Capillary Electrophoresis for Separation of Biomolecules and Viruses

by

Ana Gargaun

Thesis Submitted to the

Faculty of Graduate and Postdoctoral Studies

In partial fulfillment of the requirements

For the Doctorate of Philosophy degree in

Chemistry

Department of Chemistry and Biomolecular Sciences

Faculty of Science

University of Ottawa

Abstract

This thesis examines the use of capillary electrophoresis for the study of several biomolecules and their interactions and viruses.

The first two experimental chapters focus on its utility for thermodynamic and kinetic analysis of molecules. Chapter one focuses on the use of non-equilibrium capillary electrophoresis of equilibrium mixtures (NECEEM), to calculate the dissociation constant for the interaction between double stranded microRNA-122 and protein p19. NECEEM was used to calculate the rate constants (k_{off} = 0.059 ± 0.013 s^{-1}, k_{on} = 0.0022 ± 0.0008 $s^{-1}M^{-1}$) and the dissociation constant between miR-122 and wild type p19 (K_d = 27 ± 9 nM). A new method was developed to calculate the rate constant k_{off}, by using multiple electric fields; which resulted in a k_{off} value of 0.072 ± 0.022 s^{-1}.

In chapter two, the dissociation constant, K_d, was determined between HIV trans-activation response element and nuclear protein TOE1. It was demonstrated that TOE1, more specifically peptides ER19 and ED35, were binding to TAR with K_d values of 4.08 ± 0.19 μM for ER19 and 7.43 ± 1.60 μM for ED35. The discovery of the peptides' inhibitory action of viral replication at the transcription level is a significant step towards further elucidating mechanisms for host response to HIV-1 infection.

The third chapter focuses on the use of capillary electrophoresis for studying vesicular stomatitis virus (VSV) and vaccinia virus (VV). A new method was developed for quantification of VSV, using dithiothreitol. Furthermore, CE was used to study the preservation of VSV by a previously selected aptamer construct (quadramer) during freeze-thaw cycles. It was found that the infectivity of quadramer and aptamer pool-protected virus was higher than pure virus after 60 freeze−thaw

cycles. It was also found that adding quadramers to the virus without freezing (cycle 0) increased the virus infectivity by 30%. We also investigated the potency of a carbohydrate-based ice recrystallization inhibitor, *N*-octyl-*D*-gluconamide (NOGlc) for its ability to eliminate the cold chain and stabilize the potency of VV. Viral potency after storage at room temperature demonstrated that NOGlc conserved the infectivity of VV, during 40 days.

Acknowledgements

First, I would like to thank my supervisor during my doctoral studies, Dr. Maxim Berezovski. The fascinating nature of the research in which his lab specializes motivated me to join it. I am thankful to have been given the opportunity by Dr. Maxim Berezovski to take part in interesting and absorbing research. I acquired a diverse set of skills and the opportunity to participate in national conferences, where I had the chance to connect with scientists in the same field. My time in the lab has provided me with an excellent foundation for my career.

I would like to express special thanks to my co-supervisor, Dr. Tony Durst, who provided supervision, counsel and the outstanding example that inspired me to enter into graduate studies in the biosciences. He has become a formative influence on my career as a chemist and has always been a source of support. For that, and for opening their home to me here and in Costa Rica, I am truly grateful to Dr. Tony and Mrs. Mary Durst.

I would like to thank the Natural Sciences and Engineering Research Council, and especially the CREATE program, and the University of Ottawa for their generous support of my graduate studies. I would also like to thank the administrative staff at the University: Josée, Annette, Linda, Gabryelle, Elvira, Manon, Lorraine and Geneviève. A special thank you to the science store staff for ensuring that items were delivered quickly.

I would also like to thank my past and present lab mates for having helped make this time of my life a memorable one, and for helping build a culture of curiosity and learning at the Berezovski lab. In particular, I would like to acknowledge Shahrokh Ghobadloo, Dr. Anna Zamay, Dr. Nasrin Khan, Dr. Pavel Milman, Thao Nguyen, Dr. Gleb Mironov, Evan Bushnik, Ryan Girgrah, Nadia Al-Youssef, Mohamed Wehbe, Danny Pau, Dr. Mahmoud Labib and Alexey Chechik. I would

like to particularly highlight the friendship and contributions of my friends and former lab mates who generously provided their time to review this thesis and provide insightful and important commentary – Dr. Darija Muharemagic and Afnan Azizi. Their friendship has been a constant support throughout my studies.

I would like to thank Dr. Sabina Sperandio, Dr. Ian de Belle, Dr. John Pezacki, and Dr. John T. Arnason, all of whom have provided significant help and insight into developing my scientific knowledge. My collaboration with them and with students from other labs, including Dr. Chieu Anh Ta, has allowed me to develop a strong knowledge base that will last beyond our joint projects.

I would as well like to highlight the people who provided an unforgettable experience of graduate studies at the Durst lab. In particular, I would like to mention Dr. Asim Muhamed, Dr. Christine Choueiri, Daria Klonowska, Dr. Ana Francis Carballo and Amanda Saikaley.

My time at the University of Ottawa would not have been the same without friends that I made on campus in the Department of Chemistry and Biomolecular Sciences. I am thinking especially of Dr. Tabussom Qureshi, Alex Foo, Dr. Mirka Strmiskova, and Dr. Mark Dornan.

Finally, I would like to extend my love and appreciation to my family, without whom none of this would have been possible. I owe a debt of gratitude to my parents, who from an early age shared with me their astounding knowledge and passion for the scientific field; to Elena, for being exceedingly understanding of my busy schedule and her words of encouragement; to Marcus, who has been a great source of inspiration and joy for all of us; and to Eric, I can't imagine this journey without you.

To my mother and father,

Drs. Liubov and Serghei Gargaun

“Science, which deals with the infinite, is itself without bounds.”

Dmitri Mendeleev

Table of Contents

List of Tables

List of Figures

List of Abbreviations

Symbol	Description
^{1}H	Proton NMR
^{13}C	Carbon 13 NMR
AIDS	Acquired immune deficiency syndrome
BSA	Bovine serum albumin
C10-HSL	*N*–decanoyl–L–homoserine lactone
CAF	CD8+ anti-viral factor
CE	Capillary electrophoresis
CNAR	CD8+ T-cell non-cytotoxic anti-viral response
DCM	Dichloromethane
DEPT	Distortionless enhancement by polarization transfer
DTT	Dithiothreitol
DNA	Deoxyribonucleic acid
dsRNA	Double-stranded RNA
ds-siRNA	Double-stranded small interfering RNA
eGFP	Enhanced green fluorescent protein
EMSA	Electrophoretic mobility shift assay
EtOAc	Ethyl acetate
FAM	6-Carboxyfluorescein
$\Delta G°$	Standard state Gibbs free energy of a reaction
GFP	Green fluorescent protein
ΔH	Change in enthalpy
HEPES	4-(2-hydroxyethyl)-1-piperazineethanesulfonic acid
HIV-1	Human immodeficiency virus type-1

HPLC	High-performance liquid chromatography
HR-ESI-MS	High Resolution Electrospray Ionization Mass Spectrometry
KCEVEF	Kinetic capillary electrophoresis with variable electric fields
LC	Liquid chromatography
$MeOD_4$	Methanol-D_4
MeOH	Methanol
$MgSO_4$	Magnesium Sulfate
mRNA	Messenger RNA
miRNA	microRNA
MS	Mass spectrometry
NECEEM	Non-equilibrium capillary electrophoresis of equilibrium mixtures
NLS	Nuclear localization sequence
NOGlc	*N*-octyl-*D*-gluoconamide
NMR	Nuclear magnetic resonance
PBS	Phosphate-buffered saline
PFU	Plaque-forming units
qCE	Quantitative capillary electrophoresis
RNA	Ribonucleic acid
ΔS	Change in Entropy
SDS	Sodium dodecyl sulfate
siRNA	Small interfering RNA
TAR	Transactivation response
TCEP	*tris*-(2-carboxyethyl)phosphine
TLC	Thin layer chromatography

TOE1	Target of Egr1
tRNA	Transfer RNA
UPLC–QTOF –MS/MS	Ultra-performance liquid chromatography quadrupole time-of-flight tandem mass spectrometry
vqCE	Viral quantitative capillary electrophoresis
VSV	Vesicular stomatitis virus
VV	Vaccinia virus
WT	Wild type

Chapter 1

1. Introduction

1.1 Biomolecular interactions

Among biomacromolecular complexes, those formed between proteins and nucleic acids by non-covalent bonds are of much interest due to their regulatory role in the cell. One way to study non-covalent binding is by investigating the strength of the binding, also known as its affinity. If a target (T) binds to a ligand (L) and forms a complex (C), its interaction can be described by Equation 1.1. K_d, can then be calculated by the ratio of unbound to bound molecules, and is described by Equation 1.2. A lower K_d signifies stronger binding. K_a is the association constant and is inversely related to the K_d. The kinetics are studied by investigating the rate constants k_{off} and k_{on}, which describe how fast a complex associates and dissociates and are related to K_d through Equation 1.4.[1-3] Various methods are used to measure affinity, as described in the subsequent sections.

$$T + L \rightleftharpoons C \tag{1.1}$$

$$K_d = \frac{(T+L)}{C} \tag{1.2}$$

$$K_a = \frac{1}{K_d} \tag{1.3}$$

$$K_d = \frac{k_{off}}{k_{on}} \tag{1.4}$$

1.2 Capillary electrophoresis instrumentation

Capillary electrophoresis (CE) is a versatile technique that uses small diameter capillaries (20-200 μm) for the separation of both large and small molecules in solution under the influence of an electric field.[4] In 1969, Virtanen was the first to describe a separation of analytes in glass capillaries (200-500 μm) to improve resolution by decreasing thermal gradients.[5] Jorgensen further developed this idea by using 75 μm capillary tubes to analyze dansyl amino acids and fluorescamine-labelled peptides from a tryptic digest of egg white lysozyme,[5,6] which set a foundation for "high-performance" capillary electrophoresis as an effective tool in analytical and bioanalytical science. Its versatility in separation modes makes it an attractive and powerful tool, which can be applied to study many types of molecules and mixtures. A schematic diagram is shown in Figure 1.1 where a buffer-filled capillary is suspended between two reservoirs filled with buffer. Samples are injected in the capillary at the positive (high voltage) end and migrate towards the negative (grounded) electrode. Before they exit the capillary, sample zones pass by a detector (laser induced fluorescence, photodiode array or ultraviolet light) and the signal response is recorded over time.[7]

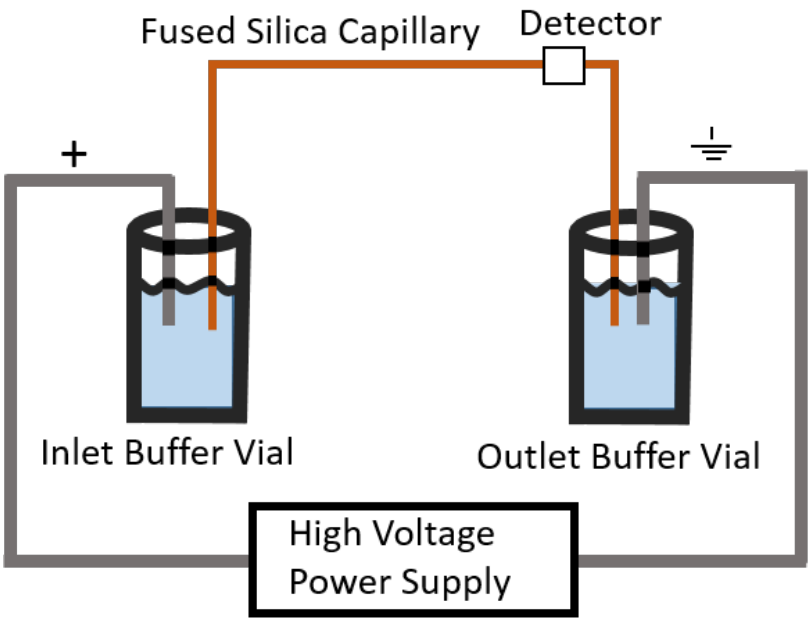

Figure 1.1 Simplified capillary electrophoresis schematic of apparatus set-up, which shows two buffer vials with the anode at the inlet side and the cathode at the outlet side.
High voltage power supply is applied for efficient separation of compounds in the narrow-bore capillary. As the compounds separate, they must pass by a detector, where there is a detection window. Several types of detectors are available, such as ultraviolet, photodiode array or laser-induced fluorescence. The detector records a signal over time and this data can later be analyzed on a computer.

The most common and most frequently used mode is capillary zone electrophoresis, which is also known as free solution capillary electrophoresis. Capillary zone electrophoresis separates molecules based on difference of charge to mass ratio under the influence of an electric field. It is a powerful technique as it can separate molecules where the difference is quite small. As the analyte and buffer molecules migrate along the direction of the electric field, the analyte ions separate according to their charge to size ratio. Figure 1.2 compares schematics of observed profiles of hydrodynamics in high performance liquid chromatography (HPLC) and electroosmotic flow in capillary electrophoresis. Hydrodynamic flow, also known as laminar flow, is affected by a pressure difference (high at the injection site and low at the exit) and results in highest velocity at the center of the capillary and zero velocity at the walls. In contrast to this, electroosmotic flow

is created by cations that are close to the walls (~10 nm) of the capillary to form a uniform plug of the solution across 99.9% of the cross section of the capillary. Electroosmotic flow refers to the migration of the buffer along with the analytes, usually from the anode towards the cathode, which results in narrower peaks and higher resolution than in HPLC.[4]

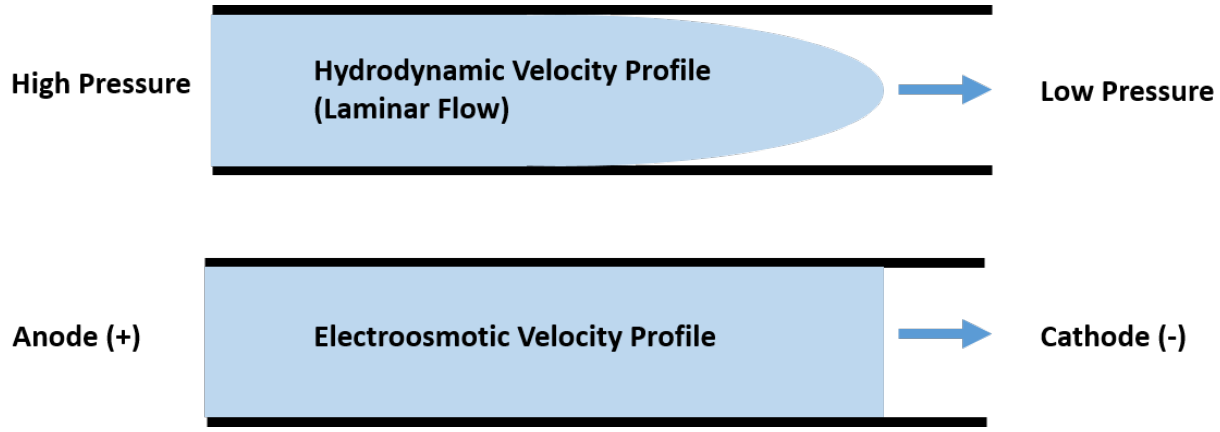

Figure 1.2 Laminar flow versus electroosmotic flow profiles, which compares the parabolic flow of HPLC with the flat flow of CE.

The inside of the capillary is made up of silanol groups (Figure 1.3A), which are deprotonated at pH levels higher than ~2. As a result, a double layer is created next to the capillary wall (Figure 1.3B). The first part of the layer is made up of the fused silica and fixed negative charge on the wall, as well as adsorbed excess cations near the wall, which partially neutralizes the negative charge. The second part of the double layer is the diffuse layer, rich in cations, which neutralizes the rest of the negative charge and drives the net flow toward the cathode. The thickness of the diffuse part varies based on ionic strength of the buffer, and it ranges from ~10 nm at a low ion strength of 1 mM to ~0.3 nm with an ionic strength of 1 M. The analytes in the solution migrate faster than the electroosmotic flow due to the difference in ionic strength between the sample plug and the run buffer.[5] Due to the small diameter of the capillary, heat is easily dissipated, which

allows for separation at high voltage (~30 kV) to result in fast, efficient separation with high plate numbers.

A)

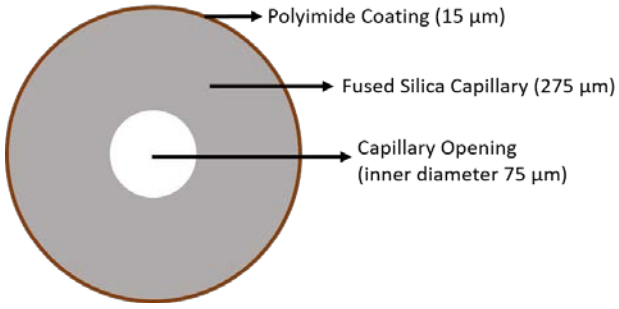

B)

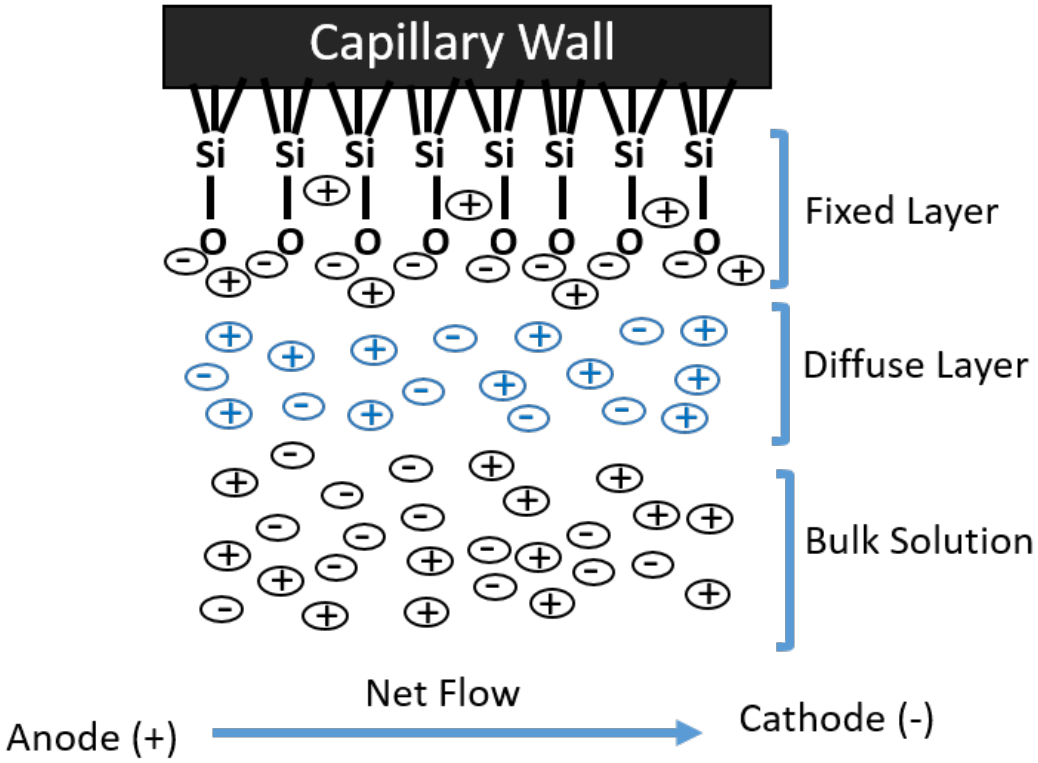

Figure 1.3 Schematics of cross section of the inside of a capillary, which shows different layers of the capillary and electroosmotic flow.
A) a 15 µm polyimide protective coating envelops the fused silica capillary for enhanced separation, which is about 275 µm in thickness. Inner diameters range from approximately 50-75 µm. B) The electroosmotic flow from anode to cathode and the formation of the double layer (fixed and diffuse), as well as the flow of the bulk solution.

Separation of analytes by CE relies on various factors, such as the mass and charge of the analyte, temperature, pH and length of the capillary, and voltage applied on the capillary. The effects of these parameters can be calculated using different mathematical formulae. Different molecules have different mobilities and therefore migrate through the capillary at different speeds (*v*). The electrophoretic mobility (μ_{ep}) is defined by the ratio of the charge of the analyte ion (*q*) to the friction coefficient (*f*) and the strength of the electric field (*E*) (Equation 1.5):

$$v_{ep} = \frac{q}{f}E = \mu_{ep}E \tag{1.5}$$

The high resolution of CE is regulated by a uniform electroosmotic flow, and changes in uniformity caused by Joule heating (generated by the flow of ions) decrease resolution.[4] Joule heating, also referred to as resistive heating, is the release of heat due to an electric current in a conductor - in this case, the capillary. Equation 1.6 defines the apparent or observed mobility (μ_{app}) as the sum of the electrophoretic mobility of the ion plus the electroosmotic mobility (μ_{eo}) of the solution.[4]

$$\mu_{app} = \mu_{ep} + \mu_{eo} \tag{1.6}$$

Cations move in the same direction as the electroosmotic flow; therefore, both μ_{ep} and μ_{eo} have the same sign, which makes apparent mobility greater than electrophoretic mobility. However, anions are transported by electrophoresis in the opposite direction from electroosmosis, which makes the μ_{ep} and μ_{eo} terms have opposite signs. pH can greatly influence the migration of ions to the cathode; therefore, changing it would affect the speed and separation of the sample. For example, at neutral or high pH electroosmosis is greater than electrophoresis, which results in the migration of ions towards the cathode. However, at low pH the opposite is true, and so the anions may never reach the cathode. The apparent mobility of a species is defined by Equation 1.7 and is the net speed (μ_{net}) divided by the electric field (*E*). Where L_d is the length of the capillary from

the injection to the detector, t is the time it takes for the species to migrate from the injection to the detector, V is the voltage applied on the capillary, and L_t is the total length of the capillary:

$$\mu_{app} = \frac{\mu_{net}}{E} = \frac{L_d/t}{V/L_t} \tag{1.7}$$

For quantitative analysis, it is necessary to normalize the peak areas by time (Equation 1.8). The normalized area is the area of the peak (A_p) divided by the migration time (t_m) of the analyte to the detector. Peak area is proportional to the quantity of analyte. The migration time is influenced by the apparent mobilities; the higher the apparent mobility of an analyte, the shorter the migration time and the less time spent in the detector. Dividing the area of the peak by the migration time corrects for time spent in the detector:

$$A_n = \frac{A_p}{t_m} \tag{1.8}$$

In 2011, an interesting capillary zone electrophoresis method was developed by Wegman, D. W. and S. N. Krylov to quantify microRNA from cell lysates.[8] Excess of labelled DNA probes with drag tags (e.g. biotin, hairpin structure) were annealed to their complementary microRNA targets in cell lysates. Drag tags were added to the probes in order to change the velocities of the different microRNA duplexes, and single-strand DNA binding protein was added to the run buffer in order to separate the single-stranded DNA probes from the duplexes, which is difficult to otherwise achieve. In one of the experiments, MCF7 cells, known to upregulate microRNA-21 and downregulate both microRNA-125b and microRNA-145, were analyzed and the results were compared with cell lysate that was spiked with the three microRNAs. MicroRNA-21 was detected and quantified, whereas the other two microRNAs were below the limit of detection of the instrument, suggesting that commercial CEs may not be suitable for detecting downregulated microRNA without pre-concentration. Based on the resolution of the three microRNA, they

suggest reliable analysis of up to 20 microRNA at once. Due to the potential of this method for microRNA profiling, it has been applied by other labs[9] and further developed for microRNA analysis by the Krylov group.[10,11]

Another separation technique in CE is capillary gel electrophoresis, where the capillary is pre-filled with a matrix, such as cross-linked polyacrylamide,[12] instead of aqueous solution. Capillary gel electrophoresis is commonly applied for size-based separation of macromolecules, such as proteins[13-15] and nucleic acids.[16-19] A similar mode is capillary isoelectric focusing, usually used for separation of peptides or proteins, and combines conventional gel isoelectric focusing with the advantages that arise from a small capillary, such as improved resolving power, quantitation and automation.[20-22] For this mode, the capillary is filled with ampholytes, polymer and the sample, and a pH gradient is created with a basic solution at the cathode and an acidic solution at the anode. Under the influence of an electric field, the analytes migrate until their overall charge is neutral.

In 2006, O'Neil *et al*. was the first to describe capillary isoelectric focusing immunoassays, which is an expansion of the previously described capillary isoelectric focusing.[23] After the peptides are separated based on isoelectric focusing, they are photochemically cross-linked to the inside of the capillary and probed with antibodies. Chemiluminescence-based detection was used to quantify post-translational modifications of proteins in 25 cells. Multiple isoforms and phosphorylated forms of endogenous extracellular signal-regulated kinase proteins were detected, quantified and compared to conventional Western blot experiments. Due to its high sensitivity and its ability to determine the percent phosphorylation for a target protein, this technology has been recently applied for detection of protein post-translational modifications in tissue biopsies.[22,24-26]

Another common mode that is used and has become an alternate to HPLC is micellar electrokinetic chromatography,[27] which creates a pseudo-stationary phase by use of micelle-forming surfactant

solutions for separation of neutral as well as charged molecules; in the presence of micelles, molecules equilibrate between the free solution and the inside of the micelles; the longer the analyte spends in the micelle, the longer its migration time.[27]

Due to the small volume that can be injected in the capillary, the limit of detection of a capillary is hindered, especially for ultraviolet detection, where the light path length is reduced compared to liquid chromatography (LC)[28] or laser-induced fluorescence. As a result, various stacking techniques for online sample concentration and separation of low concentrations of analyte are used to increase the sample concentration by orders of magnitude and therefore increase the sensitivity of the capillary.[29] Capillary isotachophoresis uses discontinuous buffer to separate a range of types of molecules, from small charged analytes to proteins, and is most useful for analysis of biological samples that are in buffer rather than water.[28] Isotachophoresis preconcentrates analytes at the leading and trailing electrolytes to perform focusing as high as 10,000 fold; the interface migrates throughout the capillary at constant velocity.[30] Stacking techniques can be combined with other modes, such as micellar electrokinetic chromatography or capillary zone electrophoresis, to provide an effective way to enrich a sample in the sample capillary prior to analysis.[27] It is important to have low salt concentrations in the sample solution, as band broadening and a low signal to noise ratio can otherwise occur. Furthermore, if the volume that is injected is very large, the resolution of the peaks can decrease.

In 2013, Garcia-Schwarz, G. and J. G. Santiago described an interesting application of capillary isotachophoresis for microRNA detection.[30] By using a two-stage hybridization assay, only 5 ng of total RNA sample was required to detect let-7a microRNA with single-nucleotide specificity. ITP was used to preconcentrate and hybridize microRNA and reporters at the interface between the leading and trailing electrolyte. Once the hybridization is complete, the ITP zone migrates

through a purification region that contains a hydrogel with the complementary sequences for the reporters, allowing for excess unhybridized reports to bind and become immobilized. The reports hybridized to microRNA migrate focused and are detected downstream. To achieve the single nucleotide specificity, reporters were designed with hairpin secondary structure; this enhanced specificity by introducing competition between self-hybridization and hybridization with other molecules.[8,30] Comparatively, reverse-transcription polymerase chain reaction can detect as few as 10 molecules.

1.3 Kinetic capillary electrophoresis

Kinetic capillary electrophoresis involves the separation of molecules that interact during electrophoresis. The affinity interaction is of a non-covalent nature and usually involves at least one biopolymer.[31] The complexes formed in these interactions can be protein/protein, protein/nucleic acid, protein/ligand, protein/small molecule, nucleic acid/small molecule, etc. Non-covalent biomolecular interactions are the cornerstone of many biological processes. Protein–protein interactions are significantly involved in the formation of multiprotein complexes, many of which are responsible for both human development and disease.[32] Furthermore, protein-DNA and protein-RNA interactions play a significant role in regulating gene expression.[33] Therefore, understanding the properties of these biomacromolecular interactions is of pivotal importance in decoding their organization, function and pathogenesis. Kinetic and thermodynamic parameters of these interactions constitute the fundamental attributes of such interactions. However, development of rapid, standard methods to accurately capture these parameters in a realistic manner remains elusive due to the inherent complexity of macromolecules and their interactions.

For studying RNA-protein interactions, a number of popular methods exist that are used for measuring these parameters; however, they all have limitations. Surface Plasmon Resonance spectroscopy is a useful technique for label-free, real-time monitoring of molecular interactions.[34,35] For example, Yao, C. *et al*. used an aptamer-based biosensor array to quantify Immunoglobulin E concentrations (2.5 to 200 μg L^{-1}) in both buffer and human serum.[36] Some of the advantages of this method include the ability to regenerate the aptamer biosensor after antigen binding, low sample volume, low detection limit and no labelling. The drawback to this method is the need for immobilizing one of the molecules; immobilization could alter the folding of the nucleic acid or protein and drastically alter its ability or likelihood to bind.

Stopped flow spectroscopy is another technique used for finding protein-RNA kinetic parameters.[37-39] Hopkins, J. *et al*.[39] used stopped-flow experiments to study binding between RNA-binding Hfq protein and small non coding RNAs. The experiments showed that annealing accelerated with Hfq concentration but was impaired by mutations in the RNA binding site of Hfq or by competition with excess RNA substrate. A fast k_{on} rate, ~10^8 M^{-1} s^{-1}, was observed, as was a slow transition, 0.5 s^{-1}, to a stable Hfq-RNA complex that exchanges ligands at a slower rate. Some advantages of stopped-flow spectroscopy include the ability to investigate kinetic molecular processes in the time range from milliseconds to hundreds of seconds, low sample volume and the fact that immobilization is not required. Shortcomings exist insofar as the observation window can be very narrow and fail if the dead time of the instrument is longer than the kinetics of the reaction.[40]

CE is particularly well suited for studying interactions between protein and nucleic acids since it can separate negatively charged nucleic acids from positively charged or slightly negatively charged proteins and protein-nucleic acid complexes, based on charge and size in solution.

Furthermore, Berezovski *et al*. have previously developed Non-Equilibrium Capillary Electrophoresis of Equilibrium Mixtures (NECEEM) as a tool for determining kinetic and thermodynamic parameters of species in equilibrium.[41,42] It is very sensitive, quick and highly reproducible, and it requires minimal amounts of the equilibrium mixture.[43] In NECEEM, a target and a ligand are incubated together to allow formation of a complex (Equation 1.5) prior to injection; as the separation starts, the equilibrium is lost and the complex dissociates.[44]

NECEEM can be used to calculate the dissociation constant (K_d) as well as dissociation and association rate constants (k_{off}) and (k_{on}) by relating these parameters to the area under the peak of the free target, the complex and complex decay in between these two peaks (Figure 1.4).[45, 46] CE advantages include its high sensitivity, the lack of any need for immobilization and its application to many systems.[47] Disadvantages include low detection limit (in a range of 10^{-6} M) for ultraviolet-based detection, whereas laser-induced fluorescence's detection limit can reach 10^{-12} M; however, this is based on the strength of the purchased laser, which can lose power over time. Furthermore, reproducibility of migration time and peak heights (areas) is poorer compared to HPLC due to variations in electroosmotic velocity. CE applications are also difficult to adjust for preparative purposes.

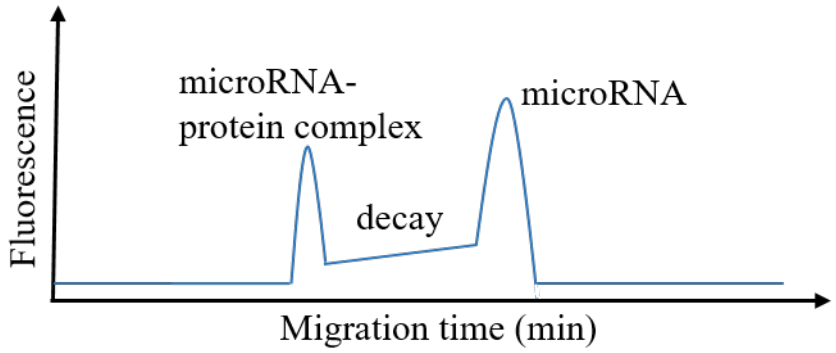

Figure 1.4 Schematic of non-equilibrium capillary electrophoresis of equilibrium mixtures where a complex is observed between microRNA and protein as well as the free microRNA.

In NECEEM, the target (T) and the ligand (L) are incubated prior to injecting the mixture in the capillary in order to allow complex (C) to form.

$$T + L \rightleftharpoons C \tag{1.9}$$

Once an external voltage is applied, the separation of the equilibrium complex from free ligand is observed under non-equilibrium conditions; the separation is based on differential electrophoretic mobility of T, L and C. The run buffer, however, does not contain any target or ligand species, so the mixture is no longer in equilibrium and starts to dissociate as it migrates through the capillary. The dissociation constant K_d can be directly calculated from the areas under the peaks of the free ligand, the complex and the decay between the two (Equations 1.10):[43]

$$K_d = \frac{[T]_0\left(1 + A_L / \left(A_D + A_C\right)\right) - [L]_0}{1 + \left(A_D + A_C\right) / A_L} \tag{1.10}$$

where $[T]_0$ is the initial concentration of the target species, $[L]_0$ is the initial concentration of L, A_L is the area under the peak of free ligand, A_D is the decay area between L and complex peaks, and A_C is the area under the peak of the complex. The decay represents the dissociation of the complex. Furthermore, one of the rate constants can be similarly determined using these parameters and time of migration of C. For instance, the formula for calculating the rate constant for the reverse reaction in Equation 2.1, k_{off}, is found as follows (Equation 1.11) and has been previously derived[1],

$$k_{off} = \frac{\ln\left(\left(A_C + A_D\right) / A_C\right)}{t_C} \tag{1.11}$$

The other rate constant can easily be found from its relationship with the two parameters (Equation 1.12),

$$k_{on} = \frac{k_{off}}{K_d} \tag{1.12}$$

1.4 Capillary electrophoresis for kinetic rates analysis, k_{off} and k_{on} and dissociation constant, K_d

Proteins interact with different types of RNA, such as nascent transcripts, mRNA, ribosomal RNA, microRNA and tRNA, and are important in transcription, translation and RNA processing.[33] An interesting interaction is between a protein p19 and short interfering RNAs (siRNAs) and microRNAs (miRNAs). MicroRNAs are endogenous RNA molecules about 22 nucleotides in length that are produced through the RNA interference pathway.[48] Protein p19 is expressed by RNA viruses, such as *Cymbidium ringspot virus* and *Tombusvirus*, as an evolutionary tool against RNA silencing.[49] Viruses produce p19 to sequester siRNAs and miRNAs by forming non-covalent p19-RNA complexes,[50,51] decreasing the amount of siRNA available for RNA silencing of viral genes.[51] Protein p19 has size-specific, sequence-independent high affinity for ds-siRNAs in its homodimer form.[51] It has recently found wide applications, particularly as a tool for trapping endogenous miRNAs,[9,52] which are used as biomarkers for profiling human cancers[33] and other disorders, including neurological and autoimmune diseases.[53]

For example, Nasheri *et al.*[54] developed an enzyme-linked microRNA and p19 sandwich assay to profile microRNA levels. One of the described experiments used surface plasmon resonance to validate p19's application as a biosensor for microRNA levels. Immobilized thiolated RNA-probes were used to trap microRNAs isolated from Huh7.5 hepatocarcinoma cell line, and signal was amplified upon binding of p19 to the miRNA duplex. A signal was produced only when the target microRNA annealed to its respective probe. More specifically, they monitored the binding

of p19 for detection of liver-abundant microRNA-122. MicroRNA-122 has been found to regulate cholesterol and fatty-acid metabolism.[55] In addition, its repression has been shown in liver cancer.[56] Furthermore, microRNA-122 positively regulates hepatitis C virus RNA abundance and is essential in the replication of infectious hepatitis C virus.[57] Therefore, understanding the binding affinity and kinetic parameters between p19 and microRNA122, as well as other miRNAs, is important in order to improve its utility.

In this work, we also studied the 23 nucleotide long microRNA-122 and p19 isolated from the *Carnation Italian Ringspot Virus*[58]. Cheng, J. *et al*. used fluorescence polarization and electrophoretic mobility shift assays to study the interactions between p19 and microRNA-122, as well as other micro and small interfering RNA. It was found that p19 binds with nanomolar affinity to ds-microRNA-122 and binds exceptionally well to double stranded RNA with the highest affinity for small RNA that are 21-23 nucleotide long.[58]

We have devised a new method, Kinetic Capillary Electrophoresis with Variable Electric Fields (KCEVEF), based on similar principles to NECEEM, that would do away with measurement of complex decay, since it is difficult to distinguish this variable from background noise when the K_d is very low, k_{on} is high or the concentration of analytes in solution is small. KCEVEF simply relies on the difference in the amount of complex that reaches the detection window of the capillary under different separation conditions; therefore, one of the disadvantages is that multiple runs are required for the experiments. Therefore, by varying the applied electric field and comparing the peak areas of the free target and the complex, the above mentioned parameters are calculated using Equation 1.13, where t_c is migration time of the complex and A_c is the area of the complex. Equation 1.12 is derived and explained in further detail in Chapter 2, Section 2.3.2. The non-

covalent biomolecular interaction between p19 and microRNA-122 served as a proof of principle study and can be applied for other protein-RNA interactions to study rate constants *via* KCEVEF.

$$k_{off} = \frac{\langle t_c \rangle \langle \ln A_c \rangle - \langle t \ln A_c \rangle}{\langle t_c^2 \rangle - \langle t_c \rangle^2} \tag{1.13}$$

In another study, we looked at biomolecular interactions between an important regulatory RNA sequence in the human immunodeficiency virus type 1 (HIV-1) called the transactivator response element (TAR) with the nuclear protein, target of Egr1 (TOE1). TAR, a known sequence required for replication,[59] forms a stable secondary structure that has a base-paired stem, a tripyrimidine bulge in the upper stem and an unpaired six-nucleotide loop.[60] TOE1 is found mostly in the nucleoli and Cajal bodies, and was identified as a downstream target of the immediate early gene Egr1. It has a functional deadenylation domain and participates in spliceosome assembly. Fourtounis *et al*. have developed a capillary-based method for studying the well-known interaction of TAR, Tat (a protein essential for viral replication) and neomycin (a known inhibitor).[61] They were interested in demonstrating the method's application for compound screening. The method was fluorescent-based multi-well CE, also referred to as a microfluidic mobility shift assay. The sample is introduced onto microscopic channels and then separated by pressure after application of potential difference. Nanoliter volumes of FAM-labelled TAR was titrated with Tat to find an optimal TAR/Tat ratio before screening for inhibitors. Neomycin, a known inhibitor, decreased the binding between TAR/Tat, as shown by a decrease in the TAR/Tat peak. IC_{50} was calculated as 1 µM and found comparable to previously published data. Due to the compatibility of the microfluidic system with 384-well screening, it is useful for screening compounds.

1.5 Capillary electrophoresis for quantification of viruses

Viruses are currently being used as important medical tools for various applications. T-VEC, an engineered herpes virus, was recently approved in the United States to treat melanoma.[62] Furthermore, multiple oncolytic viruses are currently being studied as well as tested in clinical trials,[63] with some in phase 3 as they have shown promising results.[64] Viruses are also used in many other applications, from vaccines, gene therapy[65] to engineering, material science, nanotechnology and building blocks in chemistry, electronics and biomedical sciences.[66] Due to popular use of viruses, it is important to have analytical methods that can quickly and accurately quantify them.

For vaccination therapy, according to the World Health Organization, in order for a vaccine to be considered "effective", there should be less than 1 log decrease in the original titer and no more than 10 ng of contaminating DNA should be present at time of use.[67] Current methods that are used for quantification of viruses can be categorized into infectivity-based techniques, antigen concentration and particle count. Plaque forming assays, an infectivity-based technique, are considered to be one of the most accurate methods for quantification of virions through the counting of discrete plaques.[68] For the assay, a confluent monolayer of host cells is infected with a lytic virus of an unknown concentration that has been serially diluted to a countable range. The infected cells are then covered with an immobilizing overlay medium such as agarose, methyl cellulose or carboxymethyl cellulose to prevent viral infection from spreading. Modern methods use liquid overlays such as Aveicel5-7, which can be applied at room temperature, reducing the chance of damaging heat sensitive viruses.[68] Although this is a well-established method for determination of infectious dose used in academic, commercial and clinical settings, it lacks the ability to quantify contaminating viral or cellular DNA debris.

Quantitative Polymerase Chain Reaction is another well-established technique used to quantify viruses based on their viral DNA or RNA; it is relatively quick and highly reproducible. A drawback can be the overestimation of intact virus by as much as five orders of magnitude, since the amount of viral DNA or RNA in a virus sample is usually higher than intact virus due to degradation of virus.[69]

Several groups have developed methods for CE-based detection of virus.[70] In protein-based virus detection, E. van Tricht *et al*. used capillary gel electrophoresis to identify various virus strains based on their protein profiles.[71] In nucleic acid based detection, a specific region is amplified, usually using polymerase chain reaction steps[70], and so it suffers from some of the same drawbacks as were mentioned for quantitative polymerase chain reaction. In our method, we used vesicular stomatitis virus (VSV-Δ51) that contains a mutation in the M protein provided by Jennerex Inc. VSV is being developed for oncolytic therapy[72] due to its selective, potent responses in human tumour cells.[73-76] It is a bullet-shaped, non-segmented negative-strand RNA-based virus from the family *Rhabdoviridae*; its diameter is ~70 nm wide and it is ~ 170 nm long. Our lab has been developing methods that can quantify the number of intact virus particles and the amount of contamination in a viral sample for quality control purposes, which gave rise to viral quantitative capillary electrophoresis (qCE). Some drawbacks include lengthy analysis time due to aggregation of the virus. Other research labs have tried to solve this problem by using detergents such as Triton X-100, deoxycholate, and/or sodium dodecyl sulfate (SDS) and have found that SDS works best.[77] We tried these detergents, as well as other reagents, in an effort to make the method quicker.

1.6 Capillary electrophoresis for monitoring the preservation of viruses

As mentioned earlier, viruses play an important role in many aspects of our lives. One area where viruses have truly changed our lives for the better is through vaccination. According to the Public Health Agency of Canada, vaccination has saved more lives than any other health intervention in the past 50 years.[78] Vaccination is important for all age groups, with an emphasis on more vulnerable groups, such as young children and the elderly. Vaccination programs have been responsible for eliminating, containing and controlling diseases that were common in Canada, such as diphtheria, hepatitis B and measles.[78] However, it is important to note that globally, millions die yearly because of preventable diseases[79] rarely seen in Canada that can be imported through travel and transmitted to people who are not immunized. This is why it is crucial to help vaccination programs become more successful in other parts of the world.

Vaccines, as defined by the Journal of Vaccines and Vaccination, are biological preparations that provide active acquired immunity to a particular disease; they usually contain a disease-causing microorganism, which is often prepared from killed or inactivated forms of the microbe, its toxins or one of its surface proteins.[80] This enables the immune system to recognize the antigen as a threat without severe side effects, destroy it, and upon subsequent exposure, eliminate it more easily. Besides the use of vaccines for the prevention of infectious diseases, vaccines have also been used in oncolytic therapy for treatment or prevention of cancer.[81]

One of the major problems with vaccine delivery is their thermal instability, and so having the vaccines in a form that can be stored and remain biologically active until use is a challenge.[79] To minimize this issue, a term has been developed in the 1970s called the “cold chain”, which refers to the refrigerator containers that are used to store the vaccines at protective temperatures until

use.[82] In 1974, the World Health Organization Expanded Programme on Immunizations helped establish operational standards, which provide low cost storage equipment for use in different environments. Since then, significant improvements have been made; however, it is estimated that half of supplied vaccines are wasted, mostly due to thermal instability.[79] High temperatures damage live viruses, and much effort has been put towards keeping the vaccines at low temperatures, which led to developing systems that cause accidental freezing. Freezing also damages viral integrity, and this is increasingly important as the number of vaccines that are freeze-sensitive increases.[83] An estimated 31% of the US$439 million that the United Nations Children's Fund spent on all vaccines in 2005 was on freeze-sensitive vaccines. It is important to note the strict guidelines mentioned earlier for vaccination therapy in terms of virus preservation.[67] Therefore, different attempts have been made to find formulations that are able to stabilize the virus.

Enveloped viruses in particular are likely to decrease in infectivity after freeze-thaw cycles.[84] Some compounds that have been used to stabilize blood cells have also been used to stabilize viruses; they include glycerol, sorbitol, sucrose, gelatin, monosodium glutamate and dimethyl sulfoxide, and have been shown to be helpful in stabilizing viruses to some degree.[84-86] Some of these compounds are toxic or immunogenic, and the viruses still require careful handling and storage conditions. Stabilization of the virus or cell by these agents is most likely achieved by the disruption of destructive ice crystals and by decreasing the effective concentration of electrolytes, thereby preventing the denaturation of cells by toxic concentrations of salts or solutes.[84] Potent ice recrystallization inhibitors include antifreeze glycoproteins isolated from the blood of fish, such as Artic cod.[87] Unfortunately, these are poor cryoprotectants, as they irreversibly bind ice crystals, and promote premature cryoinjury and cell death during freeze-thaw cycles.[88] Adam, M.

K. *et al*. reported the synthesis of a panel of carbohydrate-based surfactants, some of which acted as ice recrystallization inhibitors as well as cryoprotectants of TF-1α erythroleukimic cells during freeze-thaw cycles.[88] This work demonstrates the potential of carbohydrate-based surfactants as stabilizers of cells. In our work, we screened a panel of glycoproteins and carbohydrate-based surfactants for their ability to preserve the stability of vaccinia virus.

In 2012, Zang *et al*.[85] investigated silk fibroin protein polymer for its ability to stabilize live measles-mumps-rubella vaccine. The vaccine was encapsulated in silk film, air-dried or lyophilized, and then exposed to elevated temperatures as high as 45°C. When stored at 45°C, the vaccine encapsulated in silk film retained 53% activity after 24 weeks, whereas vaccine that was not stored in silk film lost all potency after 20 weeks. The copolymer structure of silk film contains nanoscale pockets that can immobilize bioactive molecules by minimizing water content and reducing protein chain mobility, thereby preventing a transition from the native to denatured form.[85, 89, 90]

More recently, Grosz, D. D. *et al*.[91] showed the stabilizing effect of sucrose on respiratory Syncytial virus, a common respiratory pathogen that can cause pneumonia. After testing various concentrations of sucrose (0-20%) as a cryo- and nebulization protectant *in vitro*, *in vivo* experiments were performed on a lamb model. They found that in cells, virus stored in 20% sucrose displayed a 0.297 log reduction, which was higher than the 0.580 log reduction displayed when stored in 0% sucrose. *In vivo* experiments showed that virus stored in 20% sucrose enhanced respiratory Syncytial virus lesions and antigen distribution. This research demonstrates the potential of carbohydrate-based compounds for stabilization of viruses.

Aptamers are single-stranded DNA or RNA that are evolved from a large pool of sequences to bind a target of interest. They fold into three-dimensional structures, and interact with and bind to

their targets through structural recognition, similar to antigen-antibody reactions; hence, they are often referred to as "chemical antibodies".[92] The use of aptamers for stabilizing proteins has been recently demonstrated by Jain, N.K. *et al*., where they used aptamers selected against tetanus toxoid vaccine to reduce moisture-induced aggregation of tetanus toxoid *in vitro* and to maintain its antigenicity.[93] In 2015, Chaudhary, R. *et al*. selected RNA aptamers against the elongated polyglutamine stretch of huntingtin protein, responsible for Huntington's disease, to reduce its aggregation *in vitro.*[94] This research demonstrates the potential for aptamers as bioanalytical agents for reducing aggregation of viruses. In our work, we used anti-vesicular stomatitis virus aptamers and investigated their effects on preserving the virion after various freeze-thaw cycles.

1.7 Research objectives

This thesis is divided in two parts. Part I, which is the main part of the work (Chapters 2-4) revolves around the study of biomolecular interactions by CE. We use it to look at peptides, proteins, miRNA and viruses. Part II describes the phytochemical analysis, as well as the biofilm and quorum sensing inhibitory effects, of material isolated from neotropical plants.

The second chapter of the thesis explores the use of CE for studying rates. We developed a new method for calculating rate constants that is particularly useful for systems where the decay is very low. For this, we used a model system comprised of protein p19 and microRNA-122. This work was done in collaboration with Dr. Victor Okhonin, Afnan Azizi, and John P. Pezacki's laboratory group.

The third chapter of the thesis looks at an important and newly identified interaction in HIV-1 infected T-cells between trans-activation response element and TOE1 protein. We were able to

show the direct interaction of various TOE1 peptide sequences by CE. This work was done in collaboration with Dr. Sabina Sperandio and Dr. Ian de Belle.

The fourth chapter of the thesis uses capillary electrophoresis for quantification of intact virus particles. This work has three themes. The first part focuses on the development of a new method for quantification of virus using dithiothreitol. We also looked at the stabilizing effect of previously selected aptamers on vesicular stomatitis virus; this work was done in collaboration with Shahrokh Ghobadloo and Dr. Darija Muharemagic, and is contained in the second part of the chapter. The third part of chapter four focuses on the use of CE for monitoring the stability of vaccinia virus by *N*-octyl-*D*-gluconamide, which was done in collaboration with Shahrokh Ghobadloo, Dr. Darija Muharemagic, and Dr. Robert Ben's laboratory group.

Part II of this thesis presents preliminary results arising out of work done in collaboration with Dr. John T. Arnason's laboratory group, Dr. Chieu Anh Ta, as well as Laura Picado and her supervisor, Dr. Ana Francis Carballo from the Universidad Nacional de Costa Rica, located in Heredia, Costa Rica. Bioassay-guided fractionation was used to study neotropical plants from Costa Rica for their potential to inhibit biofilm formation and quorum sensing in bacteria. More specifically, five plants-*Blakea cuneata, Piper papantlense, Piper aequale, Piper lanceaefolium* and *Ruptiliocarpon caracolito* - were found to have biofilm inhibitory activity against *Pseudomonas aeruginosa* and quorum sensing inhibitory activity against *Chromobacterium violaceum.*

Chapter 2

2. Study of non-covalent interactions between miRNA and protein p19 using non-equilibrium capillary electrophoresis of equilibrium mixtures

2.1 Background

The first part of this chapter focuses on the use of non-equilibrium capillary electrophoresis of equilibrium mixtures (NECEEM), a separation-based affinity method, to calculate the dissociation constant for the interaction between double stranded microRNA-122 and protein p19. MicroRNAs (miRNA) are short, non-coding RNAs that regulate gene expression; their expression profiles are emerging as potential non-invasive markers for classification of human cancers and other diseases.[95-103] A plant RNA silencing suppressor from the Carnation Italian Ringspot Virus, p19, has size-specific, sequence-independent high affinity (nanomolar) to siRNA and miRNA that are between 21-23 nucleotides in length.[104] p19 binds to miRNA as a dimer by electrostatic interactions and hydrogen-bonding with the sugar-phosphate backbone, and capping interactions with the last base pairs of the duplex region with two tryptophan residues in the N-terminal subdomain of p19.[52,105] The miRNA used in this project, miR-122, is 22 nucleotides long, and correlates strongly with liver enzyme levels and necroinflammatory activity.[106] Antagonizing miR-122 is being investigated as a hepatitis C virus therapeutic, with an antagonist in phase II

clinical trials.[107-109] It is important to study the interactions between p19 and miRNA, as p19 is often used to study various systems in plants, human and stem cells.[52]

Previously, Khan, N. *et al*., have used equilibrium capillary electrophoresis of equilibrium mixtures to develop an assay for quick quantification of miRNA in blood serum using p19 or single-stranded DNA binding protein as separation enhancers.[110] Although a recent method published by Mironov, G.G. *et al.*, demonstrated the utility of equilibrium capillary electrophoresis of equilibrium mixtures for determining the affinity of non-covalent interactions,[111] neither equilibrium capillary electrophoresis of equilibrium mixtures nor NECEEM have been previously used to investigate the rate of dissociation between p19 and miRNA-122. In a study where Cheng *et al*. perform mutational analysis on p19 in order to engineer p19 with better binding to miR-122, they found the K_d of p19 and miR-122 by electrophoretic mobility shift assays (EMSA) as 19 ± 4 nM. In a previous study by the same group, fluorescence polarization experiments and EMSA revealed the K_d as 15 ± 7 nM and 21 ± 3 nM, respectively[58]. Rawlings *et al*. studied the k_{off} of siRNA and p19 and found a relatively high k_{off} (0.062 ± 0.002s^{-1}). To the best of my knowledge, k_{off} for miR-122 and p19 have not yet been reported.

In this work, capillary electrophoresis was used to calculate the rate constants (k_{off} = 0.059 s^{-1} ± 0.013, k_{on} = 0.002 ± 0.001 $s^{-1}M^{-1}$) and dissociation constant between miR-122 and wild type p19 (K_d = 27 nM ± 9 nM) when separated at 21°C. NECEEM was used to study the non-covalent interactions between miR-122 and p19. A new method, which we named Kinetic Capillary Electrophoresis with Varying Electric Fields (KCEVEF), was also used to calculate the rate constant k_{off} by using multiple electric fields; this method gave a value of 0.072 ± 0.022 s^{-1}. A representation of the method is described in Figure 2.1 and will be discussed in more detail in the results and discussion sections of this chapter. This method can be applied to other biological

molecules that are known to interact with each other and that can be detected by capillary electrophoresis. The work in this chapter has been done in collaboration with Dr. Victor Okhonin, who developed the mathematical equation, and Dr. John P. Pezacki's lab members (Dana C. Danielson and Megan Powdrill), who provided the p19 protein. I performed all capillary electrophoresis experiments.

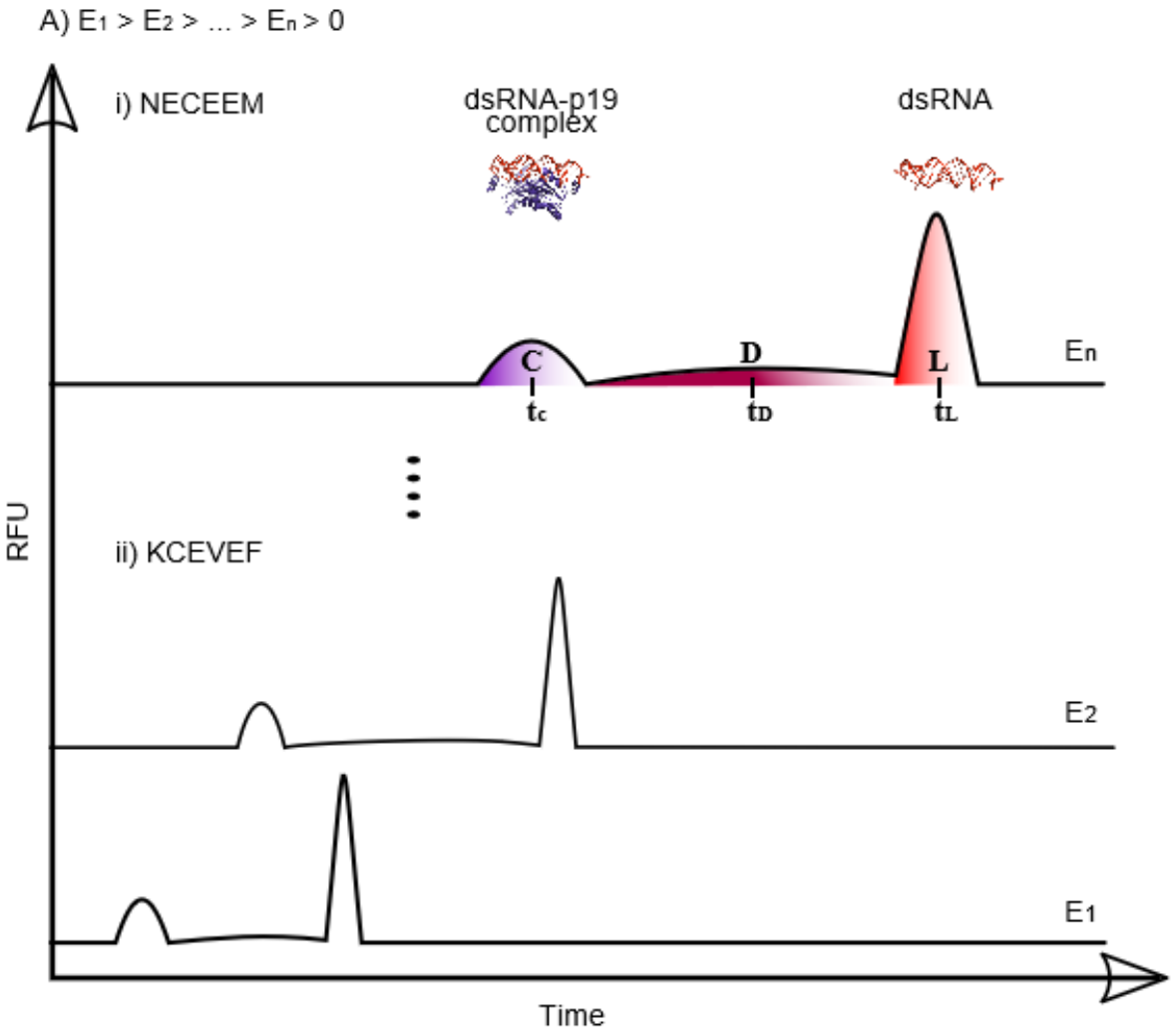

B)

(i) $$k_{off} = \frac{\langle t \rangle \langle \ln(C) \rangle - \langle t \ln(C) \rangle}{\langle t^2 \rangle - \langle t \rangle^2}$$

(ii) $$K_d = \frac{[T]_0 (1 + A_{ligand}) - [L]_0}{1 + (A_{decay} + A_{complex})/A_{ligand}}$$

(iii) $$k_{on} = \frac{k_{off}}{K_d}$$

K_d, k_{off}, k_{on}

Figure 2.1 Schematic representation for determination of kinetic and thermodynamic constants of p19-dsRNA interaction using NECEEM and KCEVEF experiments.
A) An equilibrium mixture of p19 and miRNA-probe hybrid is separated by capillary electrophoresis using various electric fields denoted by E, where E1>E2. B) Area of signals are used in equations, i), ii) and iii) to calculate the kinetic and thermodynamic constants of this interaction. For i) C, D and L are complex, decay and ligand area, respectively; and C_t, D_t, L_t are migration time of complex, decay and ligand, respectively. The angle brackets represent the average of the variable within them, under different electric fields. For ii) A represents area, T, target and L, ligand.

2.2 Materials and Methods

2.2.1 Hybridization

MicroRNA miR-122 and its hybridization FAM-labelled probe were purchased from IDT DNA Technologies (Coralville, USA). miR-122 has the sequence 5'-/Phos/UGGAGUGUGACAAUGGUGUUUG-3'. The sequence of the fluorescently labeled complementary probe with 6-carboxyfluorescein (FAM) is 5'-/5Phos/CAAACACC-AUUGUCACACUCCAA/36-FAM/-3'.

The hybridization was performed in a polymerase chain reaction thermocycler (Mastercycler pro S, Eppendorf, Germany). miR-122 and the probe were mixed together in a microvial and heated to 70°C for 1 min. The temperature was then dropped to 55°C for 5 min and then left at 20°C for 15 min. A 1:2 ratio of probe to miR-122 was used in order to ensure that all the miR-122 is hybridized. Yeast tRNA was used as masking RNA to prevent degradation of the microRNA complex by RNases that may have been present in the purified p19.

2.2.2 *Carnation Italian Ringspot Virus* p19 expression purification

Recombinant histidine-tagged *Carnation Italian Rignspot Virus* p19 was expressed and purified from pTriEx vector in *E. coli* BL21, as described in Danielson, D.C. *et al*.[112] Briefly, transformed cells were grown with 100 μg mL^{-1} of ampicillin until an optical density of 0.5 was reached. Protein expression was then induced with 1 mM isopropyl-β-D-thiogalactopyranoside and grown for 3 h. Cells were then lysed with sonication. The lysate was applied to a 1 mL Nickel FF column and washed with 10 mL buffer (50 mM Tris, 300 mM NaCl, 60 mM imidazole, pH 8) followed by elution with 10 mL elution buffer (50 mM Tris, 300 mM NaCl, 250 mM imidazole, pH 8) directly into 100 μL of 1 M DTT. Size exclusion chromatography was used to purify the proteins. Bradford protein assay was used to quantify the fraction in reference to BSA standards.

Carnation Italian Rignspot Virus p19 protein was expressed and purified as previously described.[112] p19 was prepared by Dana Danielson and Megan Powdrill.

2.2.3 Capillary electrophoresis

A ProteomeLab PA 800 capillary electrophoresis system from Beckman-Coulter, Brea, California, USA, was used to separate the equilibrium mixture in each experiment. Fluorescence was induced by a 488-nm line of an Ar-ion laser and detected at 520 ± 10 nm. A bare silica-fused capillary was

used of a total length of 59 cm, with 49 cm from injection to the detection point and an outer diameter of 365 µm and an inner diameter of 75 µm. The injections were done by a pressure pulse with varying hydrodynamic injection volumes of 23.02 nL. The electric field was varied between 305 V cm^{-1} to 406 V cm^{-1}, with the positive charge at the inlet and ground at the outlet. The capillary temperature was maintained at 15°C for the duration of the variable electric fields experiments.

For thermochemical experiments, temperatures for both the capillary and sample vials were controlled between 15°C-31°C. The run buffer was 25 mM sodium tetraborate at pH 9.86. Prior to each injection, the capillary was rinsed with 100 mM HCl for 2 min, 100 mM NaOH for 2 min, ddH_2O for 2 min, and 25 mM Borax for 2 min.

32 Karat^{TM} software (Beckman-Coulter, Brea, California, USA) was used for recording the electropherograms, and final electropherograms were produced by Excel (Microsoft).

To find the limit of detection for miR-122, a range of concentrations of miR-122 (1 pm-100 nM) were hybridized with 10 nM FAM-labelled complementary RNA probe. The limit of detection was found to be 5 nM, having been calculated for the lowest concentration of miR-122 when its duplex had a signal-to-noise ratio of 3:1.

2.2.4 Capillary electrophoresis optimization experiments

Various length capillaries (30 cm, 40 cm and 60 cm), injection conditions (29 nL-89 nL) and buffers (25 mM Tris-acetate, 25 mM borax) were tested in order to optimize separation conditions.

2.2.5 Active site titration of p19

The activity of p19 was calculated by fitting a curve to the titration graph of ds-microRNA complex formed with p19 and determining the concentration at which the complex reaches the saturation level. The curve in each graph was fit by Afnan Azizi, using an arctan function in Microsoft Excel by minimizing the squared difference between the obtained data and theoretical values found from an equation of the form:

$$y = a \cdot \arctan(bx + c) + d \qquad (3.2)$$

where y is the theoretical value, x is the concentration of protein p19, and a, b, c and d are automatically modified to minimize the squared difference.

The following values of the four modifiable coefficients were obtained: a = -19.01, b = 13.98, c = 0.00055, and d = 3.8×10^{-5}.

The saturation level of the complex is indicated by the horizontal asymptote of the curve of best fit as x tends to $+\infty$ which is located at $(a\pi/2)+d$. To calculate the concentration of p19, the apparent K_d was first calculated. To do so, the value of x at $y_{1/2}$ was determined, where $y_{1/2} = ((a\pi/2)+d)/2$. The curve suggests cooperative binding, which is likely because p19 is a dimer. Saturation level is at approximately 56 nM, based on the curve.

2.3 Results and Discussion

2.3.1 Non-Equilibrium Capillary Electrophoresis of Equilibrium Mixtures (NECEEM)

The thermodynamic and kinetic binding parameters of p19-miR-122 complex were independently calculated using both NECEEM and KCEVEF. Figure 2.2 presents a representative experimental

electropherogram of NECEEM experiments with the complex and decay shown more clearly in the inset.

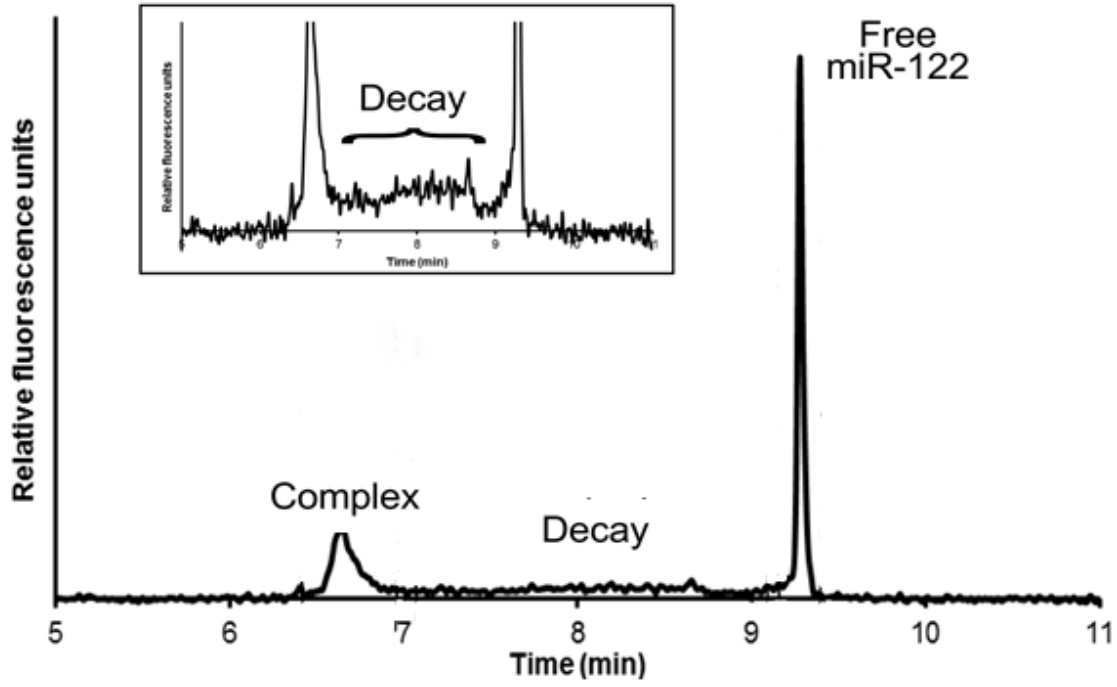

Figure 2.2 Classical picture of NECEEM, with an inset that focuses on the complex, decay, and free ligand.
For the experiment, 2.5 µM of p19 and 50 nM of double-stranded miR-122 and 50 nM of single-stranded FAM-labelled miR-122 were incubated and separated using an electric field of 407 V cm^{-1} at 15°C with hydrodynamic injection volume of 20 nL. The complex between ds-miRNA and p19 migrates at approximately 6.5 minutes, the decay is observed between 7 min and 9 min and single stranded miRNA-122 is observed at approximately 9.2 minutes. The peak for ds-miRNA is completely shifted to complex and decay.

We used equations 1.10-1.12 to determine K_d, k_{off} and k_{on} for the complex formation between p19 and miR-122: the rate constants (k_{off} = 0.059 ± 0.013 s^{-1}, k_{on} = 0.002 ± 0.001 $s^{-1}M^{-1}$) and dissociation constant between miR-122 and wild type p19 (K_d = 27 ± 9 nM) when separated at 21°C using an electric field of 407 V cm^{-1}. The K_d value is similar to the ones reported by Cheng *et al.*: 21 ± 4 nM and 15 ± 7 nM.[52] The differences in value may be due to the different experimental conditions used, such as the pH of the buffer. We used a borate buffer (pH of 9.8), whereas the one used by this group was PBS (pH 7.4), which is much closer to physiological

conditions. Figure 2.3, the bottom electropherogram, demonstrates the two peaks observed for single-stranded and double stranded miR-122. From here on in, I will refer to the FAM-labelled complementary strand of miR-122 as FAM-probe. An excess amount of FAM-probe was used in order to ensure full annealing of miR-122. For this experiment, 10 nM of miR-122 was incubated for annealing with 20 nM of FAM-probe; this should result in 10 nM of double-stranded miR-122 and 10 nM free FAM-probe, which can be represented by a 1:1 ratio of the two peaks in an electropherogram. However, this is not the case, as the two peaks are not equal in size; this may be because the concentrations of FAM-probe may be lower than expected or miR-122 is higher than expected. Free FAM-probe migrates faster than double stranded miR-122, as can be confirmed by a decrease in the peak on the right upon the formation of the complex peak, which appears at approximately 6 min, when increasing concentrations of p19 are added. The decay is observed between 6 minutes and 8 minutes and represents the dissociation of the complex, and FAM-probe is observed at approximately 8.2 minutes. The peak for free ds-miRNA disappears, as it is completely shifted to complex and decay at 1 μM of p19 with 20 nM of ds miRNA. A peak for FAM-probe does not shift because p19 does not bind to single stranded microRNA.

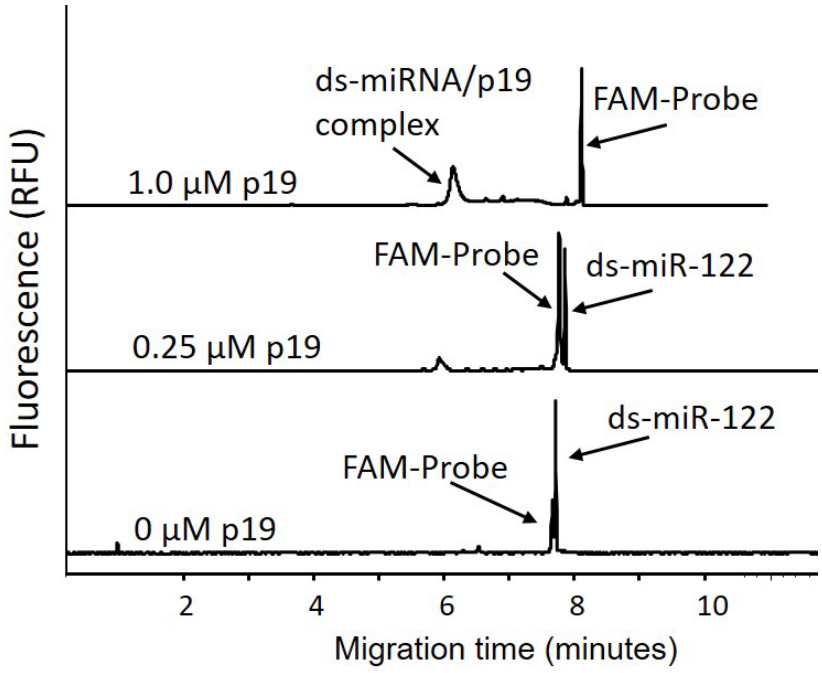

Figure 2.3 Electropherograms of double stranded miRNA-122 and p19.
10 nM miRNA-122 annealed with 20 nM FAM-labelled complementary miR-122 incubated for 10 min at room temperature with bottom, 0 µM p19, middle, 0.25 µM p19, and top, 1.0 µM p19. All separated by capillary electrophoresis under 433 V cm-1 in a 58 cm long capillary, with a hydrodynamic injection volume of 23 nL. Capillary temperature was maintained at 15°C.

To ensure that binding between p19 and single-stranded miRNA does not occur, we incubated 500 nM of p19 with 20 nM FAM-probe, and binding was not observed, as shown in Figure 2.4. There is a slight shift in migration time because of the change in electroosmotic flow.

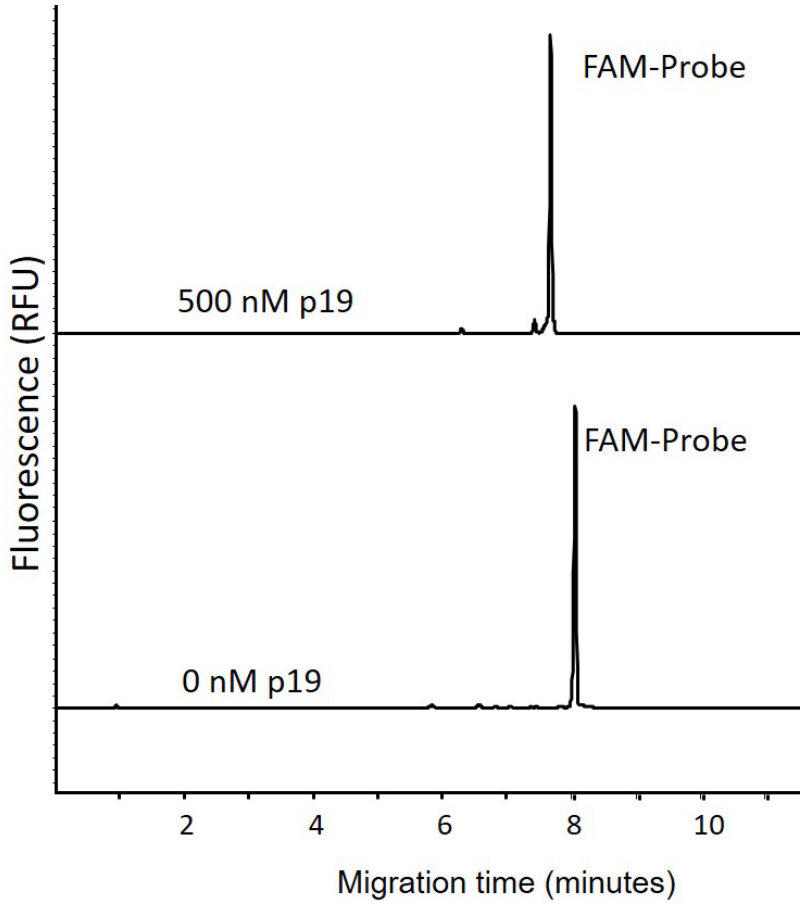

Figure 2.4 Electropherograms of FAM-labelled probe complementary to miRNA-122, and p19. Electropherograms of bottom, 10 nM FAM-probe, and top, 10 nM FAM-probe incubated with 500 nM p19. Both separated by capillary electrophoresis. 433 V cm^{-1} was used for the separation in a 58 cm long capillary, with a hydrodynamic injection volume of 23 nL; capillary temperature was maintained at 15°C.

Various separation conditions were tested prior to finding conditions under which the double stranded microRNA could be separated from the FAM-probe. Some of the conditions tested are shown in Figure 2.5, where a 40 cm long capillary and then a 60 cm long capillary are used. The 60 cm long capillary proved more effective at separating the double-stranded microRNA from the single stranded microRNA. We also tested different volumes of hydrodynamic injections (53-89 nL, shown in Figure 2.5). The higher injections however resulted in bigger peaks, due to the fluorescent impurities that appear with FAM-probe; we decided to use 23 nL in order to have better resolution of the peaks and fewer impurities detected by the CE.

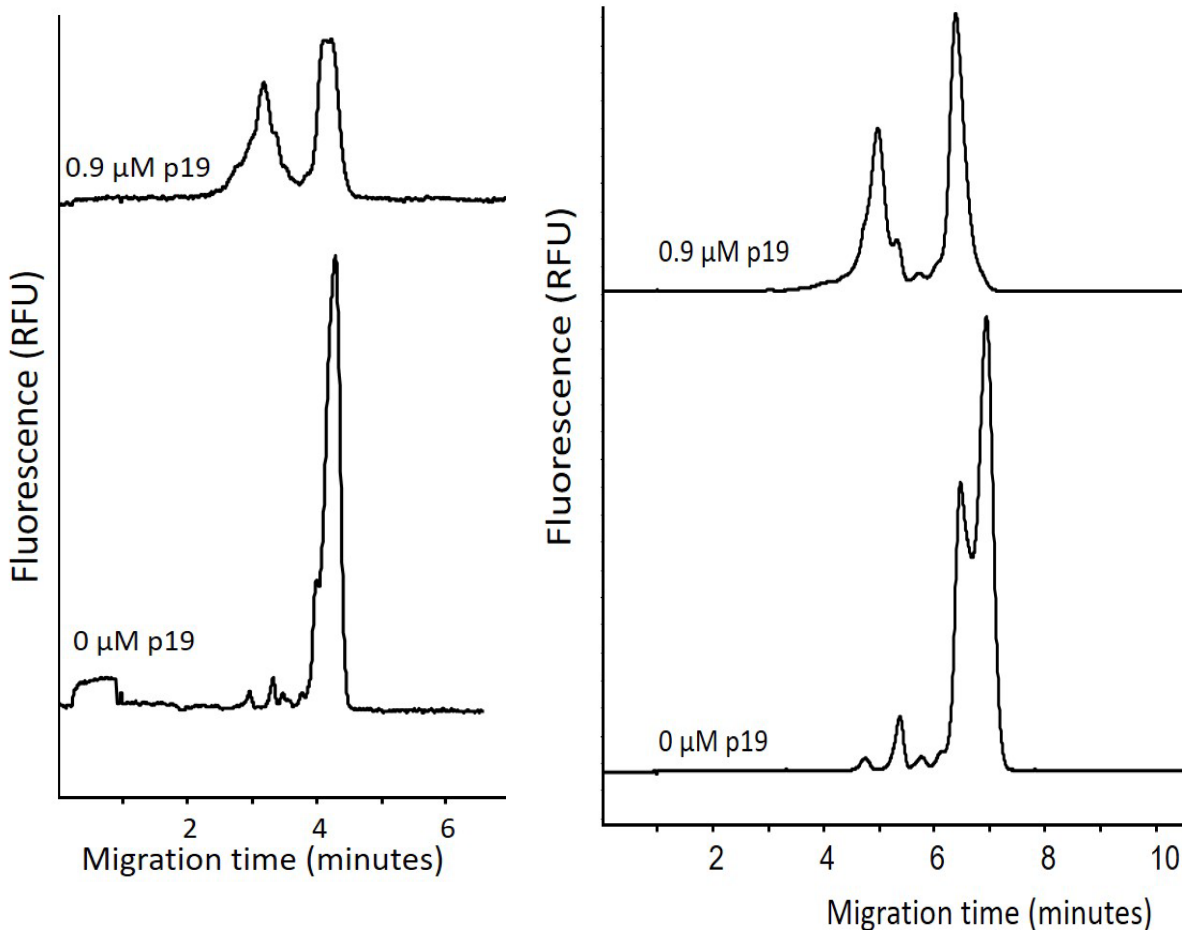

Figure 2.5 Separation of miRNA-122 and p19 by 40 and 60 cm long capillaries.
Separation of 0.9 µM p19 incubated with 20 nM ds-miRNA-122 and 20 nM FAM-probe at 20 °C in A) 40 cm capillary at 500 V cm^{-1}, 53 nL hydrodynamic injection. B) 60 cm long capillary, under 466 V cm^{-1}, hydrodynamic injection 89 nL.

To calculate the active concentration of p19, an active site titration was performed where increasing concentrations of ds-miRNA-122 (1.5 to 200 nM) were added with a constant concentration of p19 (400 nM), Figure 2.6. An arctan function was used to calculate the active concentration of p19 based on the line of best fit. The sigmoidal shape of the curve suggests cooperative binding, which is realistic considering that p19 is a dimer. The graph plateaus at approximately 56 nM; therefore, 14% of the protein was active for the experiments. The activity was very low because it had been kept for an extended period of time in the refrigerator

(approximately 4°C). We took this into consideration when calculating the thermodynamic and rate constants because the protein loses activity when it is stored at 4°C over an extended period of time.

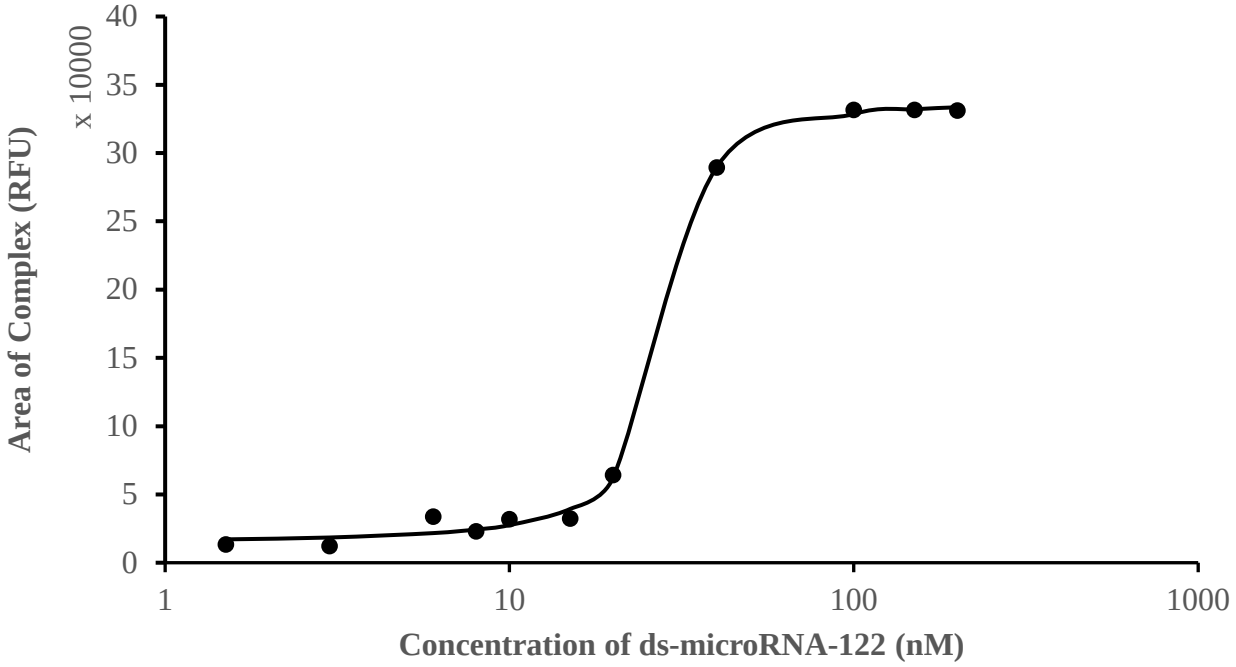

Figure 2.6 Active site titration of p19 with miRNA-122.
Relative fluorescence area of complex between 400 nM p19 with increasing concentrations of ds-miRNA (1.5 -200 nM).

2.3.1.1 Dissociation constant at different temperatures

NECEEM is a powerful and rapid way to measure thermodynamic constants. We took advantage of this property to further characterize the binding between p19 and miR-122 at different temperatures and to find the optimal temperature for complex formation. We performed a thermochemical study to obtain thermodynamic values such as standard Gibbs Free Energy of the reaction, $\Delta G°$, change in enthalpy, ΔH, and change in entropy, ΔS. We conducted the experiments by varying the temperature of the capillary and the sample holder between 15°C and 31°C in increments of two degrees Celsius. Plotting the dissociation constant as a function of temperature,

Figure 2.7A shows that as temperature passes 23°C, affinity of miR-122 for p19 decreases sharply and in a linear manner. This may indicate that beyond this temperature the complex is not very stable and readily dissociates. Furthermore, the complex appears to be most stable at temperatures between 19°C-23°C. Below 19°C, the affinity begins to decrease, but not significantly. Interestingly, while the pattern of variation in k_{off} (Figure 2.7B) is similar to that of K_d, at 25°C k_{off} remains low while K_d begins its sharp increase. This discrepancy suggests that this decrease in affinity is caused by a large drop in k_{on} and that these two kinetic parameters' change with temperature is independent of each other.

A)

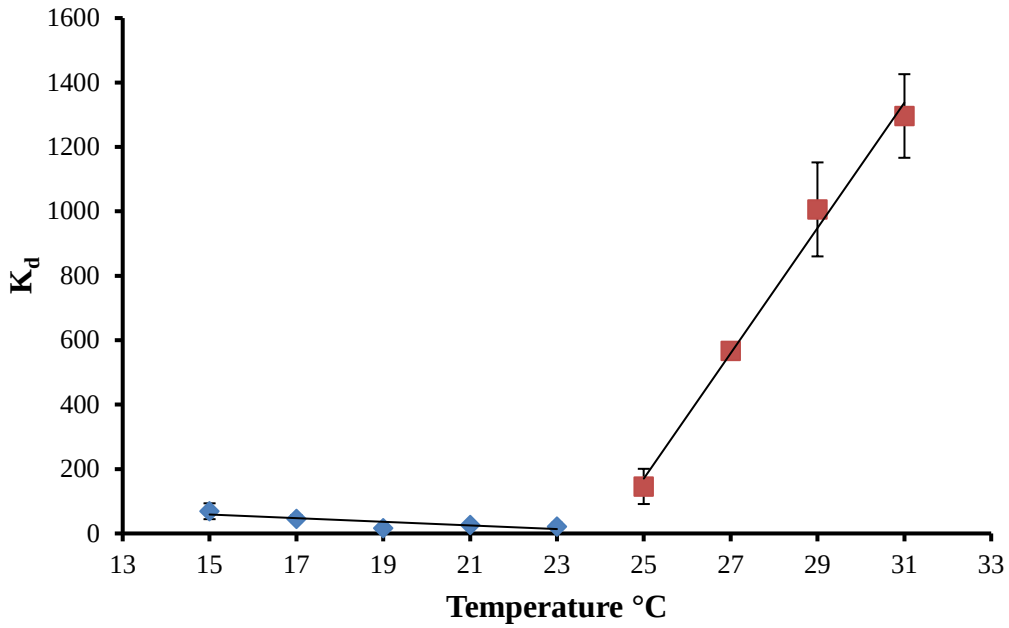

B)

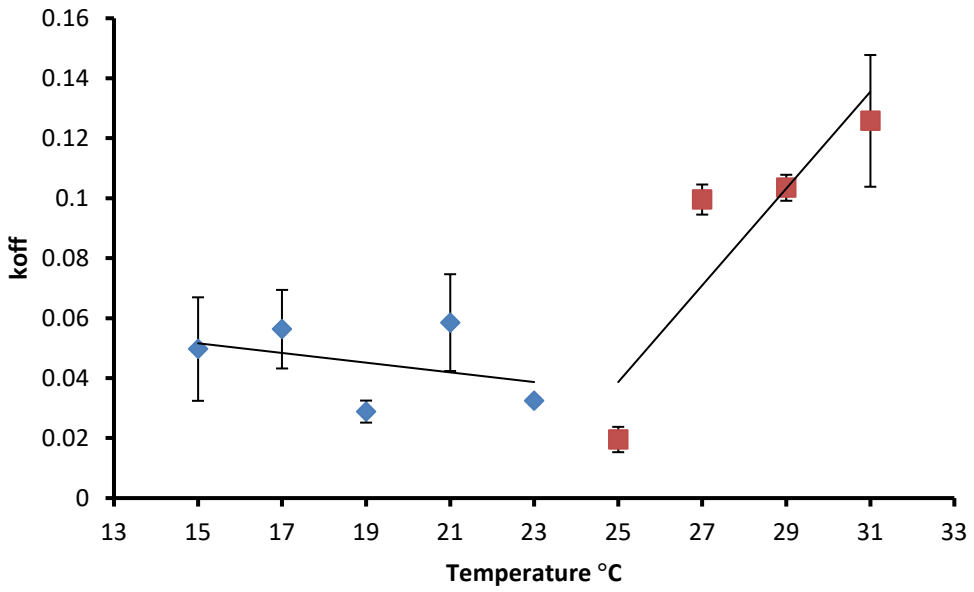

Figure 2.7 NECEEM-measured temperature dependencies of thermodynamic and kinetic binding parameters for 100 nM miR-122 and 500 nM p19 at 407 V cm^{-1}.
A) The dissociation constant, K_d, as a function of temperature. Two trends are observed: a decrease in K_d from 15°C to 23°C (blue) and an increase from 25°C to 33°C (red). B) The dissociation rate constant, k_{off}, as a function of temperature.

ΔG° is the thermodynamic constant that determines which way a biomolecular equilibrium will go and how much work needs to be done in order to shift a reaction in that direction.[113] We found the value of ΔG^o to be +40 kJ mol^{-1} for the dissociation of p19 with miR-122. This could be controlled by two effects: the inclination to fall to lower energy states by different types of bond formation (which results in a negative change of enthalpy) or by the inclination for thermal motion to increase disorder, causing a positive change of entropy.[113] To further explore these effects, we constructed a Van't Hoff plot (Figure 2.8) to calculate ΔH and ΔS. We noticed two regions, which possibly correspond to different conformations of the complex. One occurs at high temperatures, where complex formation is driven by change in entropy, while at lower temperature (where affinity is much higher) change in enthalpy is the driver for the formation of the complex.

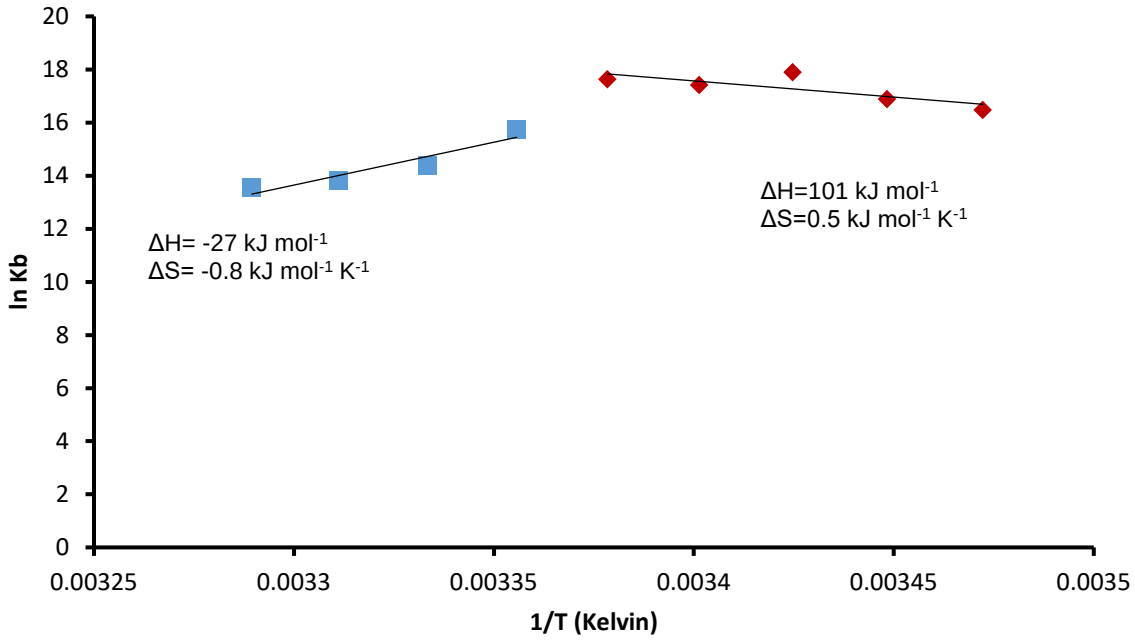

Figure 2.8 Van't Hoff plots for miR-122 and p19.
ΔH and ΔS were calculated from the plot for miR-122 and p19. Blue plot: $y = 32287x - 92.901$, $R^2 = 0.8935$; Red plot: $y = -12179x + 58.978$, $R^2 = 0.6209$.

2.3.2 Kinetic Capillary Electrophoresis with Varying Electric Fields (KCEVEF)

NECEEM is a powerful technique due to the ability to extract both the dissociation constant, K_d, and the rate constant, k_{off}, from one electropherogram. However, its reliance on the ability to distinguish the decay signal from noise causes some limitations. In cases where K_d is small and the complex does not dissociate well in the capillary, the decay signal may be barely separable from background noise (see Figure 2.2 and inset). To address this issue, we have designed a new method, KCEVEF, for determining k_{off} only from the areas of the complex peak and the corresponding migration times.

KCEVEF is principally based on the fact that, under non-equilibrium conditions in the capillary, the amount of complex that reaches the detection window is a function of the time it requires to do so and the value of k_{off} for that complex:

$$A_{ci} = (\varepsilon/\eta) A_c^0 \exp(-t_{ci} k_{off}) \quad (2.5)$$

where i is an indexing variable, A_c is the area under the peak of the complex, ε/η is a scaling constant, t_c is migration time of the complex, and k_{off} is the dissociation rate constant.

When the migration time is varied by changing the electric field strength applied to the sample, corresponding areas under the complex peak also change (see Figure 2.1 for a schematic representation). From N experiments, one can fit an exponential curve to Equation 2.5 using standard programs for fitting exponential dependencies. However, this process is labour-intensive and unnecessary. A good approximation could be made by using linear regression for the logarithms,

$$\ln(A_{ci}) \approx \ln(\varepsilon A_c^0/\eta) - (t_{ci} k_{off}) \quad (2.6)$$

Furthermore, applying linear regression to $\ln(A_{ci})$ and t_{ci}, we would obtain the following,

$$\ln\left(\frac{\varepsilon A_c^0}{\eta}\right) = \frac{\langle t_c^2 \rangle \langle \ln A_c \rangle - \langle t_c \ln A_c \rangle \langle t_c \rangle}{\langle t_c^2 \rangle - \langle t_c \rangle^2} \quad (2.7)$$

where all variables are the same as above and angle brackets denote an average of the variable within them under different electric fields. The value of k_{off} may now be calculated from Equations 2.6 and 2.7 directly from experimental values as follows, assuming no loss of signal due to changing peak shape and diffusion. A second assumption is that the formation and dissociation of the complex will not be affected by the different electric field.

$$k_{off} = \frac{\langle t_c \rangle \langle \ln A_c \rangle - \langle t \ln A_c \rangle}{\langle t_c^2 \rangle - \langle t_c \rangle^2}. \quad (2.8, \text{same as } 1.13)$$

We recorded peak areas and migration times for capillary electrophoresis of p19 and miR-122 complex under four electric field strengths, as shown in Figure 2.9. An excess amount of p19 was added to ensure total shift of ds-miRNA peak. The areas under complex peaks decreased as the electric field strength decreased, demonstrating an inverse relationship between complex area and migration time, as expected from Equation 2.5. We employed Equation 2.8 to determine the value of k_{off} and found it to be $0.072 \pm 0.022\ s^{-1}$, which is in excellent accord with the value found using NECEEM. Besides this, they are also in accordance with the rate constants found by Rowlings *et al*. for siRNA and p19 by fluorescence polarization.[114] Although a siRNA was used for their studies instead of miRNA, the values should still be close. siRNAs differ from miRNAs insofar as they are naturally found in double stranded duplex form, are fully complementary and are found in sizes between 21-22 basepairs.[115] However, since the miRNA that we are working with is 22 base pairs long and fully complementary, the value found by Rawlings *et al*. should reflect the one found by our lab.

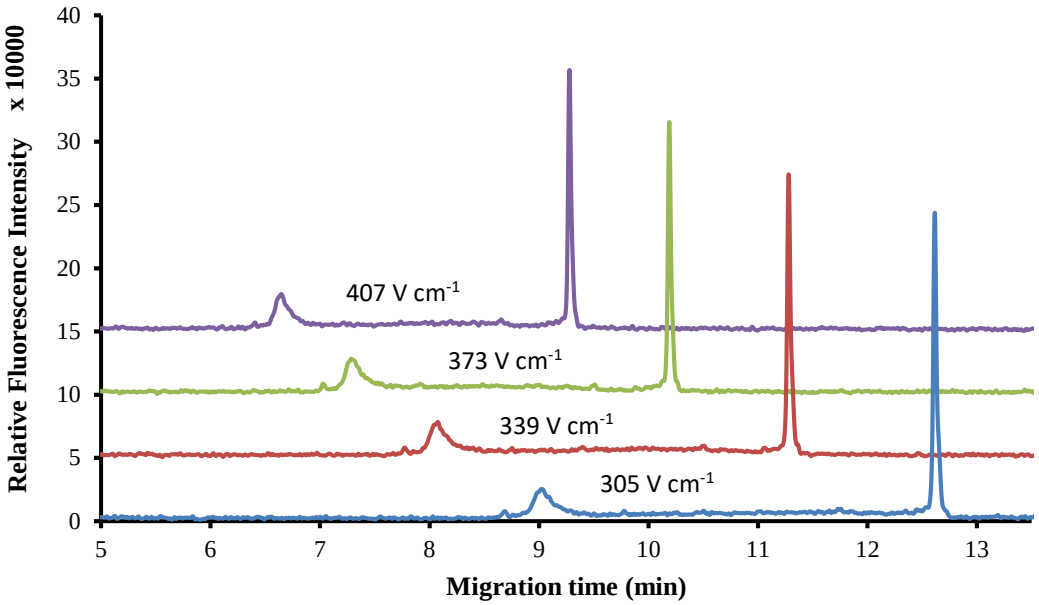

Electric Field	Area
407	49035
373	39913
339	40241
305	38256

Figure 2.9 Experimental electropherograms of the variable electric field experiments. A) Bottom to top: 305 V cm^{-1}, 339 V cm^{-1}, 373 V cm^{-1}, 407 V cm^{-1}; used for separation of 2.5 µM of p19 with freshly annealed 100 nM FAM-labelled complementary miRNA-122 with 50 nM miR-122. B) Areas of complex signals.

2.4 Conclusions

In the first part of this chapter, NECEEM was successfully used for calculating the thermodynamic and kinetic constants for the binding between microRNA-122 and p19; the rate constants (k_{off} = 0.059 ± 0.013 s^{-1}, k_{on} = 0.002 ± 0.001 $s^{-1}M^{-1}$) and dissociation constant between miR-122 and wild type p19 (K_d = 27 ± 9 nM). The K_d values found were in accordance with previously published values by the Pezacki group. We also found ΔG^o to be +40 kJ mol^{-1} for the dissociation of p19

with miR-122. Although the kinetics of microRNA-122 and p19 have not been previously studied, the k_{off} value for siRNA and p19 were found to be 0.062 s^{-1} which is, again, in accordance with our results.

In the second part of this chapter, we use a newly developed method we called Kinetic Capillary Electrophoresis with Varying Electric Fields (KCEVEF) for calculating the dissociation rate constant k_{off} (0.072 ± 0.022 s^{-1}). We found this value in agreement with the one obtained by NECEEM. This method is useful for instances where the signal of the decay is close to the signal of the noise.

Chapter 3

3. Investigation of binding affinity of TOE1 with HIV-sequence TAR

3.1 Background

Target of Egr1 (TOE1), a 510 amino acids-long protein, functions as an immediate early transcription factor.[116] Among other effects, Egr1 expression decreases growth and tumourigenic potential of several tumour cell types.[116] Besides its role in cell growth inhibition through cell cycle modulation,[116,117] TOE1 plays other roles within the cell: in Cajal body formation,[118] RNA splicing,[118] and RNA deadenylase catalytic activity *in vitro*[119]. TOE1 was found to be overexpressed in a study aimed at identifying the CD8+ T-cell non-cytotoxic anti-viral response (CNAR).[120] CNAR refers to CD8+ cells from HIV-infected individuals that inhibit virus production by infected CD4+ cells without killing the infected cell, demonstrating control of HIV-1 replication, while protecting the host from harmful effects of cytotoxic T-lymphocytes.[121, 122] Furthermore, in another study of discordant HIV-positive twins, differential genetic analysis revealed three genes, one of them being TOE1.[120] Individuals with these genes possess what is called the sought factor, CAF (CD8+ anti-viral factor), which leads to anti-HIV activity and protection from the acquired immune deficiency syndrome (AIDS) without requiring anti-viral therapy, as they are able to maintain a low viral load.[120,123] Subsequent studies failed to confirm

TOE1 as a CNAR overexpressed gene, and so the identity of CAF is still unknown.[120,124] It is presumed that CAF functions by a transcriptional mechanism acting on the viral long terminal repeats.[123] This study was conducted to further understand the function of TOE1 in HIV-1 replication and assess whether TOE1 functions in an innate immune, CAF-like manner.

Tat is a well-known cell penetrating peptide (86 to 101 amino acids long, depending on the type) produced by the HIV virus and essential for its transcription.[125,126] It functions by binding to an RNA region in the viral long terminal repeats, called the TAR element, through a basic domain of nine amino acids.[127] TAR is characterized by a loop sequence (residues 30-35) and a bulge that is a result of three non-base-paired residues (residues 23-25) located near the apex of the double helical system. The TAR loop and bulge sequences are conserved in HIV-1 and the first stem-loop of HIV-2.[128,129] The minimal TAR sequence that is functionally active contains both regions.[130, 131] Research groups have tried to interfere with the binding of Tat to TAR *in vitro* as a way to target virus inhibition through the use of complementary RNA sequences,[132] small compounds,[133-135] microRNA,[136] siRNA,[137] peptides,[138] and artificial nucleobase-amino acid conjugates[139].

Our work, recently published with Sperandio *et al*., identified protein TOE1 as similar to Tat insofar as it also contains a lysine/arginine rich sequence that interacts with TAR[140] (Table 3.1). In addition, it possesses cell-penetrating ability similar to Tat, and its interaction with TAR can inhibit Tat binding.[140] Besides this, full length TOE1 is digested by serine protease granzyme B, and several of its peptide sequences, which contain the basic nuclear localization sequence (NLS), were shown to penetrate the cell membrane and inhibit viral replication[140]. We hypothesized inhibition occurred as a result of direct binding of these peptides to TAR; therefore, we titrated

these peptides with TAR in capillary electrophoresis experiments and electrophoretic mobility shift assays. We found that peptides containing the nuclear localization sequence bound to TAR.

Table 3.1 Comparison of Tat and TOE1 regions and peptides.

Protein	**Sequence**
HIV-1 Tat	49-RKKRRQRRR-57
TOE1 basic region	335-KRRRRRRREKRKR-347
329-363 (ED35)	329-EAAAED**KRRRRR RREKRKR**ALLNLPGTQTSGEAKD-363
329-347 (ER19)	329-EAAAED**KRRRRR RREKRKR**-347
280-363ΔNLS	280-HIDYRCCLPPATHRPHPTSICDNFSAYGWCPLGPQCPQSHDI DLIIDTDEA AAEDALLNLPGTQTSGE-363
364-510	364-GPPKKQVCGDSIKPEETEQEVAADETRNLPHSKQGNKNDLE MGIKAARPEIADRATSEVPGSQASPNPVPGDGLHRAGFDAFMTG YVMAYVEVSQGPQPCSSGPWLPECHNKVYLSGKAVPLTVAKSQ FSRSSKAHNQKMKLTWGSS-510

The work presented in this chapter was done in collaboration with Dr. Sabina Sperandio and Dr. Ian de Belle at the Ottawa Hospital Research Institute and has been previously published.[140] Sabina Sperandio and Ian de Belle prepared recombinant peptides, TAR RNA and synthetic peptides, and performed RNA-gel shift assays. I performed capillary electrophoresis experiments and K_d measurements. This chapter focuses on the experiments that were conducted to test the binding ability of TOE1 and several of its peptide sequences to TAR by electrophoretic mobility shift assays (EMSA) and capillary electrophoresis. We demonstrated that TOE1, and more specifically two basic regions, ER19 and ED35, that contain the lysine/arginine rich nuclear localization sequence (NLS), binds to TAR with K_d values of 4.08 ± 0.19 μM for ER19 and 7.43 ± 1.60 μM for ED35. The discovery that full length and cleaved nuclear protein TOE1, secreted from T-cells, can spontaneously cross the plasma membrane and penetrate cells, as well as their inhibitory action of viral replication at the transcription level, is a significant step towards further

elucidating mechanisms for host response to HIV-1 infection; this has the potential to help with designing better strategies for inhibiting HIV-1 spread in infected patients.

3.2 Materials and Methods

3.2.1 Preparation of TOE1 recombinant peptides, Tat protein, synthetic peptides and FAM-labelled TAR

Preparation of recombinant peptides was done as described by Sperandio *et al.*[140] Briefly, TOE1, its deletion mutants and Tat were subcloned into the pET vector system (Novagen) for bacterial expression, including a 6×His tag at the C-terminal end. To form fusion proteins, Enhanced Green Fluorescent Protein (EGFP) was inserted at the C-terminal end of TOE1. Competent BL21(DE3) *Escherichia coli* bacteria were transformed with the vector and were grown for 16 h, induced with 0.2 mM isopropyl-β-D-thiogalactopyranoside for 3 h, and then resuspended in PBS + 0.05% Triton X-100 +1 mM PMSF. After two rounds of sonication consisting of eight pulses of 30 s followed by a 30-s pause, Triton X-100 was adjusted to 0.5% and the lysates were cleared by centrifugation. His-tagged recombinant proteins were purified on a TALON metal affinity resin (Clontech) and a NiNTA affinity resin (Qiagen) was used for EGFP fusion purification. Fractions of eluates were collected and analyzed by both Coomassie staining and Western blot to assess purity. Fractions highly enriched (>80–90% purity) in TOE1 proteins were collected and dialyzed against PBS. After dialysis, proteins were quick frozen and stored at −80 °C with the addition of 10% glycerol. The peptides used for capillary electrophoresis experiments are not EGFP-labelled unless otherwise specified. Peptides ED35 and ER19 were synthesized by Biomatik, and FAM-labelled TAR was purchased from Life Technologies, Fisher.

The preparation of recombinant peptides was performed by Sabina Sperandio.

3.2.2. Capillary electrophoresis of ED35, ER19 and 280-363ΔNLS

FAM-labelled TAR was incubated with peptide ED35, ER19 or peptide 280-363ΔNLS in a buffer containing 10 mM Tris pH 8.0, 50 mM KCl, 5 mM $MgCl_2$, 1.0 mM dithiothreitol (DTT), 10% glycerol, 1 mg mL^{-1} bovine serum albumin (BSA), and 0.1 mg mL^{-1} yeast transfer RNA (tRNA) for 15 min at room temperature, and then subjected to separation by capillary electrophoresis in 25 mM borax buffer, unless otherwise specified.

A ProteomeLab PA 800plus capillary electrophoresis system from Beckman-Coulter, Brea, California, USA, was used to separate FAM-labelled TAR from FAM-labelled TAR-peptide complex. Fluorescence was induced by a 488-nm Argon-ion laser and detected at 520 ± 10 nm. A bare silica-fused capillary was used, 60 cm in total length with 50 cm from injection to the detection point, with an outer diameter of 365 µm and an inner diameter of 75 µm. The injections were done by a pressure pulse with hydrodynamic injection volumes of 46.7 nL. The electric field during the separation was 500 V cm^{-1}, with the positive charge at the inlet and ground at the outlet. The capillary temperature was maintained at 22 °C for the duration of the experiment. The run buffer was 25 mM borax (pH 8.9), unless otherwise specified. Prior to each injection, the capillary was rinsed by applying 50.0 psi of 100 mM HCl, 100 mM NaOH, ddH2O and 25 mM borax, unless otherwise specified buffer, for 4 minutes each. 32 Karat™ Software Version 9.1 (Beckman-Coulter, Brea, California, USA) was used for recording the electropherograms. This results in a total of 20 minutes of incubation for the TAR with peptides or protein in order to reach equilibrium.

3.2.3. K_d calculations

NECEEM was used to calculate the K_d values between FAM-labelled TAR and the peptides. Briefly, the target T (in this case, the peptide) and the ligand L (FAM-labelled TAR) are incubated

prior to injecting the mixture in the capillary to allow complex (C) to form. Once an external voltage is applied, the separation of the equilibrium complex from free ligand is observed under non-equilibrium conditions; the separation is based on differential electrophoretic mobility of T, L and C. The run buffer, however, does not contain any target or ligand species, so the mixture is no longer in equilibrium and starts to dissociate as it migrates through the capillary. The dissociation constant K_d can be directly calculated from the areas under the peaks of the free ligand, the C and the decay in between the two[43]:

$$K_d = \frac{[T]_0\left(1 + A_L / \left(A_D + A_C\right)\right) - [L]_0}{1 + \left(A_D + A_C\right) / A_L} \qquad (3.1), \text{(same as equation 2.2)}$$

where $[T]_0$ is the initial concentration of the target species, $[L]_0$ is the initial concentration of L, A_L is the area under the peak of free ligand, A_D is the decay area in between the ligand and complex peaks, and A_C is the area under the peak of C.

Alternatively, K_d was calculated by fitting a curve to the titration graph of TAR complex formed with either peptide and determining the concentration of the peptide required to form a complex at half the saturation level. The curve in each graph was fit using non-linear regression in Microsoft Excel by minimizing the squared difference between the obtained data and theoretical values found from an equation of the form:

$$y = \frac{a+bx}{c+dx} \qquad (3.2)$$

where y is the theoretical value, x is the concentration of the peptide, and a, b, c and d are automatically modified to minimize the squared difference. This line of best fit was used because, although it is assumed that there is only one binding site on each peptide, it was difficult to fit a rectangular hyperbola due to insufficient data points.

For ER19, the following values of the four modifiable coefficients were obtained: a = 216.12, b = 80.26, c = 0.00103, and d = 0.000273. Similarly, for ED35, these values were: a = 278.14, b = 110.87, c = 0, and d = 0.0024.

The saturation level of the complex is indicated by the horizontal asymptote of the curve of best fit, which is located at y = b/d. Therefore, to calculate K_d, the value of x at $y_{1/2}$ is determined, where $y_{1/2}$ = b/2d.

3.2.4. RNA gel shift assays and competition assays

Recombinant TOE1 proteins or synthetic peptides were incubated at the indicated concentrations and the following carboxyfluorescein (FAM)- or Cy5-labelled TAR probes: wild type (WT) TAR, 5′-GGCCAGAUCUGAGCCUGGGAGCUCUCUGGCC-3′, or mutant bulgeless TAR, 5′-GGCCAGAGAGCCUGGGAGCUCUCUGGCC-3′, in a buffer containing 10 mM Tris, pH 8.0, 50 mM KCl, 2.5 mM $MgCl_2$, 10 mM DTT, 10% glycerol, 1 mg mL^{-1} BSA, and 0.1 mg mL^{-1} yeast tRNA for 15 min at room temperature. Binding competition was performed using the indicated fold molar excess of a TAR probe equivalent to that described above without the FAM label. TAR/TOE1 complexes were visualized on a BioRad GelDoc+ apparatus with ImageLab software following separation on 6% acrylamide gels. RNA gel-shift assays were performed by Sabina Sperandio and Ian de Belle.

3.2.5. Capillary electrophoresis separation of Tat

FAM-labelled TAR (50 nM) was incubated with Tat protein (1 μM) in 10 mM Tris-HCl (pH 7.5), 50 mM $MgCl_2$, 5% glycerol, 0.01% NP-40, 0.01 mg mL^{-1} yeast tRNA, and 10 mM DTT added fresh. The ProteomeLab PA 800 capillary electrophoresis system was used to separate FAM-labelled TAR from FAM-labelled TAR/Tat complex as described previously except for the

following modifications: The injections were done by a pressure pulse with hydrodynamic injection volumes of 46.7 nL, the electric field during the separation was 433 V cm^{-1}, the capillary temperature was maintained at 15°C or 0°C for the duration of the experiment, and the run buffer was 25 mM phosphate buffer (pH 7.3).

3.2.6. Capillary electrophoresis buffer optimization for binding experiments with peptides and proteins TOE1 and Tat

Various buffer conditions, such as 25 mM Tris-acetate, 25 mM phosphate buffer saline and 25 mM borax, were tested. Various pHs (7-9), injection times (0.5 psi for 5 sec, 1 psi for 5 sec), and voltages (20-30 kV) were also tested in order to optimize conditions for separation of peptides and proteins with TAR.

3.2.7. Capillary electrophoresis of TOE1 protein with photodiode detector

The PA800 capillary electrophoresis system was used for detection of 4 µM TOE1 protein by photodiode array detection with readings recorded at 190 nm and 214 nm. The separation was done as described previously except for the following modifications: hydrodynamic injection volumes of 26 nL were separated, the electric field was 433 V cm^{-1}, the capillary temperature was maintained at 15°C for the duration of the experiment, and the run buffer was 25 mM borax buffer (pH 8.9).

3.3 Results and Discussion

Sperandio *et al.* showed that TOE1 was able to inhibit Tat activity by examining the effect of exogenous expression of TOE1 in an *in vitro* assay; viral long terminal repeats transcriptional activation driven by Tat was measured and expression decreased by as much as 85% at the highest

concentration of TOE1.[140] Due to the similarity of the basic region of TOE1 with that of Tat, they postulated that TOE1 may act similarly to Tat so as to bind TAR, preventing the binding of Tat. This hypothesis was initially tested by performing gel shift assays to test the competition between labelled and non-labelled TOE1 in binding TAR. Capillary electrophoresis was used to further evaluate the binding affinity between TOE1 and TAR. CE is a proven method for determining dissociation constants (K_d) and it has a lower limit of detection compared to electrophoretic mobility shift assays (EMSA).[41] For both gel-shift assays and CE experiments, a FAM-labelled probe was used with synthetic peptide sequences and the formation of a complex between cleaved TOE1 and TAR was successfully observed (Figure 3.1). Prior to separation by CE, the sample was incubated for a total of 20 minutes in order to establish equilibrium.

Synthetic peptides ED35 and ER19, both containing the nuclear localization sequence (KRRRRRRREKRKR located at position 335-347), show binding to TAR by CE and EMSA. ED35, containing amino acids 329-363 of TOE1, was chosen for evaluation since it corresponded to the smallest active peptide capable of inhibiting HIV- long terminal repeats activity. Further analyses later identified ER19, an even smaller sequence that contains amino acids 329-347 and shows binding by CE (Figure 3.1A). In the absence of the peptides, one single peak is observed at approximately 7 min, which is attributed to free TAR RNA. As the peptides are not fluorescently labeled, they are not visible in the electropherogram, but experiments with full length TOE1 and EGFP-labelled TOE1 indicated that the protein migrates before the complex peak; this will be described later. Upon titration of TAR with each peptide, another peak forms that migrates at a faster rate than free TAR and consistently appears at approximately 6 min. This peak can be attributed to the complex formed between TAR and peptide, which has a faster electrophoretic

mobility than free TAR because the overall charge to size ratio is decreased once the peptide, which carries both negative and positive charges, binds the negatively charged TAR molecule. Figure 3.1 shows that increasing the concentrations of ER19 (left electropherogram) and ED35 (right electropherogram) increases complex formation to the left of free TAR. The area under the peak for free TAR decreases as more peptide is added. In order to ensure non-specific binding did not occur, BSA and yeast tRNA were used in the incubation buffer. Yeast tRNA serves as masking RNA and is also beneficial in dampening the effect of any RNases that may be present in the solution.[141] DTT is used to help with the stabilization of proteins and peptides, more specifically, to prevent aggregation due to disulfide bond formation between cysteine amino acids.[142]

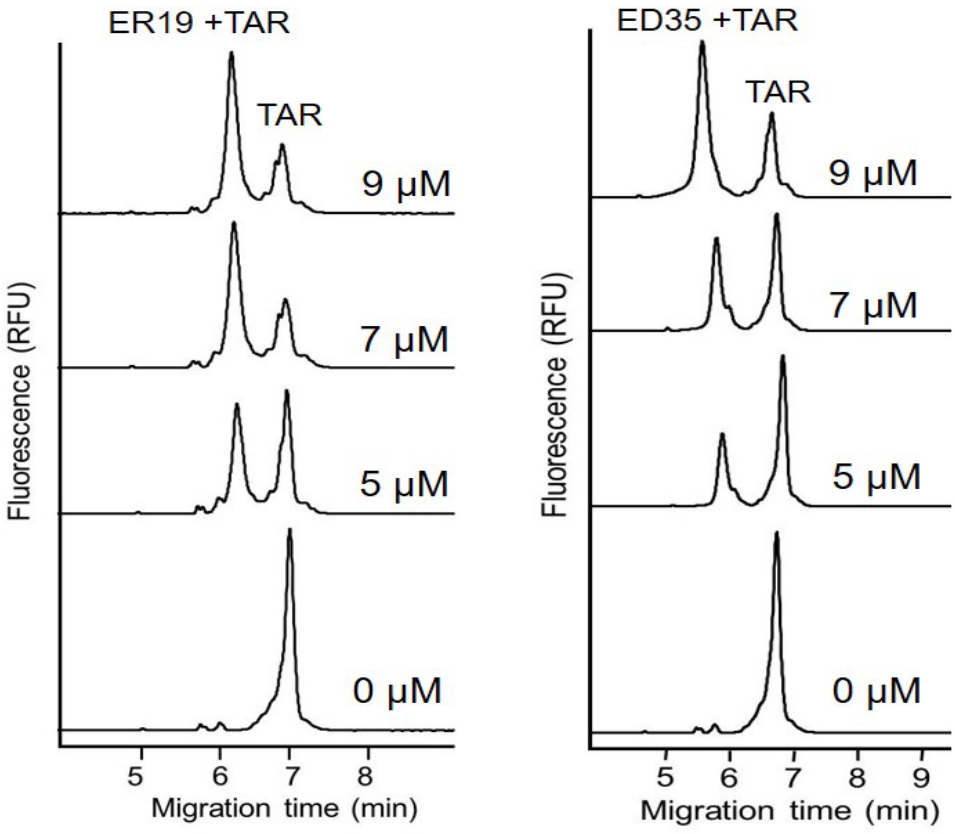

Figure 3.1 Electropherograms of FAM-labelled TAR with TOE1 synthetic peptides separated by capillary electrophoresis after incubation at 75°C for 5 min followed by a 5 min incubation at room temperature.

The ER19 synthetic peptide consists of amino acids 329-347. Left: TAR incubated with ER19 (0, 5, 7, 9 µM). Right: TAR incubated with ED35 (5, 7, 9 µM). The complex between each peptide and TAR is observed as a peak at 6 min and free TAR is observed at 7 min. All samples were also incubated with BSA and yeast tRNA, and were separated under 500 V cm^{-1} in a 60 cm long capillary in 25 mM borax buffer at 22 °C.

The binding affinities of ED35 and ER19 to TAR were calculated using NECEEM, with corresponding K_d values of 7.43 ± 1.60 µM and 4.08 ± 0.19 µM, respectively. As an alternative way of evaluating the binding affinity of the peptides to TAR, titration plots were constructed for both (Figure 3.2). By constructing a curve of best fit for each set of data, a K_d value of 9.1 µM was obtained for ER19 and 5.0 µM for ED35. The discrepancy in the values may be explained by the fact that a plateau was not reached and so it was difficult to fit a good line of best fit. Furthermore, the experiments were not performed in triplicate due to time constraints and more data is necessary at the low end; this too may also explain the discrepancy.

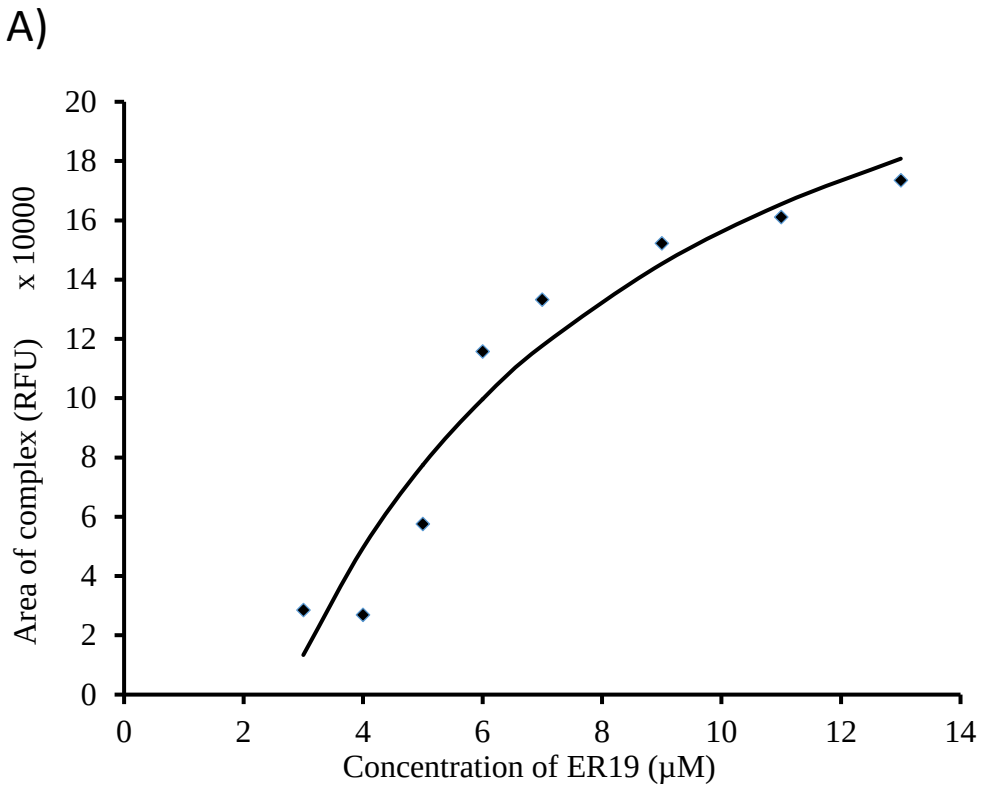

B)

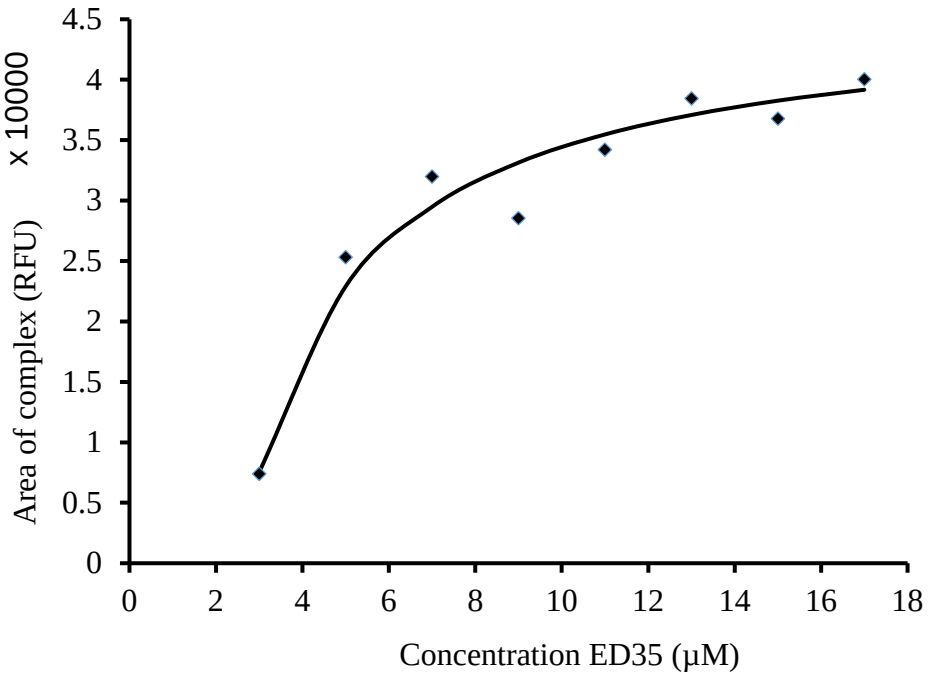

Figure 3.2 TAR titrated with A) ER19 and B) ED35, then subjected to separation by capillary electrophoresis, N=1.
Area of complex peak was plotted versus the concentration of peptide and the following equation was used for fitting ER19 data: $y = \frac{216.12+80.26x}{0.00103+0.0024x}$ and for ED35 data: $y = \frac{278.14+110.87x}{0.0024x}$

Figure 3.3A shows that binding does not occur between TAR in the absence of the nuclear localization sequence, as no complex is observed with increasing concentrations (10, 15, 25 µM) of recombinant peptide 280-363ΔNLS. It is interesting to note that Sperandio *et al*. showed that deletion of this nuclear localization sequence resulted in the peptide localization in the cytoplasm rather than the nucleus, which confirms that this sequence is responsible for nuclear targeting.[116] Another recombinant peptide, 364-510, of the C-terminal of 150 amino acids and lacking the NLS, was also tested and again no binding was observed (Figure 3.3B). The peaks for free TAR migrate at a different time than in Figure 3.3A because different separation conditions were used, as described in the caption.

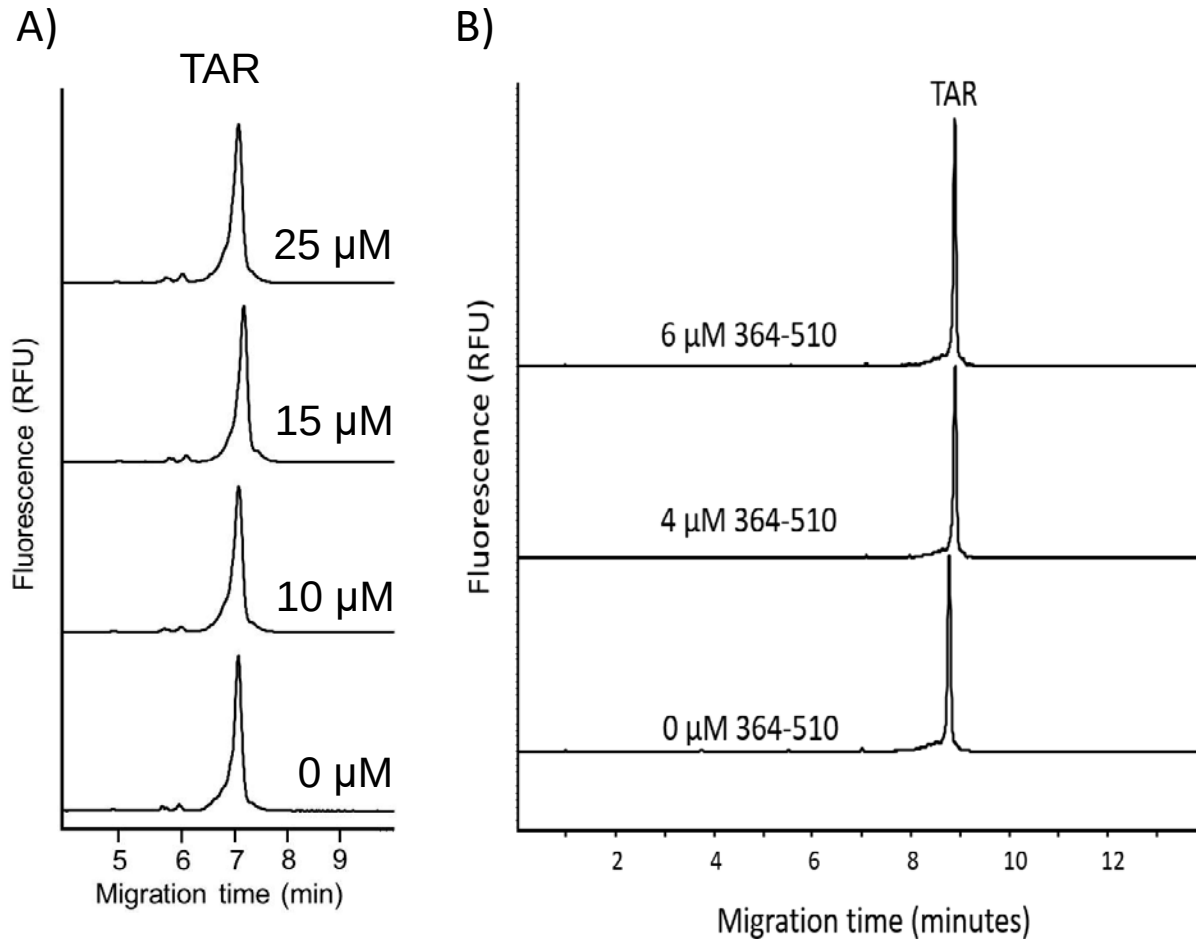

Figure 3.3 Electropherograms of FAM-labelled TAR titrated with peptides lacking NLS.
A) Electropherograms of FAM-labelled TAR (1 nM) incubated with 6xHis-tagged recombinant protein 280-363ΔNLS (0, 10, 15, 25 µM). All samples were also incubated in 10 mM Tris pH 8.0, 50 mM KCl, 5 mM $MgCl_2$, 10 mM DTT, 10% glycerol, 1 mg mL^{-1} BSA, 0.1 mg mL^{-1} yeast tRNA and were separated under 500 V cm^{-1} in a 60 cm long capillary in 25 mM borax buffer at 22 °C, with hydrodynamic injections of 46 nL. B) Electropherogram of FAM-labelled TAR (153 nM) incubated with 6xHis-tagged recombinant protein 364-510 (2, 4, 6 µM), in 10 mM Tris-HCl (pH 7.5), 50 mM $MgCl_2$, 5% glycerol, 0.01% NP-40, 0.01 mg mL^{-1} yeast tRNA, and 10 mM DTT added fresh. Separation was performed under 433 V cm^{-1} in a 60 cm long capillary, 25 mM borax buffer, with a hydrodynamic injection of 26 nL, at 15°C.

For gel shift analyses, TAR RNA probe was tested with either recombinant 329-363 TOE1 fragment or a synthetic peptide comprising the identical amino acid sequence but lacking the 6xHis tag present in the recombinant peptide. Figure 3.4A, B, D, confirms the binding of both recombinant peptide 329-363 TOE1 and its identical synthetic peptide to the TAR RNA probe. The binding is higher than that observed by CE experiments; this may be a result of the different

conditions that are required for the two types of experiments. A competition assay was also performed by adding 10-20x excess of unlabelled TAR, as demonstrated in Figure 3.4A, B. For both, complete displacement was observed at 10x excess of TAR, as the complex between FAM-labelled TAR disappeared and the free FAM-labelled TAR band was observed on the gel. EMSA performed with a mutant TAR lacking the UCU bulge (Figure 3.4C) demonstrated that this bulge is required in order for binding to occur, as there was no complex otherwise observed. Figure 3.4D shows the formation of the complex at lower concentrations of ED35 (0.5-1.25 μM) with WT TAR. The last two lanes in Figure 3.4D displayed a competition assay with WT unlabelled TAR competitor and mutant TAR competitor, both added at a 10x molar excess. It is observed that upon addition of WT unlabelled competitor, the complex of ED35/TAR disappears, whereas with addition of mutant TAR, the complex does not dissociate, as the mutant TAR does not compete for binding with WT TAR.

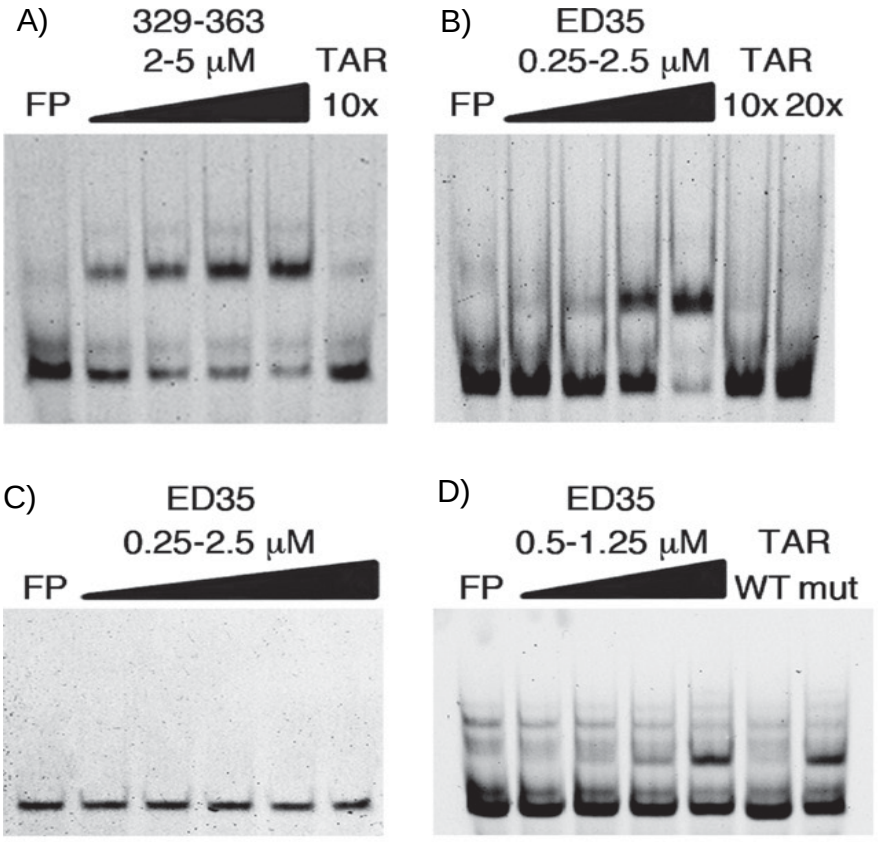

Figure 3.4 TOE1 peptides directly interact with HIV TAR sequence. RNA EMSA of a FAM-labelled TAR RNA probe in the presence of TOE1 peptides.
Increasing amounts of either A) purified recombinant 6xHis-tagged 329-363 or B) a synthetic peptide ED35 consisting of amino acids 329-363 of TOE1 were incubated for 15 min at room temperature with FAM-TAR. C) EMSA performed with a mutant TAR lacking the UCU bulge. D) EMSA with WT TAR in the presence of mutant (lacking the UCU bulge) or WT unlabelled competitor at 10x molar excess. Left lane in all images corresponds to FAM-TAR free probe (FP). EMSA was performed by Ian de Belle and reproduced with permission[140].

We also looked at binding between recombinant protein 283-363, which contains NLS, and which was observed binding with TAR (Figure 3.5). The separation conditions were not sufficiently optimized for calculating the K_d; however, it can be seen that a complex peak forms slightly to the left of free TAR at approximately 13 minutes. The separation was done at 333 V cm^{-1}; however, higher voltage would have resulted in better separation, as demonstrated in the earlier experiments. Some of the peaks that migrate between 11-12 minutes, prior to complex formation, can be attributed to fluorescent particles also observed in the TAR-only sample.

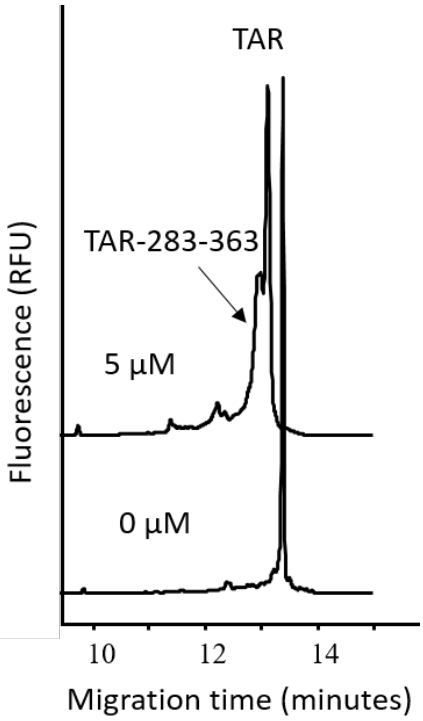

Figure 3.5 TOE1 recombinant peptide 283-363 directly interacts with HIV TAR sequence. Electropherogram of His-tagged recombinant protein 283-363 (5 µM) and 100 nM TAR. The buffer for incubation was 10 mM Tris-HCl (pH 7.5), 50 mM $MgCl_2$, 5% glycerol, 0.01% NP-40, 0.01 mg mL^{-1} yeast tRNA, and 10 mM DTT added fresh. The separation buffer was 25 mM borax (pH 9) and the separation was carried out by applying an electric field of 333 V cm^{-1}.

During these studies, we learned the importance of using tRNA or RNase inhibitor, as without either, TAR RNA was more susceptible to degradation by RNases, if any were present. This is observed in Figure 3.6, where Tat protein is incubated with TAR with and without yeast tRNA. In the absence of yeast tRNA, several peaks form to the left of the complex. With the addition of tRNA, the peaks disappear. Contamination of RNases can easily occur if stringent working conditions are not respected. This includes, but is not limited to, contamination from bench spaces, tips, water, and buffers, as well as from preparation of protein since it was grown in bacteria.[143] Although proper lab protocol was followed to the best of our ability, such contamination is sometimes difficult to avoid. Addition of excess yeast tRNA creates a system where the RNases are more likely to degrade the yeast tRNA than TAR, which is present in a much smaller amount.

RNase inhibitors are also frequently added to buffers to help with this issue, as they can inhibit various RNases under a range of conditions.[144]

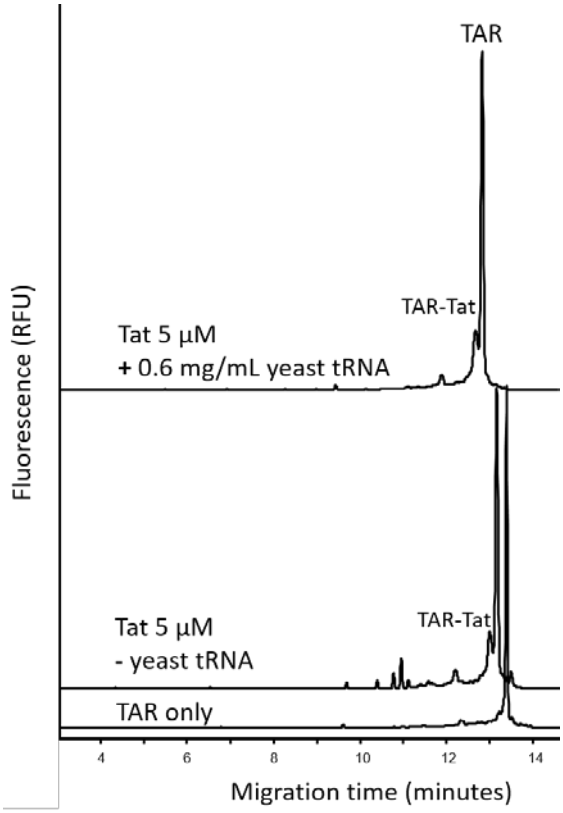

Figure 3.6 Comparison of TAR and Tat binding experiments with and without yeast tRNA. 100 nM FAM-labelled Tar (bottom) incubated with 5 µM Tat protein, and incubated without (middle) or with (top) 6 mg mL^{-1} yeast tRNA. The buffer for incubation was 10 mM Tris-HCl (pH 7.5), 50 mM $MgCl_2$, 5% glycerol, 0.01% NP-40, and 10 mM DTT added fresh. The separation buffer was 25 mM borax (pH 9) and the separation was carried out by applying an electric field of 333 V cm^{-1}.

We also observed binding between full length TOE1 and TAR. In these experiments, a recombinant mammalian RNase inhibitor (RNasin®Plus) was used in order to ensure that TAR degradation did not occur (Figure 3.7A) as a result of digestion by eukaryotic RNases (e.g. RNase A and RNase B). A complex is observed upon addition of 4 µM full length TOE1 to 0.8 µM TAR. To investigate the migration of full length TOE1, capillary electrophoresis with photodiode array detection was used (Figure 3.7B). Strong absorbance is observed between approximately 3.1-3.7 min at 190-220 nm wavelengths. At 190 nm, another peak is also observed at approximately 4.2 min. The intensity of the bands is high at 190 nm-214 nm; this is because of the strong absorbance

due to peptide bonds that absorb at 200 nm. Two peaks are observed on the electropherogram; the first is the electroosmotic flow and the second is the peak that corresponds to the migration of the protein. Absorption at 280 nm is not observed because there are only 41 aromatic rings in the 510 amino acid protein, which is below the limit of detection for the photodiode array used in the experiment. Laser induced fluorescence detection was used to detect EGFP-tagged TOE1 (Figure 3.7C). One major peak is detected at approximately 4 min. The protein migrates at a slightly different time than observed by ultraviolet detection because the EGFP tag, which has the molecular weight of 27 kDa, changes the electrophoretic mobility of TOE1 (57 kDa). Besides this, a different voltage was applied for the separation. To ensure that the complex was not a result of non-specific binding between yeast tRNA and TOE1, we used various concentrations of yeast tRNA and incubated with EGFP-labelled TOE1; we did not observe any complex formation, as shown in Figure 3.7C.

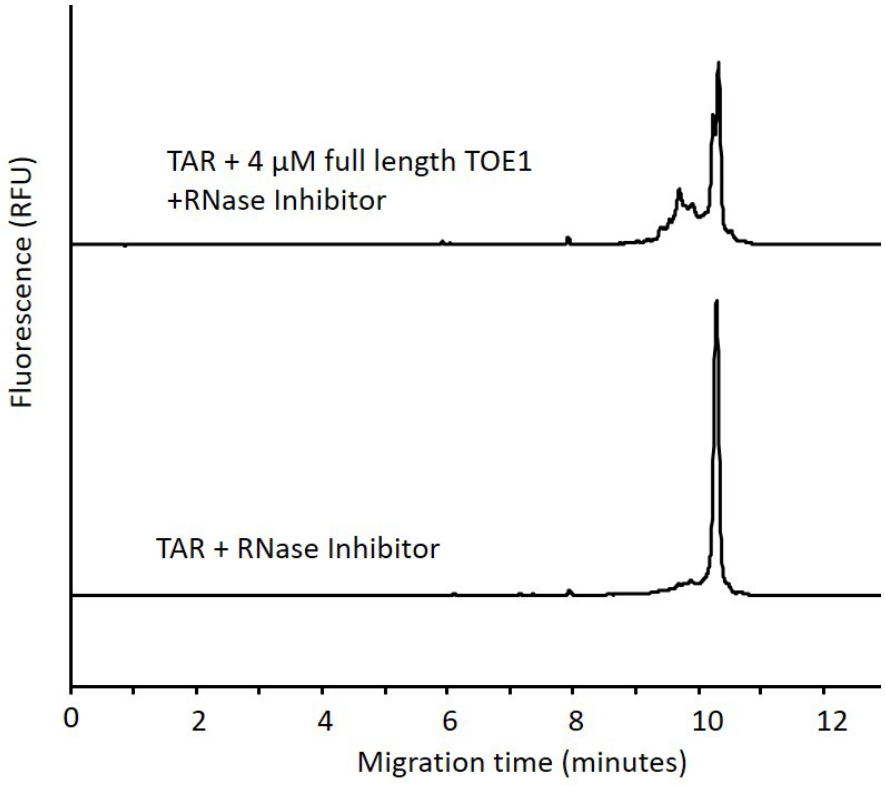

3.7 A) TAR and TOE1 experiments determining the importance of RNase and yeast tRNA. Electropherogram of FAM-labelled TAR (0.8 µM) incubated with His-tagged recombinant full length TOE1 (4 µM), RNase inhibitor, in 10 mM Tris-HCl (pH 7.5), 50 mM $MgCl_2$, 5% glycerol, 0.01 % NP-40, 0.01 mg mL^{-1} yeast tRNA, and 10 mM DTT added fresh. Separation was performed under 433 V cm^{-1} with a hydrodynamic injection of 26 nL in borax buffer.

B)

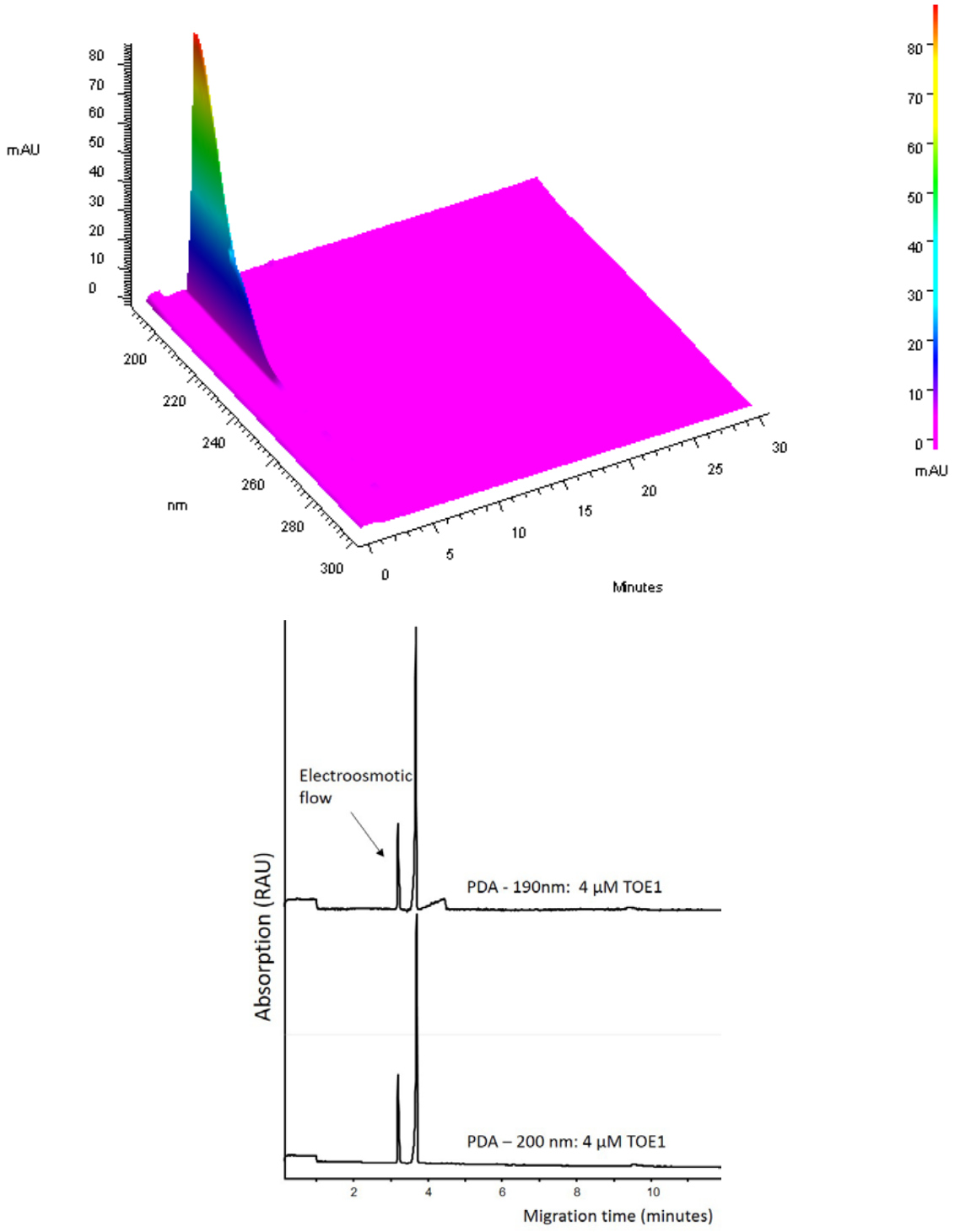

Figure 3.7 B) 3D contour of absorption spectrum and electropherograms (top), and electropherograms (bottom) at 190 nm and 214 nm, of full length protein TOE1 (4 µM) as detected by photodiode array detection when separated under 433 V cm^{-1} in 25 mM borax.

C)

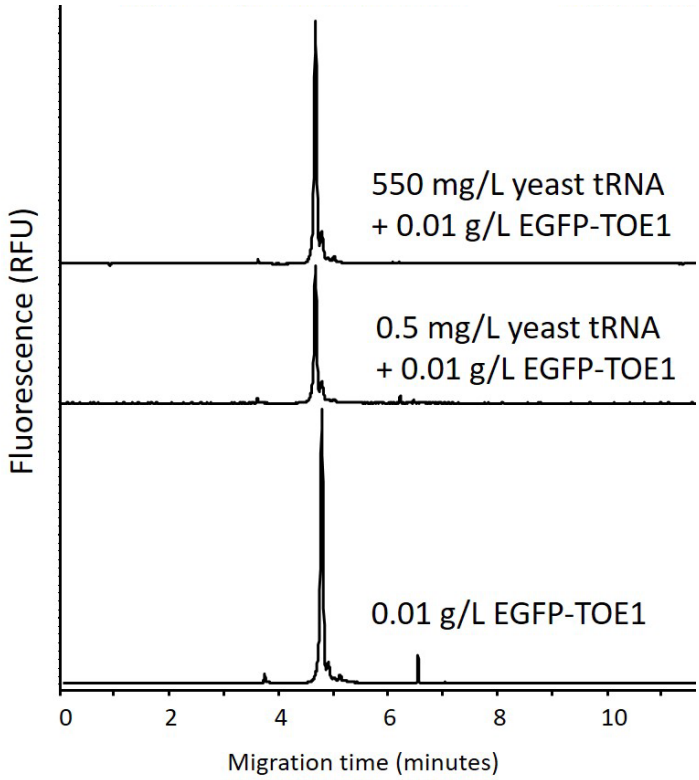

Figure 3.7 C) TAR and TOE1 experiments determining the importance of RNase and yeast tRNA, B) 3D contour of absorption spectrum and electropherograms of full length TOE1 C) 125 µM EGFP-TOE1 (0.01 µg µL^{-1}) full length protein as detected by laser induced fluorescence (bottom), EGFP-TOE1 with 0.5 mg L^{-1} yeast tRNA (middle), EGFP-TOE1 with 550 mg L^{-1} yeast tRNA, separated under 400 V cm^{-1}.

We also looked at binding between Tat and TAR by CE. Tat is a monomeric protein, but with the addition of Zn^{2+} or Cd^{2+} it can form dimers.[145] Long *et al*. showed by solution nuclear magnetic resonance (NMR) spectroscopy that the basic peptides from the carboxy terminus of the HIV-1 Tat protein bind to the apical stem-loop region of TAR.[146] Tat/TAR interactions are heavily studied, such as in Olsen *et al*., where solid-state NMR was used to characterize RNA structure and dynamics in order to demonstrate the plasticity of the RNA at its binding site; a 29 nucleotide long TAR RNA strand showed that binding to a Tat peptide led to a decrease in 3.7Å at its binding site.[147] Flexibility of TAR demonstrates the potential for therapeutic targeting of the interaction.

Previously reported analysis of optimal binding conditions for Tat and TAR showed that binding is most favourable at pH 8.0, 0°C, and that ionic strength of NaCl or KCl higher than 0.08 M can hamper the binding between the two.[148] Fourtounis *et al*. were able to observe favourable binding between Tat and TAR when incubating at room temperature for 10 min in Tris-HCl pH 7.5, where the ionic strength was kept at 50 mM NaCl; the separation buffer used in the capillary was 100 mM HEPES pH 7.3. We decided to test the affinity at 0°C and 15°C to see how temperature influenced the binding because other research groups reported good binding at both temperatures. We observed binding at 0°C when incubated for 10 to 40 min on ice, and then maintained the sample at 4°C in the CE tray with the temperature of the capillary set to 15°C with a K_d of 1.11 ± 0.04 µM (Figure 3.8). We also studied the complex after incubation at room temperature for 10-40 minutes, with separation carried out at room temperature as well (sample tray set at room temperature and capillary coolant at 22°C); the K_d was found to be 2.10 ± 0.45 µM. Phosphate buffer, pH 7.3, was used for all separations. Ideally, both experiments should be carried out at the same temperature to compare affinities because it is expected that the affinity will change based on temperature. This is because the possibility that a reaction will happen is dependent on enthalpy, entropy, and temperature of the system when binding affinity is translated to Gibbs free energy of dissociation. Although the K_d found after incubating on ice was slightly lower than the K_d of the sample incubated at room temperature, it is important to take into account that the electropherogram of the peaks separated at the lower temperature shows overlap of the two peaks; which is to say that the resolution is low and this affects the results. Furthermore, the experiments carried out at room temperature also do not show optimal resolution conditions, as the peaks are very close together. Due to the higher temperature, the peaks are wider, which may have also contributed to skewed results.

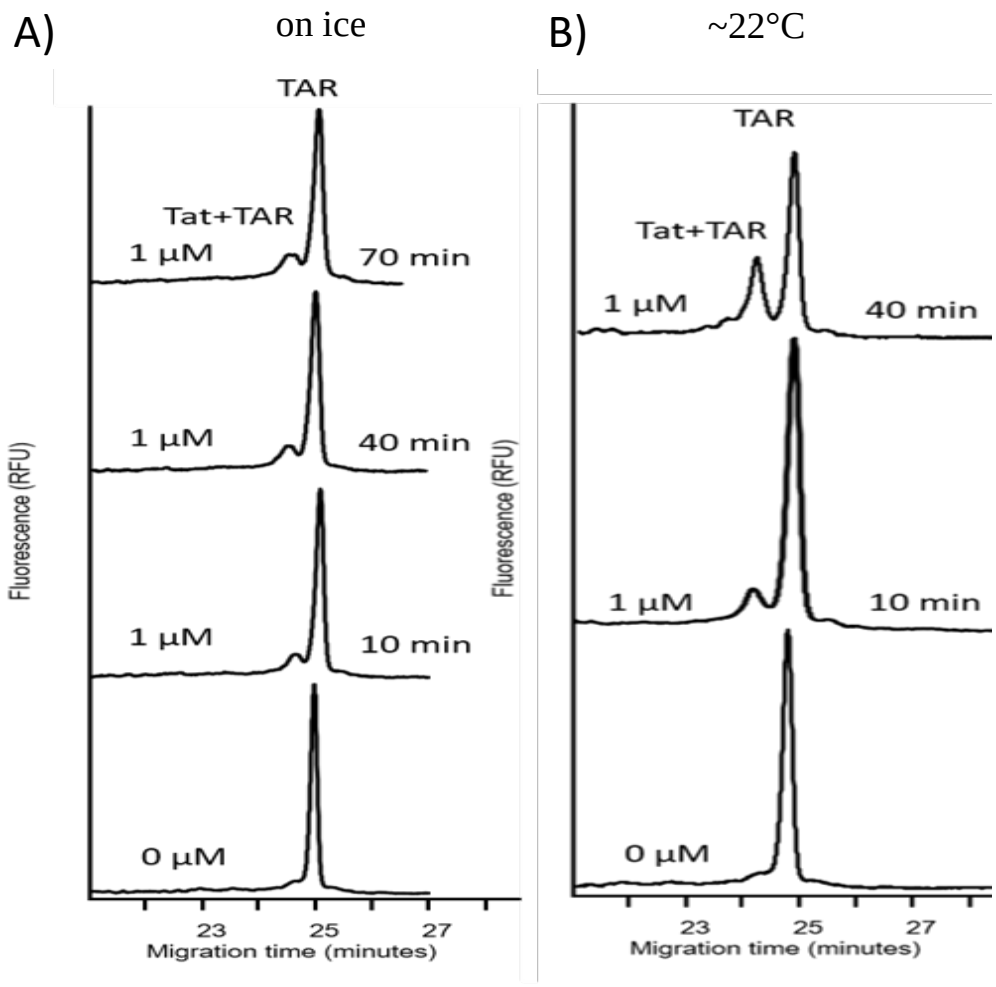

Figure 3.8 Electropherograms of FAM-labelled TAR with Tat recombinant protein separated by capillary electrophoresis and detected by laser induced fluorescence.
After incubation of FAM-labelled TAR at 60°C for 5 min followed by a 5 min incubation at room temperature, 1 µM of Tat recombinant protein was incubated with 50 nM TAR for various times A) on ice or B) at room temperature (~22°C). The complex between Tat and TAR is observed as a peak at approximately 24 min and free TAR is observed closer to 25 min. All samples were incubated with yeast tRNA and were separated under 433 V cm^{-1} in a 60 cm long capillary in 25 mM phosphate buffer at 15°C, pH 7.3.

For optimization of separation conditions of synthetic peptides ED35 and ER19, 25 mM Tris-acetate was also tested at pH 7.0. Although these conditions are considered gentler for complex formation, as the pH is closer to being physiological, it was not as useful for separation by CE. As can be observed in Figure 3.9, the resolution obtained when using this buffer is quite poor; free TAR migrates over the span of approximately 2 minutes, which is quite extensive. We also observed that a higher voltage helps with obtaining sharper peaks with better resolution.

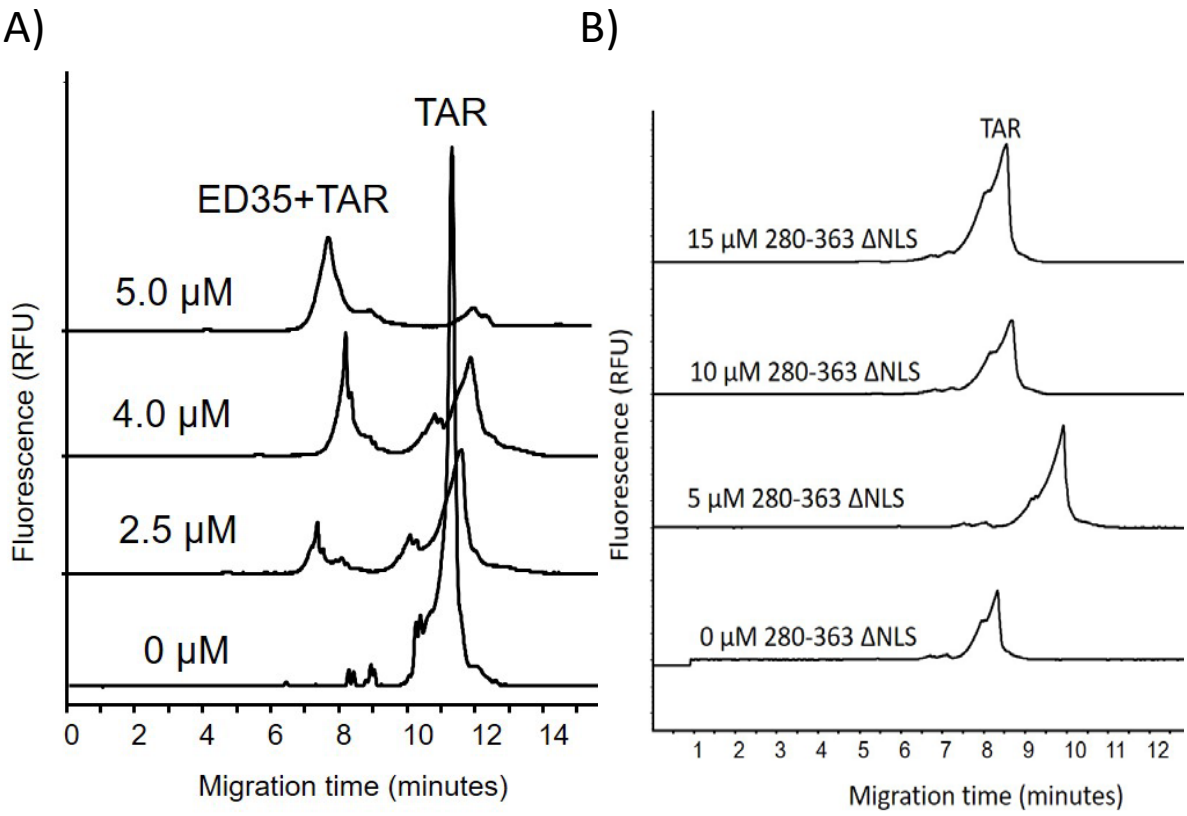

Figure 3.9 Electropherogram of capillary electrophoresis separation of TAR and ED35 using 25 mM Tris-acetate run buffer
A) ED35 (2.5, 4.0, 5.0 µM) and TAR subjected to 433 V cm^{-1}, B) TAR and 280-363ΔNLS (5, 10, 15 µM) subjected to 500 V cm^{-1}. All samples were incubated in 10 mM Tris, pH 8.0, 50 mM KCl, 2.5 mM $MgCl_2$, 10 mM DTT, 10% glycerol, 1 mg mL^{-1} BSA and 0.1 mg mL^{-1} yeast tRNA for 15 min at room temperature.

3.4 Conclusions

Protein TOE1 was identified as an inhibitor of HIV-1 replication. Its mechanism of action is through direct binding to the trans-activator response element TAR. The ability of TOE1 to bind TAR is partly due to a nuclear localization sequence within the protein. This sequence was found to be similar to Tat's lysine/arginine rich TAR-binding sequence. We demonstrated the binding between full-length and cleaved TOE1 by capillary electrophoresis and gel-shift assays. The K_d was calculated using NECEEM for ED35 and ER19, and found to be 7.43 ± 1.60 µM and 4.08 ±

0.19 μM, respectively. We also observed the significance of the nuclear localization sequence by demonstrating that without this sequence, binding is not observed with TAR, where two recombinant peptides lacking this sequence were tested: 280-363ΔNLS and 364-510. We calculated the K_d for Tat when incubated with TAR on ice and at room temperature; the K_d values were 1.11 ± 0.04 μM and 2.10 ± 0.45 μM, respectively. It is challenging to compare the K_d values of TOE1 peptides with Tat because the experiments were carried out under different experimental conditions. However, the values are within the same order of magnitude, which shows that they show similar affinity for TAR. Further experiments performed under the same conditions are required in order to obtain directly comparable values. Cell luciferase assays described by Sperandio *et al.,* which show that TOE1 was able to inhibit TAR/Tat binding,[140] demonstrated that TOE1 has even higher affinity for TAR than Tat. These results, together with the experiments performed by Sperandio *et al.,* describe the similarities between TOE1 and the sought factor, CAF (CD8+ anti-viral factor), insofar as the inhibitory activity at the level of long terminal repeats transcription, secretion from CD8+ T-cells and participation of a protease in its activity.[140] This is significant because it paves the way for further understanding of HIV-infection in patients and shows potential for inhibiting Tat/TAR interaction, which is essential for HIV-1 replication.

Chapter 4

4. Capillary Electrophoresis for Studying Viruses

4.1 Background

Viruses play an important role in many different aspects of everyday life. The research described in this chapter focuses on the study of vesicular stomatitis virus (VSV) and vaccinia virus (VV), both currently investigated in clinical trials as candidates for oncolytic therapy. One important aspect of oncolytic therapy delivery is to ensure that viral preparations are free of contaminants. According to the World Health Organization, no more than 10 ng of contaminating DNA should be present in a sample for clinical use.[67] Besides this, viruses play a critical role in our lives through vaccination programs. Although vaccines are considered one of the greatest health interventions, vaccination programs still face challenges due to the innate instability of viruses.[79] The term "cold chain" has been used to describe the refrigeration process required to transport vaccines at protective temperatures.[82] Nonetheless, due to fluctuations in temperature during transport, as much as half of all vaccines are discarded.[79] In seeking to reduce such waste, researchers have been working towards finding a better solution for making vaccination programs more successful.

The first part of this chapter describes a new method for quantification of VSV using capillary electrophoresis. Recent publications in our research group have demonstrated the use of capillary

electrophoresis for quantification of DNA and RNA viruses, and then expanded further for detection of DNA contamination.[67,149] When a viral sample is injected into the capillary electrophoresis, it gives two major fractions: one for the virus particles and another for the nucleic acid fraction, which may be present as a result of poor purification or degraded virus (Figure 4.1). During purification, DNA from the host cells may be carried over or nucleic acid can be present as a result of viral degradation. To visualize the virus and the nucleic acid, we used a nucleic acid intercalating dye, YOYO-1. Its fluorescence increases by 400 and 250 times when it binds to double stranded and single stranded DNA, respectively.[150] It has also been successfully used by other groups for visualizing RNA.[151-154] This results in a cluster of peaks for the virus particles that migrate faster than the nucleic acid. A cluster of peaks, rather than one peak, may appear because of aggregates that form, which may be a result of disulfide bonding between cysteine proteins or other interactions.[155] We tested dithiothreitol (DTT), a redox reagent commonly used for preventing this type of agglomeration in proteins,[156] for its ability to suppress cluster formation in VSV. We compared the results with the previously established method and with plaque forming assays. I performed capillary electrophoresis experiments. Preparation of virus and plaque forming assays were performed by Dr. Darija Muharemagic.

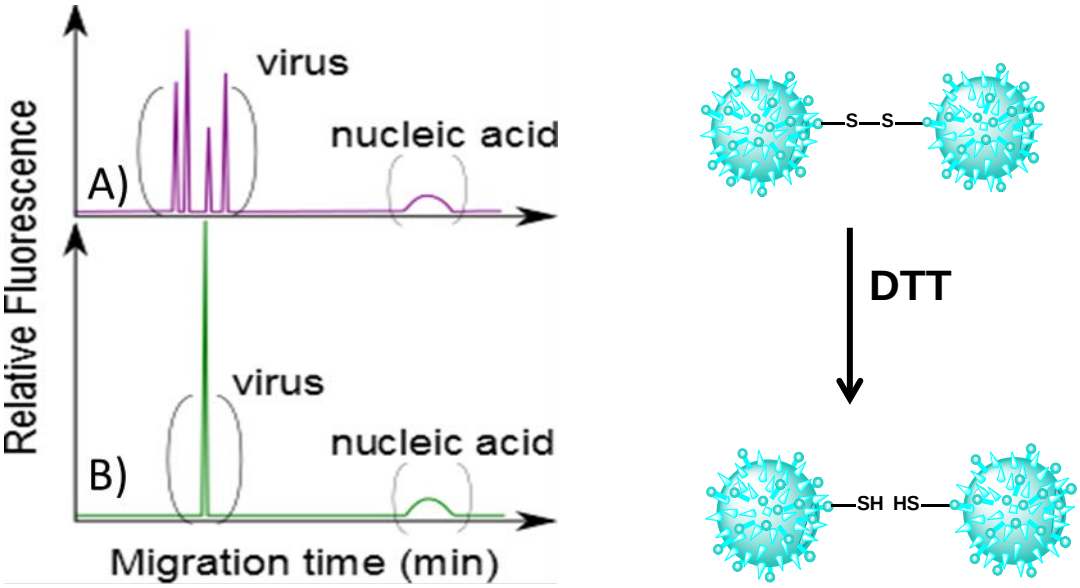

Figure 4.1 Schematic diagram of lysis-free viral quantitative Capillary Electrophoresis (qCE) for viruses demonstrating the clusters that form between viruses, resulting in multiple peaks (A) prior to addition of DTT and (B) one peak after addition of DTT.

The second part of the chapter describes the use of capillary electrophoresis for qualitative purposes where it was used to monitor preservation of intact, temperature-sensitive VSV particles. Four anti-VSV aptamers previously selected by Dr. Anya Zamay[157] were tested as a mixture for their ability to preserve virus infectivity during various freeze-thaw cycles. Furthermore, an aptamer construct was tested where a bridge containing complementary sequences to the four aptamers was annealed to the four aptamers in equimolar amounts[158] (Figure 4.2A). The infectivity of quadramer and aptamer pool-protected virus was 25 and 5 fold higher, respectively, than pure virus after 60 freeze−thaw cycles. It was also found that adding quadramers to the virus without freezing (cycle 0) increased the virus infectivity by 30%. CE supported plaque forming assay results, as more intact virus was observed when VSV was incubated with quadramer than with aptamer or with library alone. The results from this research have been published by our research group.[158] Virus was prepared by Darija Muharemagic and plaque-forming assays were performed by Shahrokh Ghobadloo. I performed capillary electrophoresis experiments.

A)

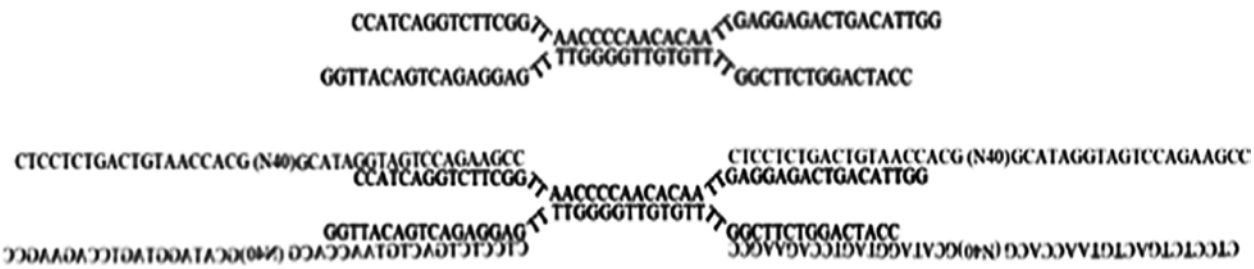

B)

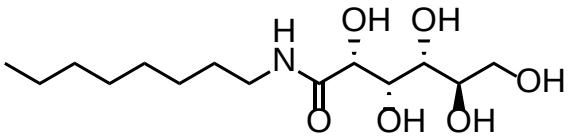

Figure 4.2 A) Schematic of bridge (top) and bridge annealed to four aptamers, described as quadramer (bottom). Reprinted.[158] Copyright {2014} American Chemical Society. B) Chemical structure of *N*-octyl-*D*-gluconamide, an ice re-crystallization inhibitor.

We also investigated the potency of a carbohydrate-based ice recrystallization inhibitor, *N*-octyl-*D*-gluconamide (NOGlc)[159,160] (Figure 4.2B) for its ability to eliminate the cold chain and stabilize the potency of VV; this work has been published.[161] Ice recrystallization inhibitors help to prevent re-organisation of smaller ice crystals into larger ice crystals, which are damaging to biological samples such as cells, tissues and viruses. NOGlc can be described as an open chain carbohydrate with fibers morphology and is a hydrogelator capable of immobilizing water molecules into three dimensional networks.[162,163] One hypothesis for the mechanism of simple carbohydrates is that they disrupt the bulk water present between ice crystal boundaries.[164] The impact of the hydrogelator was tested using plaque forming assays and CE was used to evaluate the impact on intact virus particles. Viral potency after storage at room temperature demonstrated that NOGlc conserved the infectivity of VV, 4.0 x 10^5 plaque-forming units (PFU) mL^{-1}, during 40 days. I performed capillary electrophoresis experiments in collaboration with Darija Muharemagic. Darija

Muharemagic and Shahrokh Ghobadloo prepared virus and plaque forming assays were performed by Shahrokh Ghobadloo.

4.2 Materials and Methods

4.2.1 Chemicals and Materials.

VSV was obtained from Jennerex Inc. (Ottawa, ON, Canada). More virus samples were produced in the lab using Vero kidney epithelial cells originally extracted from an African Green monkey (donated by the Bell lab, originally obtained from American Type Culture Collection (Manassas, Virginia, USA)) as previously described.[165] Sodium borate (cat. no. SX0355-1, EMD Chemicals, USA), boric acid (VWR, USA), YOYO-1 (Invitrogen, USA), *Escherichia coli* ribosomal RNA (Thomas Scientific), lambda DNA (New England Biolabs), DTT (Fisher Scientific) and bare silica capillary with an outer diameter of 365 µm and an inner diameter of 75 µm (Polymicro Technologies, USA) were used.

4.2.2 Preparation of ribosomal RNA and DNA standard and sample

Ribosomal RNA standard samples were prepared from a 100 µg mL^{-1} stock solution in borax by performing 1 in 3 serial dilutions. Phage DNA standard samples were prepared from a 200 µg mL^{-1} stock solution by performing 1 in 3 serial dilutions. DNA virus samples were diluted with borax from the stock solution originally in PBS. YOYO-1 stock solution in DMSO was diluted with borax to a final concentration of 2 µM. Both ribosomal RNA standards and virus were stained with YOYO-1 for 30 min prior to injection. DTT was added to the virus samples and incubated for 30 minutes prior to injection. The DTT concentration ranged from 15 mM to 60 mM from a stock concentration of 1 M.

4.2.3 Capillary electrophoresis for sample analysis

The capillary system used for the experiments was a ProteomeLab PA 800 (Beckman Coulter, California, USA). Laser-induced fluorescence was used to detect the virus and ribosomal RNA. YOYO-1 was excited at 488 nm using an Argon laser and detected at 520 nm. The experiments were performed in a 60 cm long capillary under 250 V cm^{-1} in 25 mM borax buffer at 15°C. Prior to each injection, the capillary was rinsed for 2 minutes with 100 mM HCl, 100 mM NaOH, H_2O, and 25 mM Borax at pH 8.9.

4.2.4 Vesicular stomatitis virus preparation

VSV was prepared and purified according to the protocol described by Diallo, J.S. *et al*.[166]

4.2.5 Cell and culture conditions

Vero cells were maintained in Dulbecco's modified Eagle's medium supplemented with 10% fetal bovine serum (Gibco BRL, Gaithersburg, Maryland, USA).

4.2.6 Vaccinia virus incubation with NOGlc and analysis by capillary electrophoresis

Two aliquots of VV were prepared with PBS and with 41 µM NOGlc, and incubated at room temperature (~22°C) for 12 days. Prior to separating each sample by CE, they were stained with 2.0 µM YOYO-1 fluorescent nucleic acid dye for 30 min. As a control, a sample from the two aliquots of VV was stained with 2.0 µM YOYO-1 dye and subjected to separation by CE without any incubation (Day 0). Duplicates of each run were performed. To calculate the areas of the virus peaks, 32 Karat Software was used. The total area of the virus peak fraction, which ranges between approximately 8 min-12 min, was selected and divided by the migration time.

4.2.7 DNA aptamers

The aptamers used in the experiments are 80 nucleotides long with a central sequence of 40 nucleotides flanked by 20 nucleotide long primer hybridization sites (5'-CTC CTC TGA CTG TAA CCA CG-$(N)_{40}$-GCA TAG GTA GTC CAG AAG CC-3'). The central N_{40} sequences are described in Table 4.1:

Table 4.1 Sequences of aptamers used in preservation studies with VSV

Aptamer	Sequence
Z-23	F_GGGACCTATCAGGCGATGTGAAAACTCTTATACCACTGG_cR
Z-29	F_ACATCCTACGTTTGCCACGCGCTACTCCGCCATCTACCC_cR
S39	F_GCACTTCACTTCTCCTCTGACTGTAACCACGC_cR
M50	F_CCATCACCCTATTATCTCATTATCTCGTTTTCCCTATGCG_cR

All four oligonucleotides were synthesized by Integrated DNA Technologies (Iowa, USA). To prepare a pool of single aptamers, each of the four aptamers was incubated separately at 95°C for 5 minutes, and then an equimolar amount of each aptamer was mixed together. For incubation with VSV, the aptamer pool was used at a final concentration of 8 µM.

4.2.8 Quadramer design

Four aptamers were linked together by a bridge, which consists of two oligonucleotide strands connected by a central complementary sequence. Each end of the bridge consists of a complementary flank, which allows aptamers to anneal. The quadramer is prepared by heating at 95°C, with equal amounts of the sides of the bridge, followed by addition of the aptamer pool in equimolar amounts. Subsequently, the complex results in four aptamers annealing to each bridge construct.

4.2.9 Preparation of aptamer/quadramer coated-VSV

Three groups were tested: aptamer- and quadramer-treated VSV, with untreated VSV as a control. For each group, 75 µL of virus (3×10^9 PFU) was aliquoted, followed by the addition of PBS (15 µL) to the control group, a pool of aptamers (15 µL) to the second group, and quadramers (15 µL) to the third. The mixtures were incubated for 60 min at 37°C and then used for plaque forming assays.

4.2.10 Freeze-thaw cycles with aptamer/quadramer coated-VSV

For testing the dosage effect of aptamers and quadramers, we used 3×10^9 PFU of VSV with nine dilutions of aptamers and quadramers, as well as nine samples with PBS used as a control. These samples were subjected to 30 freeze-thaw cycles. To study the effect of different freeze-thaw cycles after we determined the optimal concentration of DNA, seven samples for each group were prepared and were exposed to 0, 10, 20, 30, 40, 50 and 60 freeze-thaw cycles. Freezing was conducted at -80ºC, whereas the thawing was performed at room temperature. The groups were tittered for VSV infectivity after each set of 10 freeze-thaw rounds.

4.2.11 Plaque-forming assays with VSV

After each experiment, each sample group containing the virus was titered using the Vero cell line (0.4×10^6 per well) in twelve-well culture plates. After infecting the cells with serial dilutions of each sample in serum free media, the plates were incubated for 1 hour at 37°C in a 5% CO_2 humidified incubator. Afterwards, medium was removed and the cells were overlaid with 1 mL of 0.5% low melting agarose with 1x Dulbeco's Modified Eagle's medium supplemented with 10% fetal bovine serum. After incubation for 24 hours, cells positive for Yellow fluorescent protein fluorescence were visualized using Alfa Innotech Imaging System, Version 3.0.3.0. Additionally,

a standard plaque assay was performed, where the plates were fixed with methanol–acetic acid fixative (3:1 ratio) and stained with Coomassie blue solution; then the white/ clear plaques were counted.

4.2.12 Vaccinia virus propagation

VV was propagated in U2OS monolayer cultures at 37°C. Cells were infected with VV for 1 hour in Dulbeco's Modified Eagle's medium at 37°C. The media was then replaced with fresh Dulbeco's Modified Eagle's medium containing 10% fetal bovine serum. After 48 hours, the supernatant of the infected cells was harvested by centrifugation at 650 g for 30 minutes at 4°C. The pellets were then suspended in Dulbeco's Modified Eagle's medium and the virus was subsequently used as the stock of vaccinia.

4.2.13 Vaccinia virus titration

The serial dilutions of VV were added to U2OS cells maintained in 12-well plates. Following virus binding to the cells at 37°C for 1 hour, virus inoculum was aspirated and an overlay solution (mixture of 1:1 volumes of 3% carboxymethylcellulose: 2x Dulbeco's Modified Eagle's medium, 20% fetal bovine serum) was added. After 48 hours of incubation, cells positive for Green Fluorescent Protein (GFP) fluorescence were visualized by using Alfa Innotech Imaging System, Version 3.0.3.0. In addition, a standard plaque assay was performed, where the overlay was removed and the cell monolayer was stained with crystal violet for enumeration of the virus plaques.

4.3 Results and Discussion

VSV particles and VV are known to aggregate and create clusters, which greatly influences the final titre of a sample.[167,168] VV is released from the cytoplasm of the cell as it is made, and at this point has the opportunity to aggregate.[167] Due to this agglomeration, separation by CE results in a collection of multiple peaks, each representative of a cluster of virus particles, which is displayed by a different ratio of peaks from run to run.[67,149] The nucleic acid migrates much slower than the virus to the cathode due to its highly negative charge. This can be seen in Figure 4.3A. In the past, a multi-step procedure was used for viral quantification, where the first step was to separate the virus fraction from the nucleic acid fraction by CE. The second step required lysis with proteinase K for 2 hours, whereby the DNA is released. Afterwards, the virus is again separated by CE and quantified based on the difference in the area (before and after the lysis) for the DNA/RNA degradation fraction. We have now improved this method by shortening the number of steps and reagents that are needed for viral quantification, as well as making it more direct by counting the virus particles rather than using the difference in nucleic acid peak before and after lysis of virus.

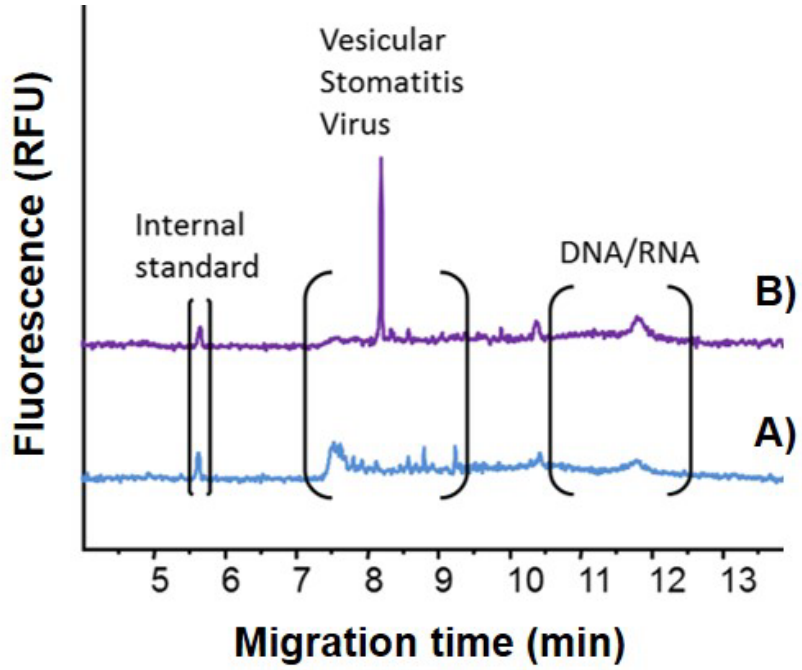

Figure 4.3 Experimental viral qCE electropherograms of VSV A) without DTT incubation, B) with 15 mM DTT incubation. All samples were stained with 2 µM YOYO-1. CE separations were performed in a 59 cm-long uncoated capillary with 25 mM borax buffer pH 8.9 under 250 V cm-1 at 15°C using laser-induced fluorescence detection.

DTT is commonly used for effectively maintaining the thiol groups in their reduced states.[154] It is effective in basic conditions and useful for our purpose since the borax running buffer used is at a pH of 8.9. It takes about 2 hours for DTT to be fully oxidized under such basic conditions; therefore, it was an important factor to consider during the experimental design process.[169] One of the most popular uses of DTT is for reducing protein disulfide bonds prior to running sodium dodecyl sulfate polyacrylamide gel electrophoresis gels. T*ris*(2-carboxyethyl)phosphine (TCEP) is similar to DTT insofar as it too reduces disulfide bonds; furthermore, it is a stronger and irreversible reagent that has the benefits of also being odourless.[156]

Our approach consists of the addition of DTT to the viral sample. DTT reduces the thiol-thiol bonds that may be encountered between virus particles and which lead to aggregation. Surface glycoprotein G, 70 kDa, forms spikes on the virion with approximately 90% of the polypeptide

chain external to the lipid bilayer.[170] The 495 amino acid protein contains 13 cysteine residues.[171] DTT treatment results in one major peak for the virus fraction, as observed in Figure 4.3B, and so lysis of the virus is no longer necessary.

The quantification of the virus was done in two steps. First, two nucleic acid curves were built (Figure 4.4) by performing 1 in 3 dilutions: ribosomal 13S and 23S RNA was used for the first curve because VSV is an RNA-based virus and a DNA curve using lambda DNA for quantifying the contamination. The fluorescent area for the nucleic acid was plotted against the concentration of nucleic acid, as seen in Figure 4.3. To quantify the amount of virus particles, the area for the virus peak was used and interpolated from the RNA standard curve for VSV (Figure 4.4). The DNA curve was used to calculate the level of contaminating nucleic acid (Figure 4.5). Sigmoidal curves fit the data best, and this may be because the amount of YOYO-1 used was kept constant and in excess, which might have resulted in photobleaching of the dye at low concentrations of nucleic acid, whereas at high concentrations of nucleic acid, there may have been an insufficient amount of YOYO-1. This was based on the assumption that nucleic acid present in the fraction is DNA from host cells. Although VSV was purified using a sucrose gradient prior to running the CE experiments, DNA contamination was still present in some cases.

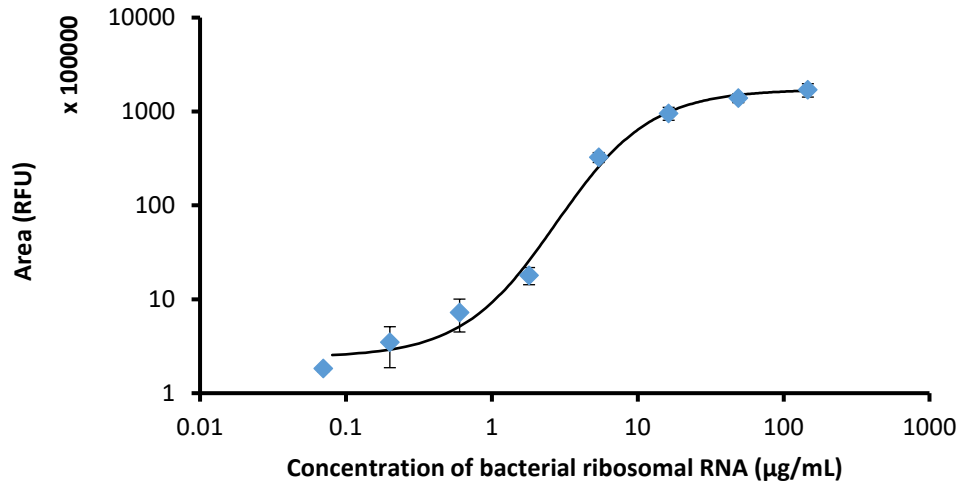

Figure 4.4 Calibration curves for area and concentration of bacterial ribosomal RNA.
The ribosomal RNA was stained with 2 µM YOYO-1 dye prior to injection. The area of the peak(s) was taken and plotted against the concentration of ribosomal RNA.

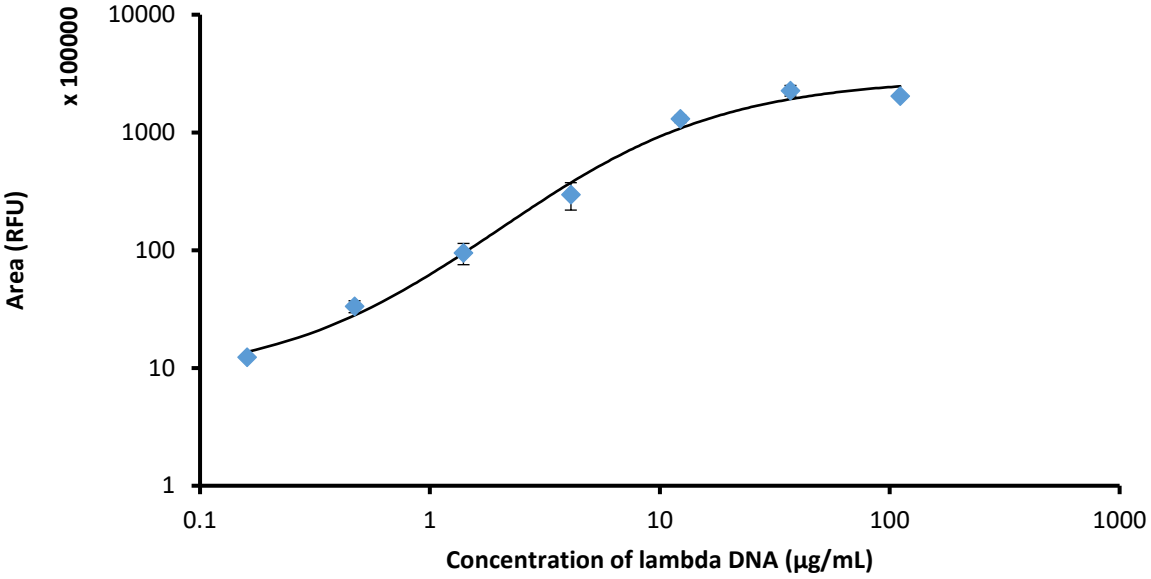

Figure 4.5 Calibration curve for phage DNA, λDNA, stained with 2 µM YOYO-1 dye used for the correlation of fluorescence and concentration for VSV.

There are several advantages to our approach. Firstly, it is a much quicker method since it only requires the addition of DTT to the virus sample. Secondly, it is advantageous insofar as it provides better resolution between the virus peak and the degraded DNA/RNA peak from host

cells if contamination is present. Furthermore, since there are fewer peaks, it is much easier to analyze for quantification purposes.

4.3.1 Quantification of intact virus

Our results were then compared to two methods for the quantification of the virus and corresponding DNA contamination. The results are summarized in Table 4.2, where two batches of virus were tested. This is useful, as no more than 10 ng of DNA is allowed in a human dose of viral therapeutics.

Table 4.2 Concentrations of virus and DNA contamination in two batches comparing viral qCE with lysis-free viral qCE and plaque forming assays.

	Batch 1	**Batch 2**
Viral concentration		
Viral qCE (ivp mL^{-1})	(3.45 ± 0.63) x 10^{12}	(3.22 ± 0.40) x 10^{12}
Lysis-free viral qCE (ivp mL^{-1})	(9.15 ± 0.39) x 10^{11}	(5.29 ± 0.14) x 10^{11}
Plaque forming assay (PFU mL^{-1})	7 x 10^{9}	5 x 10^{9}
Contamination		
DNA using viral qCE (µg mL^{-1})	0.64 ± 0.13	2.77 ± 0.23
DNA/RNA using lysis-free vqCE (µg mL^{-1})	1.42 ± 0. 02	2.35 ± 0.82

The viral sample was incubated with YOYO-1 and DTT for 30 minutes prior to injection. Once it was subjected to separation, the area for the virus peak (A_v) was then calculated using the 32 Karat Software. Calibration curves were built with the area of YOYO-1-stained nucleic acid as a function of RNA concentration for VSV. Using the line of best fit, the concentration of virus was interpolated from the graph. The concentration of intact virus units was calculated using Formula 4.1 and described in intact viral particles (ivp) mL^{-1}.

$$[Virus] = \frac{N_A D_{buffer} [NucleicAcid]}{10^6 (MM)_{NucleicAcidofVirus}} \tag{4.1}$$

Where N_A is Avogadro's number, D_{buffer} is the dilution factor that is taken into account for diluting the virus upon the addition of buffer, DTT, Bodipy and YOYO-1. Although there are differences

in the staining ability of virus particles and free nucleic acid, they were both incubated with an excess of YOYO-1 and subjected to the same conditions for the separation to decrease errors. An excess of YOYO-1 dye was used in the experiments. Batch 1 was found to have (9.15 ± 0.39) x 10^{11} ivp mL^{-1} and batch 2 was found to have (5.29 ± 0.14) x 10^{11} ivp mL^{-1}. These values were then compared to the values obtained when using the previously developed method, where the virus is lysed. Using the previous method, batch 1 contained (3.45 ± 0.63) x 10^{12} ivp mL^{-1} and batch 2 contained (3.22 ± 0.40) x 10^{12} ivp mL^{-1}. The values obtained by using the lysis-free method of quantification are three to six fold lower than the ones obtained where lysis of the virus is required. This may be because of a difference in intercalating efficiency of the YOYO-1 dye in the intact virus versus the free RNA. Both methods, however, give values that are higher than ones obtained by plaque forming assays in infectious viral particles (ivp) per mL, where batch 1 has 7 x 10^9 ivp mL^{-1} and batch 2 has 5 x 10^9 ivp mL^{-1}. These values show that plaque forming assays underestimate the amount of virus particles. This might be due to the aggregation of the viruses during plaque forming assays. It is of the highest importance to know the number of infective virus particles for vaccine therapy. The number of intact virus particles can give more information about the sample and how these values relate to infectivity. The working range for CE experiments was found to be 1.14-1.83 x10^{10} ivp mL^{-1} (Figure 4.6). Unfortunately, this is a very narrow working range, and so the virus concentration needs to be optimized prior to analysis. The limit of detection was found to be 2.05 x10^8 ivp mL^{-1} based on the calibration curve built by incubation of increasing amounts of VSV with 60 mM DTT (Figure 4.7).

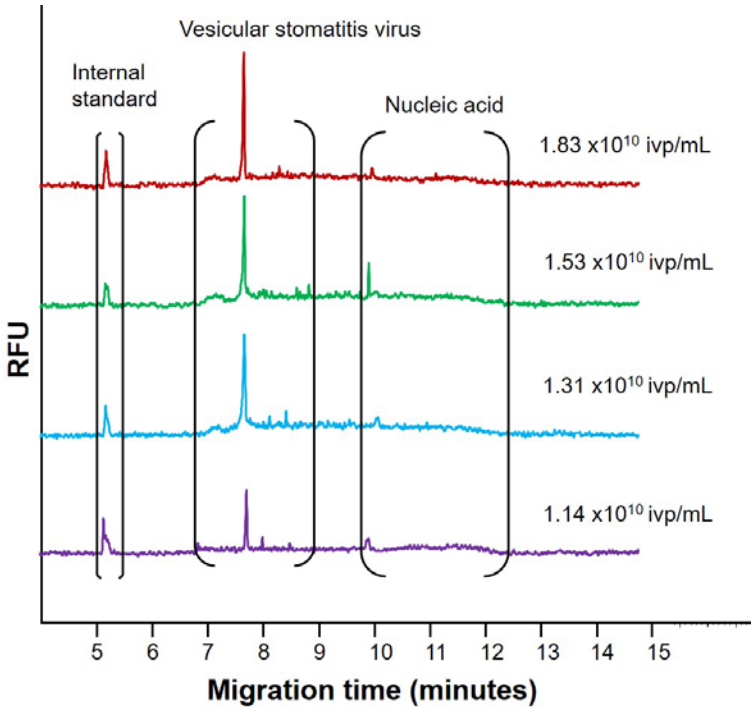

Figure 4.6 Representative electropherograms for increasing dilutions of VSV from bottom to the top.

The limit of detection of VSV was found to be 2.05 x10^{8} ivp mL^{-1}. CE separations were performed in a 59 cm-long uncoated capillary with 25 mM borax buffer pH 8.9 under 250 V cm^{-1} at 15°C using laser-induced fluorescence detection. This graph represents the dynamic working range for VSV virus with 60 mM DTT.

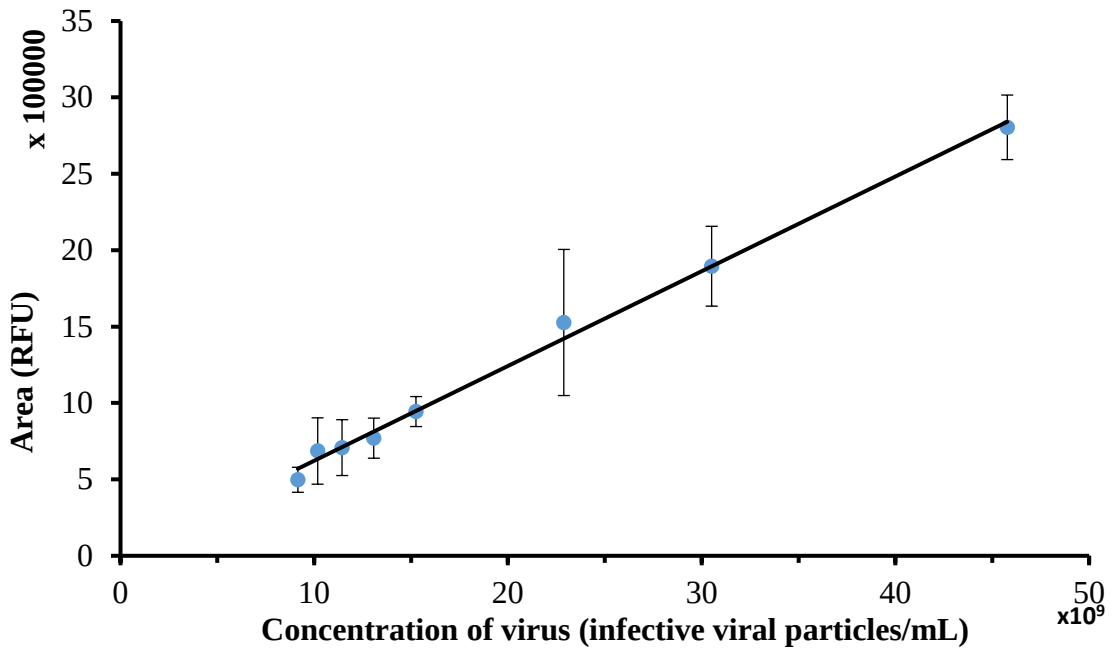

Figure 4.7 Graph for determination of the limit of detection of VSV.
VSV stained with YOYO-1 dye and incubated with internal standard, Bodipy. CE separations were performed in a 59 cm-long uncoated capillary with 25 mM borax buffer pH 8.9 under 250 V cm^{-1} at 15°C using laser-induced fluorescence detection.

4.3.2 Quantification of nucleic acid-lysis-free viral qCE

To quantify the amount of DNA/RNA in the sample using the lysis-free method, the area for the fraction that corresponds to nucleic acid is measured. The DNA concentration in the sample was determined by using a calibration curve of fluorescent area as a function of the concentration of λDNA incubated with YOYO-1 (Figure 4.3b). Equation 4.2 was used for the calculations under the assumption that the nucleic acid peak is mostly due to DNA contamination, as RNA would be more quickly degraded.

For both RNA and DNA calibration curves, the following equation is used to calculate the area (*A*) dependence of concentration (*C*), where *M*, *K*, *N*, *L*: are constants for fitting (all are non-negative).

$$A = \exp(M + K(C^N)/(L + C^N) \quad (4.2)$$

Using our lysis-free method of quantitation, the first batch contained a lower amount of DNA with 1.42 ± 0.02 μg mL^{-1} and the second batch had 2.35 ± 0.82 μg mL^{-1}. These values were then compared to the previously established method, where batch 1 had 0.64 ± 0.13 ivp mL^{-1} and batch 2 had 2.77 ± 0.23 ivp mL^{-1}. The values using the previously established method are higher than the ones using the lysis-free method. Furthermore, the level of contamination is above the required level for clinical use; according to the World Health Organization, no more than 10 ng per sample is acceptable.

4.3.3 Effect of TCEP and other surfactants

We also tested the irreversible redox reagent TCEP and several detergents, such as sodium dodecyl sulfate (SDS), Triton X-100 and sodium cholate. The addition of surfactants is common when studying proteins since severe adsorption interaction with the capillary wall can lead to peak distortion or even to loss of analyte if irreversible adsorption occurs.[172] After titration of TCEP and other detergents with the virus, we were unable to find concentrations that were suitable for reproducible results (Figure 4.8). Increasing concentrations of TCEP showed the appearance of multiple peaks. TCEP has been shown to have deleterious stability when in the presence of phosphates;[156,169] TCEP may have not proved useful for our purposes because the virus was suspended in PBS. SDS, an amphiphilic surfactant, was added to the run buffer at concentrations below and above the critical micelle concentration; the critical micelle concentration of SDS is 8.3 mM, which corresponds to the concentration at which 50% of the surfactant is in micelles and 50% is free.[173] SDS effectively denatures proteins at millimolar concentrations, at or even below the critical micelle concentration, by binding strongly to charged and hydrophobic side chains.[174] We also tested triton X-100, which often preserves the conformation of proteins; its critical micelle concentration has been found to be 0.22 mM.[175] Sodium cholate was also tested. It is a water

soluble, anionic detergent with a critical micelle concentration of 8-14 mM, which helps solubilize and reduce aggregation of protein solutions.[176] It is composed of a steroid ring with three hydroxyl groups and a carboxylic group on the terminus of the structure.

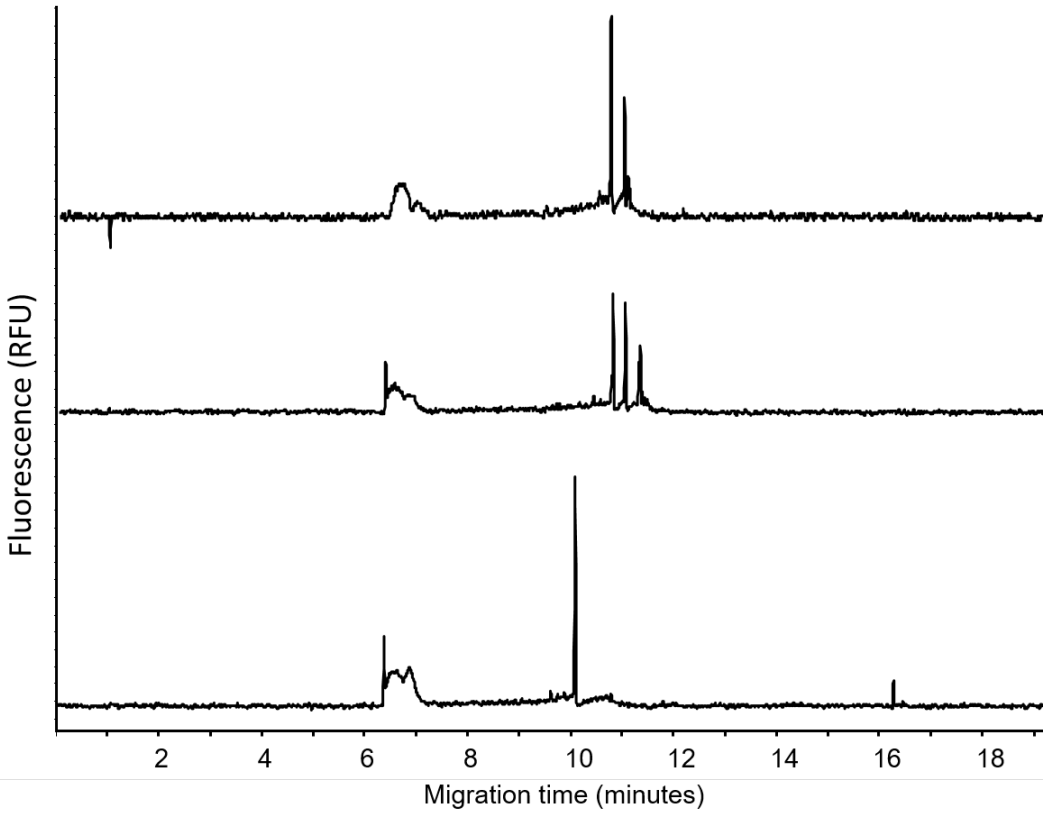

Figure 4.8 VSV incubated with TCEP (top to bottom) 25 mM, 50 mM and 63 mM TCEP.
CE separations were performed in a 59 cm-long uncoated capillary with 25 mM borax buffer pH 8.9 under 250 V cm^{-1} at 15°C using laser-induced fluorescence detection.

Okun *et al*. found that the addition of 0.05% SDS with 0.5% Triton X-100 and 0.5% sodium deoxycholate to boric acid run buffer was helpful for the separation of human rhinovirus subviral particles.[172] Based on this, we tested concentrations that are similar to the reported ones. The virus is too big to partition in the micelles, which are only 1.8 nm,[177] but the detergent is still able to form complexes with the surface proteins of VSV. Upon addition of SDS to the run buffer, we found that at higher concentrations the virus peaks would disappear and irreproducible peak patterns were observed on the electropherograms (Figure 4.9). The disappearance of the virus

peaks may be because SDS lyses the virus at higher concentrations during the separation process. Although the nucleic acid peaks are not observed, this may be because there is not enough time for YOYO-1 to intercalate with the released DNA during the CE separation. Furthermore, it can be observed that above the critical micelle concentration of SDS, Bodipy (4,4-difluoro-4-bora-3a,4a-diaza-s-indacene), the internal standard migrates at a much slower time than below the critical micelle concentration (Figure 4.9). This could be due to the fact that it was trapped in the SDS micelle. SDS is an anionic surfactant and, as a consequence, it is attracted towards the anode, which makes it migrate with a slower velocity towards the cathode than if it were at a concentration above the critical micelle concentration.[178] Yang *et al.* found that the size of the analyte molecule and its hydrophobicity both play roles in interaction with surfactants; furthermore, hydrogen bond accepting basicity of the analyte was an important factor for selectivity with anionic surfactants, such as SDS and sodium cholate.[179] Surface proteins of VSV are most likely partly charged, and this will also affect the separation of the virus. Figure 4.10 shows multiple runs with 0.0025% (0.01 mM) SDS; due to the irreproducibility of the peaks, we decided to try another surfactant.

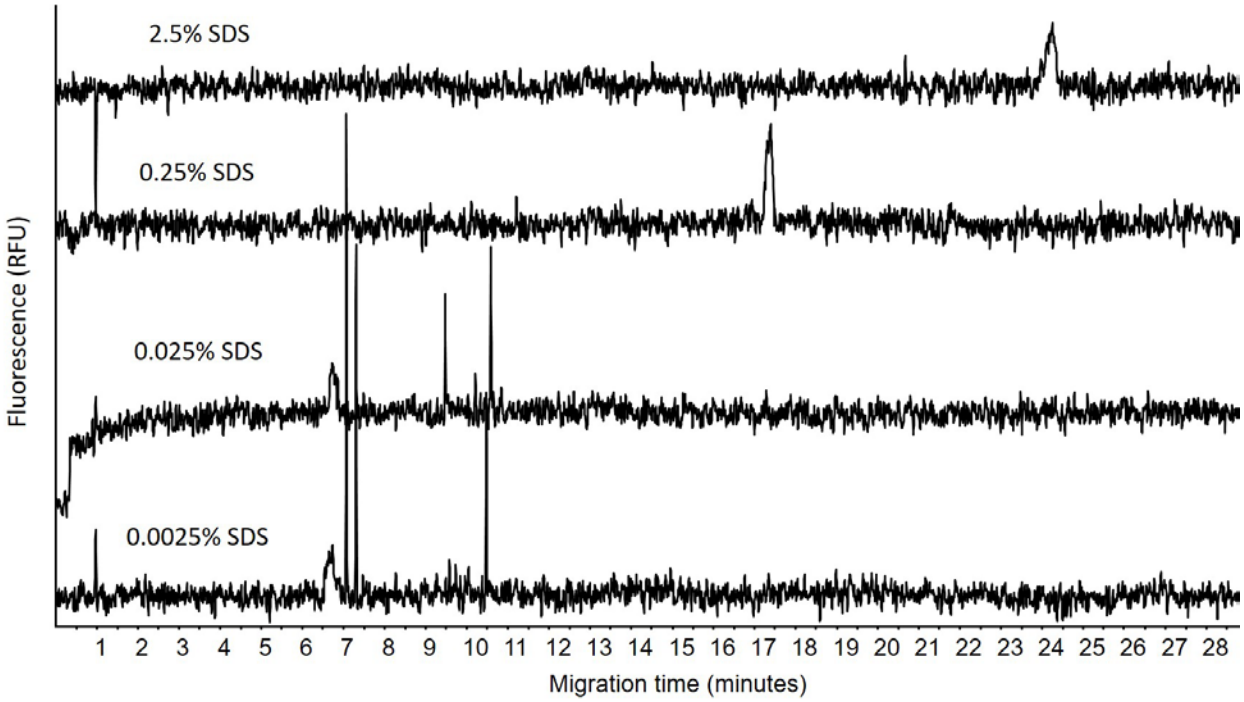

Figure 4.9 VSV separated by capillary electrophoresis with SDS in run buffer.
From bottom up: 0.0025%, 0.025%, 0.25%, 2.5% (i.e. 0.01 mM to 10 mM). CE separations were performed in a 59 cm-long uncoated capillary with 25 mM borax buffer pH 8.9 under 250 V cm^{-1} at 15°C using laser-induced fluorescence detection.

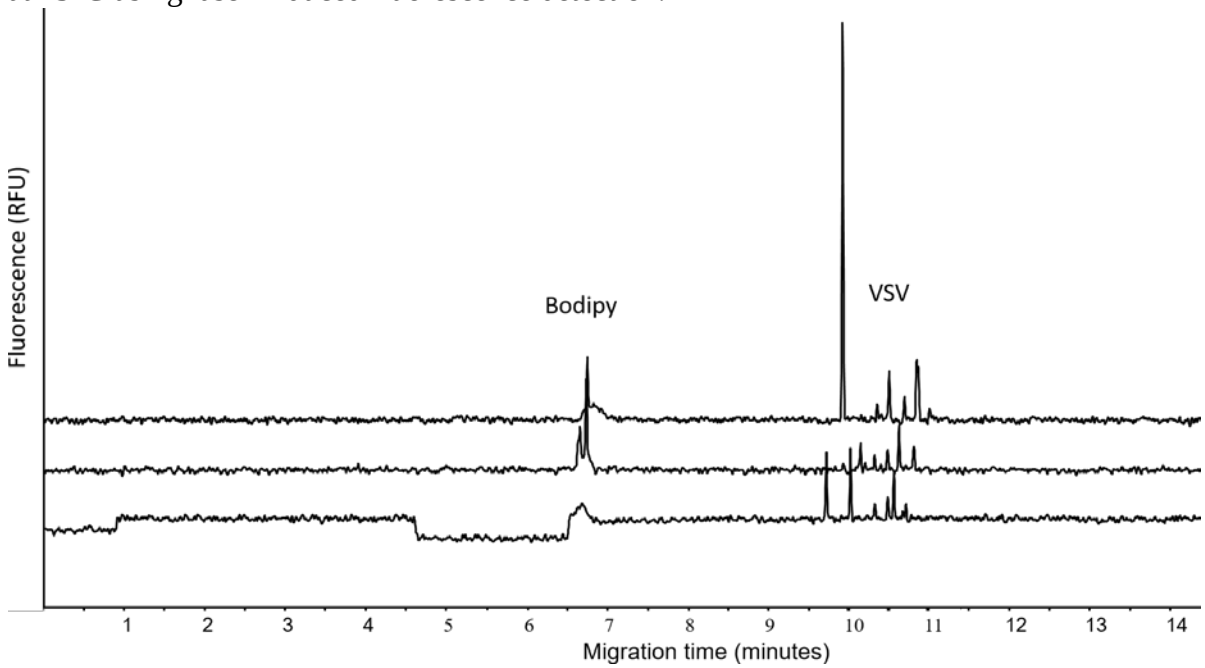

Figure 4.10 VSV separated with 0.0025% SDS (0.01 mM) in run buffer.
CE separations were performed in a 59 cm-long uncoated capillary with 25 mM borax buffer pH 8.9 under 250 V cm^{-1} at 15°C using laser-induced fluorescence detection.

Next, we tested a mild, nonionic polyoxyethylene surfactant, Triton X-100. Triton X-100 is made up of a mixture of oligomers with varying lengths of ethoxylate chain.[180] However, under basic pH the alcohol group at the terminus becomes deprotonated. Triton X-100, like other surfactants, is usually used to lyse cells and to extract and solubilize proteins. Besides this, it is also used in CE for improving separation conditions.[172] We found that addition of increasing concentrations of Triton X-100 did not affect the separation of VSV (Figure 4.11).

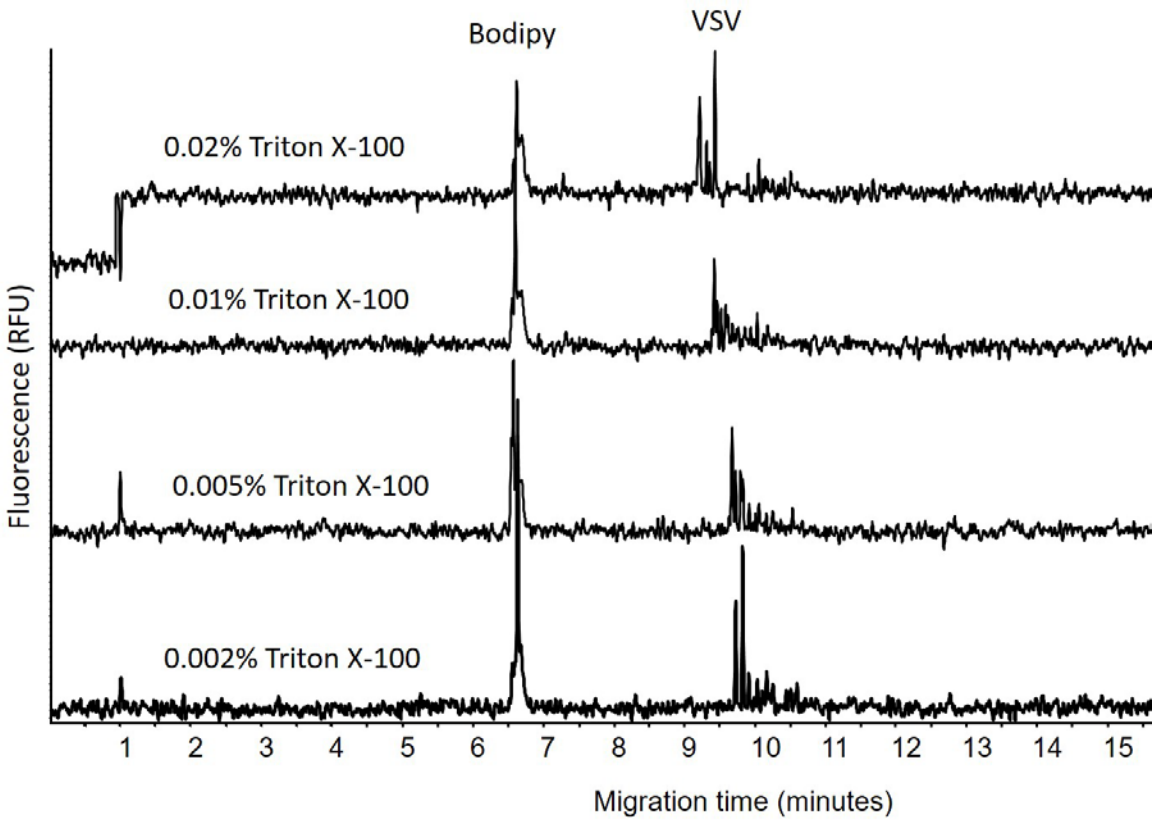

Figure 4.11 Experimental viral qCE electropherograms of VSV with Triton X-100 in run buffer. From bottom up: 0.1 %, 0.05%, and 0.01% Triton X-100. All samples were stained with 2.0 µM YOYO-1. CE separations were performed in a 59 cm-long uncoated capillary with 25 mM borax buffer pH 8.9 under 250 V cm^{-1} at 15°C using laser-induced fluorescence detection.

Next, we decided to try sodium cholate, another commonly used surfactant for solubilizing proteins. With low concentrations of sodium cholate, the electropherogram showed a reduction in the average number of virus peaks, but the number of peaks would still vary. The results looked

more promising at concentrations above the critical micelle concentration (25 mM), where the size of virus peaks increased and the number of peaks decreased (Figure 4.12). In accordance with micellar kinetic electrochromatography, at this concentration, Bodipy, the internal standard, which is small enough to fit in the micelles, migrated at a later time than the virus, which is too big to fit in the micelles and so migrates with the buffer. After further experiments, we found that the peaks were irreproducible (Figure 13 and 14), where the same concentration of cholic acid was added (5 mM or 25 mM) and therefore did not find sodium cholate useful for our purposes.

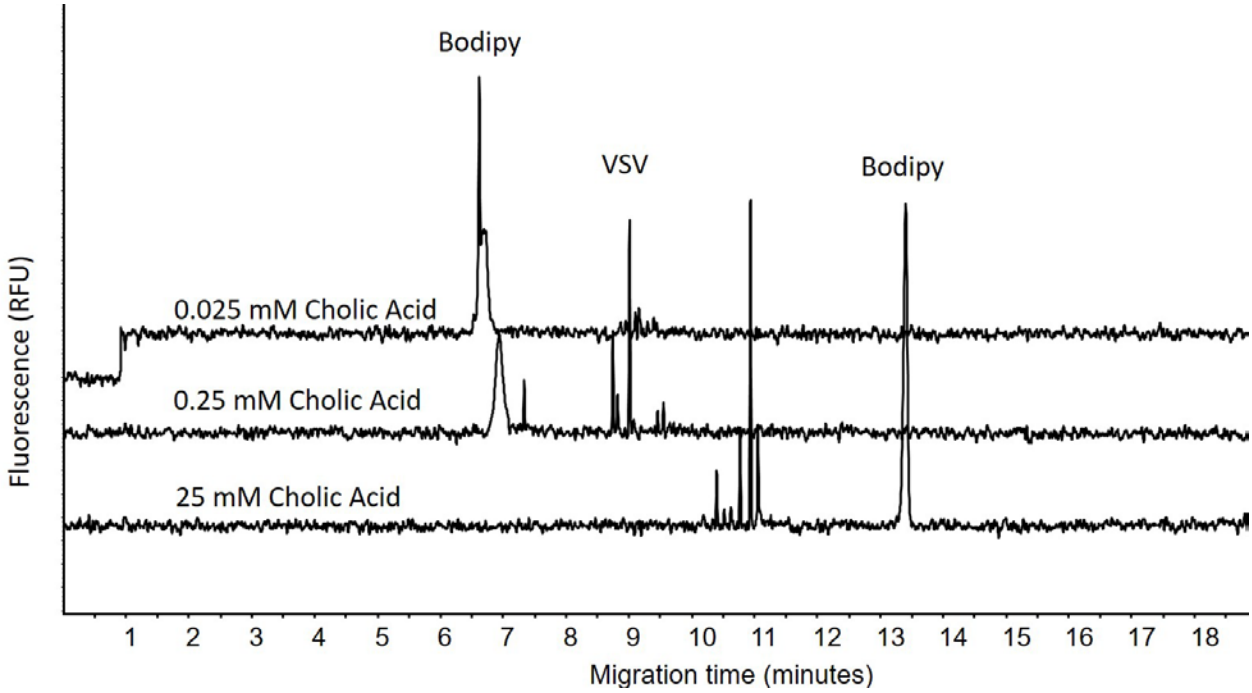

Figure 4.12 VSV with several concentrations of cholic acid/sodium cholate in run buffer. From bottom to top: 25 mM, 0.25 mM, 0.025 mM. CE separations were performed in a 59 cm-long uncoated capillary with 25 mM borax buffer pH 8.9 under 250 V cm^{-1} at 15°C using laser-induced fluorescence detection.

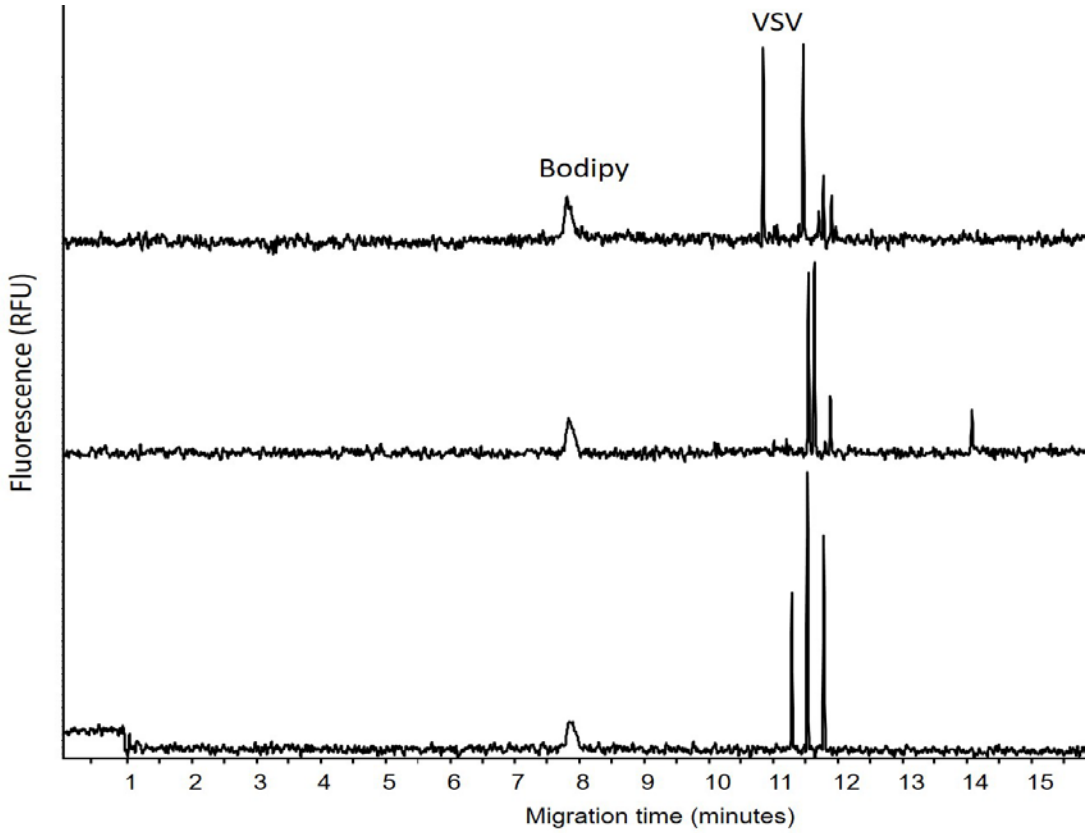

Figure 4.13 VSV with 5 mM cholic acid/sodium cholate in run buffer.
CE separations were performed in a 59 cm-long uncoated capillary with 25 mM borax buffer pH 8.9 under 250 V cm^{-1} at 15°C using laser-induced fluorescence detection.

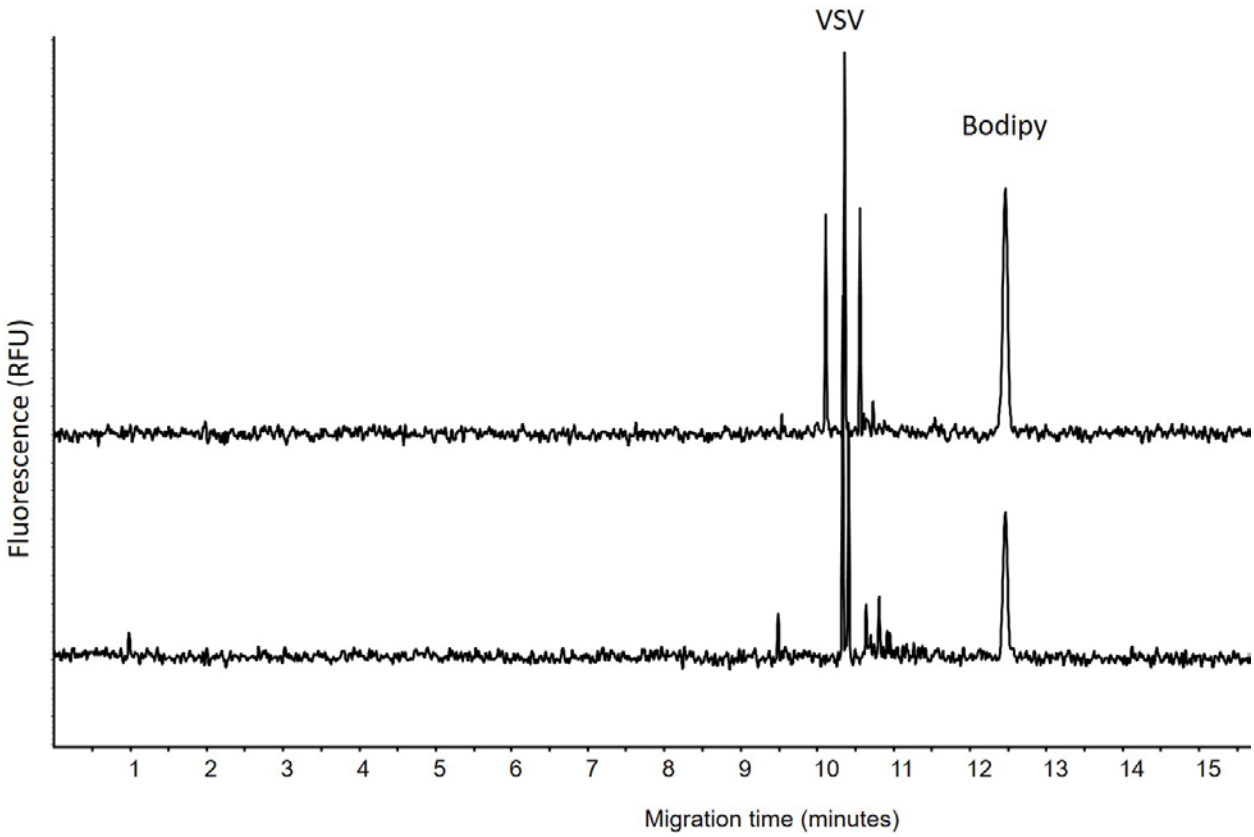

Figure 4.14 VSV with 25 mM of cholic acid in run buffer; repeat runs.
CE separations were performed in a 59 cm-long uncoated capillary with 25 mM borax buffer pH 8.9 under 250 V cm^{-1} at 15°C using laser-induced fluorescence detection.

Although the surfactants that were tested did not prove useful under the specified conditions, it is important to note that optimization can be a lengthy, complex and difficult task.[181] Furthermore, although not tested, a combination of non-ionic and anionic mixed micelles may have proven more effective. Furthermore, other macromolecular structures, such as oligomers, micro-emulsions or dendrimers, have the potential to be effective additives for the analysis and quantification of viruses by CE.[181]

4.3.4 Capillary electrophoresis for qualitative studies of preservation of virus

Previously selected anti-VSV aptamers were investigated for their ability to protect VSV during freeze-thaw conditions. Four aptamers were tested as a mixture and a quadramer was prepared,

where a bridge connected all four aptamers together. The apparent K_d for the monomeric mixture determined by flow cytometry was found as 71 ± 15 nM, and for the quadramer as 22 ± 9 nM. Plaque-forming assays were done to evaluate the infectivity of VSV after it was subjected to 10-60 freeze-thaw cycles (Figure 4.15). CE was performed in order to evaluate the decrease of intact virus particles after one freeze-thaw cycle when incubated with the aptamers. More freeze-thaw cycles were not performed because the concentration of VSV used was very close to the limit of detection of the CE once it underwent more cycles. CE experiments were used for extraction of relative amounts of virus rather than quantifying amount of virus.

Plaque-forming assays demonstrated that after 60 freeze-thaw cycles, the infectivity of quadramer and aptamer-mixture protected virus was 25 and 5 fold higher, respectively, than virus stored in buffer alone. Adding aptamers to the virus increased infectivity by 30%, which may be attributed to the ability of aptamers to decrease aggregation of the virus. When the negatively charged aptamers bind to the virus, they may cause the virus particles to repel each other due to the negative charges on the aptamers. This type of coating may further protect the virus from ice crystals that would otherwise damage the virus envelope and capsid.

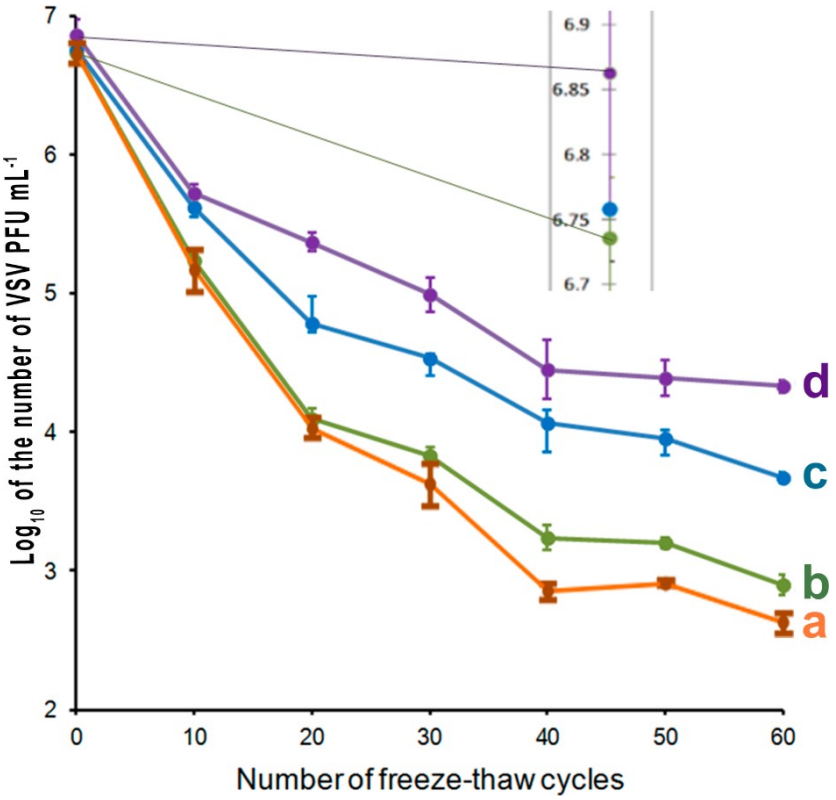

Figure 4.15 VSV infectivity correlation curve for DNA library (A), pure virus (B), with an aptamer pool (C), and with the quadramer (D) depending on the number of freeze−thaw cycles. The inset represents the initial infectivity before any freeze−thaw (cycle 0). Reprinted.[158] Copyright {2014} American Chemical Society.

CE experiments revealed that at the first freeze-thaw cycle, incubation of VSV with aptamers, the naïve library (non-specific DNA) or buffer alone all had a similar effect on the amount of virus particles damaged, as the areas were very similar: about 5 times less than before freeze-thawing (Figure 4.16). Incubating with quadramer showed that the area was much higher, only about 40% less than the original area, and that it protects the virus about three fold better than with aptamer mix, buffer or library.

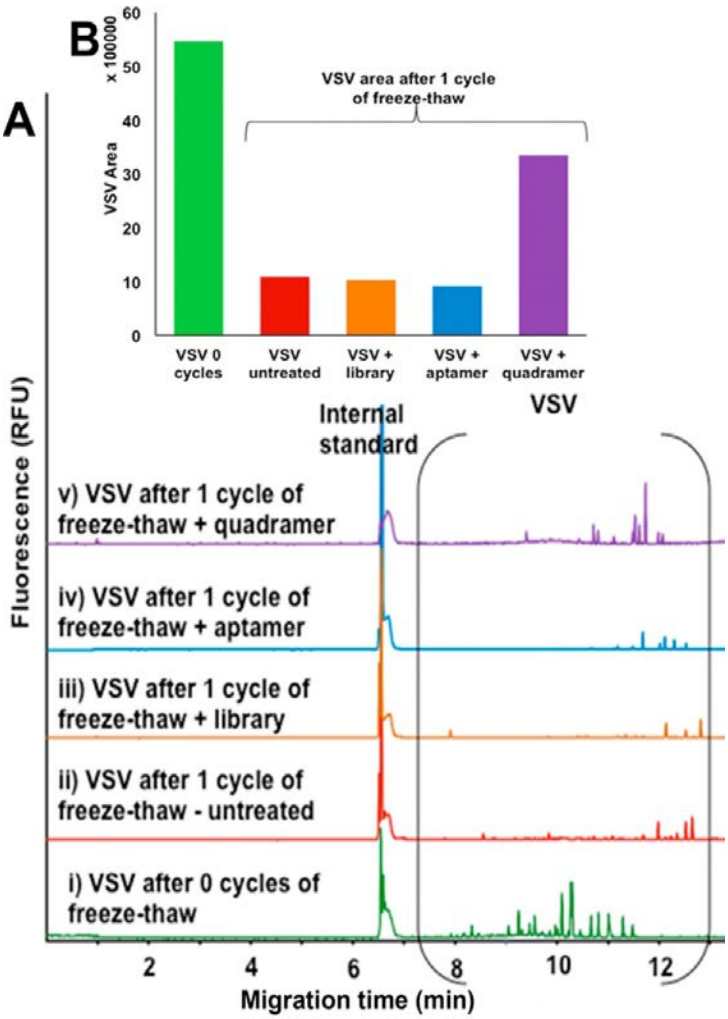

Figure 4.16 VSV separated by viral qCE after incubation with aptamer and subjection to freeze-thaw cycles.
Electropherograms for VSV separated by capillary electrophoresis and detected by laser-induced fluorescence. VSV was stained with YOYO-1 dye. CE separations were performed in a 60 cm long capillary under 250 V cm−1 in 25 mM borax buffer at 15 °C. (i) fresh, not frozen VSV; (ii−v) VSV after 1 cycle of freeze−thaw, untreated and treated with the library, the aptamers and the quadramer, respectively. (B) Areas of intact virus peaks for all experiments. Reprinted.[158] Copyright {2014} American Chemical Society.

NOGlc was identified as a potent carbohydrate for stabilization of VV. VV was stored in 41 µM NOGlc and in PBS as a control at room temperature (~22°C). Afterwards, the infectivity of the virus was tested using plaque forming assays in cells. The data was plotted against time as a logarithmic infectivity, as presented in Figure 4.17. It was observed that VV stored in PBS lost approximately 50% of its infectivity after approximately 3 weeks, and was completely ineffective after 40 days of storage at room temperature. In contrast to this, VV stored in NOGlc had preserved

its ability to infect, with a loss that was less than 10 PFUs per mL, even after 40 days of storage at room temperature.

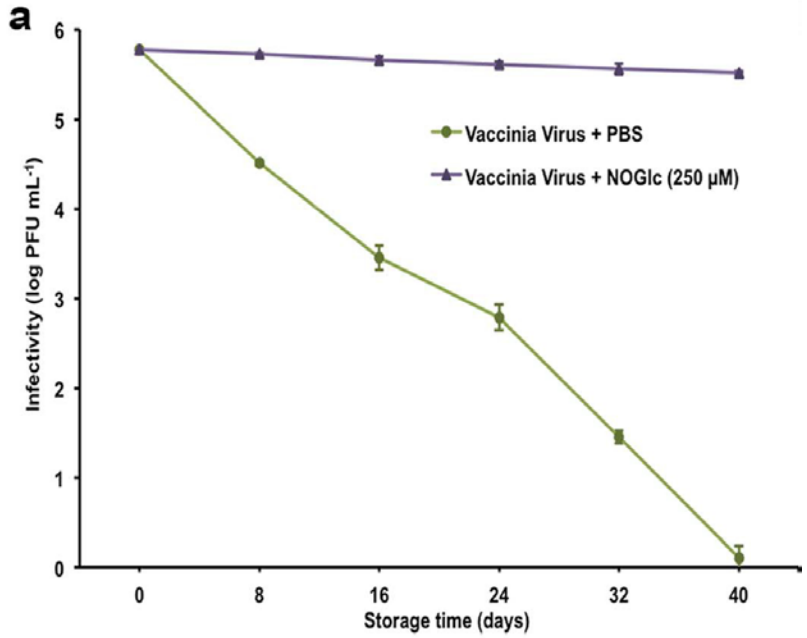

Figure 4.17 Stabilization of VV by NOGlc while stored at 22°C.
VV infectivity over the span of 40 days. Data obtained by Shahrokh Ghobadloo. Reprinted from Nature Publishing Group: Scientific Reports (4):5903, freely available under the terms of the Creative Commons Attribution License.

To investigate further, we used CE to study the intact virus particles over the span of 12 days (Figure 4.18). It was observed that the amount of intact virus particles decreased over time for both groups; however, on day 12 (Figure 4.19) the amount of intact virus particles was 4 ± 0.56 times higher for VV stored in NOGlc than the one stored in PBS. An independent sample t-test was conducted to compare how much VV was present on day 12 after storage in PBS and NOGlc. A significant difference was found between the condition means for PBS (M=50262.7, SD=4174.5) and for NOGlc (M=191689.8, SD=23294.3) $t(2)=8.45$ and $p=0.014$. Our results suggest that when the virus is incubated in NOGlc instead of PBS, the virus is preserved more in NOGlc. Another t-test was conducted in order to evaluate the difference between Day 0 (M=1083879.0, SD= 537704.5) and Day 12 in PBS in order to evaluate if there is significantly less virus on Day 12 than on Day 0; it was found that $t(2)= 2.72$, $p=0.11$. Unfortunately, this

data suggests that the difference is not significant; this may be a result of the high standard deviation on Day 0. A test was also conducted in order to evaluate the difference between Day 0 (M=561941, SD=110321) and Day 12 in NOGlc to see if the virus area has reduced significantly; it was found that t(2)=4.64, p=0.04. These results suggest that the amount of virus is significantly less on Day 12 than on Day 0. This is in contrast to the PBS findings, as mentioned earlier; this may be because of the high standard deviation that was obtained from the PBS Day 0 experiments. Finally, a t-test was also conducted between the means for PBS and NOGlc for day 0 to evaluate if the area of the virus peak is significantly different when the virus is incubated with PBS or NOGlc; it was found that the areas are not significantly different: t(2)=1.34 and p=0.31. This suggests that the areas were not affected by incubating in either solution on Day 0.

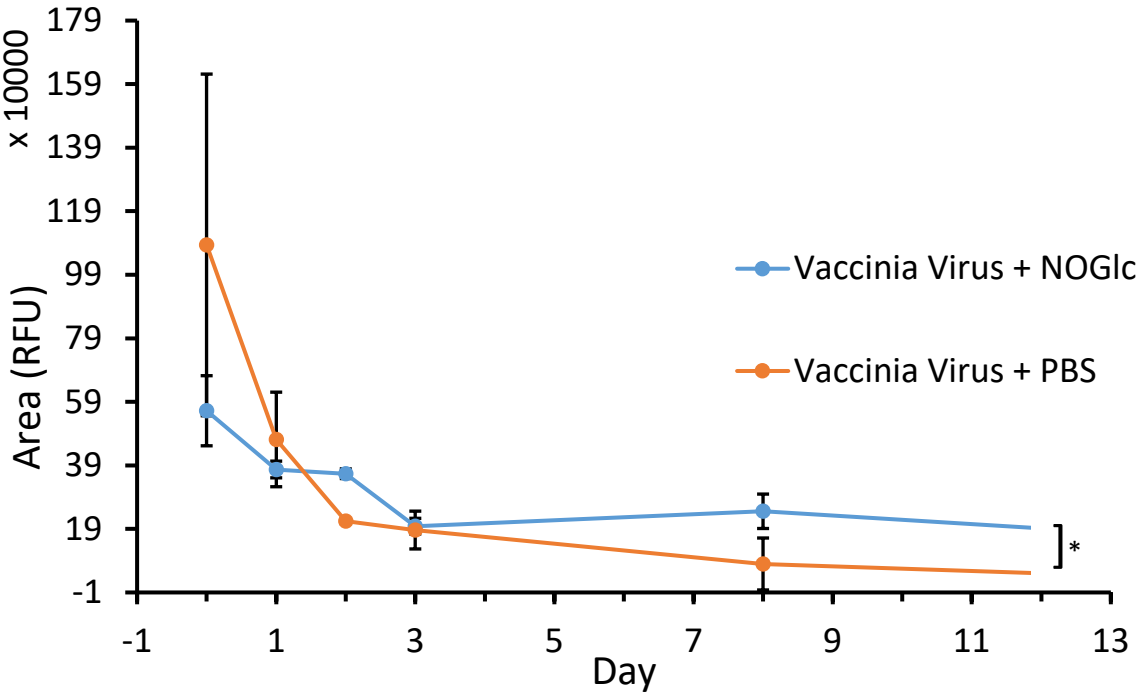

Figure 4.18 Capillary electrophoresis separation of VV with NOGlc and PBS.
Area of VV fraction after incubation with NOGlc (blue) and in PBS (red), over the span of 12 days. (* $p < 0.02$)

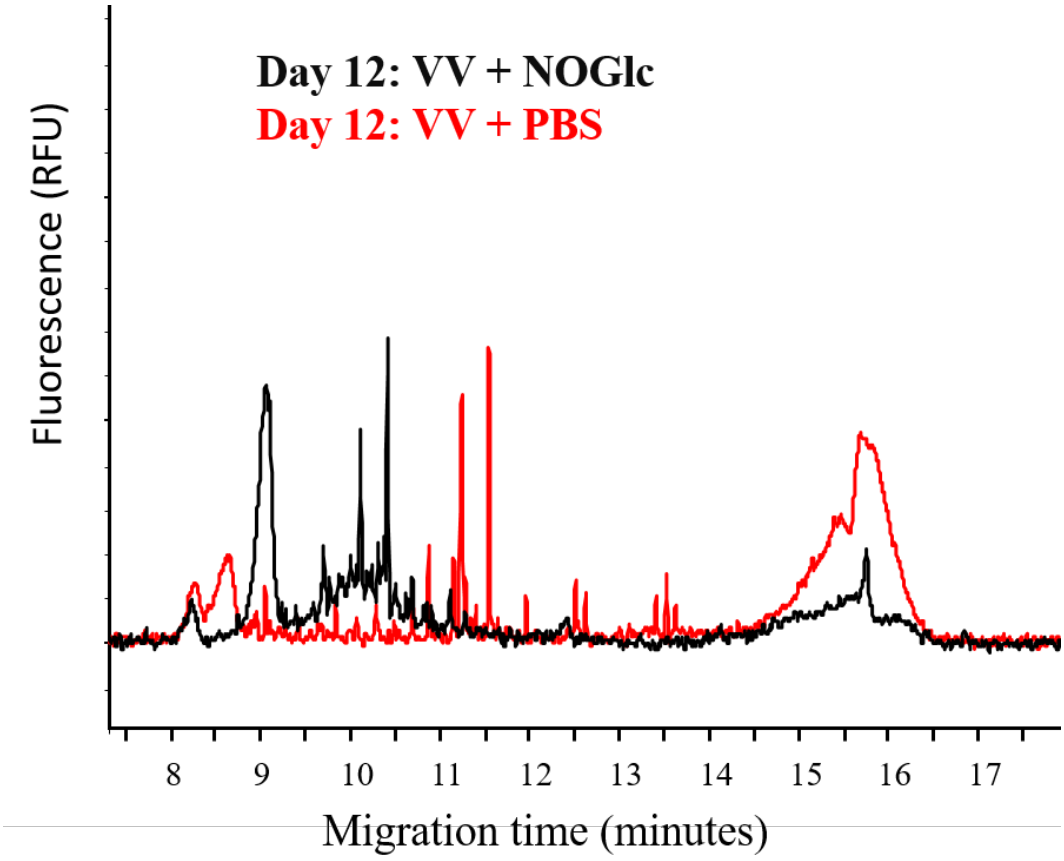

Figure 4.19 Electropherograms for VV separated by capillary electrophoresis and detected by laser induced fluorescence after incubation with PBS (red) or NOGlc (black) at 22°C for 12 days. All samples were stained with YOYO-1 dye. CE separations were performed in a 60 cm long capillary under 250 V cm^{-1} in 25 mM borax buffer at 15°C. Modified and reprinted from Nature Publishing Group: Scientific Reports (4):5903, freely available under the terms of the Creative Commons Attribution License.

One hypothesis for the mechanisms by which NOGlc helps stabilize VV is that it helps decrease virus agglomeration. This may also explain why the addition of NOGlc to VV increased infectivity by approximately 20%. CE electropherograms show that the patterns for the virus are different; virus stored in PBS creates spikes, whereas virus stored in NOGlc produces broader peaks. This too may be a result of different aggregation patterns or fewer clusters. NOGlc's hydrophobic octyl tail and chiral carbohydrate head are known to form non-covalent quadrupole helices in aqueous media. These structures are likely to disrupt the agglomeration of the virus.

4.4 Conclusions

The current method allows for quicker quantification of VSV than the previously published method. It utilizes the redox capacities of DTT to decrease the amount of aggregation between virus particles, allowing for a more homogenous mixture that then displays as one major peak in the CE electropherograms. Furthermore, this technique is advantageous because of the small amount of sample that is required for quantification, and its ability to separate virus particles and DNA/RNA contamination.

Furthermore, anti-VSV aptamers have proven useful for reducing the damaging effects of freeze-thawing VSV for infectivity purposes. These aptamers were found to help stabilize VSV by achieving a 25 fold increase in infectivity when compared to VSV stored in buffer, after 60 freeze-thaw cycles using plaque forming assays. These studies demonstrate the potential for anti-virus aptamers as tools in cryo-preservation, especially for oncolytic viruses, where infectivity of viruses is crucial.

One of the major concerns for immunization programme success worldwide is the stability of vaccines and whether or not they will remain potent on the way from the manufacturer, through the distribution channels, to the vaccine recipients.[182] Reconstituting vaccines that have been lyophilized results in a 50% loss of infectivity when stored for 1 h at 20-25°C, and in the full loss of infectivity when stored at 37°C. NOGlc has shown potential for use as a stabilizer of VV when stored at room temperature for 40 days.

Chapter 5

5 Phytochemical analysis in search of biofilm and quorum sensing inhibitors in neotropical plants (preliminary results)

5.1. Background

The scope of this project was to find new phytochemical compounds that can disrupt biofilm growth and quorum sensing in bacteria. Biofilms are matrix-enclosed microbial accumulations that adhere to biological or non-biological surfaces.[183] Depending on the environment, single-species populations or multimember communities of bacteria can form microcolonies, which constitute the biofilm.[184] Biofilm formation begins with the attachment of the bacteria to a surface; afterwards, it can move or settle and become a focal point for microcolony development.[185] The microcolonies become wrapped in a protective exopolymeric matrix made of polysaccharides, DNA and proteins.[185] Bacteria use quorum sensing, a mode of communication that uses chemical signaling molecules called autoinducers or bacterial pheromones, which are released by the bacteria as a function of increasing cell population density.[186,187] Quorum sensing regulates gene expression and is important at all stages of biofilm development, as well as in antibiotic production, symbiosis, virulence, competence, conjugation, motility and sporulation.[188] Autoinducers in gram-negative bacteria are usually N-acyl homoserine lactones and gram-positive bacteria usually

use processed oligo-peptides to communicate.[188] Quorum sensing can occur both within and between bacterial species.[188,189]

Biofilm formation can be beneficial; for example, rhizobacteria, bacteria that live in symbiosis with plants, are used as biofertilizers.[190,191] Rhizobacteria colonize on the plant's roots and provide plant growth through nitrogen fixation. In return, the host provides the bacteria with amino acids and oxygen. In contrast to this example of a good symbiotic relationship, biofilm formation can also have negative clinical and economic effects. For example, bacteria can live in well-developed biofilm matrices embedded on medical implants in humans, such as heart valves, coronary stents, fracture-fixation devices, intraocular lenses and dental implants, to name a few.[192] Approximately 80% of implant-related infections are caused by the gram-positive *Staphylococci* species bacteria, with *Staphylococcus aureus* being responsible for 34% of all hospital-related infections.[193] Infections can occur peri-operatively or post-operatively and, depending on the implant, often result in removal of the implant, infected tissue and bone, followed by long-term antimicrobial treatment.[193] This makes infections associated with surgical implants difficult to treat and expensive, with the estimated average cost of $175,000 per year for combined medical and surgical treatment in the United States for cardiovascular implants.[194]

Furthermore, biofilm-mediated infection plays a key role in patients with cystic fibrosis, as the patients are already susceptible to the gram-negative *Pseudomonas aeruginosa.*[184] This type of infection can result in hyperactive inflammatory response in the lung, leading to the death of the patient.[184] Periodontitis is another example of biofilm-related disease; in this case, caused by the gram-negative *Porphyromonas gingivalis.*[184] Infection can lead to chronic inflammation of the tissue supporting the gums, followed by tooth loss.[184] Other conditions caused by biofilm formation include, but are not limited to, chronic sinusitis, musculoskeletal infections,

osteomyelitis, urinary tract infections and biliary tract infections.[185] As highlighted here, biofilm formation can have many devastating effects on human health and, in turn, on the economy. This emphasizes the importance of having effective ways to disrupt biofilm formation.

According to the 2014 World Health Organization report on global surveillance of antimicrobial resistance, the ability to treat patients with common infections may soon be over due to the rise in antimicrobial resistance, as well as a rise in range of infections, making the 21st century an era where minor injuries can kill.[195] The World Health Organization calls for governments to make a collaborative effort in the surveillance of antimicrobial resistance and its mitigation.[195] Currently, there are several types of therapeutic approaches towards interfering with biofilm growth, such as: phytochemicals, small molecule inhibitors, antimicrobial peptides, enzymes and antibody-based therapy.[196] A variety of small molecule phenolics have been reported to have biofilm and quorum sensing inhibitory action. Phenolics or polyphenols comprise one of the largest groups of plant secondary metabolites and have been reported to exhibit a myriad of biological effects.[197] It is not surprising that polyphenols have the highest amounts of reported biofilm inhibitors compared to other classes, such as terpenoids, quinones, coumarins, alkaloids and sulfur-containing phytochemicals.[198]

Some of the most active natural products are halogenated furanones produced by marine alga *Delisea pulchra*,[199] which inhibit biofilm formation of *Escherichia coli*,[200] *Baccilus subtilis*,[201] *Pseudomonas aeruginosa*[202] (Figure 5.1).

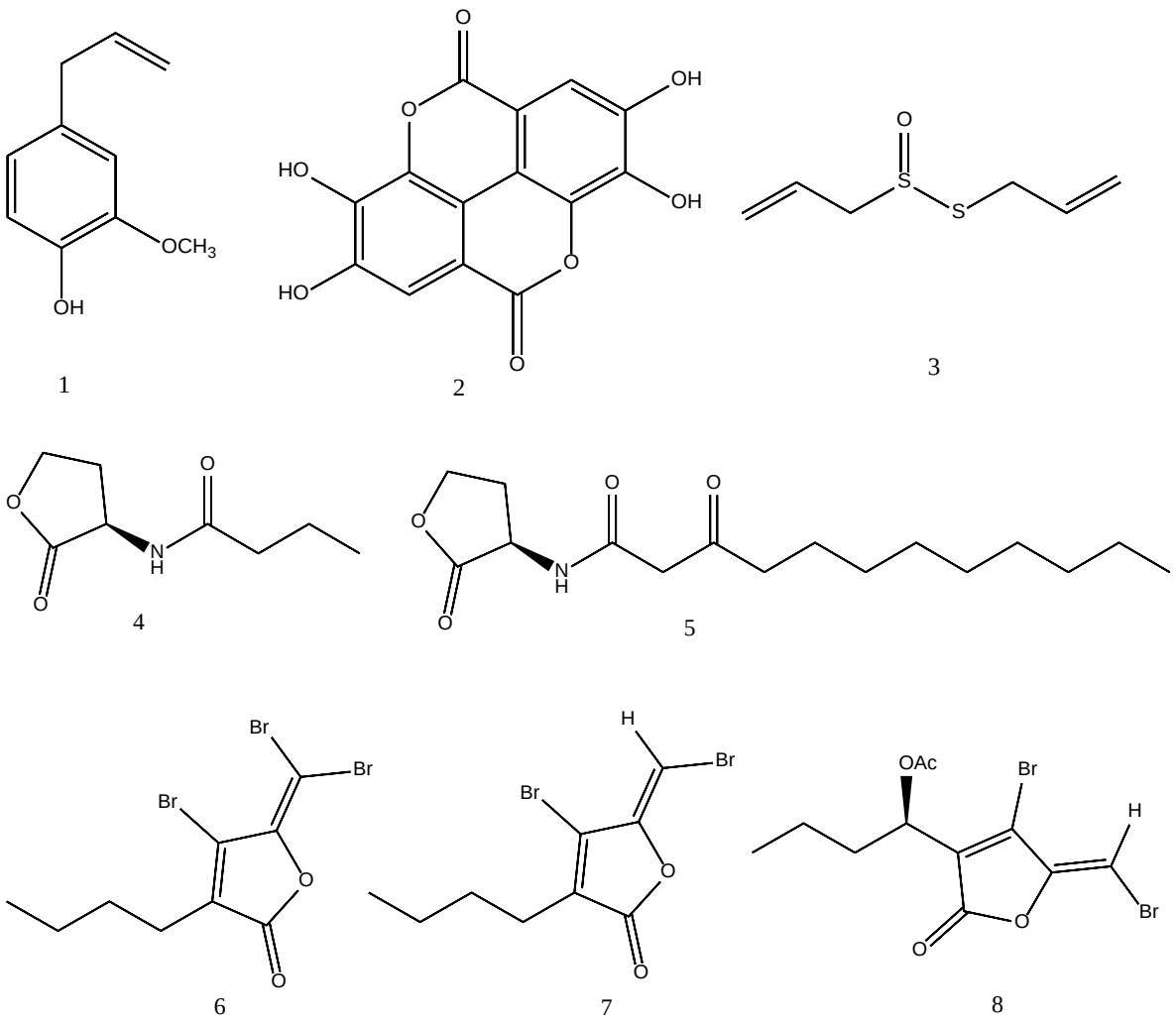

Figure 5.1 Structures of biofilm inhibitors such as eugenol (1), ellagic acid (2) and allicin (3). Structures (4) and (5) are N-acyl homoserine lactones produced by *Pseudomonas aeruginosa* and (5) is also produced by *Chromobacterium violaceum*. Structures (6), (7), and (8) are halogenated furanones produced by marine alga *Delisea pulchra*.

We proposed a study of neotropical plants collected in the rainforests of Costa Rica and Belize, based on the premise that they thrive in humid conditions optimal for biofilm growth. Hence, we hypothesized that they are likely candidates for the possession of compounds that can inhibit biofilm formation and quorum sensing in bacteria.

5.2.Results and Discussion

A large number of plants were collected from various humid regions in Costa Rica and crude extracts were prepared, mainly by Dr. Chieu Anh Kim Ta, of Dr. John T. Arnason's laboratory group, as part of her doctoral studies. The 95% ethanol crude extracts of several plants revealed biofilm inhibitory action.[203] Several plants whose extracts showed biofilm activity were chosen for further investigation, with the hope of isolating and identifying the active components: three from the Piperaceae family (*Piper aequale, Piper papantlense, Piper lanceifolium*), and one from the Melastomataceae family (*Blakea cuneata*).

The phytochemistry of the aerial parts of *Piper aequale* from Trinidad has been previously investigated by Maxwell *et al*. They analyzed the acetone extracts and found ten benzofuranoid neolignans, three of which were new natural products at that time.[204] The chemical composition of the essential oils of *P. aequale* from Costa Rica and its *in vitro* cytotoxic activity have been studied by Setzer, W.N. *et al*.[205] To the best of our knowledge, the biofilm inhibition activity of *P. aequale* has not been studied previous to our investigations.

*P. lanceifolium (*or *P. lanceaefolium* Kunth.*)* is used in folk medicine in Colombia against skin infections that occur after drizzle accompanied by rainbow.[206] The N. Towers group at the University of British Columbia conducted bioassay-guided fractionation of *P. lanceifolium* leaves in search of antifungal activity. They isolated four new benzoic acid derivatives and found that lanceaefolic acid methyl ester and pinocembrin chalcone had anti-fungal activity against *Candida albicans* with a minimal inhibitory concentration of 100 µg mL^{-1} for both.[206] This may indicate the presence of anti-microbial compounds. The composition of the essential oils from the leaves of *P. lanceifolium* collected in Colombia has been studied by Benitez, N. P. *et al*. using gas

chromatography coupled to mass spectrometry. They investigated the antibacterial properties of the essential oils at 20 mg/mL and found it had bioactivity against *Staphylococcus aureus* and *Bacillus subtilis.*[207] Unfortunately, the minimal inhibitory concentration of the essential oils was not assessed and the bioactive compounds were not isolated. The last two plants we screened were *Piper papantlense* and *Blakea cuneata* Standl; to our knowledge, no previous studies have been done on the phytochemical analysis or bioactivities of either plant. Interviews with Q'eqchi' Maya healers described the use of *Blakea cuneata* (Oxlaho chajom) for fever, swelling, insect bites and treatment of digestive system ailments; this may indicate the presence of bioactive compounds.

The second part of the chapter focuses on bioassay-guided fractionation of *Ruptioliocarpon caracolito* L. belonging to the Lepidobotryaceae family. The phytochemistry of *R. caracolito* L. has been previously studied by the Durst and Arnason groups in collaboration with others; the bark was shown to contain novel spiro-triterpenoids.[208-210] The ethanol extracts were found to reduce the growth of European corn borer (*Orstrinia nubilalis* Hubner)[211] and the rice weevil (*Sitophilus oryzae*)[212], which was associated with the spiro-compounds. Additionally, the extracts were shown to have antimalarial activity.[213] More recently, biofilm bioassay on the crude extracts of both the leaves and bark of *R. caracolito* L. displayed biofilm inhibition, and all parts except the bark showed potent quorum sensing inhibition,[203] which prompted us to start bioassay-guided fractionation of the bark of *R. caracolito* L.

This project was carried out in collaboration with Chieu Anh Ta, who performed bioassays and statistical analysis on results presented in this thesis on *P. aequale, P. papantlense, P. lanceifolium, and B. cuneata,* and Laura Picado Abarca, a visiting student from Universidad Nacional de Costa Rica who performed biofilm bioassays on *R. caracolito* L.

5.2.1. *Piper aequale* leaves

The ethanol extracts of the leaves of *P. aequale* were chromatographed on silica gel using elution gradients hexane-EtOAc (100:0 to 0:100) and EtOAc-MeOH (100:0 to 50:50). Ten fractions were collected and assayed. One of the fractions, AG-1-1I, with similar quorum sensing activity to positive control *N*–decanoyl–L–homoserine lactone (C10-HSL), was further chromatographed to afford a solid whose ^{1}H NMR and ^{13}C NMR data (Table 5.1, Figure 5.4 and Figure 5.5) was consistent with the structure of the known tetrahydrofuran lignin grandisin (Figure 5.2). The ^{1}H NMR values of the isolated material compared well with the published values. Grandisin was initially isolated from *Litsea grandis*[214]; other sources of grandisin include, but are not limited to, the leaves of *Piper solmsianum,*[215,216] *Cryptocarya crassinervia,*[217] leaves and stem bark of *Aglaia leptantha,*[218] the leaves and stems of *Kadsura longipedunculata,*[219] and from twigs of *Virola surinamensis* Warb.[220] This compound is reported to have potent *in vitro* activity against the trypomastigote form of *Trypanosoma cruzi* Chagas,[221] and anti-inflammatory activity *in vitro.*[222]

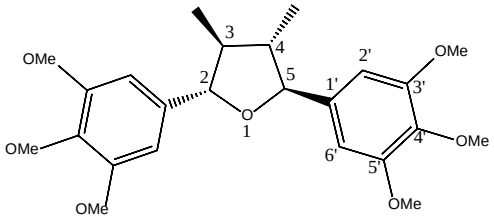

Figure 5.2 Structure of grandisin isolated from leaves of *Piper aequale,* fraction AG-I-1I.

Quorum sensing assays of *P. aequeale* (Figure 5.6) showed that grandisin fractions were about half as active as the positive control *Delisea pulchra* extract. Although some of the fractions (AG-1-1C, D, G and W) exhibited bioactivities (9-10 mm) that were similar to another positive control (C10-HSL) (10.2 mm), they were still relatively low compared to *Delisea pulchra*, which has higher quorum sensing ability (15.9 mm). The ^{1}H NMR of the most active fraction AG-1-1W (Figure 5.3) suggests the presence of fatty acids, due to high intensity peaks in the aliphatic region

of the spectrum; normally, a peak at approximately 0.88 ppm accounts for a terminal CH_3 and 1.3-1.4 ppm for $(CH_2)_n$-and the peak at 2.33 ppm, which may account for CH_2 alpha to COOH. Perhaps a carbohydrate-containing compound may also be present, as suggested by the peaks in the 3.5-4.0 ppm region.

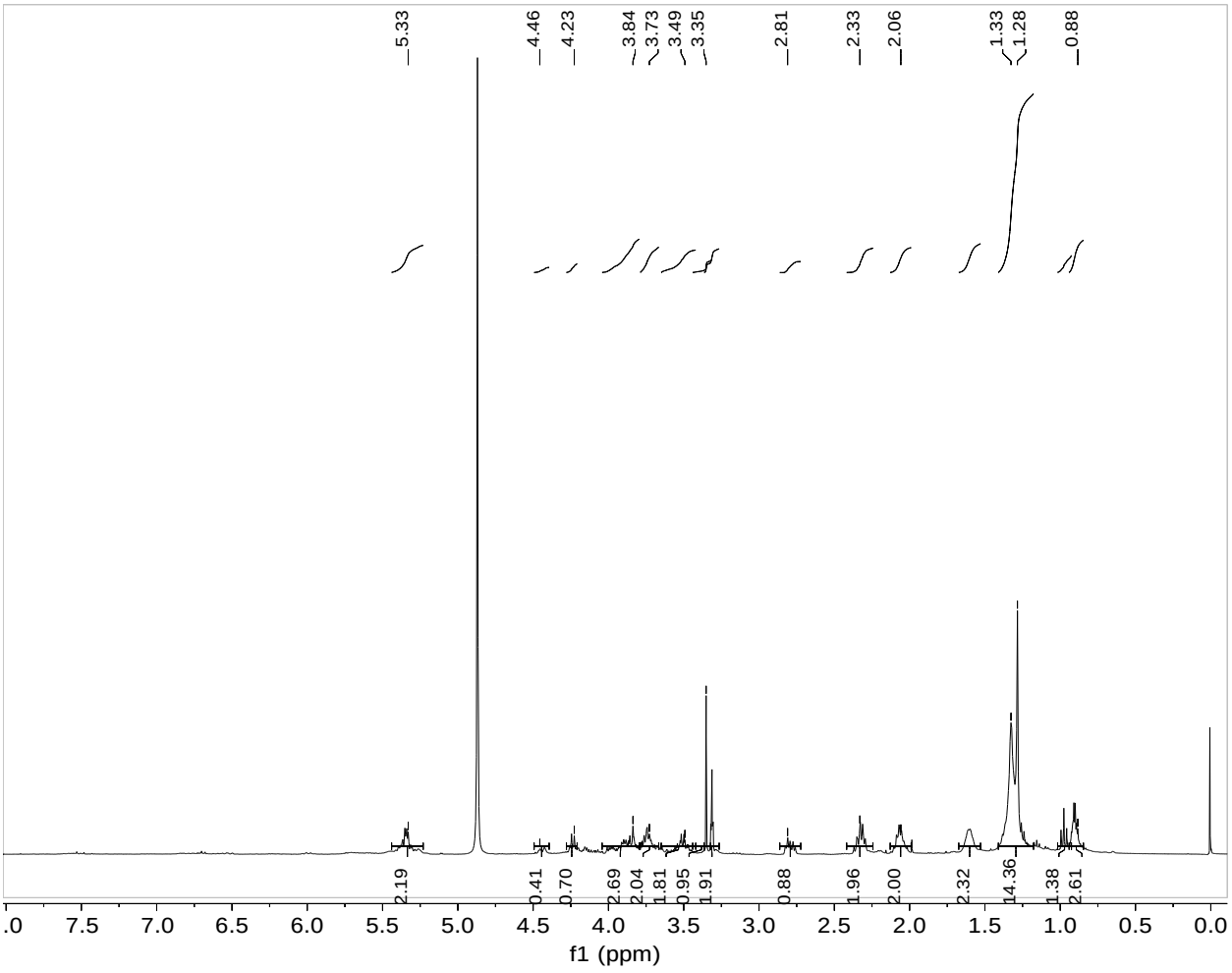

Figure 5.3 ^{1}H NMR of the most active fraction, AG-I-1W of *Piper aequale* leaf extract, $MeOD_4$.

It is recognized that the ^{1}H NMR of the isolated grandisin shows some impurities and that the purity of the sample is likely in the 85-90% range (i.e., peaks at 1.24, 1.59, 2.04, and 6.58 ppm). Since the quorum sensing inhibitory activity of this material was not very high, it was decided not to spend time on additional purification.

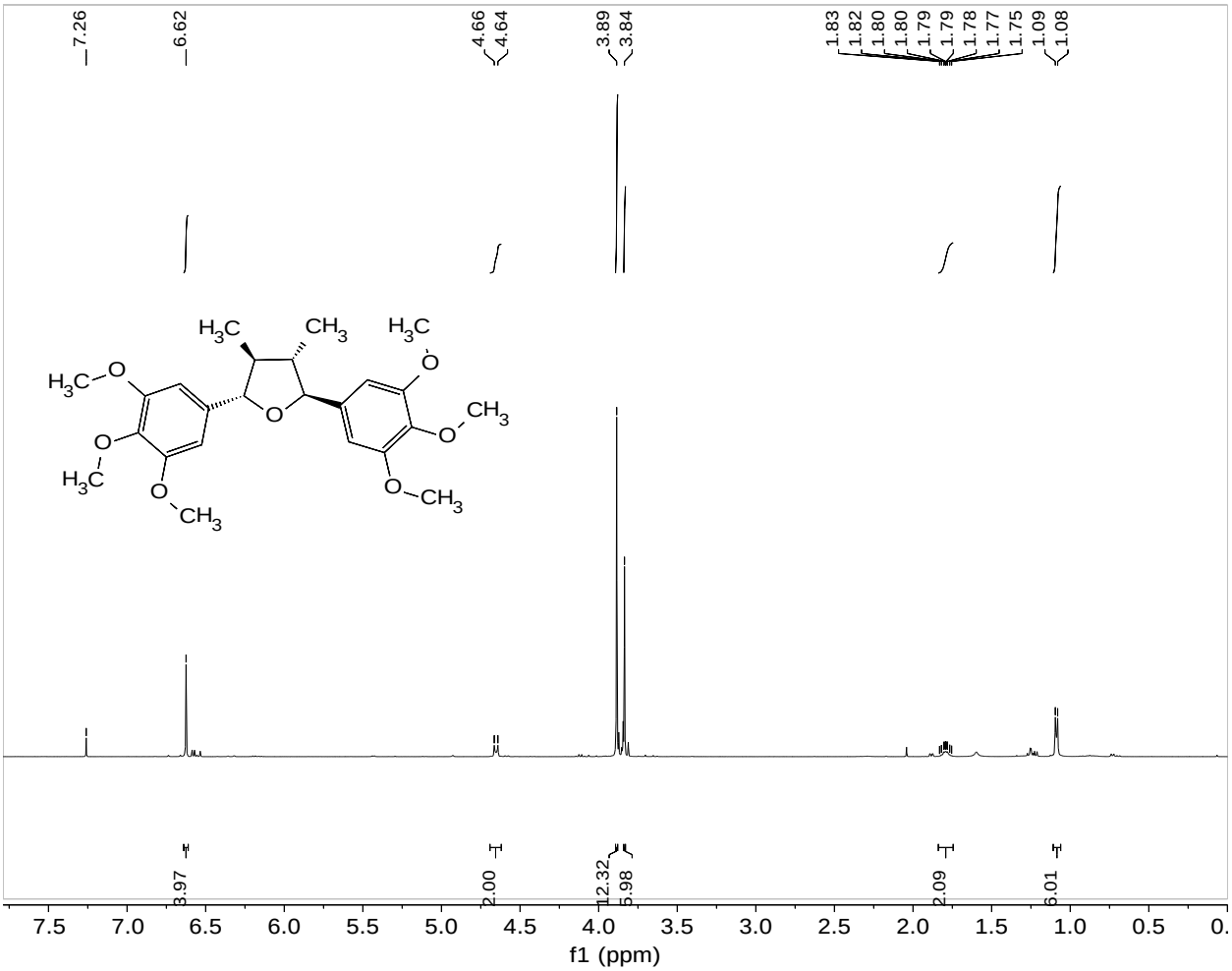

Figure 5.4 ^{1}H NMR of grandisin extracted from *P. aequale*, fraction AG-I-1I, after secondary column.

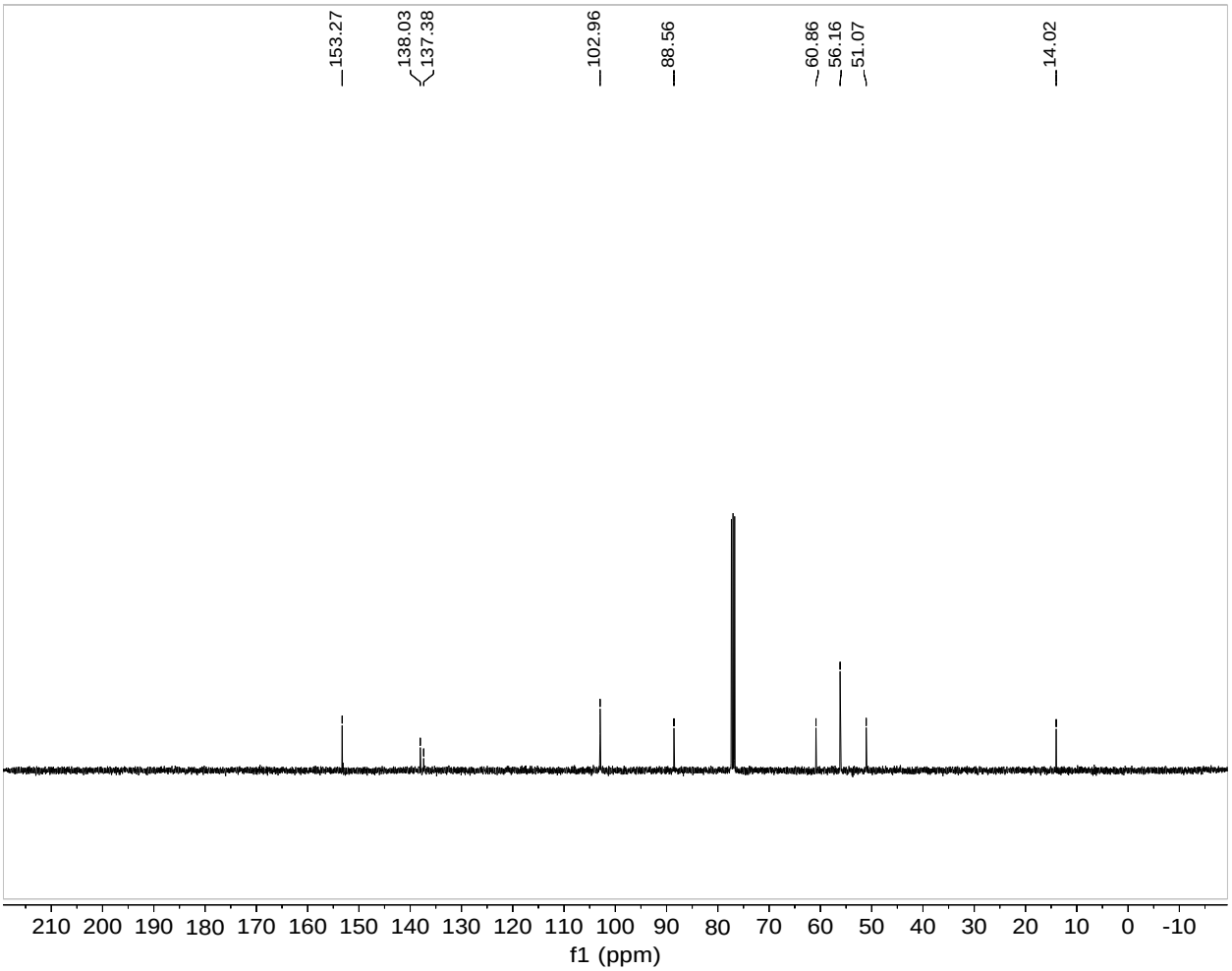

Figure 5.5 ^{13}C NMR in $CDCl_3$ of grandisin extracted from *P. aequale* leaves, fraction AG-I-1I, after secondary column.

Table 5.1 Observed δ_H and literature[214] δ_H of grandisin

Position	**Observed δ_H[a]**	**Literature δ_H[b]**	**Observed δ_C[a]**
2, 5	4.65 (d, J=9 Hz, 2H)	4.6 (d, 2H)	88.56 (2C)
3, 4	1.75-1.83 (m, 2H)	1.8 (m, 2H)	51.07 (2C)
Methyl H/C	1.09 (d, J=6 Hz, 6H)	1.1 (d, 6H)	$\underline{C}H_3$:14.02 (2C)
Aromatic H/C	6.62 (s, 4H)	6.58 (s, 4H)	1’ (137.38, 2C) 2’, 6’ : (102, 4C) 3’, 5’ (153.27, 4C) 4’ (138. 03, 2C)
Methoxy (-OCH_3)	3.84 (s, 6H), 3.89 (s, 12H)	3.75 (18H)	3’,5’ ($O\underline{C}H_3$): 56.16 (4C) 4’ ($O\underline{C}H_3$): 60. 86 (2C)

a-400 MHz

b-100 MHz, δ calculated by subtracting 10.0ppm-τ

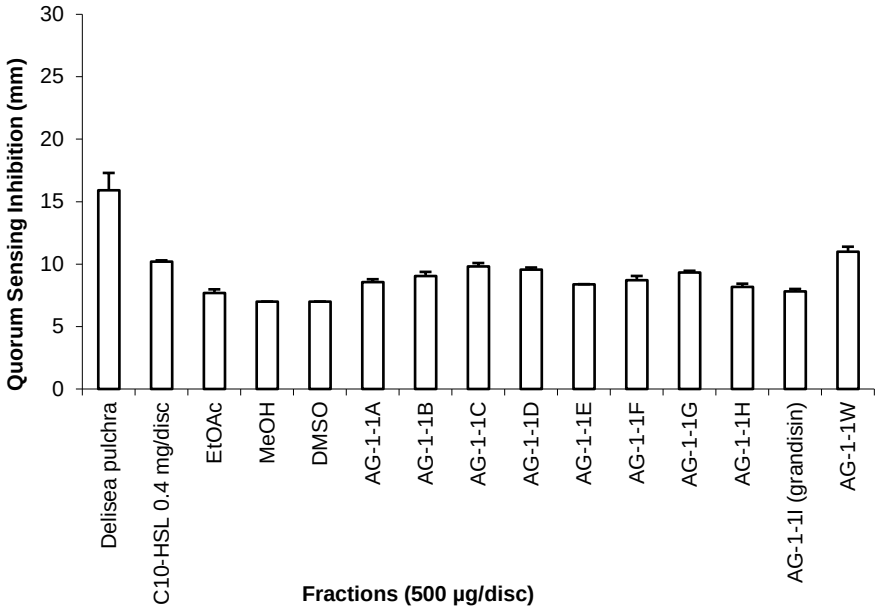

Figure 5.6 Mean ± S.E.M. quorum sensing assay by *Piper aequale.*
Fractions tested at 500 µg/disc in *Chromobacterium violaceum* ATCC 12472 compared to the positive controls *Delisea pulchra* (Greville) Montagne extract (1 mg/disc) and C10-HSL (400 µg/mL). N=3, disc diameter= 7 mm. Chieu Anh Ta performed bioassays and data analysis.

5.2.2. *Piper papantlense* leaves

Piper papantlense leaves and stem extract was fractionated by column chromatography and tested in quorum sensing bioassays. Eleven fractions of increasing polarity were collected starting with hexane-EtOAc (100:0 to 0:100) and ending with EtOAc-MeOH (100:0 to 50:50). The yields of the fractions are reported in Table 5.8 (Materials and Methods) and quorum sensing assays are presented in Figure 5.7. Although some of the fractions, such as AG-2-2B, C and D, were more active than one of our controls (C10-HSL (10.2 mm)), their quorum sensing activities were lower than the *Delisea pulchra* extract. The activity of this fraction was not considered significant enough to pursue the investigation of this plant any further. Further characterization of this plant's phytochemistry may be interesting since a small amount of literature is available on it.

The most active fractions, AG-2-2B, C and D, are complex mixtures based on NMR data, most likely containing long chain fatty acids including aromatics, among other compounds. The quorum sensing inhibitory activities of these fractions are similar to those of *P. aequale*; further investigation of these may lead to the discovery of compounds that are similarly potent with C10-HSL.

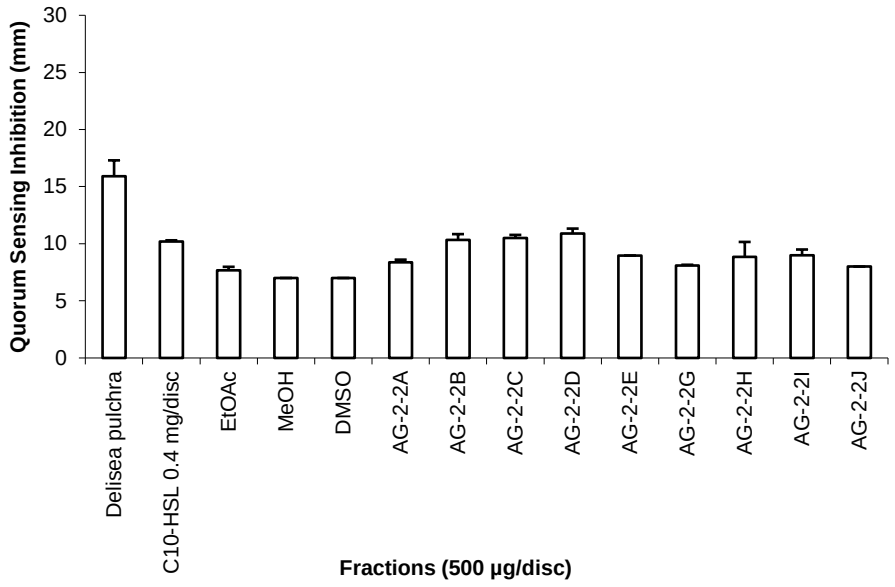

Figure 5.7 Mean ± S.E.M. quorum sensing assay by *Piper papantlense.*
Fractions tested at 500 µg/disc in *Chromobacterium violaceum* ATCC 12472 compared to the positive controls *Delisea pulchra* (Greville) Montagne extract (1 mg/disc) and C10-HSL (400 µg/mL). N=3, disc diameter= 7 mm. Chieu Anh Ta performed bioassays and data analysis.

5.2.3. *Piper lanceifolium* leaves

The 95% ethanol extracts of the leaves and stems extract of *Piper lanceifolium* were investigated next. The yields of the fractions are presented in Table 5.9 (Materials and Methods) with the corresponding quorum sensing bioassays presented in Figure 5.8. A number of fractions, such as AG-3-3B, AG-3-3C, and in particular AG-3-3L, showed quorum sensing inhibition activity

ranging from 10 mm to 12 mm, which were comparable to the standard positive controls *Delisea pulchra* (15.90 ± 1.4 mm at 1 mg/disc) and C10-HSL (10.20 mm ±0.1). Further investigations of these fractions led to the identification of dillapiol and elemicin (Figure 5.9). Dillapiol was observed by ^{1}H NMR in fraction AG-3-3C, D, E, and F. The ^{1}H NMR of fraction AG-3-3-E indicates almost pure dillapiol. The data suggests that dillapiol cannot be the most active compound since AG-3-3-E, which contains mostly dillapiol, was less active than some of the other fractions.

Elemicin was observed by ^{1}H NMR in fractions AG-3-3F and G, with fraction G containing the highest amounts of this compound (Figure 5.12). Table 5.2 and Table 3.1 present the observed and literature values for dillapiol and elemicin, respectively. Both dillapiol and elemicin have been previously reported to have antimicrobial activities.[223,224] Elemicin has been reported in the essential oils of *P. lanceifolium* collected in Colombia. Furthermore, anti-Candida[225] and anti-*Neisseria Gonorrhoeae*[226] antimicrobial activity of *P. lanceifolium* has been reported by the Towers group while studying Colombian medicinal plant extracts. They were also able to pinpoint some of the activities to specific compounds consisting of flavonoids and chalcone derivatives. In our assays, although the dillapiol and elemicin fractions displayed quorum sensing inhibitory activities comparable to the C10-HSL control, the non-polar fractions B and C and the polar fraction L had the highest activities, which suggests that the strong quorum sensing inhibitory action cannot be attributed to the two identified compounds and further phytochemical studies will be needed in order to identify the compounds.

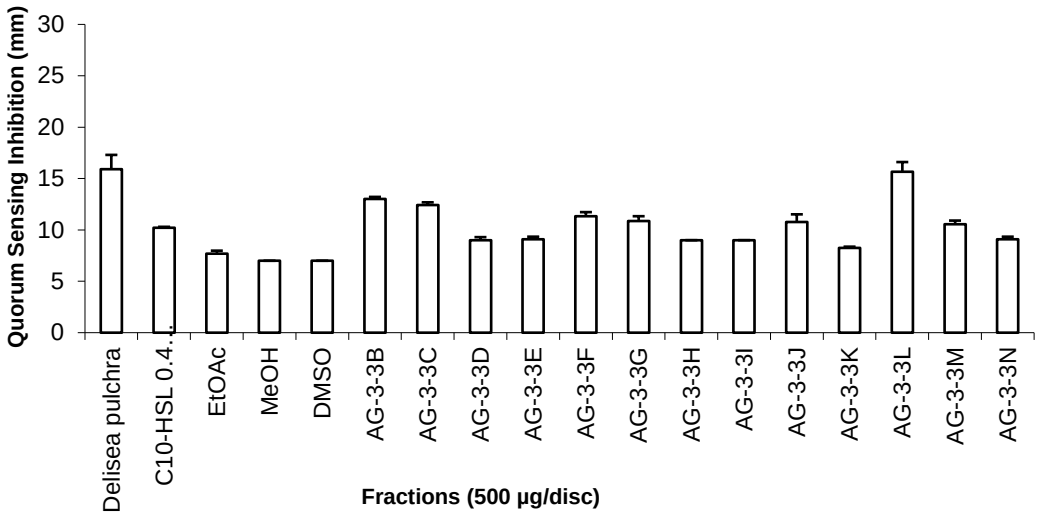

Figure 5.8 Mean ± S.E.M. quorum sensing assay by *Piper lanceifolium* leaves.
Fractions tested at 500 µg/disc in *Chromobacterium violaceum* ATCC 12472 compared to the positive controls *Delisea pulchra* (Greville) Montagne extract (1 mg/disc) and C10-HSL (400 µg/mL). N=3, disc diameter= 7 mm. Chieu Anh Ta performed bioassays and data analysis.

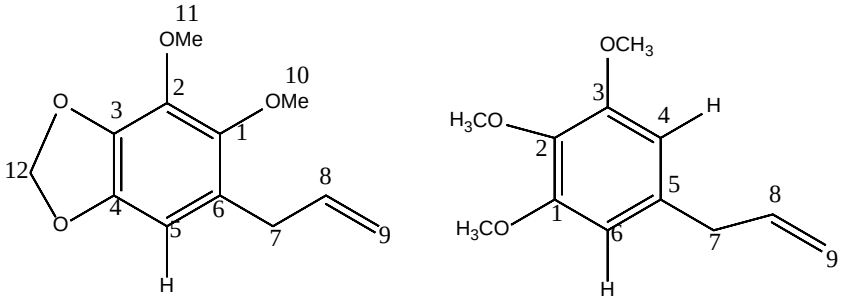

Figure 5.9 Structure of dillapiol (left) and elemicin (right), which was extracted from *Piper lanceifolium*.

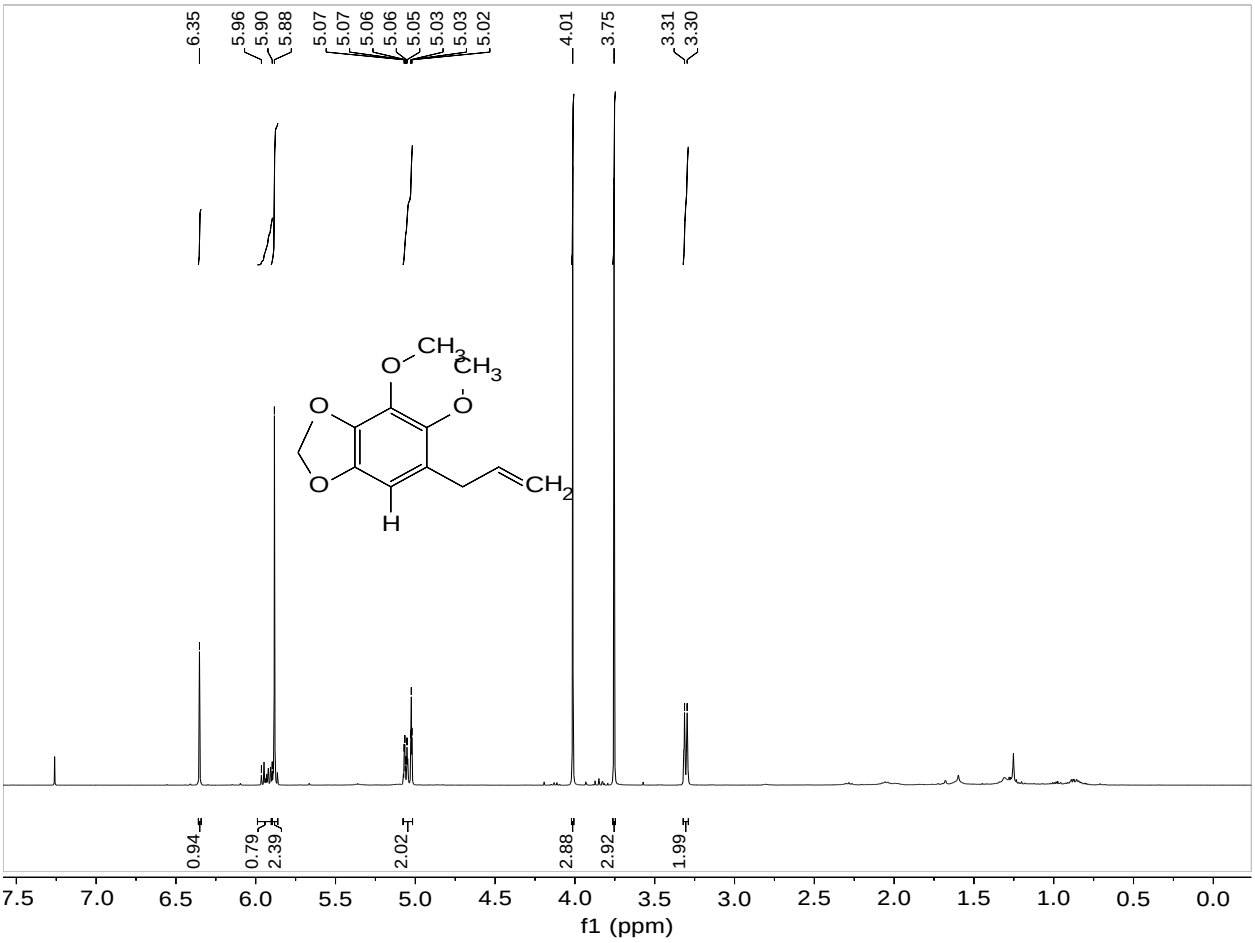

Figure 5.10 ^{1}H NMR of dillapiol isolated from *Piper lanceifolium* leaves, fraction AG-3-3E.

Table 5.2 ^{1}H NMR of dillapiol compared to literature values[227]

Position	Observed δ_H[a]	Literature δ_H[b]
1	-	-
2	-	-
3	-	-
4	-	-
5	6.35 (s, 1H)	6.37 (s, 1H)
6	-	-
7	3.33 (d, J=6.7 Hz, 2H)	3.33 (d, J=6.6 Hz, 2H)
8	5.90-5.96 (m, 1H)	5.97-5.91 (m, 1H)
9	5.02-5.07 (m, 2H)	5.02-5.10 (m, 2H)
10	3.75 (s, 3H)	3.77 (s, 3H)
11	4.01 (s, 3H)	4.02 (s, 3H)
12	5.88 (s, 2H)	5.9 (d, J=9.1 Hz, 2H)

a-400 MHz (H)

b-750 MHz (^{1}H NMR)

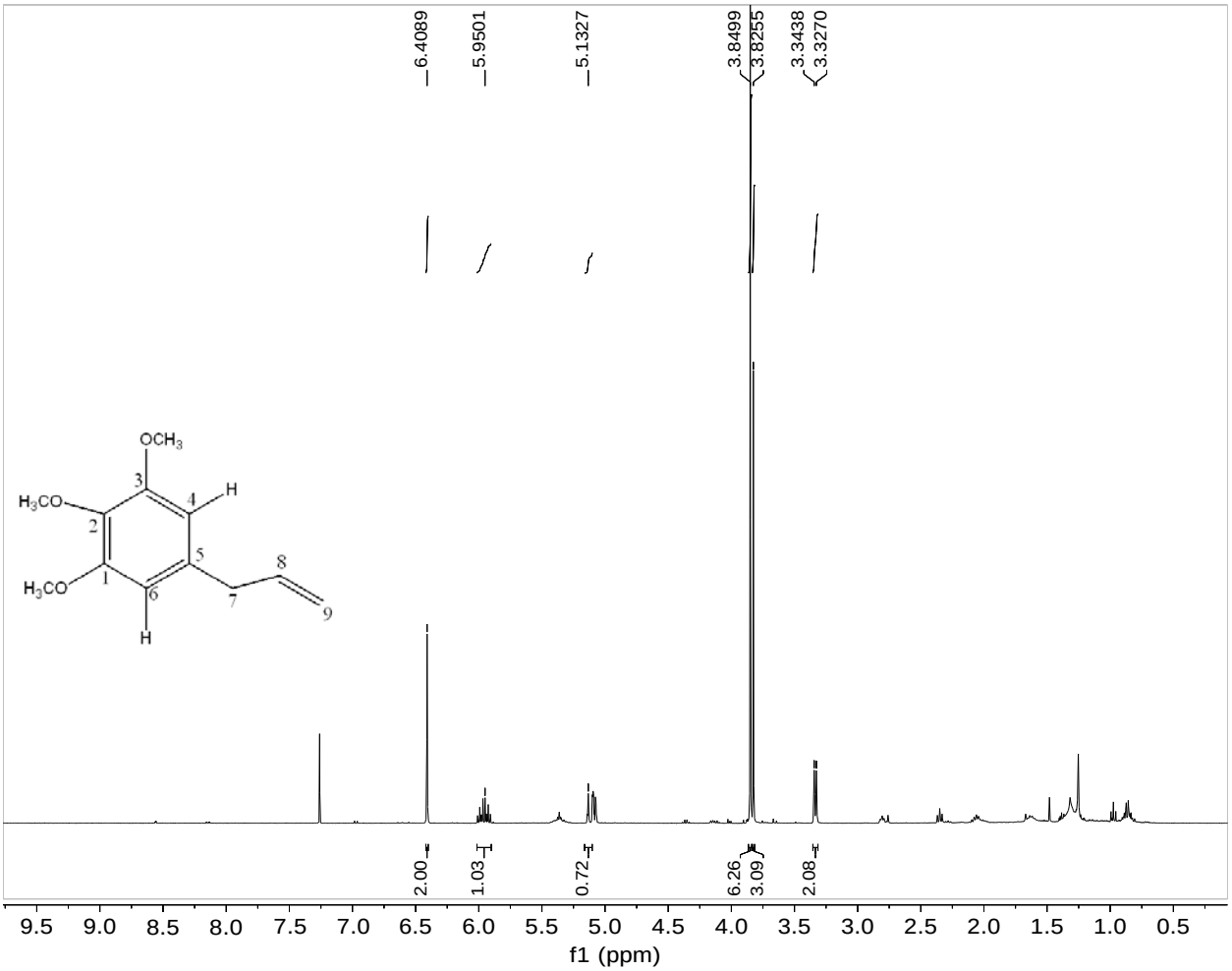

Figure 5.11 ^{1}H NMR of fraction AG-3-3G containing elemicin as the major constituent.

Table 5.3 ^{1}H NMR of elemicin, observed and literature[223] values

Position	Observed δ_H[a]	Literature δ_H[b]
1	-	-
2	-	-
3	-	-
4	6.41 (s, 2H)	6.41 (s, 2H)
5	-	-
6	6.41 (s, 2H)	6.41 (s, 2H)
7	3.34 (d, J=6.7 Hz, 2H)	3.32 (d, J=6.5 Hz, 2H)
8	5.96 (m, 1H)	5.95 (m, 1H)
9	5.13 (m), 5.08 (m) (2H)	5.12 (m, 1H), 5.08 (m, 1H)
1, 3 ($OC\underline{H_3}$)	3.85 (s, 6H)	3.85 (s, 6H)
2 ($OC\underline{H_3}$)	3.83 (s, 3H)	3.82 (s, 3H)

a-400 MHz
b-500 MHz

The most bioactive fraction, AG-3-3L, afforded a dark green compound isolated in 2.7% of the total yield from the ethanol extract of *P. lanceifolium* leaves. Based on ^{1}H NMR data, the fraction is not pure. It contains elemicin as one of its major constituents and at least one other compound (Figure 5.12). The presence of a fatty acid is suggested by the peaks in the upfield region of the spectrum, ~1.4-0.88 ppm for $-(CH_2)_n-$ and terminal $-CH_3$ in combination with the peak at 2.3 ppm (HOOC**CH_2**-).

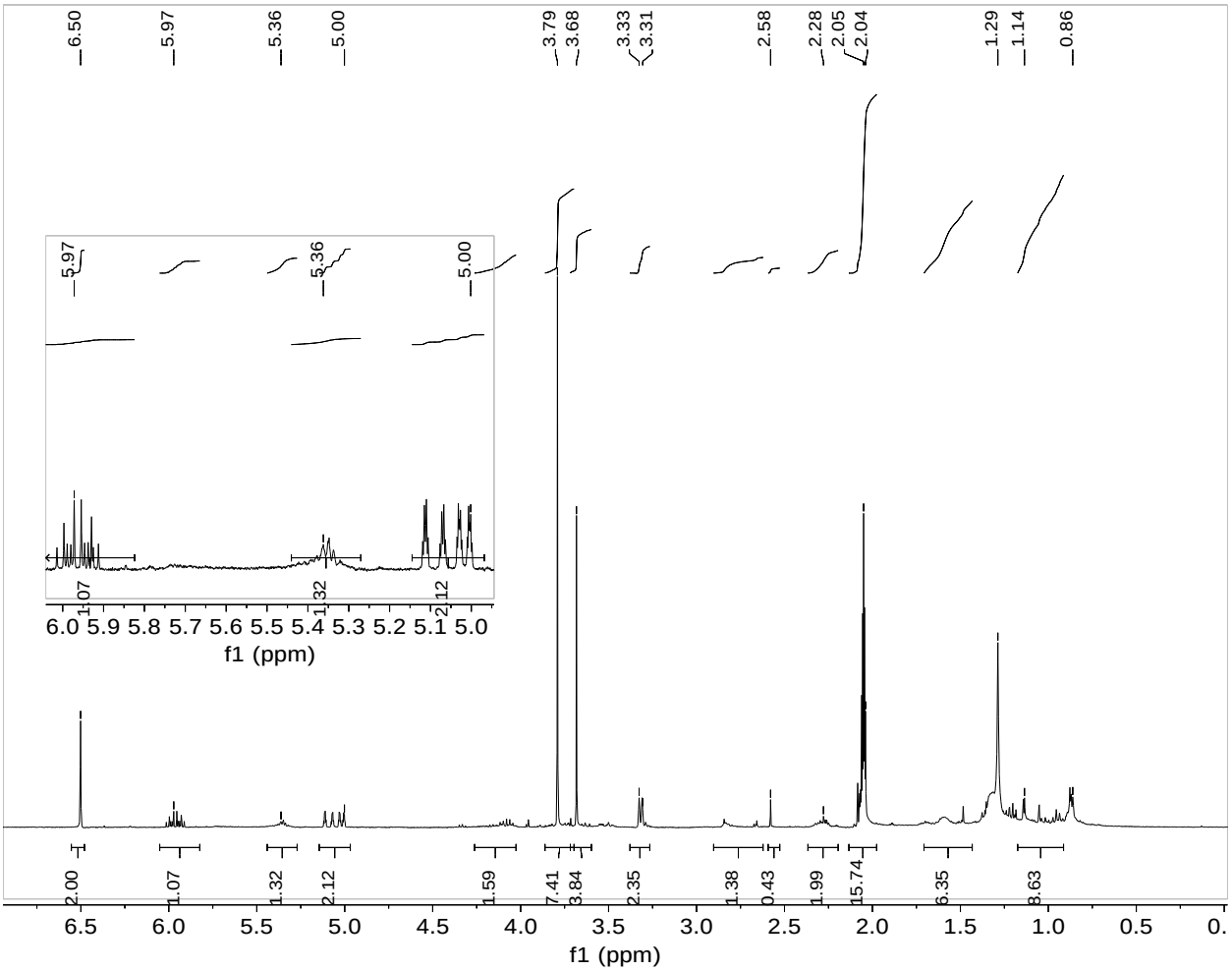

Figure 5.12 ^{1}H NMR of the most bioactive fraction AG-3-3L, from *Piper lanceifolium* leaves extract.

5.2.4. *Piper lanceifolium* fruit

Finally, the fruit of *P. lanceifolium* collected in Costa Rica was ground, extracted and fractionated by column chromatography starting with 100% hexane and ending with 50% methanol. Preliminary analysis of the ^{1}H NMR of several fractions suggests two chromone derivatives, (1) and (2). Fraction M, which contained the highest amount, was chromatographed twice more; however, in the end no pure compound was obtained. Its ^{1}H NMR data (Figure 5.15) was compared to that of the published literature in Table 5.4. Further studies such as ^{13}C NMR and mass spectrometry (MS) need to be done in order to confirm the chemical structure.

Later, steam distillation followed by extraction with ethyl acetate of *P. lanceifolium* fruit was performed by Dr. Tony Durst. The crude essential oil was re-dissolved in acetone and the mixture was separated by preparative plate chromatography with 70% ethyl acetate- 30% hexane containing a few drops of acetic acid. A spot with an R_f value of 0.35 was characterized as chromone derivative (2) based on ^{1}H and ^{13}C NMR literature values (Figure 5.13 Table 5.4). Tertiary carbon 4a and carbonyl carbon 9 was not observed by ^{13}C NMR; this may be because the sample was not run for a long enough time (5 min was used for the experiment). Lanceifolic acid methyl ester (3) and its carboxylic acid (4) (Figure 5.13) are also suggested to be present in one of the fractions separated by plate chromatography; however, the fraction is complex and needs to be further purified.

These prenylated benzoic acid derivatives (1) and (2) were tested by the G.H.N. Towers group against *Candida albicanis*; unfortunately, they did not display inhibitory activity.[206] However, Lanceifolic acid methyl ester (3) (Figure 5.13) displayed inhibitory activity against the fungus at 100 µg/mL.[206] Biofilm and quorum sensing bioassays of this fraction against different strains of bacteria are suggested for future work to investigate the bioactivity of these chromone derivatives, as chromones constitute part of a structurally diverse group of secondary metabolites and they are interesting to study due to the biological activities of their natural sources.[228] Chromone derivatives have also been found to have anti-inflammatory, anti-neoplastic, immunomodulatory and analgesic properties.[228] As *Piper lanceifolium* has been found to have other biological activities, it may be worthwhile to further characterize the chemical components of this plant.

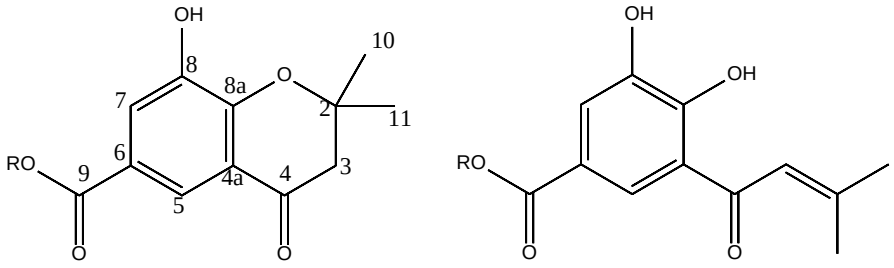

1 R=CH_3
2 R=H

3 R=CH_3
4 R=H

Figure 5.13 Chromone derivative (1) cyclolanceaefolic acid methyl ester, the methyl ester of (2) 8-hydroxy-2,2'-dimethyl-6-carboxychroman-4-one found in *Piper lanceifolium* fruit extract, fractions M and N. Lanceifolic acid methyl ester (3) and its carboxylic acid derivate (4), were previously identified in *P. lanceifolium* by the Towers group.

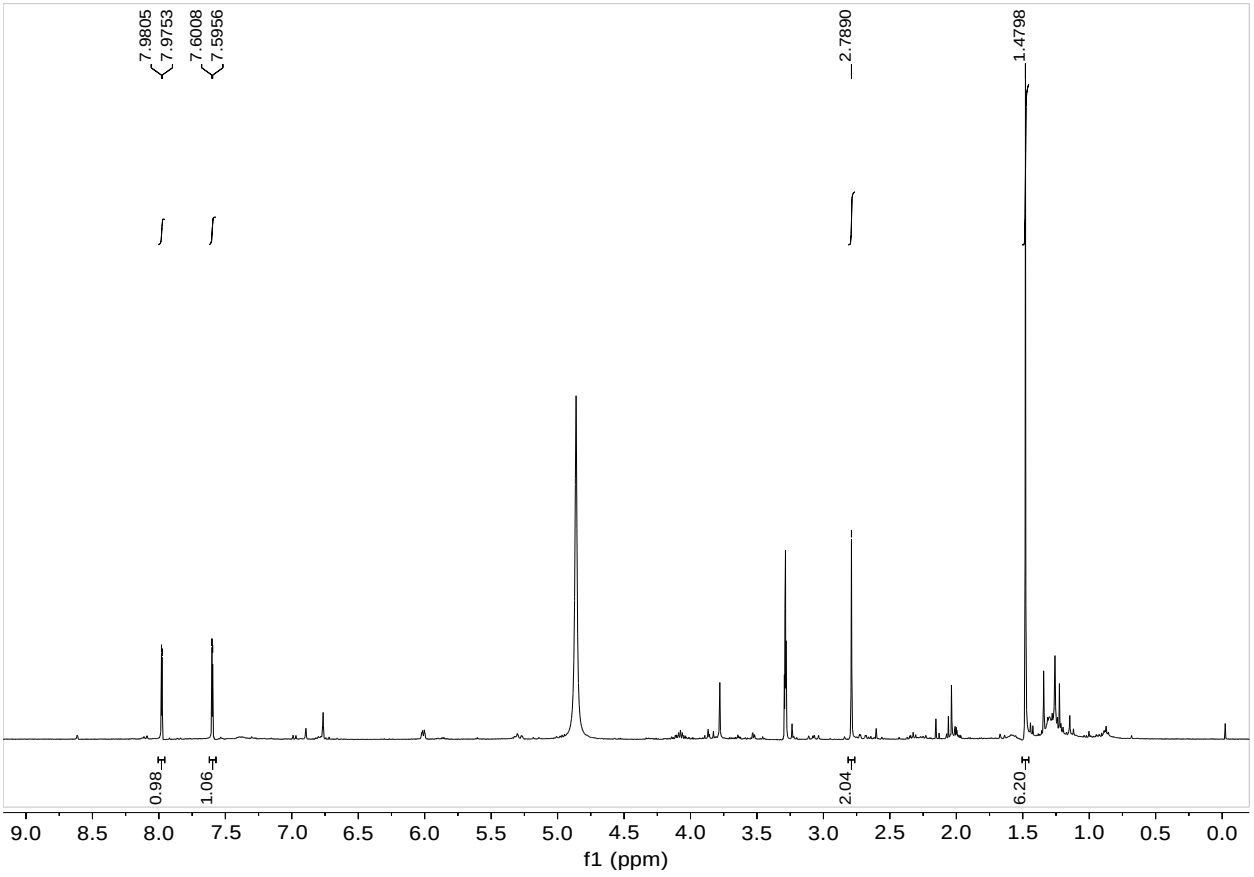

Figure 5.14 ^{1}H NMR of primary column fraction AG-I-5M of *Piper lanceifolium* fruit extract, $MeOD_4$.

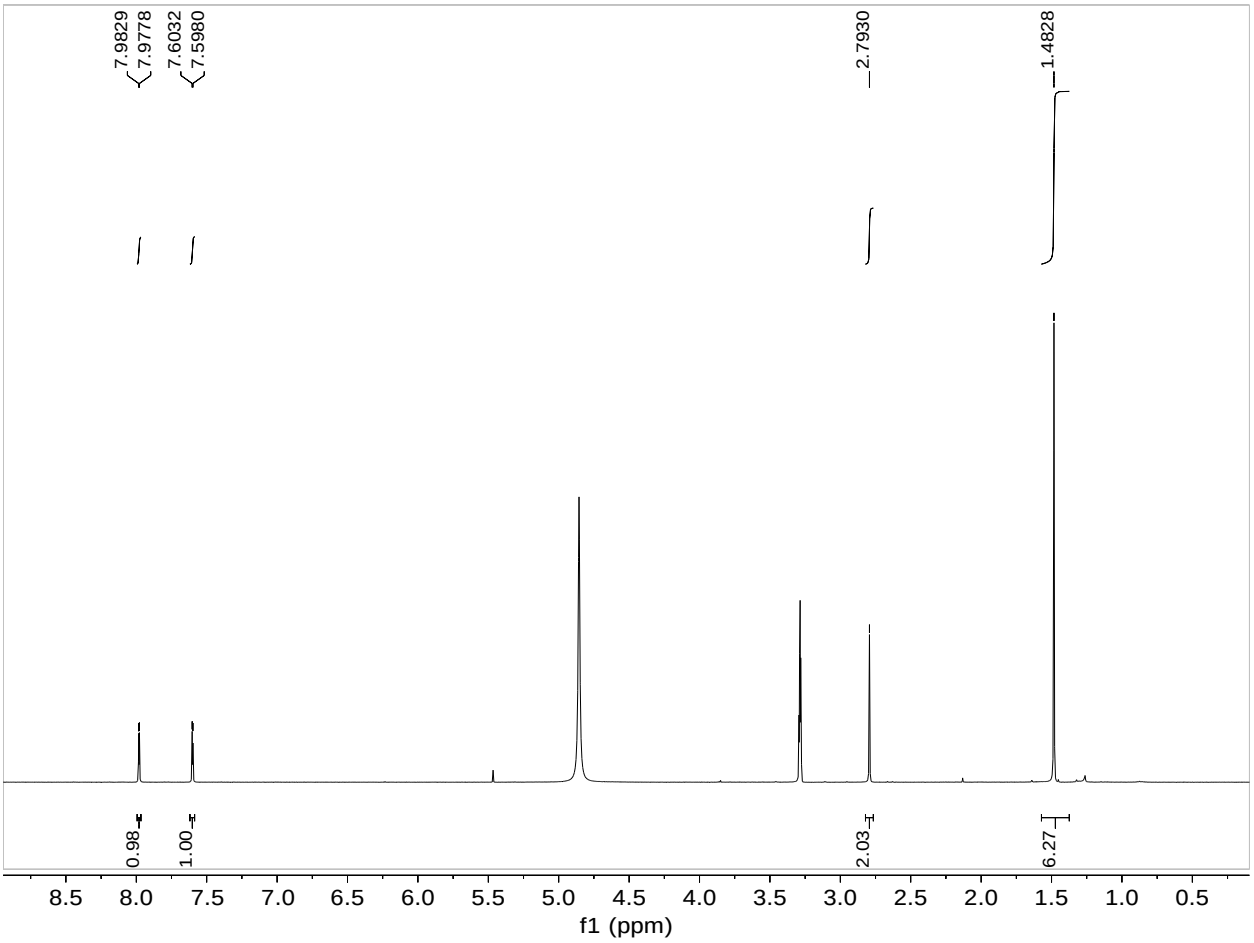

Figure 5.15 ^{1}H NMR chemical shifts of chromone (2) from *P. lanceifolium* essential oil, $MeOD_4$.

Table 5.4 ^{1}H NMR observed and literature[206] chemical shifts of chromone derivatives (1) and (2).

	1		**2**		**2**	
Position	Observed δ_H[a]	Literature δ_H[a]	Observed δ_H[a]	Literature δ_H[a]	Observed δ_C[a]	Literature δ_C[a]
2					80.9	81.7 (s)
3	2.79 (s)	2.83 (s)	2.79 (s)	2.82 (s)	48.1	48.9 (t)
4					190.9	191.8 (s)
4a					-	123.7 (s)
5	7.98 (d, 2.1)	7.96 (d, 2.1)	7.98 (d, 2.0)	7.96 (d, 2.1)	118.8	119.6 (d)
6					120.3	121.1 (s)
7	7.60 (d, 2.1)	7.62 (d, 2.1)	7.60 (d, 2.1)	7.62 (d, 2.1)	120.6	121.4 (d)
8					147.0	147.8 (s)
8a					151.7	152.6 (s)
9					-	169.9 (s)
10,11	1.48 (s)	1.48 (s)	1.48 (s)	1.48 (s)	25.6	26.5 (q)
CH_3O	3.28 (s)	3.86 (s)				

5.2.5. *Blakea cuneata* Standl leaves

To our knowledge, our work, in collaboration with the Arnason group, is the first to observe the bioactivities of *Blakea cuneata* Standl, a plant belonging to the Melastomataceae family. Quorum sensing bioassays of the fractions obtained upon initial silica gel column chromatography of the 95% ethanol extract of the leaves are shown in Figure 5.16. The amounts of material obtained in individual fractions are shown in Table 5.11 (Materials and Methods). The results clearly show that the highest quorum sensing inhibitory activities, ranging from 20.3 ± 0.4 to 26.5 ± 0.4 mm at 500 μg/disc, were in the very polar fractions (BC-I-O to U) that were eluted using solvent system of decreasing ethyl acetate to methanol ratios of (4:1 to 1:1).

We were intrigued by these preliminary results since the activity in these fractions was much higher than that of *D. pulchra* extract (15.9 ± 1.4 mm at 1 mg/disc) but also concerned since the high polarity of the active fractions strongly suggested the likelihood of glycosides or possibly even polysaccharides compounds, with which our research group had essentially no experience.

The less polar fractions exhibited quorum sensing bioactivities that were closer to that of the C10-HSL control.

The polar fractions had shown stronger biofilm inhibition than the non-polar fractions (Figure 5.17) with activities ranging from 24.4 ± 4.4 to 58.6 ± 6.5 % relative to standard control (50% methanol). The very active fraction BC-I-U showing high quorum sensing activity weighed 1.61 g. Since it was also a mixture, as shown by thin layer chromatography (TLC) and NMR, further fractionation was done using preparative high-performance liquid chromatography (HPLC). The HPLC fractions were obtained in only small amounts. They were therefore tested only in a biofilm bioassay at a lower concentration and showed activity similar to the non-HPLC-fractionated fractions from the original column (Figure 5.17).

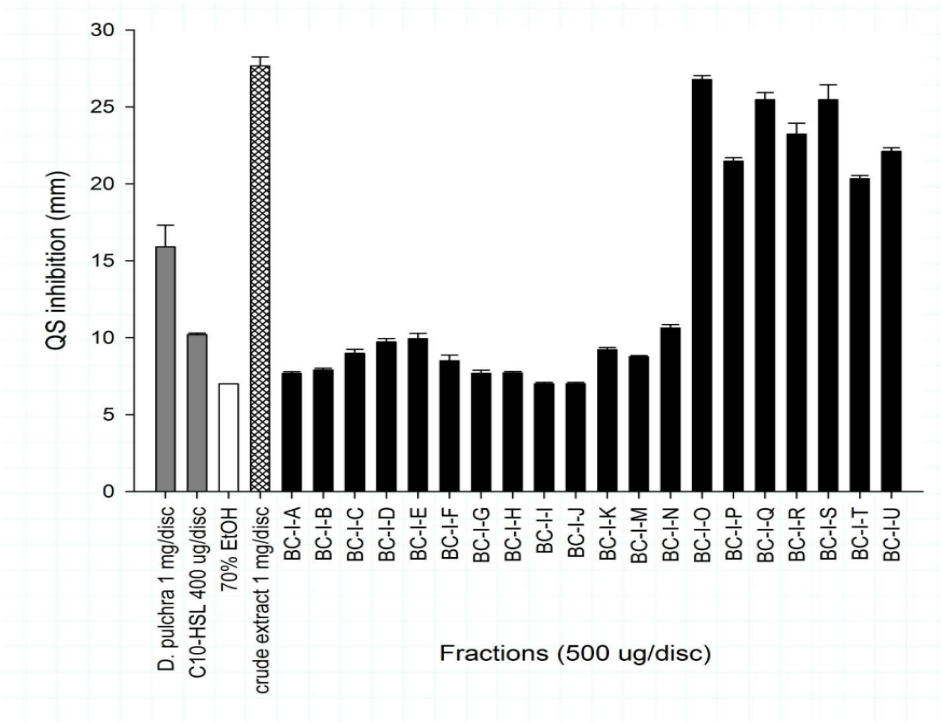

Figure 5.16 Mean ± S.E.M. quorum sensing assay by *Blakea cuneata* Standl.
Fractions tested at 500 µg/disc in *Chromobacterium violaceum* ATCC 12472 compared to the positive controls Dilsea pulchra (Greville) Montagne extract (1 mg/disc) and C10-HSL (400 µg/mL). N=3, disc diameter= 7 mm. Data reproduced with permission from Chieu Anh Ta's thesis, who performed bioassays and data analysis.

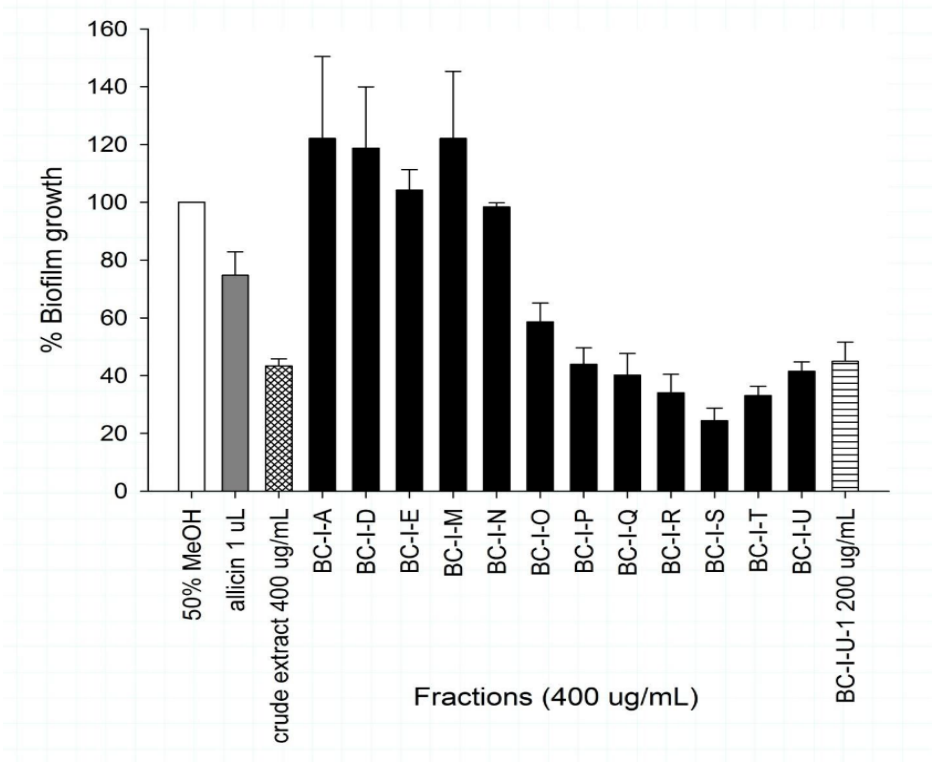

Figure 5.17 Average biofilm growth ± S.E.M. of *Pseudomonas aeruginosa* PA14 relative to vehicle control (50% MeOH) in *Blakea cuneata* Standl. crude extract (400 µg/mL) and BC-I primary (400 µg/mL) and secondary (200 µg/mL) fractions.
Positive control, allicin tested at 1 µL/mL or 1.08 mg/mL. N=3. Figure reproduced with permission from Chieu Anh Ta's thesis. Chieu Anh Ta performed bioassays and data analysis.

The ^{1}H NMR spectrum was useful insofar as we were able to suggest the possible presence of several structural features of the main compound in the active fraction (Figure 5.18). Despite our efforts at purification, the fraction was still a mixture, as observed by HPLC and NMR, which showed some impurities, potentially "grease" or column bleeding (0.88 ppm and 1.29 ppm). The observed ^{1}H NMR chemical shift peaks between ~3-4 ppm are in agreement with the presence of one or more carbohydrate units in these compounds, since -C**H**-O resonances are typically found in the 3.4 and 4.0 ppm range.[229] In carbohydrate NMR spectroscopy, the better resolved signals are usually those of the anomeric protons δ 4.4-5. Based on our NMR spectra, a doublet at 4.46 ppm with a J constant of 7.8 could account for axial-axial coupling and another doublet at 5.1 ppm with a J constant of 3.6 Hz could account for axial-equatorial or equatorial-equatorial coupling,

and indicates the presence of anomeric hydrogens in our sample. The ^{13}C NMR data supports these conclusions, showing the expected peaks between 60-80 ppm (Figure 5.19). The chemical shift of an anomeric carbon in an α-linkage is ~97-101, whereas the anomeric carbon in a β-linkage is generally higher at ~103-105.[229] The observed peak at 102 suggests a β-linkage in the carbohydrate. The quorum sensing and bioassay results were very exciting and led us to focus our efforts on isolating and identifying the compounds responsible for the activities.

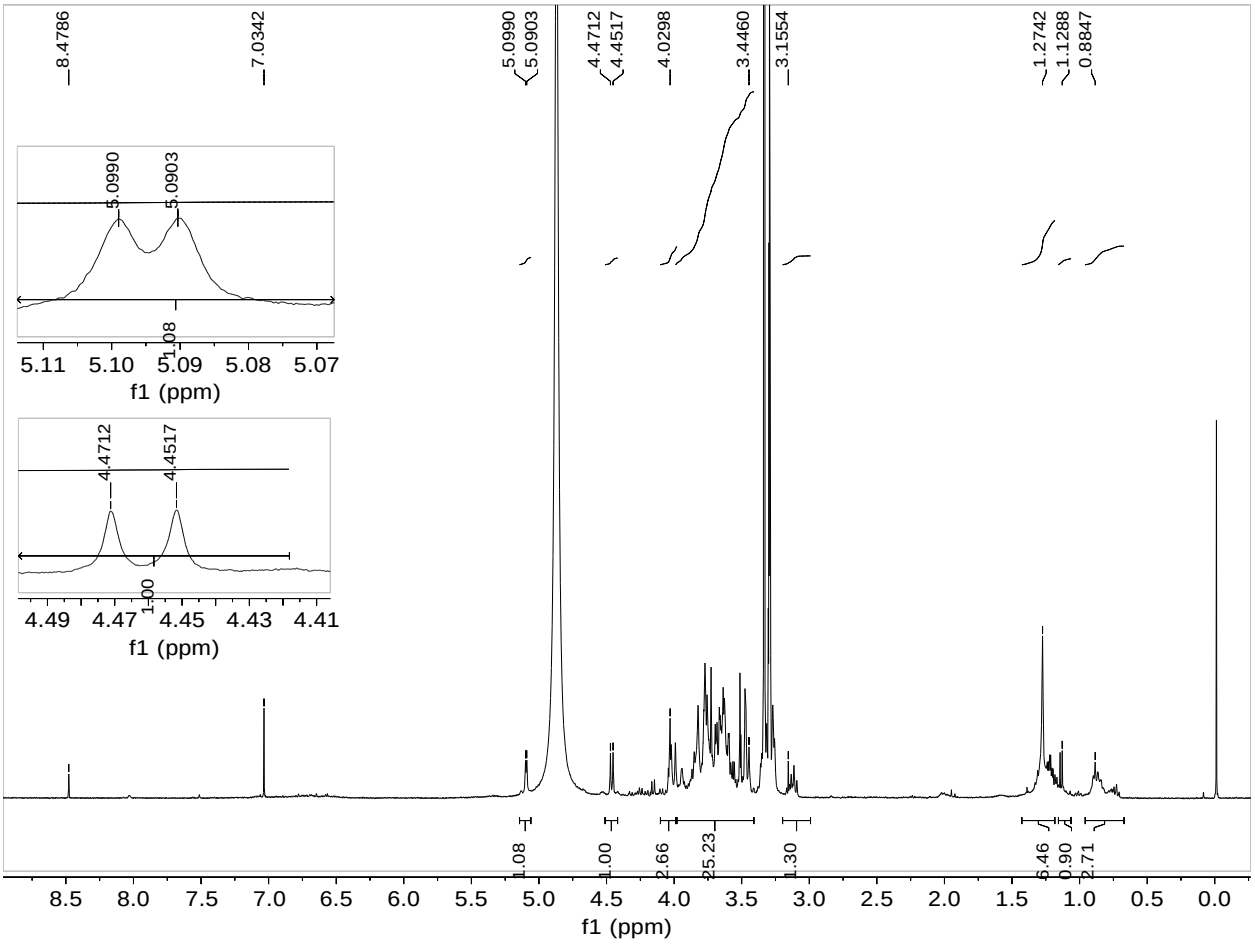

Figure 5.18 ^{1}H NMR of *Blakea cuneata* fraction BC-I-U-1, $MeOD_4$.

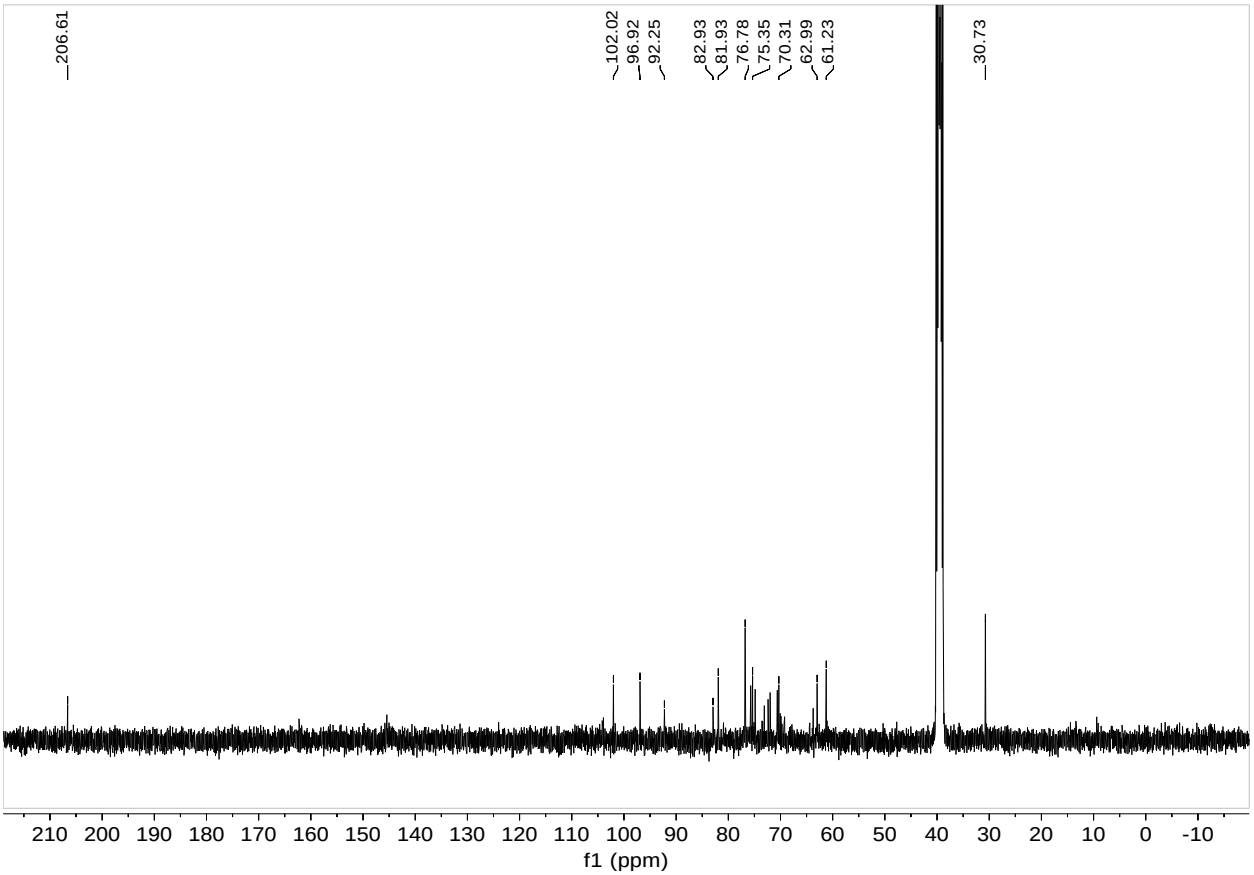

Figure 5.19 ^{13}C NMR of *Blakea cuneata* fraction BC-I-U-1, $MeOD_4$.

In order to facilitate the characterization, several acetylation reactions were performed on the polar fraction BC-I-S (Figure 5.21), whose NMR was very similar to the bioactive fraction BC-I-U. It was anticipated that acetylation would facilitate two aspects. First, it would reduce significantly the polarity of the polyhydroxyl compounds in the mixture and probably aid in the isolation of the individual components of the mixture. Secondly, we expected the NMR, ideally of any pure compound, to allow us to determine the number of primary and secondary hydroxyl groups in the molecule based on the number and the integration of the acetate methyl signals in the 1.9-2.1 ppm region of the spectrum. Additionally, acetylation of polyhydroxy compounds typically results in sharper peaks, since the product is now likely to be soluble in $CDCl_3$ rather than water. Finally, we expect a displacement of the original C**H**-OH from approximately 3.3-4 to 3.6 to about 5 ppm.

Indeed, the ^{1}H NMR of the acetylation product obtained from fraction BC-I-S after column chromatography showed these expected changes. Based on the integration of various peaks in the spectrum, seen in Figure 5.21, it appears that this fraction consists of a number of compounds in addition to a major component. It is clear that there is an absence of any significantly sized aromatic peaks in the spectrum. Since the majority of the peaks can be assigned to either -**CH**-OAc and O-C(O)-**CH$_3$** peaks, a reasonable conclusion is that the material is a polysaccharide. Approximately 13 hydrogens are observed between δ 3.5 and 5.5, which would account for the hydrogens connected to the carbohydrate backbone, and at δ 2 there are approximately 16 hydrogens that account for the acetylated hydroxyl groups (accounting for approximately 5 hydroxyl groups).

A typical acetylated disaccharide consisting of, for example, glucose and galactose units would have a ratio of 14 hydrogens bonded to carbon carrying oxygen versus 8 acetyl groups. This is a very different ratio than the approximately 13 to 5 ratio seen for the unknown compound. A structure such as a glycosylated glycerol, shown below (Figure 5.20), having a CH-O- to acetate group ratio of 26 to 12 or 13 to 6 is somewhat more consistent with the overall NMR spectrum but still not correct. The sharp singlet at 3.5 ppm is likely due to an O-CH_3 group.

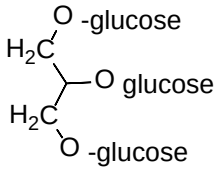

CHO- to acetate ratio

26 :12

Figure 5.20 Structure of glycosylated glycerol with CHO- to acetate group ratio

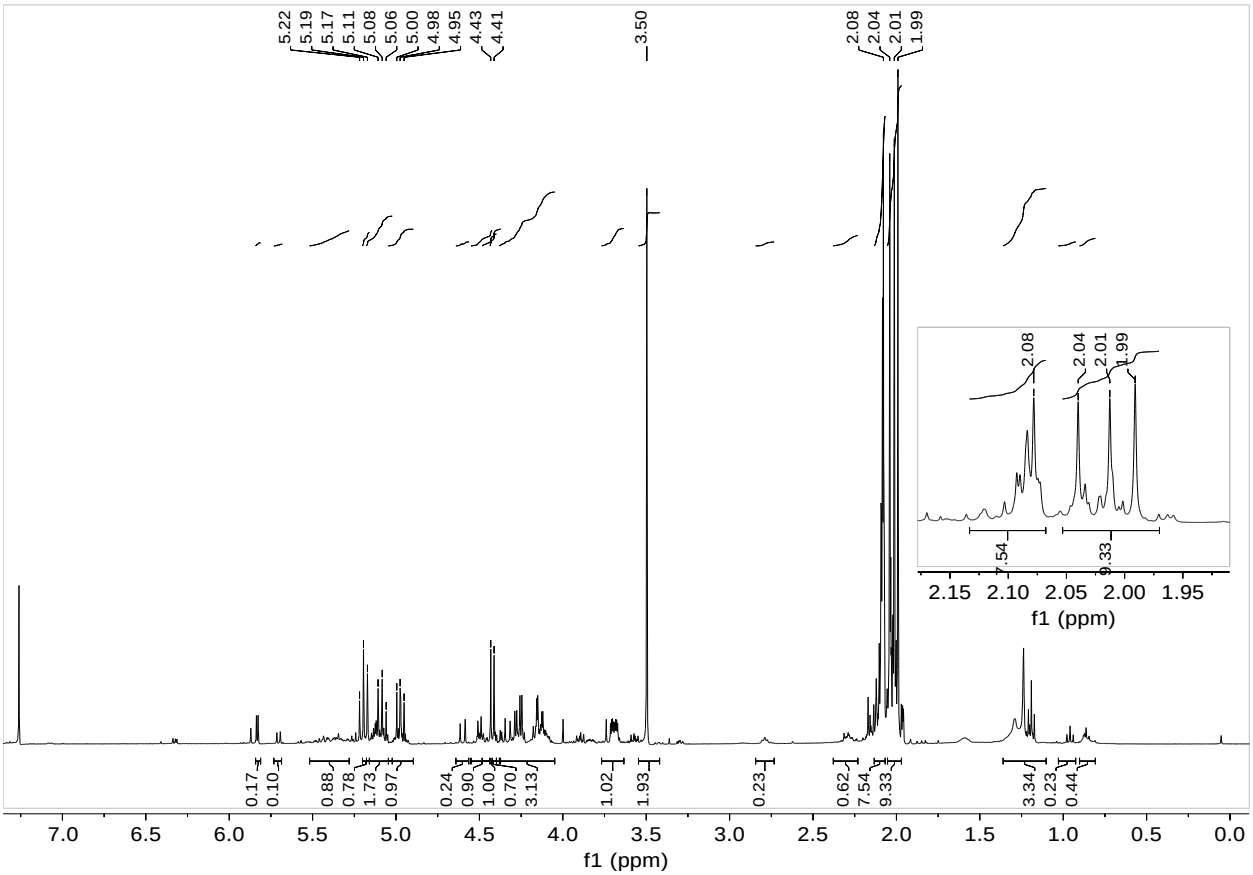

Figure 5.21 ^{1}H NMR of acetylation of *Blakea cuneata* fraction BC-I-S.

Due to the low final yield of the fractions from the primary column on the leaf extract of *Blakea cuneata*, another column was performed. This time, it was performed on 19 g of *Blakea cuneata* leaves extract, starting with 100% hexane and ending with 50% methanol. The mass yields are presented in Table 5.12 (Materials and Methods) and the corresponding bioassays in Figure 5.22. Fraction BC-II-N was chromatographed further using a Sephadex column by Chieu Anh Ta. This led to the identification of compound 1, homoplantaginin or hispidulin-7-*O*-glucoside (Figure 5.23, Table 5.5). Biofilm assays unfortunately showed no activity at the highest tested concentration of 150 µg/mL (Figure 5.22). The other fractions collected from the Sephadex column had biofilm inhibitory activities, with values ranging from 41-74% of the 50% MeOH

control. Due to the rareness of such a glycoside with respect to other phenolics, we theorize that this compound could be used as a biomarker of *B. cuneata.*

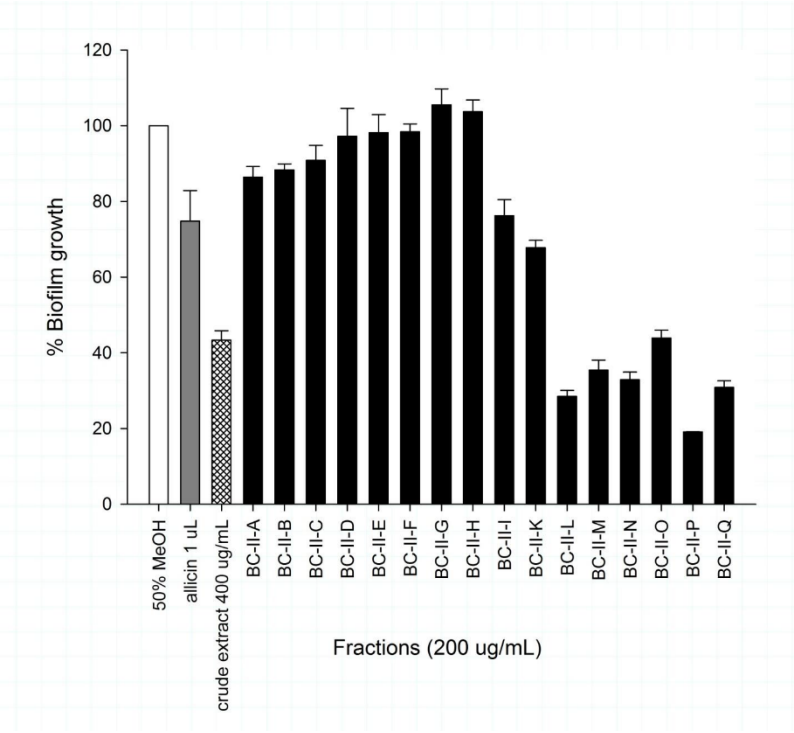

Figure 5.22 Average biofilm growth ± S.E.M. of *Pseudomonas aeruginosa* PA14 relative to vehicle control (50% MeOH) in the presence of *Blakea cuneata* Standl crude extract (400 μg/mL) and BC–II primary fractions (200 μg/mL).
The positive control, allicin was tested at 1 μL/mL or 1.08 mg/mL. N = 3. Figure reproduced from Chieu Anh Ta's thesis with permission. Chieu Anh Ta performed bioassays and analyzed the data.

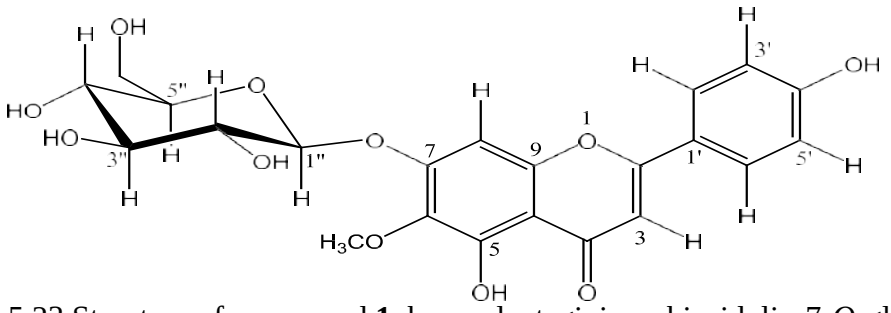

Figure 5.23 Structure of compound **1**, homoplantaginin or hispidulin-7-*O*-glucoside.[203]

Table 5.5 1D and 2D NMR spectroscopic data for compound **1**. NMR analysis was performed by Chieu Anh Ta. Table reproduced from Chieu Anh Ta's thesis with permission.

# C	**Cpos**	**δ_C**	**DEPT**	**δ_H**	**HMBC**
1	*CH_3*O-	61.5	CH_3	3.88, s, 3H	
2	6''	62.6	CH_2	Ha, 3.96, d, *J*=2.2 Hz Hb, 3.72, dd, *J* = 6.0, 12.0 Hz	
3	4''	71.3	CH	3.42, t, *J* = 9.0 Hz	
4	2''	74.8	CH	3.55, m	H-3''
5	3''	78.0	CH	3.55, m	H-4',H-2''
6	5''	78.5	CH	3.53,t, *J* = 8.8 Hz	H-6b''
7	8	95.8	CH	6.94, s	H-2''
8	1''	102.0	CH	5.12,d, *J* = 7.2 Hz	H-2''
9	3	103.7	CH	6.64, s	H-8
10	10	107.5	C		H-8, H-3
11	3', 5'	117.1	2-CH	6.91, d, *J* = 8.8 Hz	H-3',H-5'
12	1'	123.0	C		H-3',H-5'
13	2', 6'	129.7	2-CH	7.87, d, *J* = 8.8 Hz	H-2',H-6'
14	6	134.2	C		H-8, O-CH_3
15	5	154.1	C		
16	7	154.3	C		
17	9	157.9	C		H-1'', H-8
18	4'	163.1	C		H-2', H-6'
19	2	166.9	C		H-3, H-4', H6'
20	4	184.3	C=O		H-3, H-8

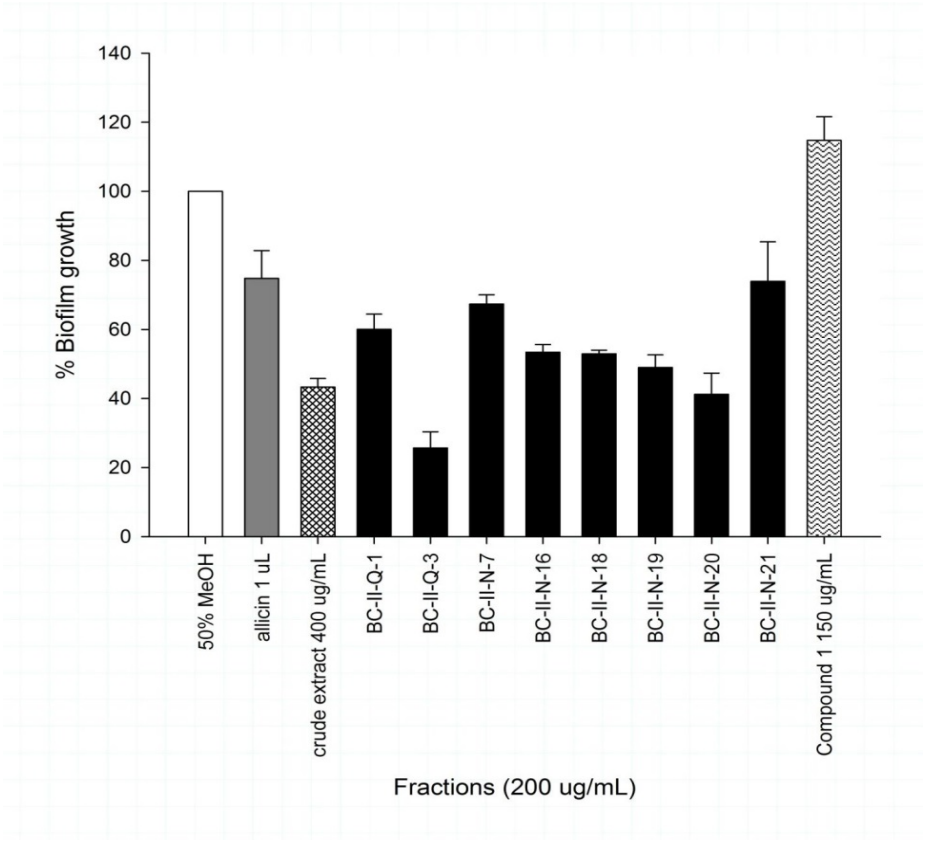

Figure 5.24 Average biofilm growth ± S.E.M. of *Pseudomonas aeruginosa* PA14 relative to vehicle control (50% MeOH) in the presence of *Blakea cuneata* Standl. crude extract (400 μg/mL), BC–II secondary fractions (200 μg/mL), and compound **1** (150 μg/mL). Fractions were compared to the positive control allicin (1 μL/mL or 1.08 mg/mL). N = 3. Figure reproduced from Chieu Anh Ta's thesis with permission. Chieu Anh Ta performed bioassays and analyzed the data.

To avoid further issues of low final amounts of materials, a column was performed on a much larger amount of *B. cuneata* ethanol extract (108 g) starting with 100% hexane and ending with 50% methanol. The yields are described in Table 5.13 (Materials and Methods) and the bioassays in Figure 5.25. Afterwards, 10 g of bioactive material, combined from fractions BC-III-G and H, was purified by secondary column chromatography. The NMR spectra of the bioactive compounds showed that the fractions were again carbohydrate-based. The fractions with sufficient yields were also included in the bioassays shown in Figure 5.25 (BC-III-G+H-81, 83, 84). These

results showed that fractions 81, 83 and 84 had lower inhibitory action than before the secondary column, and so they were not pursued further.

At this point, we took another approach in an effort to purify the compounds from the primary column, and so fraction BC-III-H was separated by preparative HPLC. HPLC chromatograms showed a complex mixture of compounds; the major peak was collected and tested in a biofilm assay, as shown in Figure 5.25 (BC-III-H-1). Again, the biofilm inhibitory activity was lower than that of the unpurified fraction, which leads me to believe that this compound is not responsible for the high bioactivity of the unpurified fraction.

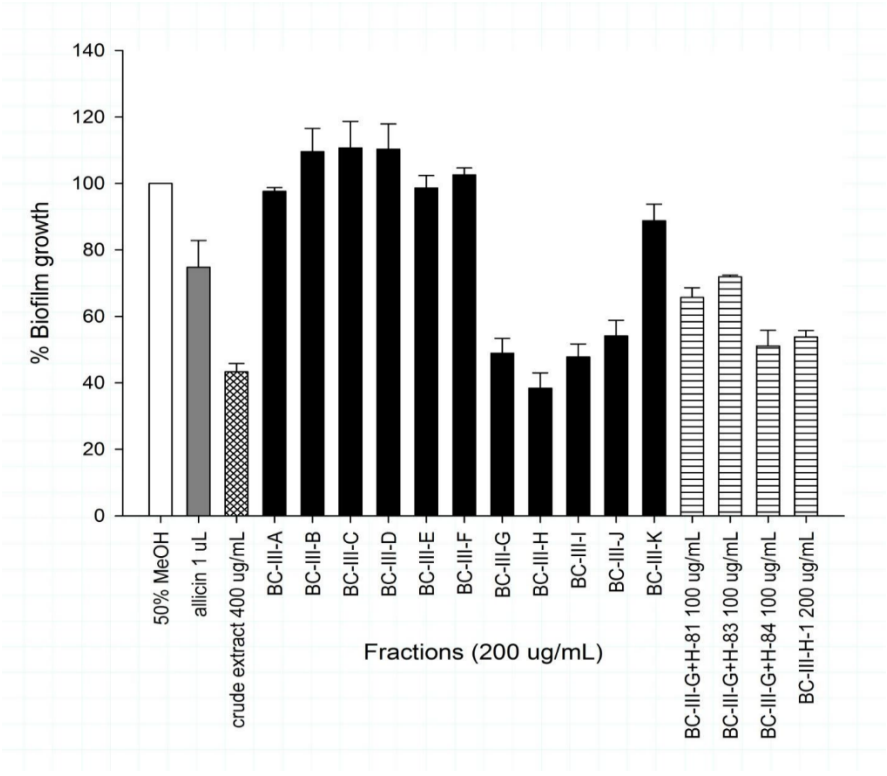

Figure 5.25 Average biofilm growth ± S.E.M. of *Pseudomonas aeruginosa* PA14 relative to vehicle control (50% MeOH) in the presence of *Blakea cuneata* Standl. crude extract (400 µg/mL), and BC–III primary (200 µg/mL) and secondary fractions (100 to 200 µg/mL). Fractions were compared to the positive control allicin (1 µL/mL or 1.08 mg/mL). N = 3. Figure reproduced from Chieu Anh Ta's thesis with permission. Chieu Anh Ta performed bioassays and data analysis.

Due to the polar nature of the fractions, they exhibited low solubility in most solvents for NMR analysis. D_2O proved to be most useful, even if the samples still precipitated after sonication and heating in a water bath prior to NMR analysis. NMR analysis at a higher temperature was explored to check if this would help with the solubility issues; however, no differences were observed between those where the samples were heated at 50°C immediately before analysis with NMR and those which were not.

Next, the 500 MHz NMR was used for analysis. The ^1H NMR spectra of fractions that dissolved are similar, with 3 major peaks in the aromatic region (as seen in fraction BC-III-H-HH), as well as broad peaks in the carbohydrate region 3-4 ppm and broad peaks at approximately 1 ppm that may account for "grease" (Figure 5.26). The NMR spectra of fraction BC-III-H-HH is nearly identical to the NMR spectra of BC-III-H-2, 3 and 4 (except that the peak signals are stronger in some due to solubility issues) when analyzed in D_2O at 500 MHz. However, according to ultra-performance liquid chromatography quadrupole time of flight mass spectrometry (UPLC-QTOF-MS/MS) analysis shown in Table 5.6, there are three different compounds that migrate as separate peaks between 26- 28 min. UPLC–QTOF–MS/MS suggests the presence of high molecular weight compounds with high degrees of unsaturation. Acetylation of one of the higher yielding fractions purified by HPLC was unsuccessfully attempted. Due to the low yields of the fractions collected after preparative HPLC and the low solubility of the compounds, which resulted in low resolution of the NMR spectra, unfortunately we were not able to identify the separated compounds or check their bioactivities, except for the first peak, which showed lower biofilm inhibitory activity than before preparative HPLC. This suggests that it is not the most active compound in the plant sample.

The pattern in the aromatic region of the spectrum in Figure 5.26 looks deceptively simple. The observed coupling constants (1.2 and 6.0 Hz) are suggestive of ortho and meta coupling. The doublet of doublets at about 7.8 and the triplet of doublets centered around 7.4 ppm would fit a di-substituted aromatic system. However, the observed integration ~1: ~1.5: ~3 does not fit partial structure. Again, we are left with the conclusion that the observed pattern is most likely due to a combination of several compounds.

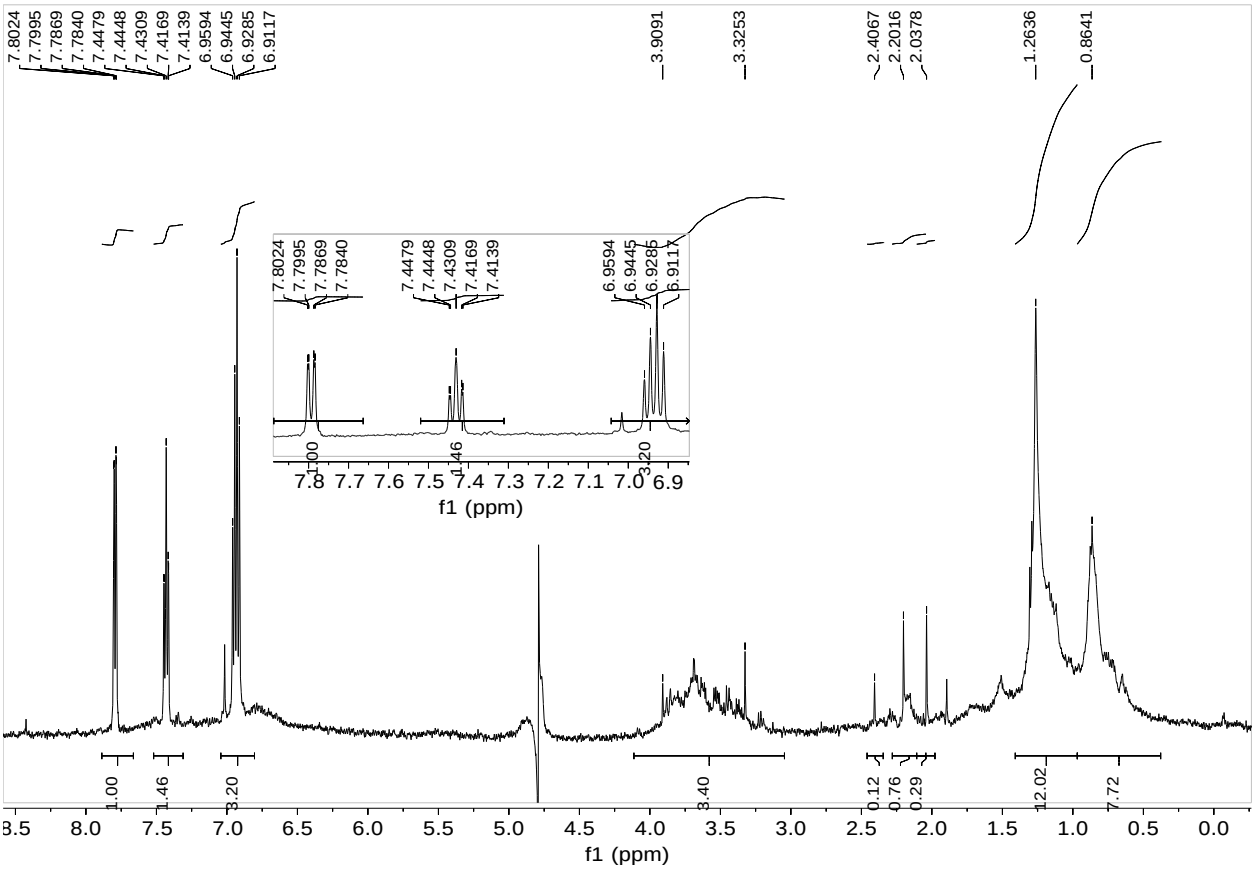

Figure 5.26 ^{1}H NMR of *B. cuneata* fraction BC-III-H-HH, prepared by column chromatography, followed by preparative HPLC. Sample in D_2O, 500 MHz NMR.

Table 5.6 Retention times, yields, masses and elemental composition of BC–III–H secondary fractions from preparative scale HPLC analyzed with UPLC–QTOF–MS/MS by Chieu Anh Ta. Table reproduced and modified with permission from Chieu Anh Ta's thesis.

Fraction	Retention time (min)	Yield (mg)	[M–H]+	Elemental composition	Degree of unsaturation
BC-III-H-1	0-24	381	N/A[a]	N/A[a]	N/A[a]
BC–III–H–2	26.15	2.7	485.1084	$C_{24}H_{21}O_{11}$	15
BC–III–H–3	27.15	2.5	615.1350	$C_{29}H_{27}O_{15}$	16
BC–III–H–4	28.16	2.3	689.3912	$C_{38}H_{57}O_{11}$	11
BC–III–H–5	29.15	2.7	463.1254	$C_{22}H_{23}O_{11}$	12
BC–III–H–6	30.15	1.6	689.3868	$C_{45}H_{53}O_{6}$	20
BC–III–H–7	31.15	1.2	669.1870	$C_{26}H_{27}O_{20}$	14
BC–III–H–8	32.71	1.4	669.1824	$C_{33}H_{33}O_{15}$	18
BC–III–H–9	35.59	2.3	689.3859	$C_{45}H_{53}O_{6}$	20
BC–III–H–10	39.28	2.1	119.1398	$C_{12}H_{18}NO$	5
BC–III–H–11	43.20	1.0	527.3350	$C_{32}H_{47}O_{6}$	10

a: complex

Further work needs to be done in order to identify the bioactive compound(s). Our approach so far has been to acetylate a bioactive fraction, separate the mixture of compounds, and then deacetylate each compound and check by bioassays. Due to the low yields, we were not able to deacetylate and then check for bioactivity and analyze by NMR. Another approach worthy of consideration would be to do a Kupchan partition for the isolation of carbohydrates in the sample[230]. Due to the high bioassay results observed for extracts of this plant, further work should be considered towards the identification of the bioactive compound(s).

5.2.6. *Ruptiliocarpon caracolito* L bark

Ruptiliocarpon caracolito bark was extracted by two methods. One involved sequential extraction with hexane, ethyl acetate followed by methanol. In the second method, we used 80% ethanol; then we did sequential liquid-liquid extractions of the ethanol extract with hexane and then dichloromethane (Table 5.14). The extracts were tested in biofilm and quorum sensing assays. The hexane extracts were not tested due to the low solubility in methanol and ethanol - the latter solvent is typically used in the assays. The biofilm assays showed that the polar fractions obtained

with either methanol or ethanol showed the highest biofilm growth inhibition, with 43.5 ± 0.1 % and 51.3 ± 0.1 % control at 500 µg/disc (Figure 5.27). Quorum sensing assays (Figure 5.28) also showed that the fractions obtained with methanol and ethanol had the highest quorum sensing inhibition, ranging from 11 to 14 mm, which is close to that of *D. pulchra* (15 mm). The less-polar dichloromethane fraction did not show any activity in the biofilm assays.

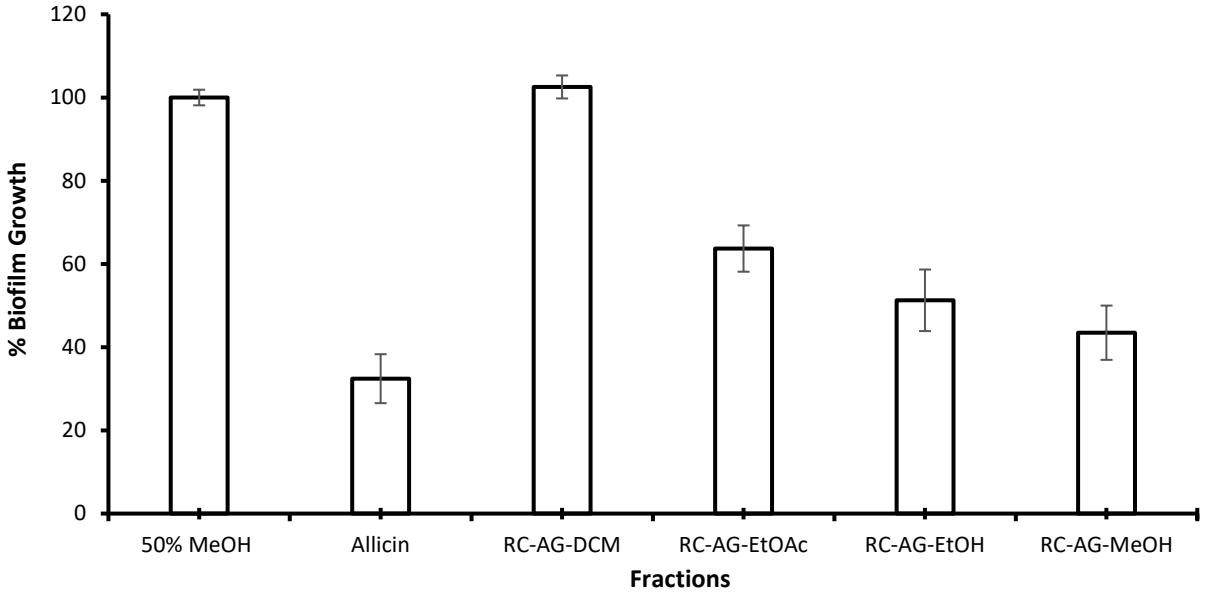

Figure 5.27 Average biofilm growth ± S.E.M. of *Pseudomonas aeruginosa* PA14 relative to vehicle control (50% MeOH) in the presence of *Ruptiliocarpon caracolito* bark extracts (800 µg/mL).
Fractions were compared to the positive control allicin (1 µL/mL or 1.08 mg/mL). N = 3. Biofilm assays were performed by Laura Picado.

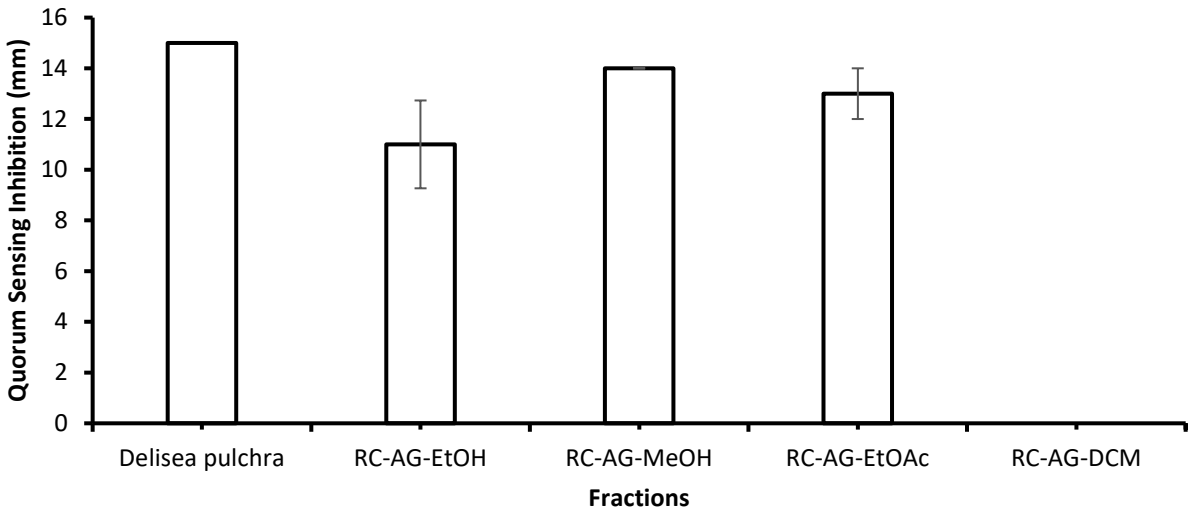

Figure 5.28 Mean ± standard deviation quorum sensing assay by *Ruptiliocarpon caracolito* bark extracts (N=3) tested at 500 µg/disc in *Chromobacterium violaceum* ATCC 12472.
Fractions were compared to the positive control *Delisea pulchra* (Greville) (N=1) Montagne extract (1 mg/disc). Disc diameter= 7 mm. I performed bioassay with the help and supervision of Agnes Cadieux.

NMR data again suggested that a carbohydrate moiety-containing compound was extracted with methanol (Figure 5.29). This NMR shows an intriguing set of peaks in the 6.8 to 7.1 ppm region. The distance between the seven large peaks (see insert) does not represent ortho- or meta- coupling constants in aromatic rings (J_{ortho}=8 -10 Hz, J_{meta}=1-2 Hz). None of the peaks can be attributed to 8 spiro-compounds previously isolated.[210] It is more likely that these peaks are due to several different compounds.

The NMR data analysis of the less polar hexane and ethyl acetate extracts indicated the presence of canophyllol (Figure 5.30, Figure 5.31), based on the diagnostic doublet of doublets at 3.61 ppm for C-C**H**$_2$OH in combination with the high field methyl groups between 0.8-2.5 ppm (δ 0.72, 0.86, 0.87, 0.88, 0.91, 0.97, 0.99, 1.05, 1.12, 1.18) and the -CH_{2-} groups in the aliphatic region. This compound was previously isolated from the bark of *R. caracolito* by S. Mackinnon.[211] NMR spectra of a reference canophyllol sample are shown in Figure 5.31 for comparison. The fraction

is not pure. The presence of plasticizer and residual ethyl acetate solvent peaks is apparent; it also shows evidence of the presence of unsaturated long chain fatty esters. Due to the low or lack of bioactivity of these non-polar fractions, it is concluded that canophyllol is not responsible for the bioactivity of the crude sample. Canophyllol had been previously examined for anti-fungal activity by the V.U. Ahmad group, and it was found that it did not display any bioactivity in their assays either.[231] Further work will be necessary to isolate in pure form the major compounds in the methanol and ethanol extracts in order to identify the compound(s) responsible for the plant's inhibitory effect in biofilm growth and quorum sensing.

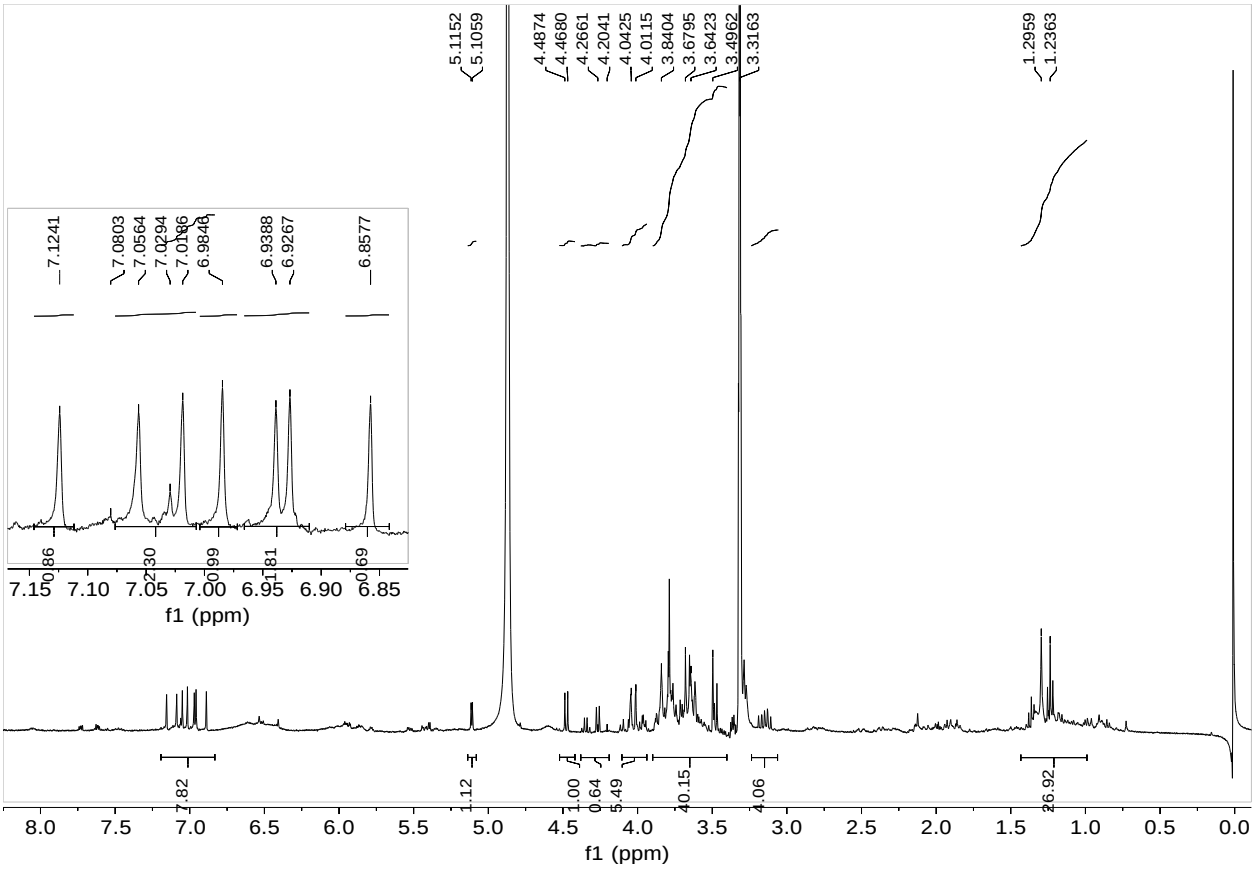

Figure 5.29 ^{1}H NMR of methanol extract of *R. caracolito* bark, $MeOD_4$.

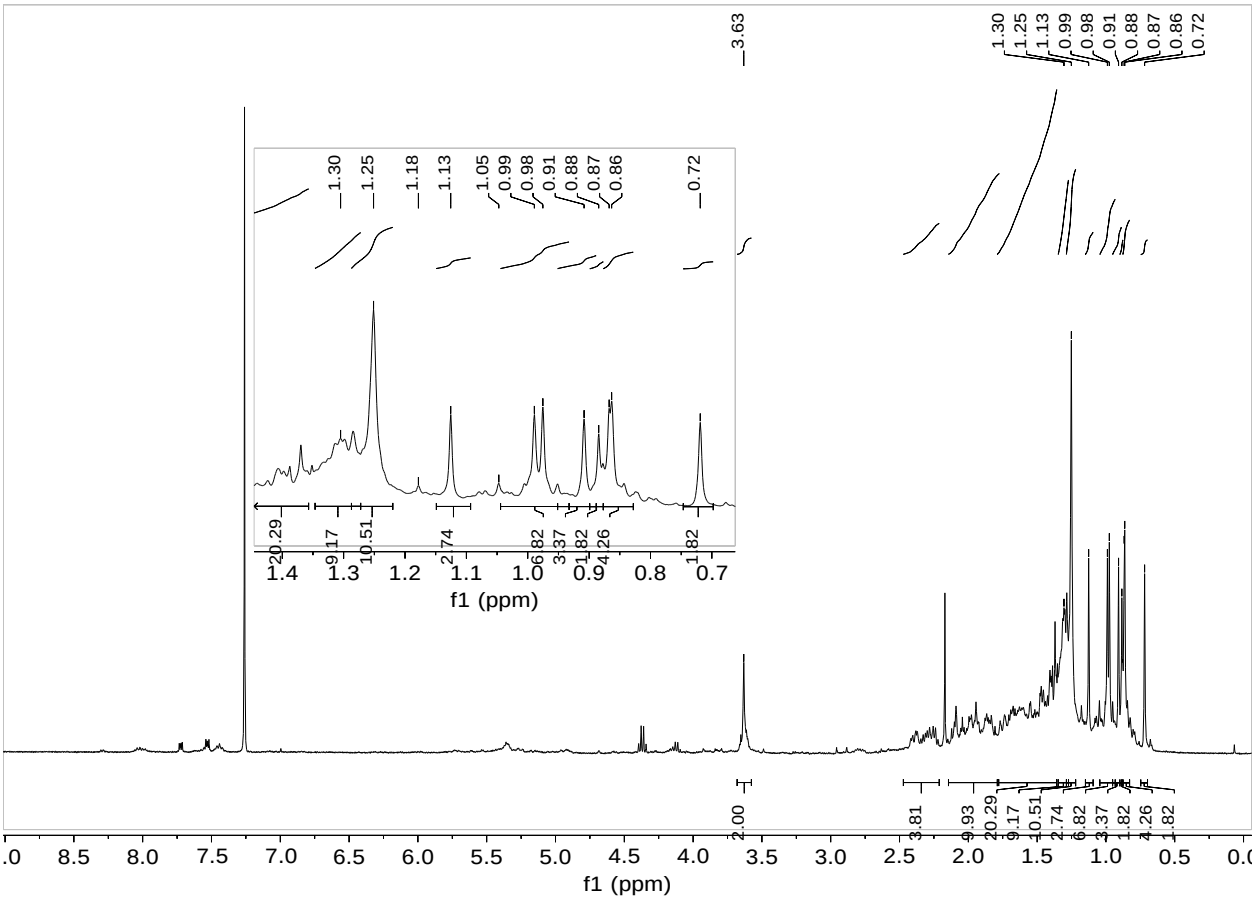

Figure 5.30 ^{1}H NMR of ethyl acetate bark extract fraction of *R. caracolito.*

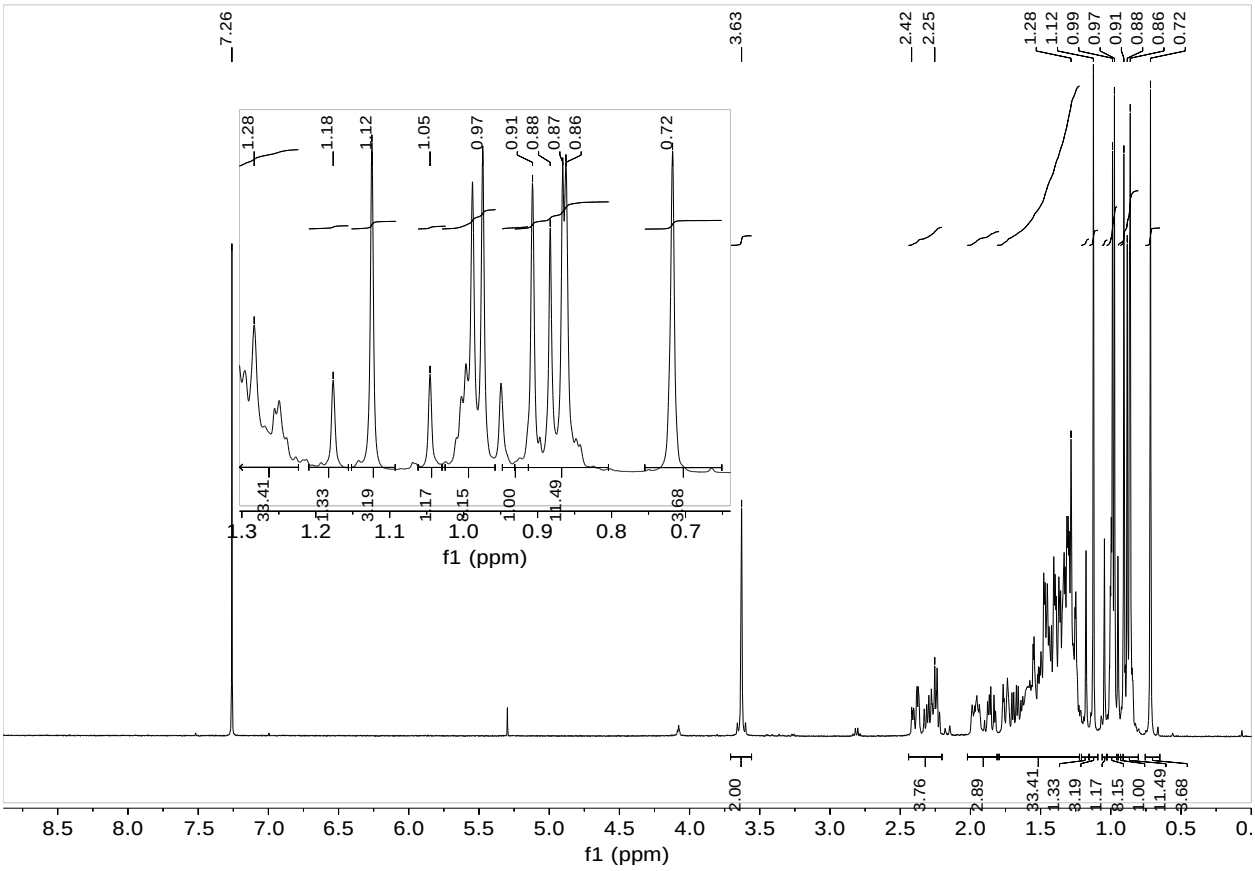

Figure 5.31 ^{1}H NMR of canophyllol reference sample.

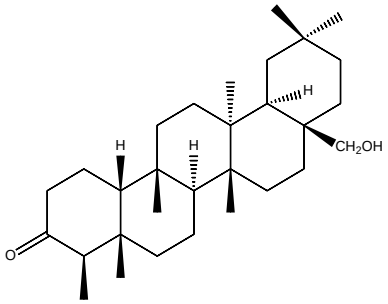

Figure 5.32 Structure of canophyllol.

5.3. Conclusions

The biofilm and quorum sensing inhibitory activities of several neotropical plants were investigated. Most plants displayed inhibitory effects. In particular, *Blakea cuneata* displayed the greatest activities, even higher than that of *Delisea pulchra*. *Ruptiliocarpon caracolito* displayed inhibitory effects close to those of *Blakea cuneata*. The findings suggest that our initial hypothesis was correct; plants that thrive in humid environments possess phytochemical activities that inhibit biofilm growth. In general, it appears that the activity is due to very polar compounds, most likely polysaccharide-type compounds.

This portion of the thesis is to a considerable extent incomplete since the key bioactive compounds from the five plants whose total extract showed activity were not isolated in pure form, despite considerable effort over a lengthy period of time. Unfortunately, due to time constraints and the demands of the major part of the thesis, I was not able to devote the time and effort required to master the relatively difficult task of dealing with the isolation and identification of polar carbohydrate-containing compounds from complex mixtures. The observed bioactivity and the importance of finding new structures that are biofilm-forming inhibitors suggest strongly that further efforts should be made to isolate and characterize the bioactive compound(s), especially from the most active plant extracts derived from *Blakea cuneata* and *Ruptiliocarpon caracolito*. In addition to this, a more complete phytochemical characterization of several of the Piper species may lead to the discovery of new compounds.

5.4.Materials and Methods

5.4.1. General methods

Blakea cuneata leaves were collected in Jalacte, Belize and *Piper aequale, Piper papantlense, Piper lanceifolium* and *Ruptiliocarpon caracolito* were collected in Costa Rica, as described in Chieu Anh Ta's thesis[203].

Piper aequale, Piper papantlense, Piper lanceifolium and Blakea cuneata Standl leaves were extracted with 80% ethanol. The plant parts were ground with a blender (Waring commercial LR 8992), then extracted with a ratio of 1:10 mass:solvent volume at room temperature with shaking overnight. The materials were extracted a second time at 1:5 (mass/volume) using the same conditions. All extracts were filtered *in vacuo* and dried using rotary evaporation (Yamato RE 500) at approximately 40°C followed by lyophilization (Super Modulyo, -55 °C). This was done by Chieu Anh Ta and Claude Denis, as described in the former's thesis.[203]

Column chromatography was performed using various solvents (hexane, dichloromethane (DCM), ethyl acetate (EtOAc), and methanol (MeOH)) supplied from Fisher and used as received. Silica Flash F60 with particle size 40-63 μm (230-400 mesh) was obtained from Silicycle. Column chromatography was monitored by TLC using thin aluminum plates with silica gel 60 $F_{254.}$ Spots were visualized initially under ultraviolet light (254 nm) followed by staining with Hanessian's stain (ammonium molybdate) (2.5 g) and cerium ammonium sulphate (1.0 g) in a solution of 10% aqueous H_2SO_4. Spots were then visualized by a heat gun. I performed all silica column chromatography fractionations.

^1H and ^{13}C NMR spectra of samples in $CDCl_3$, Acetone-d_6, DMSO-d_6, $MeOD_4$, and D_2O were recorded by Bruker AVANCE 400 at 400 MHz for ^1H and 100 MHz for ^{13}C or Bruker AVANCE

500 for ^{1}H in parts per million. Spectral analyses were performed at facilities located at the University of Ottawa. I performed all NMR experiments unless otherwise stated.

HPLC was done on an Agilent 1200 Series, reverse phase C18 Gemini Axia column 250 mm x 21.2 mm I.D., particle size 10 µm. The system consisted of a binary pump (flow rate 5-100 mL/min), a photodiode array detector and fraction collector. HPLC analyses were done by Chieu Anh Ta, Ammar Saleem and myself. An analytical HPLC 1100 Series (column 10 µm C18 110Å, length 250 x 4.6 mm, diameter of 10 µm) was also used for evaluation of the complexity of the fractions. Operation of the HPLC was performed with the help of Asim Muhammad.

Waters XEVO G2 UPLC–QTOF–ESI system was used for High Resolution Electrospray Ionization Mass Spectrometry (HR-ESI-MS). Electrospray Ionization Mass Spectrometry (ESI–MS) was done using a Shimadzu LCMS 2020 Series system by Chieu Anh Ta.

The biological activities of all fractions were evaluated by quorum sensing (QS) and biofilm growth assays. Assays were performed mainly by Chieu Anh Ta, as described in her thesis[203] unless stated otherwise (as some bioassays were also done by Laura Picado and by myself with the supervision and help of Agnes Cadieux).

5.4.2. *Piper aequale* leaves

10.0 g of *Piper aequale* leaves and stem extract was dissolved in 75 mL of H_2O due to the low solubility of the crude extract in MeOH. This was then extracted in EtOAc (100 mL, 5x). The organic layers were combined and concentrated by use of a rotary evaporator to yield 1.40 g of extract. The dry residue was then dissolved in a minimal amount of MeOH for chromatography on a glass column chromatography packed with silica gel starting with 100% hexane. The solvent polarity was increased in increments of 10% EtOAc up to 100% EtOAc. MeOH was then used to further increase the polarity of the solvent and finish elution of the column with 50% MeOH/50% EtOAc. TLC was used to monitor the separation and migration of the compounds in the column. A total of 63 fractions were collected and pooled to afford 10 fractions based on TLCs. ^{1}H NMR was done in order to evaluate the types of compounds in the fractions. Two major spots were observed by TLC in fraction AG-I-1I (0.750 g) and were further purified by plate chromatography, as follows; 50 mg of fraction AG-I-1I was dissolved in a minimum amount of solvent and then plotted on 5 plates. The solvent was left to evaporate before running the plates in dichloromethane (DCM). Ultraviolet light at 254 nm was used to monitor the separation of the compounds. Two spots were isolated by scraping off the silica and then soaking the silica in DCM for 10 min in order to extract the compounds. Afterwards, the two compounds were filtered using a glass pipette and cotton. ^{1}H NMR revealed the compound grandisin present in both fractions. ^{13}C NMR, DEPT and correlation spectroscopy were performed to confirm the identity of the compound.

In order to evaluate the biological activities of all fractions, quorum sensing (QS) and biofilm growth assays were performed by Chieu Anh Ta, as described in her thesis.[203]

Table 5.7 Primary column yields of 10 fractions collected from 10.0 g extract of *P. aequale* leaves.

Fraction	**Weight product (g)**	**Solvent system**
AG-1-1A	0.19	80% Hexane- 20% EtOAc
AG-1-1B	0.03	80% Hexane- 20% EtOAc
AG-1-1C	0.04	70% Hexane- 30% EtOAc
AG-1-1D	0.09	60% Hexane- 40% EtOAc
AG-1-1E	0.07	60% Hexane- 40% EtOAc
AG-1-1F	0.18	60% Hexane- 40% EtOAc
AG-1-1G	0.10	40% Hexane- 60% EtOAc
AG-1-1H	0.05	40% Hexane- 60% EtOAc
AG-1-1I	0.75	10% Hexane- 90% EtOAc
AG-1-W	1.10	100% EtOAc
Total	2.60	50% EtOAc- 50% MeOH

5.4.3. *Piper papantlense* leaves

10.0 g of crude ethanol extract was dissolved in a minimal amount of MeOH before column chromatography with 100% hexane. The polarity of the solvent system was increased in increments of 10% with EtOAc up to 100% EtOAc, followed by final elution with 50% MeOH/50% EtOAc. A total of 118 fractions were collected and pooled into 11 fractions based on TLC. ^{1}H NMR was done in order to evaluate the functional groups present in the fractions.

Biological activity of all fractions was evaluated with quorum sensing and biofilm growth assays, which were performed by Chieu Anh Ta, as described in her thesis.[203]

Table 5.8 Column chromatography yield of 11 fractions collected from 10.0 g ethanol extract of *P. papantlense.*

Fraction	Weight product (g)	Solvent system
AG-2-2A	0.71	90% Hexane - 10% EtOAc
AG-2-2B	1.07	80% Hexane- 20% EtOAc
AG-2-2C	0.77	70% Hexane- 30% EtOAc
AG-2-2D	1.36	60% Hexane- 40% EtOAc
AG-2-2E	0.07	60% Hexane- 40% EtOAc
AG-2-2F	0.32	10% Hexane-90% EtOAc
AG-2-2G	0.35	90% EtOAc- 10 % MeOH
AG-2-2H	1.08	75% EtOAc- 25% MeOH
AG-2-2I	1.37	75% EtOAc- 25% MeOH
AG-2-2J	0.41	75% EtOAc- 25% MeOH
AG-2-2K	0.65	50% EtOAc- 50% MeOH
Total	8.16	

5.4.4. *Piper lanceifolium* leaves

10.0 g of *Piper lanceifolium* crude extract was dissolved in a minimal amount of methanol. A few drops of distilled water were added to help dissolve the crude extract. Gradient column chromatography was done to elute the compounds, starting with 100% hexane and increasing in increments of 10% EtOAc up to 100% EtOAc. To further increase the polarity of the system, MeOH was added in increments of 10%, starting with 10% MeOH/90 % EtOAc up to 50% MeOH/50% EtOAc. A total of 158 fractions were collected and pooled into 14 fractions based on TLC with a total amount of 6.77 g of fractionated material. ^{1}H NMR was done to evaluate the compounds present in the fractions. It was observed that the compound dilapiol was present in fraction AG-3-3E (0.04 g). In fraction AG-3-3F (0.17 g), a mixture of dilapiol and elemicin was present, and in fraction AG-3-3G (1.07 g), mostly elemicin was present.

Inhibitory activity of all fractions was evaluated with quorum sensing and biofilm growth assays, which were performed by Chieu Anh Ta, as described in her thesis.[203]

Table 5.9 Primary column yield of 14 fractions collected from 10.0 g leaves ethanol extract of *P. lanceifolium.*

Fraction	**Weight product (g)**	**Solvent system**
AG-3-3A	0.01	100% Hexane
AG-3-3B	0.07	90% Hexane- 10% EtOAc
AG-3-3C	0.07	85% Hexane- 15% EtOAc
AG-3-3D	0.59	85% Hexane- 15% EtOAc
AG-3-3E	0.04	75% Hexane- 25% EtOAc
AG-3-3F	0.17	75% Hexane- 25% EtOAc
AG-3-3G	1.07	60% Hexane- 40% EtOAc
AG-3-3H	0.23	50% Hexane- 50% EtOAc
AG-3-3I	0.22	50% Hexane- 50% EtOAc
AG-3-3J	0.09	25% Hexane- 75% EtOAc
AG-3-3K	0.15	90% EtOAc- 10% MeOH
AG-3-3L	0.18	90% EtOAc- 10% MeOH
AG-3-3M	0.26	80% EtOAc- 20% MeOH
AG-3-3N	3.62	50% EtOAc- 50% MeOH
Total	6.77	

5.4.5. *Piper lanceifolium* fruit

To further characterize *Piper lanceifolium*, 20.0 g of fruit collected in Costa Rica in March 2010 was ground into a fine powder by using a blender. This was extracted with 2 L of EtOAc to yield 2.64 g of crude extract. The crude extract was mixed with silica and MeOH and dried *in vacuo* using a rotary evaporator. The dry batch was then placed on the column and the compounds were separated by column chromatography, starting with 100% hexane and increasing the polarity in increments of 10% EtOAc, up to 100% EtOAc. Then, the column was flushed with 1:1 mixture of MeOH:EtOAc. ^{1}H NMR was done to evaluate the types of compounds in the fractions.

Column chromatography was performed on fraction AG-I-5M, starting with 40% EtOAc/60% hexane. A chromone derivative seems to be the major isolated product (0.050 g). The NMR reveals the presence of impurities, and so the product is chromatographed again by column chromatography to yield 0.042 g of product, which was then analysed by ^{1}H NMR.

Table 5.10 Primary column yield of 14 fractions collected from 10.0 g of 95% ethanol extract of *P. lanceifolium* fruit.

Fraction	Weight product (g)	Solvent system
AG-I-5A	0.029	100% Hexane
AG-I-5B	0.544	90% Hexane -10 % EtOAc
AG-I-5C	0.027	70% Hexane- 30 % EtOAc
AG-I-5D	0.006	70% Hexane- 30 % EtOAc
AG-I-5E	0.019	70% Hexane- 30 % EtOAc
AG-I-5F	0.101	60% Hexane- 40 % EtOAc
AG-I-5G	0.153	60% Hexane- 40 % EtOAc
AG-I-5H	0.047	60% Hexane- 40% EtOAc
AG-I-5I	0.026	40% Hexane- 60% EtOAc
AG-I-5J	0.055	40% Hexane- 60% EtOAc
AG-I-5K	0.167	40% Hexane- 60% EtOAc
AG-I-5L	0.245	40% Hexane- 60% EtOAc
AG-I-5M	0.205	30% Hexane- 70% EtOAc
AG-I-5N	0.179	10% Hexane- 90% EtOAc
AG-I-5O	0.373	100% EtOAc
AG-I-5P	0.325	50% EtOAc- 50% MeOH

Finally, 850 g of *Piper lanceifolium* fruit was steam-distilled and then dissolved in 150 mL of H_2O by Tony Durst. Following this, extraction of this aqueous phase was done with EtOAc. The extract was dried with $MgSO_4$ and concentrated, followed by drying *in vacuo* for 10 min. Plate chromatography was done to separate 3 major spots by dissolving 100 mg of dry extract and dissolving it in a minimal amount of acetone. This was then blotted on the plate and separated by a solvent system of 70% ethyl acetate/30% hexane and a few drops of acetic acid. Based on NMR data, a chromone derivative (Rf value 0.35) was isolated in 0.016 g.

5.4.6. *Blakea cuneata* Standl leaves

10.0 g of crude extract was dissolved in a minimal amount of MeOH and then chromatographed. The compounds were eluted using gradient column chromatography, starting with 100% hexane. The polarity of the solvent system was increased in increments of 10% with EtOAc up to 100% EtOAc, followed by MeOH. A total of 21 fractions (BC-1-A to U) were pooled based on TLCs. NMR analysis was done to evaluate the types of compounds present in the fractions.

Table 5.11 Primary column weight yields of 21 fractions collected from 10.0 g of *Blakea cuneata* Standl. leaves.

Fraction	Weight product (g)	Solvent system
BC-I-A	0.16	85% hexane- 15% EtOAc
BC-I-B	0.06	85% hexane- 15% EtOAc
BC-I-C	0.02	80% hexane- 20% EtOAc
BC-I-D	0.07	80% hexane- 20% EtOAc
BC-I-E	0.05	80% hexane- 20% EtOAc
BC-I-F	0.01	80% hexane- 20% EtOAc
BC-I-G	0.00	50% hexane- 15% EtOAc
BC-I-H	0.01	50% hexane- 15% EtOAc
BC-I-I	0.01	50% hexane- 15% EtOAc
BC-I-J	0.01	50% hexane- 15% EtOAc
BC-I-K	0.05	50% hexane- 15% EtOAc
BC-I-L	0.008	90% EtOAc- 10% MeOH
BC-I-M	0.05	90% EtOAc- 10% MeOH
BC-I-N	0.05	90% EtOAc- 10% MeOH
BC-I-O	0.32	80% EtOAc- 20% MeOH
BC-I-P	0.26	80% EtOAc- 20% MeOH
BC-I-Q	0.26	75% EtOAc- 25% MeOH
BC-I-R	0.38	75% EtOAc- 25% MeOH
BC-I-S	1.21	75% EtOAc- 25% MeOH
BC-I-T	0.53	75% EtOAc- 25% MeOH
BC-I-U	1.61	50% EtOAc- 50% MeOH

Biofilm assays and quorum sensing assays were performed by Chieu Anh Ta to evaluate the biological activity of the fractions, as described in her thesis.[203]

Acetylation was then performed on fraction AG-I-4S. 0.243 g of fraction AG-I-4S was mixed with 5 mL of acetic anhydride and 5 mL of pyridine. The mixture was then heated and stirred continuously. To quench the reaction, 40 mL of saturated ammonium chloride and 10 mL of 10% HCl were added. Extraction of the organic layer was done three times with 15 mL of EtOAc. The organic phases were combined, dried over $MgSO_4$ and the organic mixture was dried *in vacuo*. Gradient column chromatography starting with 100% hexane was performed in an attempt to purify the products. A total of 5 fractions were combined. The NMR spectra showed that multiple products were obtained. A representative NMR spectrum is presented and discussed in the Results and Discussion section. Fractions 1-4 were combined to afford 0.061 g and then chromatographed by TLC again in an attempt to better separate the compounds. 8 fractions were collected; unfortunately, the yield was too low for NMR analysis.

Due to the low yield of the fractions, another acetylation was performed on 0.492 g of AG-I-4S, as described earlier, to afford 0.4228 g of acetylated products. The acetylated products were then chromatographed. A total of 11 fractions were combined based on TLCs. The yield was again too low to characterize the compounds by NMR.

Analytical HPLC and TLC was used to analyze fractions BC-I-O to BC-I-U (1.3 - 2.7 mg/mL). Both HPLC and TLC analysis showed complexity of the samples. TLC systems showed that it is difficult to separate the compounds, as they create streaks due to their polar nature. Further fractionation of *Blakea cuneata* Standl fraction BC-I-U was done with analytical HPLC with the help of Asim Muhammad. The fraction was prepared at 50 mg/mL in 50% MeOH/50% H_2O, sonicated for 5 min, filtered with PTFE 0.2 µm and then submitted to HPLC. The same analytical HPLC was used to collect 3 fractions (a=0.76 mg, b=1.42 mg, and c=2.85 mg). Additional

fractionation of BC-I-U was done by preparative HPLC, where 5 major fractions were collected: BC-I-U-1 (99 mg), BC-I-U-2 (4 mg), BC-I-U-3 (1 mg), BC-I-U-4 (1 mg), BC-I-U-5 (2 mg).

Biofilm inhibition assays were done by Chieu Anh Ta on BC-I-U-1 alone due to low yields (1 to 4 mg) of the other fractions. ^{1}H NMR was then done using DMSO-*d6*, as the fractions were highly polar and did not dissolve well in other solvents.

A second column was then performed with *Blakea cuneata* extract since not enough material was available to work with after acetylation and biofilm experiments. 19 g of product was used for column chromatography. A total of 16 fractions were collected. Biofilm assays were performed by Chieu Anh Ta (BC-II-A to BC-II-Q). Chieu Anh Ta used a Sephadex column, as described in her thesis, to further separate the compounds. This led to the identification of one compound, homoplantaginin or hispidulin-7-*O*-glucoside, which unfortunately did not show bioactivity in biofilm assays.

Table 5.12 Primary column yield of 21 fractions collected from 19.0 g of *Blakea cuneata* Standl leaves extract.

Fraction	Weight product (g)	Solvent system
BC-II-A	0.5133	85% Hexane – 15% EtOAc
BC-II-B	0.1128	85% Hexane – 15% EtOAc
BC-II-C	0.2238	80% Hexane – 20% EtOAc
BC-II-D	0.0556	80% Hexane – 20% EtOAc
BC-II-E	0.0242	80% Hexane – 20% EtOAc
BC-II-F	0.0778	80% Hexane – 20% EtOAc
BC-II-G	0.1372	50% Hexane – 50% EtOAc
BC-II-H	0.0620	50% Hexane – 50% EtOAc
BC-II-I	0.1619	30% Hexane – 70% EtOAc
BC-II-K	0.0556	30% Hexane – 70% EtOAc
BC-II-L	2.0678	80% EtOAc – 20% MeOH
BC-II-M	0.3158	80% EtOAc – 20% MeOH
BC-II-N	1.6724	80% EtOAc – 20% MeOH
BC-II-O	1.4805	75% EtOAc – 25% MeOH
BC-II-P	2.1205	75% EtOAc – 25% MeOH
BC-II-Q	6.5234	75% EtOAc – 25% MeOH
Total	15.6046	

Column chromatography fractionated 108 g of *B. cuneata* Standl extract in another attempt to increase the yields of the fractions. The column elution was started with 100% hexane, followed by 50% hexane/50% EtOAc, 100% EtOAc, 25% MeOH/75% EtOAc, and ended with 50% MeOH/50% EtOAc. A total of 10 fractions were collected after pooling. Biofilm bioassays were done by Chieu Anh Ta to evaluate inhibitory activity (fractions BC-III-A to BC-III-K).

Table 5.13 Primary column weight yields of 11 fractions collected from 108 g of *Blakea cuneata* Standl. leaves ethanol extract.

Fraction	Weight of product (g)	Solvent system
BC-III-A	0.7	100% Hexane
BC-III-B	5.593	50% Hexane – 50% EtOAc
BC-III-C	1.031	50% Hexane – 50% EtOAc
BC-III-D	1.642	100% EtOAc
BC-III-E	0.287	100% EtOAc
BC-III-F	0.036	100% EtOAc
BC-III-G	7.248	75% EtOAc – 25% MeOH
BC-III-H	8.942	75% EtOAc – 25% MeOH
BC-III-I	7.720	75% EtOAc – 25% MeOH
BC-III-J	3.044	75% EtOAc – 25% MeOH
BC-III-K	49.161	50% EtOAc – 50% MeOH
Total	85.40	

Fraction K was acetylated (1.087 g) and fractionated by column chromatography. Fraction 8 and 9 (total mass of 0.062 g) from this column were further separated by silica plate chromatography. Again, due to the low yield and low signals, it was difficult to characterize the compound based on NMR.

10.0 g of bioactive material was combined (7.0 g from fraction BC-III-G and 3.0 g from fraction BC-III-H) and fractionated by column chromatography; the dry extract was first dissolved with a minimum amount of DCM and 25 g of silica. After fractionation, the silica/extract mixture was dried *in vacuo* using a rotary evaporator. 1 kg silica column was used for the separation (long and narrow). 100 mL of H_2O was added to 1 kg of silica and mixed well. The column was then loaded with 1:1 Hexane:EtOAc (1 L) and left overnight to settle. The next day, the sample was loaded and allowed to settle on column for 30 min prior to addition of the solvent. The total number of fractions after pooling was 86 with biofilm inhibitory bioactivity in fractions 81-86 (assays performed by Chieu Anh Ta). The selected fractions were then analyzed by NMR.

3.0 g of fraction BC-III-H was used for HPLC separation using time-based collection to afford Pools A through Q. Peak-based collections were also made from one run. All of these fractions were analyzed using UPLC–QTOF–MS/MS by Chieu Anh Ta and Ammar Saleem. NMR spectra of these compounds were then taken. At this point, we encountered a poor solubility issue. Acetone-*d6*, $MeOD_4$, and D_2O were tested in attempts to dissolve the fractions. 1 mg of several fractions (Fractions A, BB, HH, II, JJ, KK, LL, NN, OO) were suspended in 0.5 mL of each deuterated solvent; sonication in a water bath at 40°C were also used. NMR spectra recorded with Bruker 400 gave poor resolution. After this, with the help of Glenn A. Facey (the NMR facility manager), we recorded NMR spectra of several fractions in D_2O on the Bruker 300. The water peaks were suppressed at approximately 4 ppm. Fraction NN revealed several aromatic peaks (2:2:1 m-ring). 32 scans were used to record the spectrum. The sample was then heated to 50°C and the spectra were recorded again. Heating them up did not make much of a difference with regards to solubility; therefore, there was no need to run them at a high temperature. After this, the samples were recorded on the 500 MHz NMR by Glenn A. Facey. This showed that most fractions are the same with varying intensities (Fractions A, BB, HH, II, JJ, KK, LL, NN, OO). In another attempt to get better NMR spectra, fraction A and KK were dissolved in DMSO-*d6*. This however was not successful, as no peaks were observed for the sample and only the DMSO-*d6* peaks were visible. Fraction LL was then acetylated, but assigning peaks was difficult as broad peaks between 2.5-4pm and 5-6ppm were observed.

5.4.7. *Ruptiliocarpon caracolito* L bark

100 g of *Ruptiliocarpon caracolito* bark was ground using a 1 mm mill filter to produce fine powder. The powder was divided into two equal batches. The first 50 g of milled bark was added to 500 mL of 100% hexane, shaken at 200 rpm for 48 hours while covered with aluminum foil to protect photosensitive compounds from light. The other 50 g of extract was added to 500 mL of 80% ethanol/20% H_2O, shaken at 200 rpm for 48 hours and again covered with aluminum foil to protect from light. After 48 hours, each extract was filtered and re-dissolved in hexane and ethanol correspondingly. The extracts were then left to shake at 200 rpm for another 48 hrs. The extraction was repeated 4 times.

After extraction with hexane, the first batch of crude plant extract was re-extracted with EtOAc (500 mL, 2x) with gentle shaking for 24 hours at a time and then was re-extracted with MeOH (500 mL, 2x); the first MeOH extraction was for 48 hours and the second MeOH extraction was for 24 hours. The samples were dried *in vacuo* with a rotary evaporator and pooled for bioassays.

For the ethanol extract, a liquid-liquid extraction was done with hexane (500 mL, 4x). This was followed by another liquid-liquid extraction with DCM (500 mL, 2x). The extracts were combined and dried *in vacuo* with a rotary evaporator to a minimal amount. The samples were left to air dry for bioassay. Biofilm inhibition assays were performed in triplicate by Laura Picado. I performed quorum sensing assays with the help and guidance of Agnes Cadieux. NMR spectra of the extracts and canophyllol were also recorded.

Table 5.14 Mass yields after extraction of 50.0 g of *Ruptiliocarpon caracolito* bark by each method.

Method 1		**Method 2**	
Fractions	**Mass (g)**	**Fractions**	**Mass (g)**
100% Hexane	0.40	80% Ethanol/20% H_2O	2.70
100% Ethyl Acetate	0.85	100% Hexane	0.88
Methanol	5.39	100% Dichloromethane	1.32

Chapter 6

6. Conclusions and Future Directions

Capillary electrophoresis is a powerful, well-established analytical technique used for the separation of ions. CE is applied in various analytical and bioanalytical fields, such as in clinical diagnosis[232], pharmaceutical science[233] and forensic science[234]. It is routinely used for analysis of non-covalent interactions, such as those between RNA and protein,[2] and for the analysis of macromolecules, such as viruses[67,149]. CE demonstrates great potential for use in both research and clinical settings.

As non-covalent interactions are an important part of understanding biochemical processes, in these studies we have addressed interactions between microRNA-122 and p19, as well as between trans-activation response element (TAR) and target of Egr1 (TOE1) and its peptides using non-equilibrium capillary electrophoresis of equilibrium mixtures (NECEEM). In both studies, the importance of optimization of conditions for the application of NECEEM came to light. This is because the interactions were greatly influenced by changes in capillary temperature, running buffer and binding buffer components. Furthermore, resolution of the peaks and limit of detection of the sample were also in turn affected by these parameters and others, such as capillary length, voltage and sample injection. Laser-induced fluorescence detection requires very little sample, which made it easy to conserve sample as much as possible while studying various parameters.

Until the discovery of small non-coding RNAs in 1993, even the existence of microRNA was completely unknown.[235] However, there has been much emphasis since their discovery on the

importance of these small non-coding RNAs, which regulate genes post-transcriptionally, and their roles as biomarkers of disease diagnosis and prognosis. Protein p19 has been used as a tool to study microRNA profiling.[9,54,58] Hence, understanding the thermodynamic and kinetic constants is important for the application of p19. The dissociation constant we found was similar to the literature. Although this was the first time the rate constant between microRNA-122 and p19 was published, it was found to be in agreement with that of another small non-coding RNA and p19. A newly developed method for calculating k_{off}, kinetic capillary electrophoresis with varying electric fields (KCEVEF), was also used, and these results were in agreement with those of NECEEM. This method proved to be especially useful when the dissociation rate constant, k_{off}, is high.

The interaction between protein TOE1 and HIV-1 trans-activation response (TAR) element was of particular interest because it was able to identify TOE-1 as an inhibitor of HIV-1 replication. NECEEM proved to be useful for this purpose. Various peptides were tested and it was found that only the peptides containing the nuclear localization sequence (NLS) bound to TAR. Interestingly, these sequences were similar to that of protein Tat, which is well known for its imperative role in viral transcription. Both Tat and TOE1 NLS peptides (ED35 and ER19) contain lysine/arginine-rich regions identified as crucial for binding. This research takes us one step closer towards understanding HIV-1 infection in patients and shows great potential for the inhibition of Tat/TAR interaction.

A method recently developed by our lab demonstrated the utility of CE for both DNA and RNA viruses. One of the great advantages of using CE for viral analysis is its ability to separate the viral fraction from the contaminating nucleic acid fraction, which may be present as a result of poor purification or degraded virion. The previous method required a lysis step; however, this was

optimized by addition of a redox reagent, dithiothreitol. Its use in the stabilization of proteins led us to identify its utility for decreasing virus aggregation. We found it decreased the number of clusters, which resulted in a more homogenous system, facilitating the method and making it lysis-free.

Although vaccines have been called one of the biggest breakthroughs in science, they still face distribution challenges. Due to the inherent instability of viruses and fluctuations in temperature during transportation, many methods have been considered for distribution and/or preservation and delivery of vaccines.[236] Room temperature preservation of vaccinia virus infectivity by *N*-octyl-*D*-gluconamide showed this hydrogelator's potential to stabilize the virus during transportation and in turn eliminate the "cold chain". These results are encouraging, and further studies, such as the evaluation of toxicity of *N*-octyl-*D*-gluconamide, should be pursued.

In addition to their instability at room temperature, viruses also lose infectivity when subjected to freeze-thaw conditions. An aptamer against vesicular stomatitis virus was found to preserve the infectivity of the virus after various freeze-thaw cycles. Four previously selected aptamers[237] were linked together by a nucleic acid bridge to produce a tetravalent construct, termed a quadramer. The relative amount of intact viruses before and after freeze-thawing was monitored by CE and the virus' infectivity was evaluated using plaque forming assays. The results display the potential for anti-virus aptamers as tools in cryo-preservation. This is especially important for oncolytic viruses, where infectivity of the virus is essential for successful therapy. More work needs to be done in order to investigate the use of other anti-virus aptamers as cryo-protectants, as well as agents for infectivity enhancement.

The last chapter of this thesis presented the preliminary results of bioassay-guided isolation of biofilm and quorum sensing inhibitors from neotropical plants. Besides the immunocompromised

who are highly susceptible to infections, many more infections result as outcomes of implant surgeries. The clinical and economic effects of infections due to biofilms is devastating and current therapies include the use of antibiotics. Unfortunately, current research has shown that antibiotic resistance is on the rise, and the future may be a place where antibiotics no longer prove to be useful.[195] In an effort to find new compounds, we investigated five neotropical plants that grow in humid environments. *Blakea cuneata* displayed the highest inhibitory activities against biofilm growth and quorum sensing. The results suggest the bioactive compound is a carbohydrate derivative. Further studies are required to characterize the bioactive compound(s) in *Blakea cuneata* and *Ruptiliocarpon caracolito*, which also displayed high inhibitory activity against biofilm growth and quorum sensing in bacteria. Furthermore, a more complete phytochemical characterization of the Piper species may result in discovery of new compounds.

List of Publications

1. Sperandio, S., Barat, C., Cabrita, M.A., **Gargaun, A.**, Berezovski, M.V., Tremblay, M.J. De Belle, I. TOE1 is an Inhibitor of HIV-1 Replication with Cell-Penetrating Capability. 2015 *Proceedings of the National Academy of Sciences of the United States of America*, 112 (26), E3392-E3401.

Contribution: I performed capillary electrophoresis experiments.

2. Ghobadloo, S.M., **Gargaun, A.**, Casselman, R., Muharemagic, D., Berezovski, M.V. Aptamer-Facilitated Cryoprotection of Viruses. 2014 *ACS Medicinal Chemistry Letters*, 5 (11), 1240-1244.

Contribution: I performed capillary electrophoresis experiments and edited the manuscript.

3. Ghobadloo, S.M., Balcerzack, A.K., **Gargaun, A.**, Muharemagic, D., Mironov, G.G., Capicciotti, C.J., Briard, J.G., Ben, R.N., Berezovski, M.V. Carbohydrate-Based Ice Recrystallization Inhibitors Increase Infectivity and Thermostability of Viral Vectors. 2014 *Scientific Reports*, 4, Article Number 5903.

Contribution: I performed capillary electrophoresis experiments and edited the manuscript.

4. Dabrota, C., Asim, M., Choueiri, C., **Gargaun, A.**, Korobkov, I., Butt, A., Carlson, K.E., Katzenellenbogen, J.A., Wright, J.S., Durst, T. Synthesis and Receptor Binding in *trans*-CD Ring-Fused A-CD Estrogen: Comparison with the *cis*-Fused Isomers. 2014 *Bioorganic and Medicinal Chemistry Letters*, 24 (16), 3841-3844.

Contribution: I contributed to synthesis experiments.

References

1. Krylov, S. N., and Berezovski, M. (2003) Non-equilibrium capillary electrophoresis of equilibrium mixtures--appreciation of kinetics in capillary electrophoresis, *Analyst 128*, 571-575.
2. Berezovski, M., Drabovich, A., Krylova, S. M., Musheev, M., Okhonin, V., Petrov, A., and Krylov, S. N. (2005) Nonequilibrium capillary electrophoresis of equilibrium mixtures: a universal tool for development of aptamers, *J Am Chem Soc 127*, 3165-3171.
3. Berezovski, M., and Krylov, S. N. (2005) Thermochemistry of protein-DNA interaction studied with temperature-controlled nonequilibrium capillary electrophoresis of equilibrium mixtures, *Anal Chem 77*, 1526-1529.
4. Harris, D. C. (2007) *Quantitative Chemical Analysis*, 7th Edition ed., W. H. Freeman and Company, New York, United States of America.
5. Whatley, H. (2001) *Basic Principles and Modes of Capillary Electrophoresis*, Springer Science + Business Media, LLC, University of Texas Medical Branch, Galveston, Texas.
6. Jorgenson, J. W., and Lukacs, K. D. (1981) Zone Electrophoresis in Open-Tubular Glass-Capillaries, *Anal Chem 53*, 1298-1302.
7. Jorgenson, J. W., and Lukacs, K. D. (1983) Capillary zone electrophoresis, *Science 222*, 266-272.
8. Wegman, D. W., and Krylov, S. N. (2011) Direct Quantitative Analysis of Multiple miRNAs (DQAMmiR), *Angewandte Chemie International Edition 50*, 10335-10339.
9. Khan, N., Cheng, J., Pezacki, J. P., and Berezovski, M. V. (2011) Quantitative analysis of microRNA in blood serum with protein-facilitated affinity capillary electrophoresis, *Anal Chem 83*, 6196-6201.
10. Wegman, D. W., Ghasemi, F., Stasheuski, A. S., Khorshidi, A., Yang, B. B., Liu, S. K., Yousef, G. M., and Krylov, S. N. (2016) Achieving Single-Nucleotide Specificity in Direct Quantitative Analysis of Multiple MicroRNAs (DQAMmiR), *Anal Chem 88*, 2472-2477.
11. Dodgson, B. J., Mazouchi, A., Wegman, D. W., Gradinaru, C. C., and Krylov, S. N. (2012) Detection of a thousand copies of miRNA without enrichment or modification, *Anal Chem 84*, 5470-5474.
12. Zhu, Z., Lu, J. J., and Liu, S. (2012) Protein separation by capillary gel electrophoresis: A review, *Analytica Chimica Acta 709*, 21-31.
13. Zhao, S. S., and Chen, D. D. Y. (2014) Applications of capillary electrophoresis in characterizing recombinant protein therapeutics, *Electrophoresis 35*, 96-108.
14. Polunina, T. A., Varshavskaia, I. S., Grigor'eva, G. V., and Krasnov, I. M. (2014) [Proteomic methods of protein separation and analysis], *Zhurnal mikrobiologii, epidemiologii, i immunobiologii*, 107-114.
15. Cianciulli, C., Hahne, T., and Watzig, H. (2012) Capillary gel electrophoresis for precise protein quantitation, *Electrophoresis 33*, 3276-3280.
16. Swerdlow, H., and Gesteland, R. (1990) Capillary gel electrophoresis for rapid, high resolution DNA sequencing, *Nucleic Acids Research 18*, 1415-1419.
17. Cohen, A. S., Najarian, D. R., Paulus, A., Guttman, A., Smith, J. A., and Karger, B. L. (1988) Rapid separation and purification of oligonucleotides by high-performance capillary gel electrophoresis, *Proceedings of the National Academy of Sciences 85*, 9660-9663.
18. (2001) Initial sequencing and analysis of the human genome, *Nature 409*, 860-921.
19. Greenough, L., Schermerhorn, K. M., Mazzola, L., Bybee, J., Rivizzigno, D., Cantin, E., Slatko, B. E., and Gardner, A. F. (2015) Adapting capillary gel electrophoresis as a sensitive, high-throughput method to accelerate characterization of nucleic acid metabolic enzymes, *Nucleic Acids Research*.
20. Rodriguez-Diaz, R., Wehr, T., and Zhu, M. (1997) Capillary isoelectric focusing, *Electrophoresis 18*, 2134-2144.

21. Hühner, J., Lämmerhofer, M., and Neusüß, C. (2015) Capillary isoelectric focusing-mass spectrometry: Coupling strategies and applications, *Electrophoresis 36*, 2670-2686.
22. Urasaki, Y., Fiscus, R. R., and Le, T. T. (2016) Molecular classification of fatty liver by high-throughput profiling of protein post-translational modifications, *J Pathol 238*, 641-650.
23. O'Neill, R. A., Bhamidipati, A., Bi, X., Deb-Basu, D., Cahill, L., Ferrante, J., Gentalen, E., Glazer, M., Gossett, J., Hacker, K., Kirby, C., Knittle, J., Loder, R., Mastroieni, C., MacLaren, M., Mills, T., Nguyen, U., Parker, N., Rice, A., Roach, D., Suich, D., Voehringer, D., Voss, K., Yang, J., Yang, T., and Vander Horn, P. B. (2006) Isoelectric focusing technology quantifies protein signaling in 25 cells, *Proceedings of the National Academy of Sciences of the United States of America 103*, 16153-16158.
24. Fan, A. C., Deb-Basu, D., Orban, M. W., Gotlib, J. R., Natkunam, Y., O'Neill, R., Padua, R. A., Xu, L., Taketa, D., Shirer, A. E., Beer, S., Yee, A. X., Voehringer, D. W., and Felsher, D. W. (2009) Nanofluidic proteomic assay for serial analysis of oncoprotein activation in clinical specimens, *Nat Med 15*, 566-571.
25. Tikhanovich, I., Kuravi, S., Campbell, R. V., Kharbanda, K. K., Artigues, A., Villar, M. T., and Weinman, S. A. (2014) Regulation of FOXO3 by phosphorylation and methylation in hepatitis C virus infection and alcohol exposure, *Hepatology 59*, 58-70.
26. Chen, J. Q., Lee, J. H., Herrmann, M. A., Park, K. S., Heldman, M. R., Goldsmith, P. K., Wang, Y., and Giaccone, G. (2013) Capillary isoelectric-focusing immunoassays to study dynamic oncoprotein phosphorylation and drug response to targeted therapies in non-small cell lung cancer, *Mol Cancer Ther 12*, 2601-2613.
27. Silva, M. (2013) Micellar electrokinetic chromatography: A review of methodological and instrumental innovations focusing on practical aspects, *Electrophoresis 34*, 141-158.
28. Osbourn, D. M., Weiss, D. J., and Lunte, C. E. (2000) On-line preconcentration methods for capillary electrophoresis, *Electrophoresis 21*, 2768-2779.
29. Mala, Z., Gebauer, P., and Bocek, P. (2015) Recent progress in analytical capillary isotachophoresis, *Electrophoresis 36*, 2-14.
30. Garcia-Schwarz, G., and Santiago, J. G. (2013) Rapid high-specificity microRNA detection using a two-stage isotachophoresis assay, *Angew Chem Int Ed Engl 52*, 11534-11537.
31. Krylov, S. N. (2007) Kinetic CE: foundation for homogeneous kinetic affinity methods, *Electrophoresis 28*, 69-88.
32. Philip W. Kuchel, S. E.-S., Vanessa Gysbers, J. Mitchell Guss. (2013) Schaum's Outline of Biochemistry, Third Edition, McGraw-Hill Companies, Inc.
33. Lu, J., Getz, G., Miska, E. A., Alvarez-Saavedra, E., Lamb, J., Peck, D., Sweet-Cordero, A., Ebert, B. L., Mak, R. H., Ferrando, A. A., Downing, J. R., Jacks, T., Horvitz, H. R., and Golub, T. R. (2005) MicroRNA expression profiles classify human cancers, *Nature 435*, 834-838.
34. Boozer, C., Kim, G., Cong, S., Guan, H., and Londergan, T. (2006) Looking towards label-free biomolecular interaction analysis in a high-throughput format: a review of new surface plasmon resonance technologies, *Curr Opin Biotechnol 17*, 400-405.
35. Albert, J., Lepinay, S., Caucheteur, C., and DeRosa, M. C. (2013) High resolution grating-assisted surface plasmon resonance fiber optic aptasensor, *Methods 63*, 239-254.
36. Yao, C., Qi, Y., Zhao, Y., Xiang, Y., Chen, Q., and Fu, W. (2009) Aptamer-based piezoelectric quartz crystal microbalance biosensor array for the quantification of IgE, *Biosensors and Bioelectronics 24*, 2499-2503.
37. Długosz, M., Bojarska, E., and Antosiewicz, J. M. (2002) A procedure for analysis of stopped-flow transients for protein–ligand association, *Journal of Biochemical and Biophysical Methods 51*, 179-193.

38. Lago, H., Parrott, A. M., Moss, T., Stonehouse, N. J., and Stockley, P. G. (2001) Probing the kinetics of formation of the bacteriophage MS2 translational operator complex: identification of a protein conformer unable to bind RNA1, *Journal of Molecular Biology 305*, 1131-1144.
39. Hopkins, J. F., Panja, S., and Woodson, S. A. (2011) Rapid binding and release of Hfq from ternary complexes during RNA annealing, *Nucleic Acids Research 39*, 5193-5202.
40. Bujalowski, W. M. (2012) *Spectroscopic methods of analysis : methods and protocols*, Humana Press, New York.
41. Berezovski, M., and Krylov, S. N. (2002) Nonequilibrium capillary electrophoresis of equilibrium mixtures--a single experiment reveals equilibrium and kinetic parameters of protein-DNA interactions, *J Am Chem Soc 124*, 13674-13675.
42. Berezovski, M., Nutiu, R., Li, Y., and Krylov, S. N. (2003) Affinity analysis of a protein-aptamer complex using nonequilibrium capillary electrophoresis of equilibrium mixtures, *Anal Chem 75*, 1382-1386.
43. Krylov, S. N. (2006) Nonequilibrium capillary electrophoresis of equilibrium mixtures (NECEEM): A novel method for biomolecular screening, *Journal of biomolecular screening 11*, 115-122.
44. Berezovski, M., and Krylov, S. N. (2003) Using DNA-binding proteins as an analytical tool, *J Am Chem Soc 125*, 13451-13454.
45. Berezovski, M., Musheev, M., Drabovich, A., and Krylov, S. N. (2006) Non-SELEX selection of aptamers, *J Am Chem Soc 128*, 1410-1411.
46. Berezovski, M. V., Musheev, M. U., Drabovich, A. P., Jitkova, J. V., and Krylov, S. N. (2006) Non-SELEX: selection of aptamers without intermediate amplification of candidate oligonucleotides, *Nat Protoc 1*, 1359-1369.
47. Chen, Y. L., Lu, W. J., Chen, X. G., and Teng, M. (2012) Review of recent developments of on-line sample stacking techniques and their application in capillary electrophoresis, *Cent Eur J Chem 10*, 611-638.
48. Bartel, D. P. (2004) MicroRNAs: genomics, biogenesis, mechanism, and function, *Cell 116*, 281-297.
49. Lakatos, L., Szittya, G., Silhavy, D., and Burgyan, J. (2004) Molecular mechanism of RNA silencing suppression mediated by p19 protein of tombusviruses, *EMBO J 23*, 876-884.
50. Dunoyer, P., Lecellier, C. H., Parizotto, E. A., Himber, C., and Voinnet, O. (2004) Probing the microRNA and small interfering RNA pathways with virus-encoded suppressors of RNA silencing, *The Plant cell 16*, 1235-1250.
51. Vargason, J. M., Szittya, G., Burgyan, J., and Hall, T. M. T. (2003) Size selective recognition of siRNA by an RNA silencing suppressor, *Cell 115*, 799-811.
52. Cheng, J., Danielson, D. C., Nasheri, N., Singaravelu, R., and Pezacki, J. P. (2011) Enhanced specificity of the viral suppressor of RNA silencing protein p19 toward sequestering of human microRNA-122, *Biochemistry 50*, 7745-7755.
53. Ha, T. Y. (2011) MicroRNAs in Human Diseases: From Cancer to Cardiovascular Disease, *Immune network 11*, 135-154.
54. Nasheri, N., Cheng, J., Singaravelu, R., Wu, P., McDermott, M. T., and Pezacki, J. P. (2011) An enzyme-linked assay for the rapid quantification of microRNAs based on the viral suppressor of RNA silencing protein p19, *Analytical Biochemistry 412*, 165-172.
55. Esau, C., Davis, S., Murray, S. F., Yu, X. X., Pandey, S. K., Pear, M., Watts, L., Booten, S. L., Graham, M., McKay, R., Subramaniam, A., Propp, S., Lollo, B. A., Freier, S., Bennett, C. F., Bhanot, S., and Monia, B. P. (2006) miR-122 regulation of lipid metabolism revealed by in vivo antisense targeting, *Cell Metab 3*, 87-98.
56. Coulouarn, C., Factor, V. M., Andersen, J. B., Durkin, M. E., and Thorgeirsson, S. S. (2009) Loss of miR-122 expression in liver cancer correlates with suppression of the hepatic phenotype and gain of metastatic properties, *Oncogene 28*, 3526-3536.

57. Jangra, R. K., Yi, M., and Lemon, S. M. (2010) Regulation of hepatitis C virus translation and infectious virus production by the microRNA miR-122, *J Virol 84*, 6615-6625.
58. Cheng, J., Sagan, S. M., Jakubek, Z. J., and Pezacki, J. P. (2008) Studies of the interaction of the viral suppressor of RNA silencing protein p19 with small RNAs using fluorescence polarization, *Biochemistry 47*, 8130-8138.
59. Malim, M. H., Hauber, J., Le, S. Y., Maizel, J. V., and Cullen, B. R. (1989) The HIV-1 rev trans-activator acts through a structured target sequence to activate nuclear export of unspliced viral mRNA, *Nature 338*, 254-257.
60. Braddock, M., Powell, R., Blanchard, A. D., Kingsman, A. J., and Kingsman, S. M. (1993) HIV-1 TAR RNA-binding proteins control TAT activation of translation in Xenopus oocytes, *FASEB J 7*, 214-222.
61. Fourtounis, J., Falgueyret, J.-P., and Elie Sayegh, C. (2011) Assessing protein–RNA interactions using microfluidic capillary mobility shift assays, *Analytical Biochemistry 411*, 161-163.
62. Ledford, H. (2015) Cancer-fighting viruses win approval, *Nature 526*, 622-623.
63. Health, U. S. N. I. o. (2012) Clinical Trials.gov.
64. Chiocca, E. A. (2002) Oncolytic viruses, *Nature reviews. Cancer 2*, 938-950.
65. Thomas, C. E., Ehrhardt, A., and Kay, M. A. (2003) Progress and problems with the use of viral vectors for gene therapy, *Nat Rev Genet 4*, 346-358.
66. Singh, P., Gonzalez, M. J., and Manchester, M. (2006) Viruses and their uses in nanotechnology, *Drug Develop Res 67*, 23-41.
67. Azizi, A., Mironov, G. G., Muharemagic, D., Wehbe, M., Bell, J. C., and Berezovski, M. V. (2012) Viral quantitative capillary electrophoresis for counting and quality control of RNA viruses, *Anal Chem 84*, 9585-9591.
68. Baer, A., and Kehn-Hall, K. (2014) Viral Concentration Determination Through Plaque Assays: Using Traditional and Novel Overlay Systems, *Journal of Visualized Experiments : JoVE*, 52065.
69. Patricia C. Stepp, K. A. R., Erica D. Dawson, Kathy L. Rowlen, and Matthew M. Ferris. (2011) Comparing H1N1 Virus Quantification with a Unique Flow Cytometer and Quantitative PCR, *Bioprocess International 9*, 50-56.
70. Lian, D.-S., and Zhao, S.-J. (2015) Capillary electrophoresis based on nucleic acid detection for diagnosing human infectious disease, In *Clinical Chemistry and Laboratory Medicine (CCLM)*.
71. van Tricht, E., Geurink, L., Pajic, B., Nijenhuis, J., Backus, H., Germano, M., Somsen, G. W., and Sänger-van de Griend, C. E. (2015) New capillary gel electrophoresis method for fast and accurate identification and quantification of multiple viral proteins in influenza vaccines, *Talanta 144*, 1030-1035.
72. Wu, L., Huang, T. G., Meseck, M., Altomonte, J., Ebert, O., Shinozaki, K., Garcia-Sastre, A., Fallon, J., Mandeli, J., and Woo, S. L. (2008) rVSV(M Delta 51)-M3 is an effective and safe oncolytic virus for cancer therapy, *Human gene therapy 19*, 635-647.
73. Stojdl, D. F., Lichty, B., Knowles, S., Marius, R., Atkins, H., Sonenberg, N., and Bell, J. C. (2000) Exploiting tumor-specific defects in the interferon pathway with a previously unknown oncolytic virus, *Nature medicine 6*, 821-825.
74. Parato, K. A., Senger, D., Forsyth, P. A., and Bell, J. C. (2005) Recent progress in the battle between oncolytic viruses and tumours, *Nature reviews. Cancer 5*, 965-976.
75. Wollmann, G., Davis, J. N., Bosenberg, M. W., and van den Pol, A. N. (2013) Vesicular stomatitis virus variants selectively infect and kill human melanomas but not normal melanocytes, *Journal of virology 87*, 6644-6659.
76. Ozduman, K., Wollmann, G., Piepmeier, J. M., and van den Pol, A. N. (2008) Systemic vesicular stomatitis virus selectively destroys multifocal glioma and metastatic carcinoma in brain, *The Journal of neuroscience : the official journal of the Society for Neuroscience 28*, 1882-1893.

77. Kremser, L., Bilek, G., Blaas, D., and Kenndler, E. (2007) Capillary electrophoresis of viruses, subviral particles and virus complexes, *Journal of separation science 30*, 1704-1713.
78. Canada, P. H. A. o. (2016) Canadian Immunization Guide.
79. Brandau, D. T., Jones, L. S., Wiethoff, C. M., Rexroad, J., and Middaugh, C. R. (2003) Thermal stability of vaccines, *J Pharm Sci 92*, 218-231.
80. Journal of Vaccines and Vaccination, http://www.omicsonline.org/vaccines-vaccination.php.
81. Parato, K. A., Senger, D., Forsyth, P. A. J., and Bell, J. C. (2005) Recent progress in the battle between oncolytic viruses and tumours, *Nat Rev Cancer 5*, 965-976.
82. Zaffran, M. (1996) Vaccine transport and storage: environmental challenges, *Dev Biol Stand 87*, 9-17.
83. Chen, D., and Kristensen, D. (2009) Opportunities and challenges of developing thermostable vaccines, *Expert Rev Vaccines 8*, 547-557.
84. Wallis, C., and Melnick, J. L. (1968) Stabilization of enveloped viruses by dimethyl sulfoxide, *J Virol 2*, 953-954.
85. Zhang, J., Pritchard, E., Hu, X., Valentin, T., Panilaitis, B., Omenetto, F. G., and Kaplan, D. L. (2012) Stabilization of vaccines and antibiotics in silk and eliminating the cold chain, *Proc Natl Acad Sci U S A 109*, 11981-11986.
86. Health, P. (2016) Health Guides, Understanding Vaccines; What goes into a vaccine, Public Health.
87. Harding, M. M., Anderberg, P. I., and Haymet, A. D. (2003) 'Antifreeze' glycoproteins from polar fish, *Eur J Biochem 270*, 1381-1392.
88. Adam, M. K., Poisson, J. S., Hu, Y., Prasannakumar, G., Pottage, M. J., Ben, R. N., and Wilkinson, B. L. (2016) Carbohydrate-based surfactants as photocontrollable inhibitors of ice recrystallization, *RSC Advances 6*, 39240-39244.
89. Guziewicz, N., Best, A., Perez-Ramirez, B., and Kaplan, D. L. (2011) Lyophilized silk fibroin hydrogels for the sustained local delivery of therapeutic monoclonal antibodies, *Biomaterials 32*, 2642-2650.
90. Pritchard, E. M., and Kaplan, D. L. (2011) Silk fibroin biomaterials for controlled release drug delivery, *Expert Opin Drug Deliv 8*, 797-811.
91. Grosz, D. D., van Geelen, A., Gallup, J. M., Hostetter, S. J., Derscheid, R. J., and Ackermann, M. R. (2014) Sucrose stabilization of Respiratory Syncytial Virus (RSV) during nebulization and experimental infection, *BMC Res Notes 7*, 158.
92. Sun, H., Zhu, X., Lu, P. Y., Rosato, R. R., Tan, W., and Zu, Y. (2014) Oligonucleotide aptamers: new tools for targeted cancer therapy, *Mol Ther Nucleic Acids 3*, e182.
93. Jain, N. K., Jetani, H. C., and Roy, I. (2013) Nucleic Acid Aptamers as Stabilizers of Proteins: The Stability of Tetanus Toxoid, *Pharmaceutical Research 30*, 1871-1882.
94. Chaudhary, R. K., Patel, K. A., Patel, M. K., Joshi, R. H., and Roy, I. (2015) Inhibition of Aggregation of Mutant Huntingtin by Nucleic Acid Aptamers In Vitro and in a Yeast Model of Huntington/'s Disease, *Mol Ther 23*, 1912-1926.
95. Fedorko, M., Pacik, D., Wasserbauer, R., Juracek, J., Varga, G., Ghazal, M., and Nussir, M. I. (2016) MicroRNAS in the pathogenesis of renal cell carcinoma and their diagnostic and prognostic utility as cancer biomarkers, *International Journal of Biological Markers 31*, e26-e37.
96. Lim, H. J., and Yang, J. L. (2016) Regulatory roles and therapeutic potential of microRNA in sarcoma, *Critical Reviews in Oncology/Hematology 97*, 118-130.
97. Ludvíková, M., Kalfeřt, D., and Kholová, I. (2015) Pathobiology of MicroRNAs and Their Emerging Role in Thyroid Fine-Needle Aspiration, *Acta Cytologica 59*, 435-444.
98. Moret-Tatay, I., Iborra, M., Cerrillo, E., Tortosa, L., Nos, P., and Beltrán, B. (2016) Possible biomarkers in blood for Crohn's disease: Oxidative stress and microRNAs - Current evidences and further aspects to unravel, *Oxidative Medicine and Cellular Longevity 2016*.

99. Pal, M. K., Jaiswar, S. P., Dwivedi, V. N., Tripathi, A. K., Dwivedi, A., and Sankhwar, P. (2015) MicroRNA: a new and promising potential biomarker for diagnosis and prognosis of ovarian cancer, *Cancer Biology and Medicine 12*, 328-341.
100. Paul, R., Choudhury, A., Choudhury, S., Mazumder, M. K., and Borah, A. (2016) Cholesterol in pancreatic β-Cell death and dysfunction underlying mechanisms and pathological implications, *Pancreas 45*, 317-324.
101. Thomas, J., Ohtsuka, M., Pichler, M., and Ling, H. (2015) MicroRNAs: Clinical relevance in colorectal cancer, *International Journal of Molecular Sciences 16*, 28063-28076.
102. Wallace, R. G., Twomey, L. C., Custaud, M. A., Moyna, N., Cummins, P. M., Mangone, M., and Murphy, R. P. (2016) Potential Diagnostic and Prognostic Biomarkers of Epigenetic Drift within the Cardiovascular Compartment, *BioMed Research International 2016*.
103. DiStefano, J. K., and Gerhard, G. S. (2016) Circulating microRNAs in nonalcoholic fatty liver disease, *Expert Review of Gastroenterology and Hepatology 10*, 161-163.
104. Jin, J., McReynolds, L. A., and Gullerova, M. (2014) p19-Mediated Enrichment and Detection of siRNAs, In *Animal Endo-SiRNAs: Methods and Protocols* (Werner, A., Ed.), pp 99-111, Springer New York, New York, NY.
105. Vargason, J. M., Szittya, G., Burgyan, J., and Hall, T. M. (2003) Size selective recognition of siRNA by an RNA silencing suppressor, *Cell 115*, 799-811.
106. Hayes, N. C., and Chayama, K. (2016) MicroRNAs as Biomarkers for Liver Disease and Hepatocellular Carcinoma, *International Journal of Molecular Sciences 17*.
107. Lanford, R. E., Hildebrandt-Eriksen, E. S., Petri, A., Persson, R., Lindow, M., Munk, M. E., Kauppinen, S., and Orum, H. (2010) Therapeutic silencing of microRNA-122 in primates with chronic hepatitis C virus infection, *Science 327*, 198-201.
108. Luna, J. M., Scheel, T. K., Danino, T., Shaw, K. S., Mele, A., Fak, J. J., Nishiuchi, E., Takacs, C. N., Catanese, M. T., de Jong, Y. P., Jacobson, I. M., Rice, C. M., and Darnell, R. B. (2015) Hepatitis C virus RNA functionally sequesters miR-122, *Cell 160*, 1099-1110.
109. Janssen, H. L., Reesink, H. W., Lawitz, E. J., Zeuzem, S., Rodriguez-Torres, M., Patel, K., van der Meer, A. J., Patick, A. K., Chen, A., Zhou, Y., Persson, R., King, B. D., Kauppinen, S., Levin, A. A., and Hodges, M. R. (2013) Treatment of HCV infection by targeting microRNA, *N Engl J Med 368*, 1685-1694.
110. Khan, N., Cheng, J., Pezacki, J. P., and Berezovski, M. V. (2011) Quantitative Analysis of MicroRNA in Blood Serum with Protein-Facilitated Affinity Capillary Electrophoresis, *Anal Chem 83*, 6196-6201.
111. Mironov, G. G., Okhonin, V., Gorelsky, S. I., and Berezovski, M. V. (2011) Revealing equilibrium and rate constants of weak and fast noncovalent interactions, *Anal Chem 83*, 2364-2370.
112. Danielson, D. C., Filip, R., Powdrill, M. H., O'Hara, S., and Pezacki, J. P. (2015) Suppressing RNA silencing with small molecules and the viral suppressor of RNA silencing protein p19, *Biochemical and Biophysical Research Communications 463*, 1135-1140.
113. Cooper, A. (1999) Thermodynamic analysis of biomolecular interactions, *Curr Opin Chem Biol 3*, 557-563.
114. Rawlings, R. A., Krishnan, V., and Walter, N. G. (2011) Viral RNAi suppressor reversibly binds siRNA to outcompete Dicer and RISC via multiple turnover, *J Mol Biol 408*, 262-276.
115. Mack, G. S. (2007) MicroRNA gets down to business, *Nat Biotechnol 25*, 631-638.
116. De Belle, I., Wu, J. X., Sperandio, S., Mercola, D., and Adamson, E. D. (2003) In vivo cloning and characterization of a new growth suppressor protein TOE1 as a direct target gene of Egr1, *J Biol Chem 278*, 14306-14312.
117. Sperandio, S., Tardito, S., Surzycki, A., Latterich, M., and de Belle, I. (2009) TOE1 interacts with p53 to modulate its transactivation potential, *FEBS Lett 583*, 2165-2170.

118. Fong, K. W., Li, Y., Wang, W., Ma, W., Li, K., Qi, R. Z., Liu, D., Songyang, Z., and Chen, J. (2013) Whole-genome screening identifies proteins localized to distinct nuclear bodies, *J Cell Biol 203*, 149-164.
119. Wagner, E., Clement, S. L., and Lykke-Andersen, J. (2007) An unconventional human Ccr4-Caf1 deadenylase complex in nuclear cajal bodies, *Mol Cell Biol 27*, 1686-1695.
120. Diaz, L. S., Stone, M. R., Mackewicz, C. E., and Levy, J. A. (2003) Differential gene expression in CD8+ cells exhibiting noncytotoxic anti-HIV activity, *Virology 311*, 400-409.
121. Levy, J. A., Mackewicz, C. E., and Barker, E. (1996) Controlling HIV pathogenesis: the role of the noncytotoxic anti-HIV response of CD8+ T cells, *Immunol Today 17*, 217-224.
122. Walker, C. M., Moody, D. J., Stites, D. P., and Levy, J. A. (1986) CD8+ lymphocytes can control HIV infection in vitro by suppressing virus replication, *Science 234*, 1563-1566.
123. Levy, J. A. (2003) The search for the CD8+ cell anti-HIV factor (CAF), *Trends Immunol 24*, 628-632.
124. Katz, B. Z., Salimi, B., Gadd, S. L., Huang, C. C., Kabat, W. J., Kersey, D., McCabe, C., Heald-Sargent, T., Katz, E. D., and Yogev, R. (2011) Differential gene expression of soluble CD8+ T-cell mediated suppression of HIV replication in three older children, *J Med Virol 83*, 24-32.
125. Frankel, A. D., and Pabo, C. O. (1988) Cellular uptake of the tat protein from human immunodeficiency virus, *Cell 55*, 1189-1193.
126. Green, M., and Loewenstein, P. M. (1988) Autonomous functional domains of chemically synthesized human immunodeficiency virus tat trans-activator protein, *Cell 55*, 1179-1188.
127. Romani, B., Engelbrecht, S., and Glashoff, R. H. (2010) Functions of Tat: the versatile protein of human immunodeficiency virus type 1, *J Gen Virol 91*, 1-12.
128. Emerman, M., Guyader, M., Montagnier, L., Baltimore, D., and Muesing, M. A. (1987) The specificity of the human immunodeficiency virus type 2 transactivator is different from that of human immunodeficiency virus type 1, *EMBO J 6*, 3755-3760.
129. Guyader, M., Emerman, M., Sonigo, P., Clavel, F., Montagnier, L., and Alizon, M. (1987) Genome organization and transactivation of the human immunodeficiency virus type 2, *Nature 326*, 662-669.
130. Jakobovits, A., Smith, D. H., Jakobovits, E. B., and Capon, D. J. (1988) A discrete element 3' of human immunodeficiency virus 1 (HIV-1) and HIV-2 mRNA initiation sites mediates transcriptional activation by an HIV trans activator, *Mol Cell Biol 8*, 2555-2561.
131. Hauber, J., and Cullen, B. R. (1988) Mutational analysis of the trans-activation-responsive region of the human immunodeficiency virus type I long terminal repeat, *J Virol 62*, 673-679.
132. Vickers, T., Baker, B. F., Cook, P. D., Zounes, M., Buckheit, R. W., Jr., Germany, J., and Ecker, D. J. (1991) Inhibition of HIV-LTR gene expression by oligonucleotides targeted to the TAR element, *Nucleic Acids Res 19*, 3359-3368.
133. Hamy, F., Felder, E. R., Heizmann, G., Lazdins, J., Aboul-ela, F., Varani, G., Karn, J., and Klimkait, T. (1997) An inhibitor of the Tat/TAR RNA interaction that effectively suppresses HIV-1 replication, *Proceedings of the National Academy of Sciences of the United States of America 94*, 3548-3553.
134. Mei, H.-Y., Mack, D. P., Galan, A. A., Halim, N. S., Heldsinger, A., Loo, J. A., Moreland, D. W., Sannes-Lowery, K. A., Sharmeen, L., Truong, H. N., and Czarnik, A. W. (1997) Discovery of selective, small-molecule inhibitors of RNA complexes—1. The tat protein/TAR RNA complexes required for HIV-1 transcription, *Bioorganic & Medicinal Chemistry 5*, 1173-1184.
135. Hamy, F., Brondani, V., Florsheimer, A., Stark, W., Blommers, M. J. J., and Klimkait, T. (1998) A new class of HIV-1 Tat antagonist acting through Tat-TAR inhibition, *Biochemistry 37*, 5086-5095.
136. Ouellet, D. L., Plante, I., Landry, P., Barat, C., Janelle, M. E., Flamand, L., Tremblay, M. J., and Provost, P. (2008) Identification of functional microRNAs released through asymmetrical processing of HIV-1 TAR element, *Nucleic Acids Res 36*, 2353-2365.

137. Christensen, H. S., Daher, A., Soye, K. J., Frankel, L. B., Alexander, M. R., Laine, S., Bannwarth, S., Ong, C. L., Chung, S. W., Campbell, S. M., Purcell, D. F., and Gatignol, A. (2007) Small interfering RNAs against the TAR RNA binding protein, TRBP, a Dicer cofactor, inhibit human immunodeficiency virus type 1 long terminal repeat expression and viral production, *J Virol 81*, 5121-5131.
138. Jang, S., Hyun, S., Kim, S., Lee, S., Lee, I. S., Baba, M., Lee, Y., and Yu, J. (2014) Cell-penetrating, dimeric alpha-helical peptides: nanomolar inhibitors of HIV-1 transcription, *Angew Chem Int Ed Engl 53*, 10086-10089.
139. Joly, J. P., Mata, G., Eldin, P., Briant, L., Fontaine-Vive, F., Duca, M., and Benhida, R. (2014) Artificial nucleobase-amino acid conjugates: A new class of TAR RNA binding agents, *Chemistry - A European Journal 20*, 2071-2079.
140. Sperandio, S., Barat, C., Cabrita, M. A., Gargaun, A., Berezovski, M. V., Tremblay, M. J., and de Belle, I. (2015) TOE1 is an inhibitor of HIV-1 replication with cell-penetrating capability, *Proc Natl Acad Sci U S A 112*, E3392-3401.
141. Berezovski, M. V., Lechmann, M., Musheev, M. U., Mak, T. W., and Krylov, S. N. (2008) Aptamer-facilitated biomarker discovery (AptaBiD), *J Am Chem Soc 130*, 9137-9143.
142. Cleland, W. W. (1964) Dithiothreitol, a New Protective Reagent for SH Groups*, *Biochemistry 3*, 480-482.
143. Chomczynski, P. (1992) Solubilization in formamide protects RNA from degradation, *Nucleic Acids Res 20*, 3791-3792.
144. Kim, B. M., Schultz, L. W., and Raines, R. T. (1999) Variants of ribonuclease inhibitor that resist oxidation, *Protein Sci 8*, 430-434.
145. Frankel, A. D., Bredt, D. S., and Pabo, C. O. (1988) Tat protein from human immunodeficiency virus forms a metal-linked dimer, *Science 240*, 70-73.
146. Long, K. S., and Crothers, D. M. (1999) Characterization of the solution conformations of unbound and Tat peptide-bound forms of HIV-1 TAR RNA, *Biochemistry 38*, 10059-10069.
147. Olsen, G. L., Edwards, T. E., Deka, P., Varani, G., Sigurdsson, S. T., and Drobny, G. P. (2005) Monitoring tat peptide binding to TAR RNA by solid-state 31P-19F REDOR NMR, *Nucleic Acids Res 33*, 3447-3454.
148. (1991) *Advances in Molecular Biology and Targeted Treatment for AIDS*, Plenum Press, New York, George Washington University Medical Center.
149. Mironov, G. G., Chechik, A. V., Ozer, R., Bell, J. C., and Berezovski, M. V. (2011) Viral quantitative capillary electrophoresis for counting intact viruses, *Anal Chem 83*, 5431-5435.
150. Cosa, G., Focsaneanu, K. S., McLean, J. R., McNamee, J. P., and Scaiano, J. C. (2001) Photophysical properties of fluorescent DNA-dyes bound to single- and double-stranded DNA in aqueous buffered solution, *Photochem Photobiol 73*, 585-599.
151. Janas, T., and Yarus, M. (2003) Visualization of membrane RNAs, *RNA 9*, 1353-1361.
152. Bleher, R., and Martin, R. (2001) Ribosomes in the squid giant axon, *Neuroscience 107*, 527-534.
153. Martin, R., Vaida, B., Bleher, R., Crispino, M., and Giuditta, A. (1998) Protein synthesizing units in presynaptic and postsynaptic domains of squid neurons, *Journal of Cell Science 111*, 3157-3166.
154. Miura, Y., Ichikawa, Y., Ishikawa, T., Ogura, M., De Fries, R., Shimada, H., and Mitsuhashi, M. (1996) Fluorometric determination of total mRNA with oligo(dT) immobilized on microtiter plates, *Clinical Chemistry 42*, 1758-1764.
155. Wallis, C., and Melnick, J. L. (1967) Virus aggregation as the cause of the non-neutralizable persistent fraction, *J Virol 1*, 478-488.
156. Getz, E. B., Xiao, M., Chakrabarty, T., Cooke, R., and Selvin, P. R. (1999) A comparison between the sulfhydryl reductants tris(2- carboxyethyl)phosphine and dithiothreitol for use in protein biochemistry, *Analytical Biochemistry 273*, 73-80.

157. Labib, M., Zamay, A. S., Muharemagic, D., Chechik, A., Bell, J. C., and Berezovski, M. V. (2012) Electrochemical sensing of aptamer-facilitated virus immunoshielding, *Anal Chem 84*, 1677-1686.
158. Ghobadloo, S. M., Gargaun, A., Casselman, R., Muharemagic, D., and Berezovski, M. V. (2014) Aptamer-facilitated cryoprotection of viruses, *ACS Med Chem Lett 5*, 1240-1244.
159. Williams, K. A. (2011) Synthesis and Characterization of Monosaccharide-derived Low Molecular Weight Gelators, In *Chemistry*, p 173, The University of New Orleans, United States of America.
160. Matthias, D. M., Robertson, J., Garrison, M. M., Newland, S., and Nelson, C. (2007) Freezing temperatures in the vaccine cold chain: a systematic literature review, *Vaccine 25*, 3980-3986.
161. Ghobadloo, S. M., Balcerzak, A. K., Gargaun, A., Muharemagic, D., Mironov, G. G., Capicciotti, C. J., Briard, J. G., Ben, R. N., and Berezovski, M. V. (2014) Carbohydrate-based ice recrystallization inhibitors increase infectivity and thermostability of viral vectors, *Sci Rep 4*, 5903.
162. Fuhrhop, J. H., Schnieder, P., Boekema, E., and Helfrich, W. (1988) Lipid bilayer fibers from diastereomeric and enantiomeric N-octylaldonamides, *Journal of the American Chemical Society 110*, 2861-2867.
163. Pfannemüller, B., and Welte, W. (1985) Amphiphilic properties of synthetic glycolipids based on amide linkages. I. Electron microscopic studies on aqueous gels, *Chemistry and Physics of Lipids 37*, 227-240.
164. Tam, R. Y., Ferreira, S. S., Czechura, P., Ben, R. N., and Chaytor, J. L. (2008) Hydration index-a better parameter for explaining small molecule hydration in inhibition of ice recrystallization, *Journal of the American Chemical Society 130*, 17494-17501.
165. Diallo, J. S., Vaha-Koskela, M., Le Boeuf, F., and Bell, J. (2012) Propagation, purification, and in vivo testing of oncolytic vesicular stomatitis virus strains, *Methods Mol Biol 797*, 127-140.
166. Diallo, J.-S., Vähä-Koskela, M., Boeuf, F., and Bell, J. (2012) Propagation, Purification, and In Vivo Testing of Oncolytic Vesicular Stomatitis Virus Strains, In *Oncolytic Viruses: Methods and Protocols* (Kirn, H. D., Liu, T.-C., and Thorne, H. S., Eds.), pp 127-140, Humana Press, Totowa, NJ.
167. Galasso, G. J. (1967) Quantitative studies on the quality, effects of aggregation and thermal inactivation of vesicular stomatitis virus, *Archiv für die gesamte Virusforschung 21*, 437-446.
168. Sharp, D. G., and Kim, K. S. (1966) Multiplicity reactivation and radiation survival of aggregated vaccinia virus. Calculation of plaque titer based on MR and particle aggregation seen in the electron microscope, *Virology 29*, 359-366.
169. Han, J. C., and Han, G. Y. (1994) A Procedure for Quantitative Determination of Tris(2-Carboxyethyl)phosphine, an Odorless Reducing Agent More Stable and Effective Than Dithiothreitol, *Analytical Biochemistry 220*, 5-10.
170. Rose, J. K., Welch, W. J., Sefton, B. M., Esch, F. S., and Ling, N. C. (1980) Vesicular stomatitis virus glycoprotein is anchored in the viral membrane by a hydrophobic domain near the COOH terminus, *Proceedings of the National Academy of Sciences of the United States of America 77*, 3884-3888.
171. The NCBI handbook, B. M. N. L. o. M. U., National Center for Biotechnology Information. (2002) Glycoprotein (G protein) mature peptide, NP_955548.1, October ed., http://www.ncbi.nlm.nih.gov/books/NBK21091/.
172. Okun, V. M., Blaas, D., and Kenndler, E. (1999) Separation and biospecific identification of subviral particles of human rhinovirus serotype 2 by capillary zone electrophoresis, *Anal Chem 71*, 4480-4485.
173. Bales, B. L., Messina, L., Vidal, A., Peric, M., and Nascimento, O. R. (1998) Precision relative aggregation number determinations of SDS micelles using a spin probe. A model of micelle surface hydration, *Journal of Physical Chemistry B 102*, 10347-10358.

174. Nielsen, M. M., Andersen, K. K., Westh, P., and Otzen, D. E. (2007) Unfolding of β-Sheet Proteins in SDS, *Biophysical Journal 92*, 3674-3685.
175. Tiller, G. E., Mueller, T. J., Dockter, M. E., and Struve, W. G. (1984) Hydrogenation of Triton X-100 eliminates its fluorescence and ultraviolet light absorption while preserving its detergent properties, *Analytical Biochemistry 141*, 262-266.
176. Biotechnology, P. (2006) Sodium Cholate, United States of America.
177. Duplâtre, G., Ferreira Marques, M. F., and da Graça Miguel, M. (1996) Size of Sodium Dodecyl Sulfate Micelles in Aqueous Solutions as Studied by Positron Annihilation Lifetime Spectroscopy, *The Journal of Physical Chemistry 100*, 16608-16612.
178. Hancu, G., Simon, B., Rusu, A., Mircia, E., and Gyéresi, Á. (2013) Principles of Micellar Electrokinetic Capillary Chromatography Applied in Pharmaceutical Analysis, *Advanced Pharmaceutical Bulletin 3*, 1-8.
179. Yang, S., and Khaledi, M. G. (1995) Chemical Selectivity in Micellar Electrokinetic Chromatography: Characterization of Solute-Micelle Interactions for Classification of Surfactants, *Anal Chem 67*, 499-510.
180. Norton, D., and Shamsi, S. A. (2004) Capillary electrochromatography of Triton X-100, *Electrophoresis 25*, 586-593.
181. Muijselaar, P. G., Otsuka, K., and Terabe, S. (1997) Micelles as pseudo-stationary phases in micellar electrokinetic chromatography, *Journal of Chromatography A 780*, 41-61.
182. Knezevic, I. (2009) Stability evaluation of vaccines: WHO approach, *Biologicals 37*, 357-359; discussion 421-353.
183. Hall-Stoodley, L., Costerton, J. W., and Stoodley, P. (2004) Bacterial biofilms: From the natural environment to infectious diseases, *Nature Reviews Microbiology 2*, 95-108.
184. Davey, M. E., and O'Toole, G. A. (2000) Microbial biofilms: From ecology to molecular genetics, *Microbiology and Molecular Biology Reviews 64*, 847-867.
185. Rybtke, M., Hultqvist, L. D., Givskov, M., and Tolker-Nielsen, T. (2015) Pseudomonas aeruginosa Biofilm Infections: Community Structure, Antimicrobial Tolerance and Immune Response, *Journal of Molecular Biology 427*, 3628-3645.
186. Waters, C. M., and Bassler, B. L. (2005) Quorum sensing: Cell-to-cell communication in bacteria, In *Annual Review of Cell and Developmental Biology*, pp 319-346.
187. Nazzaro, F., Fratianni, F., and Coppola, R. (2013) Quorum sensing and phytochemicals, *International Journal of Molecular Sciences 14*, 12607-12619.
188. Miller, M. B., and Bassler, B. L. (2001) Quorum sensing in bacteria, *Annu Rev Microbiol 55*, 165-199.
189. Kim, S. K., and Lee, J. H. (2016) Biofilm dispersion in Pseudomonas aeruginosa, *Journal of Microbiology 54*, 71-85.
190. Vessey, J. K. Plant growth promoting rhizobacteria as biofertilizers, *Plant and Soil 255*, 571-586.
191. Beauregard, P. B., Chai, Y., Vlamakis, H., Losick, R., and Kolter, R. (2013) Bacillus subtilis biofilm induction by plant polysaccharides, *Proceedings of the National Academy of Sciences 110*, E1621-E1630.
192. Costerton, J. W., Montanaro, L., and Arciola, C. R. (2005) Biofilm in implant infections: its production and regulation, *Int J Artif Organs 28*, 1062-1068.
193. Kucharikova, S., Gerits, E., De Brucker, K., Braem, A., Ceh, K., Majdic, G., Spanic, T., Pogorevc, E., Verstraeten, N., Tournu, H., Delattin, N., Impellizzeri, F., Erdtmann, M., Krona, A., Lovenklev, M., Knezevic, M., Frohlich, M., Vleugels, J., Fauvart, M., de Silva, W. J., Vandamme, K., Garcia-Forgas, J., Cammue, B. P., Michiels, J., Van Dijck, P., and Thevissen, K. (2016) Covalent immobilization of antimicrobial agents on titanium prevents Staphylococcus aureus and Candida albicans colonization and biofilm formation, *J Antimicrob Chemother 71*, 936-945.

194. Darouiche, R. O. (2004) Treatment of infections associated with surgical implants, *N Engl J Med 350*, 1422-1429.
195. Organization, W. H. (2014) Antimicrobial Resistance - Global Report on Surveillance 2014, p 257, http://www.who.int/drugresistance/publications/infographic-antimicrobial-resistance-20140430.pdf?ua=1.
196. Sharma, G., Rao, S., Bansal, A., Dang, S., Gupta, S., and Gabrani, R. (2014) Pseudomonas aeruginosa biofilm: Potential therapeutic targets, *Biologicals 42*, 1-7.
197. Borges, A., Saavedra, M. J., and Simões, M. (2012) The activity of ferulic and gallic acids in biofilm prevention and control of pathogenic bacteria, *Biofouling 28*, 755-767.
198. Ta, A. C., and Arnason, T. J. (2016) Mini Review of Phytochemicals and Plant Taxa with Activity as Microbial Biofilm and Quorum Sensing Inhibitors, *Molecules 21*.
199. Pereira, U. A., Barbosa, L. C. A., Maltha, C. R. A., Demuner, A. J., Masood, M. A., and Pimenta, A. L. (2014) γ-Alkylidene-γ-lactones and isobutylpyrrol-2(5H)-ones analogues to rubrolides as inhibitors of biofilm formation by Gram-positive and Gram-negative bacteria, *Bioorganic & Medicinal Chemistry Letters 24*, 1052-1056.
200. Ren, D., Sims, J. J., and Wood, T. K. (2001) Inhibition of biofilm formation and swarming of Escherichia coli by (5Z)-4-bromo-5-(bromomethylene)-3-butyl-2(5H)-furanone, *Environmental Microbiology 3*, 731-736.
201. Ren, D., Sims, J. J., and Wood, T. K. (2002) Inhibition of biofilm formation and swarming of Bacillus subtilis by (5Z)-4-bromo-5-(bromomethylene)-3-butyl-2(5H)-furanone, *Letters in Applied Microbiology 34*, 293-299.
202. Hentzer, M., Riedel, K., Rasmussen, T. B., Heydorn, A., Andersen, J. B., Parsek, M. R., Rice, S. A., Eberl, L., Molin, S., Høiby, N., Kjelleberg, S., and Givskov, M. (2002) Inhibition of quorum sensing in Pseudomonas aeruginosa biofilm bacteria by a halogenated furanone compound, *Microbiology 148*, 87-102.
203. Ta, C. A. K. (2015) Bacterial biofilm inhibition and antifungal activity of neotropical plants, In *Biology*, p 257, University of Ottawa, Ottawa.
204. Maxwell, A., Dabideen, D., Reynolds, W. F., and McLean, S. (1999) Neolignans from Piper aequale, *Phytochemistry 50*, 499-504.
205. Setzer, W. N., Park, G., Agius, B. R., Stokes, S. L., Walker, T. M., and Haber, W. A. (2008) Chemical compositions and biological activities of leaf essential oils of twelve species of Piper from Monteverde, Costa Rica, *Nat. Prod. Commun. 3*, 1367-1374.
206. Lopez, A., Ming, D. S., and Towers, G. H. (2002) Antifungal activity of benzoic acid derivatives from Piper lanceaefolium, *J Nat Prod 65*, 62-64.
207. Pino Benítez, N., Melendez, E., and Stashenko, E. E. (2009) Chemical composition and antibacterial activity of the essential oil from the leaves of Piper lanceaefolium a plant traditionally used in Colombia, *Boletin Latinoamericano y del Caribe de Plantas Medicinales y Aromaticas 8*, 301-304.
208. MacKinnon, S. L., Bensimon, C., Arnason, J. T., SanchezVindas, P. E., and Durst, T. (1997) Spirocaracolitones, CD-spiro triterpenoids from Ruptiliocarpon caracolito, *J. Org. Chem. 62*, 840-845.
209. Asim, M., Hussien, H., Poveda, L., Arnason, J. T., and Durst, T. (2010) Triterpenoids from the bark of Ruptiliocarpon caracolito, *Phytochemistry 71*, 1418-1422.
210. Asim, M., Hussien, H., Arnason, J. T., Poveda, L., and Durst, T. (2007) Spirocaracolitone triterpenoids from the bark of Ruptiliocarpon caracolito, *J Nat Prod 70*, 1228-1232.
211. MacKinnon, S. (1995) Bioactive triterpenoids of the Rutales, University of Ottawa, Ottawa.
212. Omar, S., Marcotte, M., Fields, P., Sanchez, P. E., Poveda, L., Mata, R., Jimenez, A., Durst, T., Zhang, J., MacKinnon, S., Leaman, D., Arnason, J. T., and Philogene, B. J. R. (2007) Antifeedant activities of terpenoids isolated from tropical Rutales, *J. Stored Prod. Res. 43*, 92-96.

213. MacKinnon, S., Durst, T., Arnason, J. T., Angerhofer, C., Pezzuto, J., Sanchez-Vindas, P. E., Poveda, L. J., and Gbeassor, M. (1997) Antimalarial activity of tropical Meliaceae extracts and gedunin derivatives, *J Nat Prod 60*, 336-341.
214. Holloway, D., and Scheinmann, F. (1974) Two lignans from Litsea grandis and L. gracilipes, *Phytochemistry 13*, 1233-1236.
215. Cabral, M. M., Alencar, J. A., Guimaraes, A. E., and Kato, M. J. (2009) Larvicidal activity of grandisin against Aedes aegypti, *J Am Mosq Control Assoc 25*, 103-105.
216. Martins, R. C., Lago, J. H., Albuquerque, S., and Kato, M. J. (2003) Trypanocidal tetrahydrofuran lignans from inflorescences of Piper solmsianum, *Phytochemistry 64*, 667-670.
217. Saad, J. M., Soepadamo, E., Fang, X. P., McLaughlin, J. L., and Fanwick, P. E. (1991) (-)-Grandisin form Cryptocarya crassinervia, *J Nat Prod 54*, 1681-1683.
218. Greger, H., Pacher, T., Vajrodaya, S., Bacher, M., and Hofer, O. (2000) Infraspecific variation of sulfur-containing bisamides from Aglaia leptantha, *J Nat Prod 63*, 616-620.
219. Pu, J. X., Gao, X. M., Lei, C., Xiao, W. L., Wang, R. R., Yang, L. B., Zhao, Y., Li, L. M., Huang, S. X., Zheng, Y. T., and Sun, H. D. (2008) Three new compounds from Kadsura longipedunculata, *Chem Pharm Bull (Tokyo) 56*, 1143-1146.
220. Lopes, N. P., De Almeida Blumenthal, E. E., Cavalheiro, A. J., Kato, M. J., and Yoshida, M. (1996) Lignans, γ-Lactones and propiophenones of Virola surinamensis, *Phytochemistry 43*, 1089-1092.
221. Lopes, N. P., Chicaro, P., Kato, M. J., Albuquerque, S., and Yoshida, M. (1998) Flavonoids and lignans from Virola surinamensis twigs and their in vitro activity against Trypanosoma cruzi, *Planta Med 64*, 667-668.
222. Carvalho, A. A., Galdino, P. M., Nascimento, M. V., Kato, M. J., Valadares, M. C., Cunha, L. C., and Costa, E. A. (2010) Antinociceptive and antiinflammatory activities of grandisin extracted from Virola surinamensis, *Phytother Res 24*, 113-118.
223. Lane, A. L. (2008) Marine Natural Products as Antimicrobial Chemical Defenses and Sources of Potential Drugs, In *Chemistry and Biochemistry*, Georgia Institute of Technology, U.S.A.
224. Rossi, P. G., Bao, L., Luciani, A., Panighi, J., Desjobert, J. M., Costa, J., Casanova, J., Bolla, J. M., and Berti, L. (2007) (E)-methylisoeugenol and elemicin: Antibacterial components of Daucus carota L. essential oil against Campylobacter jejuni, *Journal of Agricultural and Food Chemistry 55*, 7332-7336.
225. Lopez, A., Hudson, J. B., and Towers, G. H. (2001) Antiviral and antimicrobial activities of Colombian medicinal plants, *J Ethnopharmacol 77*, 189-196.
226. Ruddock, P. S., Charland, M., Ramirez, S., Lopez, A., Neil Towers, G. H., Arnason, J. T., Liao, M., and Dillon, J. A. (2011) Antimicrobial activity of flavonoids from Piper lanceaefolium and other Colombian medicinal plants against antibiotic susceptible and resistant strains of Neisseria gonorrhoeae, *Sex Transm Dis 38*, 82-88.
227. Rojas-Martínez, R., Arrieta, J., Cruz-Antonio, L., Arrieta-Baez, D., Velázquez-Méndez, A. M., and Sánchez-Mendoza, M. E. (2013) Dillapiole, isolated from peperomia pellucida, shows gastroprotector activity against ethanol-induced gastric lesions in wistar rats, *Molecules 18*, 11327-11337.
228. Khadem, S., and Marles, R. J. (2011) Chromone and flavonoid alkaloids: occurrence and bioactivity, *Molecules 17*, 191-206.
229. Bubb, W. A. (2006) *NMR Spectroscopy in the study of Carbohydrates: Characterizing the Structural Complexity*, Wiley InterScience, www.interscience.wiley.com.
230. Kupchan, S. M., Tsou, G., and Sigel, C. W. (1973) Datiscacin, a novel cytotoxic cucurbitacin 20-acetate from Datisca glomerata, *J Org Chem 38*, 1420-1421.

231. Ali, M. S., Mahmud, S., Perveen, S., Rizwani, G. H., and Ahmad, V. U. (1999) Screening for the Antimicrobial Properties of the Leaves of Calophyllum inophyllum Linn. (Guttiferae), *Journal of Chemical Society of Pakistan 21*, 174-178.
232. Sniehotta, M., Schiffer, E., Zurbig, P., Novak, J., and Mischak, H. (2007) CE - a multifunctional application for clinical diagnosis, *Electrophoresis 28*, 1407-1417.
233. Marsh, A., Broderick, M., Altria, K., Power, J., Donegan, S., and Clark, B. (2008) Capillary Electrophoresis for Pharmaceutical Analysis, In *Capillary Electrophoresis: Methods and Protocols* (Schmitt-Kopplin, P., Ed.), pp 205-245, Humana Press, Totowa, NJ.
234. Pascali, J. P., Bortolotti, F., and Tagliaro, F. (2012) Recent advances in the application of CE to forensic sciences, an update over years 2009-2011, *Electrophoresis 33*, 117-126.
235. Almeida, M. I., Reis, R. M., and Calin, G. A. (2011) MicroRNA history: discovery, recent applications, and next frontiers, *Mutat Res 717*, 1-8.
236. Kumru, O. S., Joshi, S. B., Smith, D. E., Middaugh, C. R., Prusik, T., and Volkin, D. B. (2014) Vaccine instability in the cold chain: mechanisms, analysis and formulation strategies, *Biologicals 42*, 237-259.
237. Muharemagic, D., Zamay, A., Ghobadloo, S. M., Evgin, L., Savitskaya, A., Bell, J. C., and Berezovski, M. V. (2014) Aptamer-facilitated Protection of Oncolytic Virus from Neutralizing Antibodies, *Mol Ther Nucleic Acids 3*, e167.